Explosive instability of magneto-elastic Waves

Oleksandr Yevstafyev

N° d'ordre : 155

ECOLE CENTRALE DE LILLE

THÈSE

présentée en vue
d'obtenir le grade de

DOCTEUR

en

Spécialité : Micro et Nano Technologies, Acoustique et Télécommunications

par

Oleksandr Yevstafyev

DOCTORAT DELIVRE CONJOINTEMENT PAR L'ECOLE CENTRALE DE LILLE ET TAURIDAV.I. VERNADSKY NATIONAL UNIVERSITE

Titre de la thèse :

Instabilité Explosive des Ondes Magneto-Élastiques

Soutenue le 17 juin 2011 devant le jury d'examen composé de :

Président	Mr. Marc LETHIECQ	Professeur à l'Université de To urs
Rapporteur	Mr. Jean-Marie LE BRETON	Professeur à l'Université de Rouen
Rapporteur	Mr. Igor LYUBCHANSKII	Professeur à Donetsk Physical et Technical Institut de l'Académie National des Sciences d'Ukraine
Examinateur	Mr. Olivier BOU MATAR	Professeur à l'Ecole Centrale de Lille
Examinateur	Mr. Yuri PYL'NOV	Professeur à l'Institut Radiotechnique, Electronique et Automation de Moscou
Directeur de Thèse	Mr. Philippe PERNOD	Professeur à l'Ecole Centrale de Lille
Directeur de Thèse	Mr. Vladimir PREOBRAZHENSKY	Professeur à l'Ecole Centrale de Lille Directeur de recherche à l'Académie des Sciences de Russie.
Directeur de Thèse	Mr. Volodymyr BERZHANS'KY	Professeur à Taurida V.I. Vernadsky National Université de Simferopol

Thèse préparée dans le Laboratoire International Associé LEMAC à l'Institut d'Electronique, de Microélectronique et de Nanotechnologie (IEMN, UMR CNRS 8520) (France) et à TauridaV.I. Vernadsky National Universite (TNU) (Ukraine) dans le cadre d'une cotutelle

Ecole Doctorale SPI 072 (Lille I, Lille III, Artois, ULCO, UVHC, EC Lille)
PRES Université Lille Nord-de-France

Table of Contents

Acknowledgement

Ces travaux ont été réalisé au sein du laboratoire Européen associé en Magnéto-Acoustique non-linéaire de la matière condensée (LEMAC), à l'Institut d'Electronique de Microélectronique et de Nanotechnologie du Nord (IEMN, CNRS/UMR 8520, France) en co-tutelle avec Taurida V.I. Vernadsky National Université (TNU, Simferopol, Ukraine).

Je remercie vivement en premier lieu mes directeurs de thèse du coté français les Professeurs Philippe PERNOD et Vladimir PREOBRAZHENSKY de l'Ecole Centrale de Lille pour m'avoir accueilli dans leur équipe (LEMAC-IEMN), pour leur encadrement et pour la confiance qu'ils m'ont témoigné tout au long de ces trois années de travail.

Je remercie au même titre mon directeur de thèse du coté Ukrainien le Professeur Volodymyr Berzhans'ky de Taurida V.I. Vernadsky National Université de Simferopol, je tiens à lui exprimer toute ma reconnaissance pour l'intensité de son partage et de son soutien.

J'associe également à ces remerciements le Professeur Jean-Marie LE BRETON de l'Université de Rouen et le Professeur Igor LYUBCHANSKII de Donetsk Physical et Technical Institut de l'Académie National des Sciences d'Ukraine d'avoir accepté de rapporter ce travail, ainsi que les membres du jury, le Professeur Marc LETHIECQ de Université de Tours, Yuri PYL'NOV de l'Institut de Radiotechnique d'Electronique et d'Automatique de Moscou et le Professeur Olivier BOU MATAR de l'Ecole Centrale de Lille.

Cette thèse a enfin été rendue possible par le soutien et l'amitié de tous les membres présents et passés du LEMAC. L'environnement de recherche varié rencontré dans cette équipe a rendu mon expérience à Lille particulièrement enrichissante. Je veux aussi exprimer ma reconnaissance à tous les personnels de l'IEMN qui ont permis ces recherches.

Enfin, je remercie évidemment toute ma famille et mes amis pour leur soutien et leurs encouragements pendent mon mon travail, sans eux, il aurait été très difficile d'en venir à bout. Merci.

Introduction

Nonlinear physical effects represent one of the topical problems in modern science. In acoustics nonlinear and parametric phenomena in solids are very diverse and serve as a powerful tool for scientific research of the properties of matter. These phenomena themselves also present great interest as they can be used in various ultrasonic applications in biomedicine and industry for non-destructive diagnostics, imaging, signals treatment, destructive applications, etc. For example, well-known effects of parametric signal amplification and wave front reversal of ultrasound are used in phase conjugators based on highly nonlinear PZT piezoelectric ceramics or magneto-acoustic ceramics that serve as active medium. Combination of this technique with nonlinear harmonics imaging allows visualization of isoechogenic phantoms and increases resolution of imaging. In the recent years also nonlinear effects in so-called "soft solids" became of an interest due to numerous possible biomedical applications for ultrasonic diagnostics, particularly supersonic shear wave elasticity imaging has been developed and is utilized in elastography.

All studied parametric effects arise from modulation of linear parameters of the system. Recently the research has broadened to effects caused by modulation of nonlinear parameters in condensed matter and in microelectromechanical systems. This type of modulation opened a new category of instabilities that manifest themselves as multi-boson coupled excitations. These effects previously have been reported only in plasma physics. Multi-boson processes present interest for fundamental physics, in particular for physics of elementary particles.

In materials where acoustic waves are coupled with excitations of other nature, as in piezoelectric or magnetic media, nonlinearities of the coupling and of piezoeffect or magnetic subsystem itself introduce effective nonlinearity to the elastic subsystem excitations, changing the nonlinear elastic moduli for low frequency quasi-elastic oscillations. In high temperature easy plane antiferromagnes (AFEP) like α-Fe_2O_3 and $FeBO_3$ the moduli change is especially high due to exchange interaction participation in long wave oscillations that introduces giant effective anharmonicity in the crystals. This makes AFEPs a convenient model media to study general problems of nonlinear dynamics in continuous media.

Acoustic excitations in antiferromagnets are usually realized in the form of hybrid magnetoelastic waves named quasi-phonons. Anomalously strong phonon-magnon coupling in AFEPs manifests itself in particular in the generation of parametrically coupled quasi-phonon pairs. These pairs can be coupled with the help of modulating electromagnetic field. Threshold of the modulation depth for these instabilities depends on the damping parameters in the medium and supercritical dynamics demonstrates exponential growth. A number of other parametric and nonlinear effects have been also theoretically predicted and experimentally observed in AFEPs, including parametric generation of sound by sound, doubling of the sound frequency, acoustic detection, etc.

The value of giant effective acoustic nonlinearity in easy plane antiferromagnets has a strong dependence on external magnetic field. Modulation of the nonlinear elastic parameters favors generation of the multi-boson excitations. First stationary excitations of three quasi-phonons in condensed matter have been theoretically predicted and experimentally observed in hematite crystal under electromagnetic pumping.

Theoretical analysis of the new instabilities has shown several specific dynamic features that differ excited quasi-phonon triads from the generation of quasi-phonon pairs. First of all nonlinear instability thresholds depend not only on amplitude of electromagnetic pumping but also on the number of initial quasi-phonons (i.e. on amplitude of an initial oscillations). Second of all supercritical mode of these instabilities demonstrates explosive dynamics with rapid increase of number of generated quasi-phonon triads up to creation of singularity of amplitudes of coupled waves at finite time of pumping.

Parametric instabilities arising from modulation of nonlinear parameters of the system have also been recently experimentally detected in MEMS structures. Nonlinear coupling between an array of nonlinearly coupled microcantilevers was modulated with alternating electric field resulting in subharmonic instabilities formation.

Further theoretical works suggested that for traveling nonlinearly interacting magneto-elastic waves the supercritical explosive behavior is accompanied by the spatial localization of the excitations. Due to energy conservation law explosive dynamics of a system is usually caused by interactions between normal waves with “negative energy” waves, for which amplitude increase corresponds to decrease of energy. Numerous theoretical works on negative and positive wave interactions have been written with very few experimental

observations, mainly in plasma physics. Nonlinear parametric instabilities anticipated in easy plane aniferromagnets demonstrate explosive supercritical behavior of all positive three magnetoelastic waves in magnetic crystal under homogeneous electromagnetic pumping with their amplitudes tending to infinity in a finite time. Three-phonon coupled excitations were experimentally observed in α-Fe_2O_3 single crystal however theoretically predicted explosive dynamics of supercritical excitations has not been manifested due to other interactions in the crystal, mainly the nonlinear frequency shift (NFS) of magneto-elastic modes. Experimental observation of explosive dynamics of magnetoelastic waves was an important milestone yet to be achieved.

The main goal of the work was set as theoretical and experimental studies of supercritical explosive dynamics arising from three quasi-phonon instabilities in "easy plane" antiferromagnets: hematite α-Fe_2O_3 and iron borate $FeBO_3$.

The **first chapter** describes physical magnetoelastic phenomena that formed the foundation of the present research and gives state of the art analysis in magnetoacoustics and multi-boson processes. Dynamics of coupled excitations of magnetic and elastic subsystems is considered in various magnetic media, including ferromagnets, ferrites and antiferromagnets. Various parametric instabilities of magnetoelastic waves that arise from modulation of linear parameters are described. Applications of these instabilities in wave phase conjugation are presented. It is shown that easy plane antiferromagnets possess unprecedented magnetoelastic coupling and giant effective anharmonicity that can be controlled by external magnetic field. Recently discovered parametric instabilities that arise from modulation of nonlinear parameters of magnetoelastic system are analyzed. Theoretical studies suggested explosive dynamics and spatial localization of supercritical dynamics of these instabilities but these suggestions that have yet to be confirmed experimentally.

In the **second chapter** the mechanisms that affect supercritical explosive dynamics manifestation in single-mode three quasi-phonon excitations are analyzed. Analysis is performed on the basis of effective anharmonic approximation for easy plane antiferromagnetic crystal. Approximation suggests that nonlinear frequency shift that comes from the cubic nonlinearity is responsible for the explosive instability limitation. Nonlinearity compensation is suggested via singular consistent pumping phase modulation law. Results of supercritical numerical simulations of the anharmonic approximation with suggested pumping

modulation law are presented that demonstrate explosive dynamics with amplitude of oscillations tending to infinity in finite time.

The **third chapter** is devoted to experimental studies of explosive supercritical dynamics of single-mode three quasi-phonon excitations. Investigation is performed on two AFEP magnetoelastic single crystal resonators mage from hematite and iron borate. Experiments on iron borate are carried out at the temperature range 77 K – 293 K where its magnetoelastic properties differ considerably. First, magnetoelastic resonance modes of the samples are determined and their properties are studied, including coupling coefficient dependences on bias magnetic field, nonlinear frequency shifts of the modes and their quality factors. For the first time cubic nonlinearity of the iron borate is researched. Obtained results are used to determine operating points and compensation laws of pumping phase modulation for supercritical dynamics research. New developed experimental continuous technique for supercritical resonator dynamics visualization under electromagnetic pumping is described. For the first time explosive dynamics of nonlinear parametric instability is experimentally observed and studied in both resonators when proper phase modulation laws are applied to the pumping.

In the **fourth chapter** strongly nonlinear model of three quasi-phonon excitations in single mode is developed. The model considers magnetoelastic nonlinearities outside of anharmonic approximation developed in the second chapter. Developed model is numerically simulated using the values of with experimentally researched hematite and iron borate characteristics at 293 K and at 77 K. The results are compared with the numerical simulations of anharmonic approximation and experimentally obtained data. Strongly nonlinear model demonstrates good correlation with experimental observations of explosive instability.

In the **fifth chapter** the phenomenon of nonlinear interaction of three magnetoelastic waves in easy pane antiferromagnetic medium is considered. Two anharmonic models of the waves' coupling are developed for parallel and perpendicular electromagnetic pumping geometries with respect to bias field. The models consider real AFEP crystal nonlinearities up to the fourth order terms. These terms are found to introduce nonlinear phase shift of ultrasonic triads' generation. Custom computer program that was written in Fortran language for numerical simulations of the coupling process in time and space domains is described. Developed models are simulated with the help of this program and thresholds of the instabilities are determined. Numerical simulations of the models in supercritical mode

demonstrate explosive dynamics and spatial localization of the triads when nonlinear phase shift is neglected. Introduction of the nonlinearities contributes nonlinear phase shift that limits instability dynamics. Pumping field modulation law is suggested that helps to overcome this limitation and manifest explosive dynamics and spatial localization of the instability with hematite crystal nonlinearities.

Thesis conclusion presented at the end of the manuscript summarizes the results obtained in the conducted studies of explosive instabilities of magnetoelastic waves and compares them with initially set goals and tasks of the work.

Chapter I

Parametric and Nonlinear Magnetoelastic Effects in Magnetically Ordered Materials

1.1 Chapter I introduction

The First Chapter presents a review of magnetoacoustics and defines its current state of the art and reveal its topical research problems. It starts from the description of the phenomenon of magnetoelastic waves in general and various parametric and nonlinear effects of these waves. Parametric instabilities in ferrites are discussed and different mechanisms that cause these instabilities under parallel and perpendicular electromagnetic pumping are analyzed. These instabilities were widely researched in the past and are currently used in various applications, notably in wave phase conjugation. Key features of phase conjugation are presented with a review of applications.

Magnetoelastic coupling is especially high in antiferromagnetic materials with easy plane anisotropy (AFEP), where the coupling introduces giant effective nonlinearity. The chapter continues with description of parametric and nonlinear processes in AFEP crystals that manifest themselves much brighter than in ferrites. Modern discoveries and trends in magnetoacoustics are discussed. Recently predicted nonlinear parametric instabilities in antiferromagnets are among the topical problems as they are anticipated to have unique features that differ them from regular parametric instabilities. Suggested explosive supercritical dynamics of these nonlinear processes is yet to be experimentally observed due to strong limitation mechanisms, but presents considerable scientific importance. In the end of the chapter as a result of presented state of the art analysis the scope of the present work is set and main goals are defined.

1.2 Magnetoelastic waves in ferromagnets and ferrites. Magnetoacoustic resonance

Condensed matter consists of subsystems of various physical natures. Excitations of these subsystems interact with each other in different ways that depend on the excitation amplitudes and coupling coefficients between the subsystems. The study of such linear and nonlinear interaction helps to understand better the materials. One of the examples of coupled systems is magnetically ordered materials. In such materials magnetic subsystem and elastic subsystem are interacting with each other via magnetoelastic coupling, causing the mixture of

spin waves and elastic waves, so they no longer exist separately, but become coupled magnetoelastic waves.

The first works that interpreted magnetoelastic coupling as a reason of interaction between the elementary excitations like magnons (spin waves) and phonons (elastic waves) [1] were done by Akhiezer back in forties. Further work by Turov and Irhin that discussed coupled magnetoelastic waves as a separate phenomenon was published later in 1956 [2] with realization, that not only magnetoelastic coupling needs to be taken into account, but magnetoelastic waves themselves with their new properties present a fundamental interest in physics.

Active research of mangetoelastic waves started in 1958 with theoretical approach of coupled magnetoelastic waves in ferromagnets and ferroacoustic resonance by Akhiezer, Baryahtar and Peletminsky [4], Kittel's work on spin waves and ultrasonic waves interaction [5], Spencer's and LeCraw's work on parametrical magnetoelastic resonance in yttrium iron garnet [3]. These works served as a foundation to the new important section of physics called magnetoacoustics and fueled up further research in this field. Yttrium iron garnet ferrite served as an important object for studies of magnetoelastic wave effects because the acoustic losses in this media were found to be an order of magnitude lower than in quartz [6]. A typical spectrum of coupled magnetoelastic waves in a ferrite is presented in Figure 1.1.

Dashed lines show "pure" spectra of spin waves Ak_m^2 and elastic waves $v_s k$. Elastic waves spectrum is determined as $\omega_s = v_s k$ where ω_s is the elastic wave frequency, k is the wave vector and v_k is the speed of sound. Spin wave spectrum is determined by the following relation [7]:

$$\omega_m = \gamma\left[(H_{eff} + Ak_m^2)(H_{eff} + 4\pi M_0 \sin^2\Theta_\mathrm{m} + \mathrm{Ak_m^2})\right]^{1/2}, \qquad (1.1)$$

where ω_m is spin wave frequency, k_m is their wave vector, Θ_m is the angle between external magnetic field and wave vector, A is exchange constant, H_{eff} is the sum of all fields that have an effect on magnetization M_0.

The interaction that exists between spin waves and elastic waves makes the spectra coupled (solid lines) and causes a number of static and dynamic phenomena in magnets

including ΔE-effect (elastic modules change due to magnetic field), spontaneous symmetry breaking, magnetoacoustic resonance (MAR) [8] and many others.

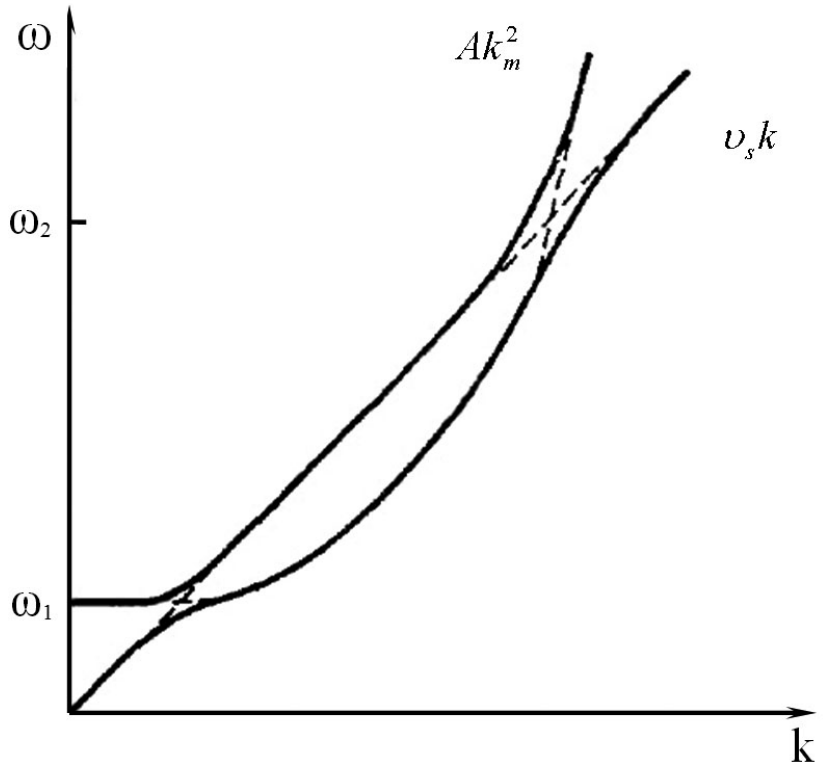

Figure 1.1. Spectrum of coupled magnetoelastic waves in ferrite. Magnon branch Ak_m^2 has two intersections with phonon branch $\upsilon_s k$.

MAR appears as a rapid energy absorption in the conditions when frequencies and wave vectors of magnetic and elastic waves become identical, i.e. in the intersection points of spin and elastic spectra. These points correspond to the strongest magnetoelastic coupling in the system and are shown in Figure 1.1. In these points the spectra are actually being pushed away from each other. The frequencies of intersections can be easily obtained from the spectra equations above, there are two of them, in case when $\Theta_m = 0$, $\omega_1 \cong \gamma H_{eff}$ and $\omega_2 \cong v^2/\gamma A$. These frequencies generally appear in the hypersound band, ω_2 generally lies in the frequencies region where elastic waves propagation is rather problematic, making MAR at ω_1 of an interest. It is also important to notice that the term "MAR" is sometimes used also to describe the process of parametric excitation of acoustic oscillations with the help of electromagnetic wave.

The coupling coefficient ζ between magnetic and elastic subsystems in general theory of oscillations is determined by the energies relation:

$$\zeta = \frac{W_{me}}{\sqrt{W_m W_e}}, \tag{1.2}$$

where W_{me} is the energy of magnetoelastic interaction, W_m is the energy of magnetic subsystem and W_e is the energy of elastic subsystem. The value of coupling coefficient ζ represents relative splitting of magnetic and elastic branches of the spectrum near the MAR point. The square of the coupling coefficient ζ^2 determines relative interaction of the magnetoelastic waves spectra as portion of energy that is being transmitted from one subsystem to another in the points far away from the MAR, including the important band of ultrasound waves, where $k \ll k_1$, or in the magnets where MAR is not possible.

Magnetoelastic waves became an interesting object to study as it was relatively easy to excite them and vary their characteristics with different alternating elastic stress and magnetic field. They found important applications in different systems, including controllable delay lines [9,10], parametric amplifiers [11,12], bandwidth compression [13], etc. The easiest way to excite magnetoelastic waves is to use parametric pumping.

1.3 Parametric magnetoelastic instabilities in ferrites

Parametric excitation in general is a method of exciting and maintaining oscillations in a dynamic system (or coupled subsystems), in which excitation results from a periodic variation of some parameter in the subsystem. So magnetoelastic waves can be parametrically excited by variation of the parameters of magnetic or elastic subsystem. Nowadays parametric excitation in ferromagnets and antiferromagnets has become a very important tool that helps studying energy flows in nonequilibrium systems. The most common way to excite magnetoelastic waves is to apply an alternating magnetic field perpendicular or parallel to the bias magnetic field; however there are multiple mechanisms of parametric instabilities formation, that are discussed in this section.

1.3.1 Parametric instabilities excited by transverse pumping

First experimental observation of parametric resonance of magnetoelastic waves in ferrites under transverse pumping (when the alternating magnetic field h is applied perpendicular to the magnetization M) were made in the works of Damon [14], and Bloembergen and Wang [15] during ferromagnetic resonance experiments. They have found abnormal energy absorption that had a clear threshold. Suhl [16] explained this effect as parametric instability of uniform magnetization precession with regards to spin waves pair excitation with frequencies ω_1 and ω_2 and wave vectors k_1 and k_2. He also formulated the condition of parametric resonance in continuous media:

$$\begin{aligned} n\omega_p &= \omega_1 + \omega_2, \\ k_1 + k_2 &= 0, \end{aligned} \tag{1.5}$$

where ω_p is the frequency of uniform precession and n = 1, 2, 3... The number n determines the order of the instability. Since $k_2 = -k_1$, parametric instability creates pairs of waves with equal but opposite wave vectors. At first theoretical studies of the parametric processes were focused mostly on determinations of the processes thresholds and instability amplitude limitations. This process was called Suhl first order instability. In further works other mechanisms of magnetic, elastic and magnetoelastic instabilities that may be excited parametrically by means of magnetic pumping field h applied transverse to the bias field H were reported [3,17,18]. An important step was made when a summarizing theory of different transversely pumping mechanisms was published by Auld in his work [19].

In his work Auld actually classified known parametric instabilities, defining Suhl first-order instability [16], Suhl second order instability, reaction instability, magnetoacoustic resonance instability (MAR). A summary of these processes is presented in Figure.1.2.

There ω_m is spin-wave dispersion relation, ω_l is longitudinal elastic waves dispersion, ω_t and ω_{td} are two shear elastic waves. $\omega_k^{(2)}$ and $\omega_k^{(1)}$ show the upper and lower branches of the coupled shear magnetoelastic waves. $\omega_k^{(3)}$ and $\omega_k^{(4)}$ are the lower and upper branches of coupled longitudinal magnetoelastic waves. Possible instabilities are shown with the numbers and described in the figure.

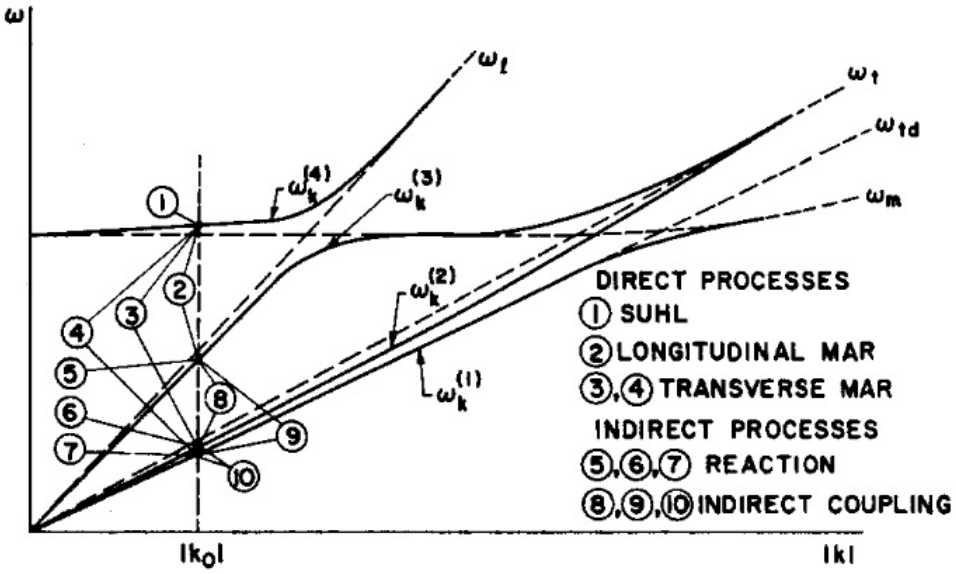

Figure 1.2. Magnetoelastic dispersion curves and classification of instability processes [19].

The thresholds here will be shown in terms of critical pump precession angles Θ. For Suhl first order instability mentioned earlier the critical pump precision threshold Θ_I depends on the dipolar coupling strength and on the damping of the spin wave. When the elastic displacement vector angle with respect to external magnetic field $\theta_k = 0$ the threshold is infinite, so general form is:

$$\Theta_I = \frac{|\omega_m^2 - \Omega_H^2 + i(\Omega_H^2/Q_M)|}{2\Omega_M\Omega_H sin\theta_k cos\theta_k}, \tag{1.4}$$

where ω_m is the frequency of uncoupled wave, $\Omega_M = \gamma 4\pi M_s$, $\Omega_H = \gamma H_i$, γ is gyromagnetic ratio, M_s is magnetization. For Suhl second order instability minimum thresholds of precession angle Θ_{II} occur when $\theta_k = 0$ [16], so the threshold equation is:

$$\Theta_{II} = \sqrt{\frac{\Delta H_k}{4\pi M_s}} = \frac{1}{\sqrt{Q_m}}, \tag{1.5}$$

where $Q_m = \omega_m / \gamma \Delta H_k$ is the quality factor. Magnetoacoustic resonance mechanism instability may involve either longitudinal or shear waves and generates a pair that consists of phonon and magnon (both branches of the magnetoelastic spectra are involved) near the point of the branches intersection. The threshold precession angle Θ_{MAR} for MAR instability is:

$$\Theta_{MAR} = \frac{1}{2K_1(0)\sqrt{Q_m Q_l}}, \tag{1.6}$$

where K_1 is magnetomechanical coupling coefficient. Reaction instability mechanism is based on the fact that the effective elastic constant has a magnetic component which can be modulated by the pump. In this process two elastic waves are excited as shown on Figure 1.2. The threshold of reaction instability is:

$$\Theta_{Re} = \frac{\omega_p^2}{4F(\theta_k)K_2^2(\theta_k)Q_{eff}} \tag{1.7}$$

Auld's numerical calculations of thresholds showed that the MAR instability and reaction instability thresholds in YIG lie above Suhl instabilities [19]. The studies of the interaction of parametric coupling and travelling waves have shown that travelling waves can be parametrically amplified experimentally with transverse pumping field [11, 20-22]. The first parametric generation of magnetoelastic waves together with their amplification was experimentally reported by Damon and van de Vaart [23] at X-band frequencies and liquid helium temperatures, and later on at room temperatures and lower frequencies [24]. In further work on the phenomenon the net gain exceeded 55 dB at the temperature 1.5 K [25].

An important specificity of all the calculated parametric thresholds is that they are proportional to $Q_m^{-1/2}$ (the reaction instability varies at approximately same rate in the vicinity of its minimum value). The amplitude of the initial oscillations does not change the threshold. This is a typical behavior of the instabilities arising from those terms in the magnetocrystalline energy which are linear in the strain variations. Recently discovered parametric instabilities that arise from nonlinear strain variations have different threshold conditions that depend also on the initial oscillations amplitude. These instabilities are discussed in the section 1.8 of this chapter.

1.3.2 Parametric instabilities excited with parallel pumping

In 1960 Morgentaller [26] and independently Schlomann, Green and Milano [27] theoretically predicted and experimentally observed [27] parametric excitation of spin waves

with longitudinal pumping (alternating magnetic field h is parallel to the magnetization). It was suggested that due to dipolar interaction, the tip of the electron precession vector follows an ellipsoidal path instead of circular one. Since the length of magnetization stays constant during precession, the length of z-component varies at twice the precession frequency during its rotation (considering that the z axis is parallel to the spin precession axis). The threshold of this instability was experimentally studied and theoretically derived as:

$$h_{||} = \frac{\omega}{\tau\gamma^2 4\pi M_0}\ , \tag{1.8}$$

where τ is energy relaxation time, H is external field, ω is the frequency of wave and M_0 is magnetization, γ is dissipation parameter. Turner [28] on the sample of yttrium iron garnet near the point of magnetoacoustic resonance demonstrated that coupled spin and elastic waves can also be parallel pumped. Comstock and LeCraw have observed another mechanism of parallel parametric instability [29] of a nearly pure elastic wave. Parallel alternating magnetic field was used to excite non-resonance parametric instability via elastic modulus C_{44} modulation in the single-crystal EuIG sample. The threshold of this instability was derived as:

$$h_{||} = \frac{[(\omega_{res}^2 - \omega^2)^2 + (\omega^2/Q)^2]^{1/2}}{\omega_{res}^2 \partial C_{44}(H_0)/\partial H} C_{44}, \tag{1.9}$$

where ω_{res} is the resonance frequency of the mode, ω is the frequency of pumping, Q is the quality factor of resonator and C_{44} is elastic module of the sample. Parallel parametric excitation became one of the main means of spin waves generation in ferromagnets in following years with a number of other works on the magnetoelastic instabilities in ferrodielectrics [30-33]. As can be seen from the equations, similar to the perpendicular pumping geometry, the thresholds of parametric instabilities with parallel pumping also depend on the dissipative forces in the media and do not depend on the level of initial oscillations. As the pumping amplitude goes beyond the threshold, the amplitude of generated oscillations starts growing exponentially until it is stabilized by other nonlinear mechanisms.

Strong magnetoelastic coupling of some acoustic resonance modes with spin modes has also been theoretically and experimentally studied by LeCraw and Kasuya [96]. A theoretical treatment of parametric coupling between magnetization and elastic strain in a ferromagnet produced by magnetic pumping has been presented by Comstock and Auld [97].

The thresholds of the parametric excitations were determined. Numerical calculations of the thresholds showed possibility of experimental observation of the effect. First experimental observation of parametric modes coupling was reported on $Eu_3Fe_5O_{12}$ ferrite [29].

1.3.3 Supercritical energy flow stabilization mechanisms of parametric instabilities

Theoretical approaches were focused not only on the thresholds of the instabilities but also on the mechanisms that were limiting the instability amplitude growth. Once the pumping surpasses an instability threshold the energy coming from the pumping exceeds the dissipations of the generated boson pairs and amplitudes of parametrically coupled waves increase exponentially with time. However the growth is not infinite and is limited by independent nonlinear processes. Suhl in his work [16] suggested that when the magnetoelastic waves are excited with the homogeneous magnetization precession the main mechanism of the limitation is their counterinfluence on the pumping that is "freezing" its amplitude on the threshold level. For parallel pumping Schlomann [27] suggested that it is important to take into account nonlinear interaction of parametrically excited waves between each other. Gottlib and Suhl [34] calculated the nonlinear influence of multi-magnon interactions on the relaxation rates that cause the amplitude limiting. Bierlein and Richards [35] in their experiments with higher harmonics showed that this type of interaction must be considered for explanation of experimentally observed spin waves frequency doubling. Zakharov et al. [36-38] have developed these ideas and constructed a theoretical model for parametrical spin waves excitations, a so called S theory, in which two independent mechanisms of energy flow stabilization are taken into account.

The first processes was noted by Schlomann [27] keeps the correlation of phases inside every parametrically generated couple of waves with opposite wave vectors and cause self-consistent total phase change in each pair. This total phase change decreases the coupling between the spin waves and pumping, and at the end, causes amplitude limitation. This process is also called nonlinear phase shift, or nonlinear frequency shift.

The second mechanism is positive nonlinear damping that increases relaxation rate of the excited waves with the increase of the square of their amplitude:

$$\gamma_k = \gamma_0 + \gamma_k|c|^2, \tag{1.10}$$

as well as other nonlinear mechanisms of higher orders. Here γ are corresponding dissipation parameters.

Exponential growth of the parametrically excited waves is also limited because of nonlinear interactions in the joint system of waves and pumping source [39], by a so-called pumping exhaustion mechanism. As parametrically excited waves reach high amplitudes they influence the pumping field and start decreasing its amplitude. When the decreased amplitude is pushed below the instability threshold, the exponential growth stops and the process stabilizes.

1.4 Magnetoelastic parametric wave phase conjugation

Phase conjugation (PC) means transformation of a wave field that results in the reversal of propagation of the waves conserving the initial spatial distribution of amplitudes and phases [40]. Phase conjugation possesses some unusual physical properties and offers unique opportunities in physical research, nondestructive testing, technology, and medicine.

1.4.1 The phenomenon of wave phase conjugation

Wave front reversal was first discovered in nonlinear optics. In sonic and ultrasonic acoustics the conditions for the reversal are available due to time invariance of the wave equation in heterogeneous nondissipative propagation medium with the density $\rho(\vec{r})$ and compressibility $\kappa(\vec{r})$. In such medium acoustic pressure field is described by a scalar $p(\vec{r},t)$ that satisfies the equation [41]:

$$\begin{gathered}(L_r + L_t)p(\vec{r},t) = 0, \\ L_r = \nabla\left(\frac{1}{\rho(\vec{r})}\nabla\right), L_t = -\kappa(\vec{r})\frac{\partial^2}{\partial t^2}\end{gathered} \tag{1.11}$$

Since the equation (1.11) contains only second order time derivatives, it is time invariant. This means that for a set of sound waves $p(\vec{r},t)$ that is emitted by a source and is

propagating in heterogeneous media, being scattered and refracted, in theory a conjugated set $p(\vec{r}, -t)$ can be generated with the help of time-domain conjugation, that experiences same scattering and refraction as if time is going backwards, and restores the original distribution of acoustic field at the source.

For a real monochromatic wave field $A_i(\vec{r}, t)$ with an amplitude $a(\vec{r})$ and field phase $\varphi(\vec{r})$ of oscillations with the frequency ω:

$$A_i(\vec{r}, t) = a(\vec{r}) \cos\big(\omega t - \varphi(\vec{r})\big), \tag{1.12}$$

the conjugated wave of the same amplitude is described as:

$$A_c(\vec{r}, t) = a(\vec{r}) \cos\left(-\omega t - \varphi(\vec{r})\right) \equiv a(\vec{r}) \cos\left(\omega t + \varphi(\vec{r})\right) \tag{1.13}$$

Thus wave propagation time reversal can be achieved also by equivalent phase conjugation $\varphi(\vec{r}) \rightarrow -\varphi(\vec{r})$ in all points of the propagation medium. Depending on the ways the experimental reversed wave is created the effect is reffered to as time reversal or Fourier-domain wave phase conjugation.

In spectral interpretation the change of time sign is equivalent to the change of the wave vector direction from $\vec{k}$ to $-\vec{k}$. If a propagating acoustic beam is reflected by an acoustic conjugation mirror, it starts propagating backwards and compensates phase distortions in inhomogeneous, acoustically transparent medium, including the compensation for acoustic losses in elastic scattering. An acousto-optical visualization of this peculiarity has been performed [47]. Scattered conjugated acoustic beams also possess auto focusing features, as propagating backwards they converge on the original source of sound scatter.

Nowadays the most efficient methods for acoustic wave front reversal are time reversal with the help of so-called acoustic retina arrays [41] and phase conjugation with the help of parametric phase conjugation in solids [42].

Time reversal acoustic mirror usually consists of 1D or 2D array of piezoelectric transducers that are used for both registration and emission of ultrasound. The array pitch has to be not more than $\lambda/2$, where λ is the shortest wavelength of spectral components of expected signal. Every transducer is connected to a separate signal registration and processing module. Incident wave is recorded with the help of this array. Obtained signal is processed separately for each transducer to generate a time-reversed waveform that is then sent to the

same transducer to emit time-reversed signal. The advantages of such wave front reversal systems are broad signal processing options and practically no limitations of the input signal. The disadvantages are high production prices and relative complicity of such systems.

Parametric wave phase conjugation is experimentally achieved in parametrically active solids by sound speed modulation with pumping field.

1.4.2 Principles of parametric wave phase conjugation in solids

Conjugated wave in a solid medium can be generated during parametric coupling of two acoustic waves of the circular frequency ω and parametric electromagnetic pumping at the double frequency $\omega_p = 2\omega$. Since the speed of electromagnetic waves is by five orders faster than the speed of sound the pumping produces nearly uniform medium modulation. Reversed wave generation can be interpreted as a two-boson process when decay of pumping photon with frequency ω_p and wave vector $k \approx 0$ results in generation of two phonons with two opposite wave vectors $k_1 = -k_2$ of equal frequencies $\omega_1 = \omega_2$. Energy and impulse conservation laws for this process can be written as:

$$\begin{cases} \vec{p}_p = \vec{p}_i + \vec{p}_c \\ E_p = E_i + E_c \end{cases} \tag{1.14}$$

These laws show that:

$$\begin{cases} \vec{k}_p = \vec{k}_i + \vec{k}_c \\ \omega_p = \omega_i + \omega_c \end{cases} \tag{1.15}$$

A vector diagram that illustrates the process of pumping phonon decay into two phonons is presented in the Figure 1.3.

Let's consider the equation describing acoustic wave propagation process:

$$\frac{\partial^2 u}{\partial t^2} = v^2(t)\frac{\partial^2 u}{\partial z^2} \tag{1.16}$$

With the speed of sound $v(t)$ being modulated by an electromagnetic field:

$$v^2(t) = v_0^2\left(1 + 2m\cos\omega_p t\right), \tag{1.17}$$

where $m = \Delta V/V_0$ is the depth of modulation, ω_p - frequency of pumping, v_0 — velocity of sound at constant value of magnetic bias field.

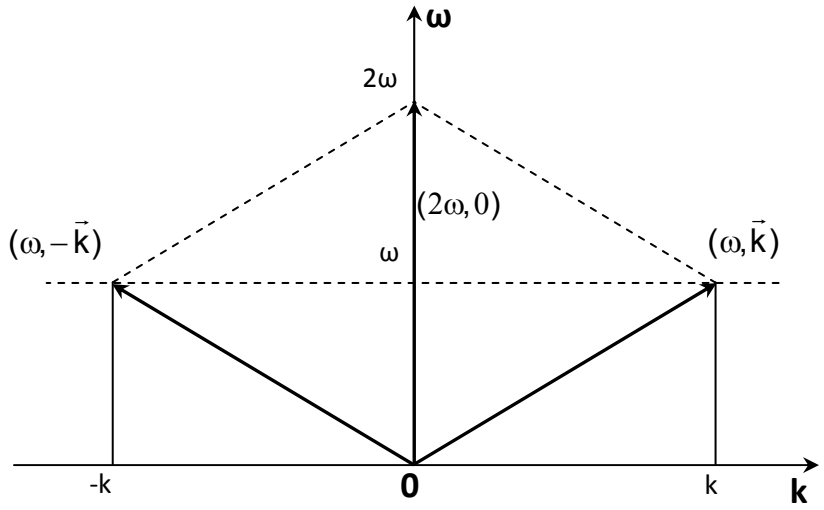

Figure 1.3. Vector diagram of energy and impulse conservation laws during two-boson parametric excitation of phase conjugated wave with electromagnetic pumping.

If an incident acoustic wave of frequency ω propagates in magnetoelastic material where pumping field at double frequency $\omega_p = 2\omega$ (parametric resonance condition) is applied, the conjugate wave is created. When the parametric instability threshold is surpassed, the amplitude of the conjugated wave starts growing exponentially. With neglected dissipation the generation of PC wave can be described by means of the system of equations [43]:

$$\begin{cases} \dfrac{\partial A}{\partial t} + v_0 \dfrac{\partial A}{\partial z} = ihB^* \\ \dfrac{\partial B^*}{\partial t} - v_0 \dfrac{\partial B^*}{\partial z} = ihA \end{cases}, \tag{1.18}$$

where $h = m\omega/2$. Within the asymptotic theory of parametric interaction, the spatial distribution of the conjugate wave amplitude B^* at linear stage of amplification is written as:

$$B^* = -iA_0 \frac{\sin(q(L-z))}{\cos(qL)}, \tag{1.19}$$

where L is the length of active zone, $q = h/v_0$. The condition $qL = \pi/2$ corresponds to threshold value of parametrical generation of sound from thermal noise. When the system is under the threshold $qL \ll \pi/2$ only linear amplification of conjugated wave is possible. The supercritical mode of giant amplification occurs when the pumping amplitude is higher than a threshold value $qL > \pi/2$. At this regime the amplitude of conjugated wave increases exponentially and giant amplifications of 80 dB and more have been reported [44,45]. Critical value of the sound speed modulation depth m is determined by a relation:

$$m_c = \frac{\lambda}{2L}, \tag{1.20}$$

where λ is the ultrasound wave length. Thus if the length of active zone L stays constant the threshold of supercritical amplification regime depends of the frequency of incident waves.

1.4.3 Parametrically active media for wave phase conjugation.

Critical parametrical modulation depth dependency (1.8) suggests that the most favorable conditions for wave front reversal are found at higher frequencies. For that reason first experimental observations of reversed wave generation in nonlinear magnetoelasic [25] and piezoelectric [43,46] media were performed in the hyper sound frequencies. The phenomenon gained more attention when it was reported that phase conjugation corresponds to wave front reversal [52, 53]. However a decrease of the frequency of incident wave dramatically decreased the effective quality factor of conjugation moving it to subthreshold regime. The studies of phase conjugation using nonlinear piezoelectric materials such as $LiNbO_3$ [48], CdS, BK7 glass [49] and PZT ceramics [50, 51] have been conducted but supercritical regime of amplifications has not been realized due to insufficient electroacoustic interaction in these crystals at ultrasound frequencies.

An extremely high efficiency of the parametric PC of a travelling ultrasonic wave was found experimentally in a magnetostriction ceramics based on nickel ferrite [61]. This discovery opened a new era of supercritical conjugation research [54-57] with the amplification coefficients of the backward wave at a frequency of 30 MHz exceeding 80 dB and estimated intensity of hundreds of Watts per cm^2 . The possibility of generation of highly intense phase conjugate ultrasonic waves by means of polycrystalline materials is of special interest because modern ceramic technology allows one to manufacture active elements for

PC devices of any size and shape, which may be required for specific applications. Most of the modern experiments in linear and especially nonlinear ultrasonic use wave phase conjugation in magnetostriction ceramics.

1.4.4 Applications of phase conjugated ultrasonic beams

The unique features of supercritical parametric PC like compensation for phase distortions, autofocusing, giant signal amplification, etc. can find use in many real life applications. Phase conjugation can be used for linear acoustoscopy to compensate phase aberrations compensation [58]. The possibility of the giant amplification of selected frequency with the help of phase conjugated waves (PCWs) in supercritical parametric mode also permits expansion of the PCW technique to nonlinear acoustic imaging to improve the resolution of images and research nonlinear properties of the media. Wave phase conjugator can be used to either amplify the initial signal frequency, so that it propagates back at higher amplitude and generated higher harmonics are analyzed [59], or it can be tuned to the frequency of a harmonic to amplify and reverse it back to the transducer [60,62].

Recent studies of nonlinear acoustic imaging are focusing on medical applications. Phase conjugation can be used in ultrasound examinations of objects that have similar linear parameters as the surrounding medium. Such objects are called isoechogenic phantoms and their nonlinear parameters usually differ. PCW can selectively amplify necessary harmonic component to visualize isoechogenic objects. It has been theoretically shown [63, 64] that for PWC second harmonic imaging the contrast of the object is expected to be of the order $\Delta\beta/\beta_0$, where $\Delta\beta = \beta - \beta_0$ is the difference between nonlinear parameters of the object and surrounding medium respectively. Experimental research of isoechogenic phantoms made from 20% and 60% methanol solutions in water medium has been reported [65] showing high contrast images of the phantoms. The results of scan imaging of the 20 % methanol phantom are presented in the Figure 1.4 (a-c). When PCW is implemented at 10 MHz for the fundamental harmonic of 10-MHz wave (a) the phantom looks to be the same as surrounding medium. When PCW is implemented at 10 MHz, but for the first harmonic of 5-MHz wave (a), contrast difference is noticeable. When the second harmonic of PCW at 20 MHz is analyzed (c) even higher contrast image can be obtained. Some other medical applications are also possible. Focusing of phase conjugate waves onto the model object through bony tissue

was experimentally studied in connection with hyperthermia of a brain tumor in [68]. Self-focused powerful acoustic beams to a bladder or kidney stone to be destroyed not only simplifies the system focusing but also continues crushing fragments of the object when it cracks and moves.

The results of acoustic imaging of two crossed thin (0.1 mm diameter) wires behind phase aberration layer are presented in the Figure 1.4 (d - h) obtained with an incident sound burst at 10 MHz. The scheme of the experiment (d) shows the wires (o), transducer (1), wave phase conjugator (2) and aberration layer (3). Images (e,g) show the pictures obtained without phase conjugation just using focused transducer and receiver at fundamental harmonic 10 MHz and first harmonic at 20 MHz respectively. Phase aberration layer completely destroyes the wires image.

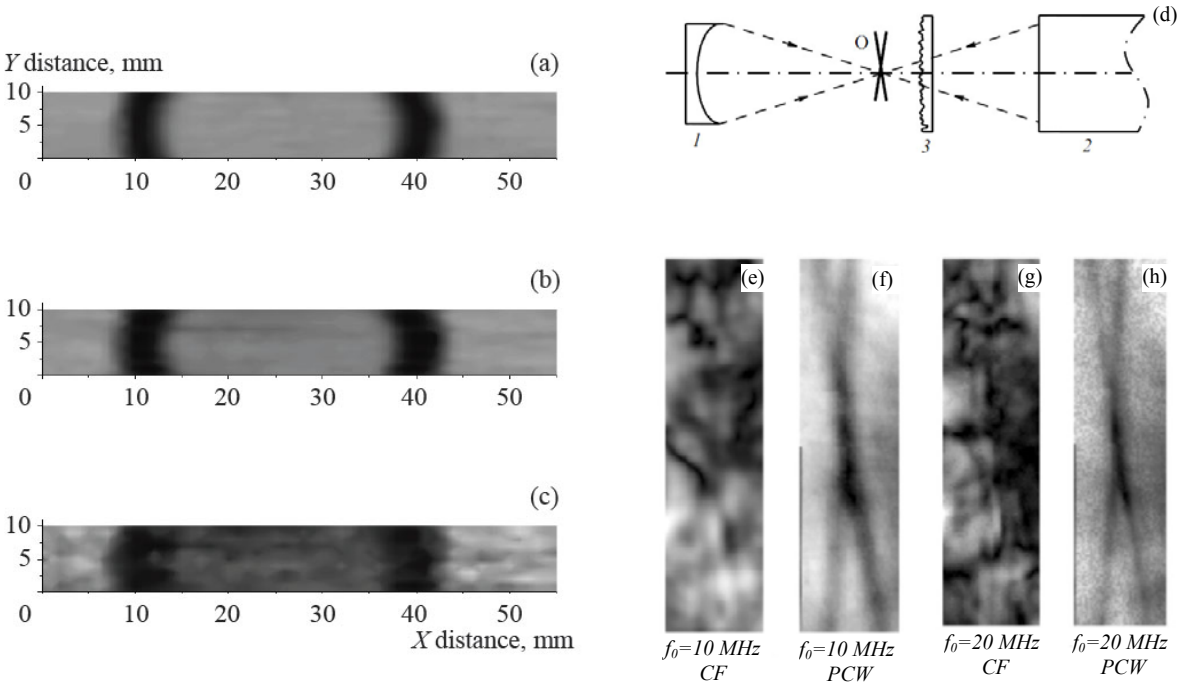

Figure 1.4. Scan imaging of the 20 % methanol phantom: (a) PCW is implemented for the fundamental harmonic, (b) first harmonic, and second harmonic analysis (c) [65]. Experimental Setup of nonlinear acoustoscopy (d) shows the object (o), transducer (1), conjugator (2), aberration layer (3). Presented imaging results use fundamental harmonic (e,g) and first harmonic (f,h) [42].

Images (f,h) show the pictures obtained with phase conjugation, also at fundamental harmonic 10 MHz and second harmonic at 20 MHz respectively. The wires can be clearly seen on both pictures, and the second harmonic image has a higher resolution.

Phase conjugate ultrasound can be also used for velocimetry of the flows [66, 67]. Moving media breaks the time reversal invariance and the registered phase shift can be used to determine velocimetry of the flow in industrial applications or in living tissues. Other industrial applications of wave phase conjugation include non-destructive testing [69], underwater communications [70] and ultrasound attenuation measurements in inhomogeneous media.

1.5 Magnetoelastic waves in antiferromagnets

1.5.1 Magnetoelastic coupling coefficient in antiferromagnets

As it was mentioned in the first section, the square of magnetoelastic coupling coefficient ζ^2 determines the interaction between magnetic and elastic branches of the medium spectrum. In general case in magnetic materials magnetoelastic interaction is relatively weak with $\zeta \ll 1$. For example for easy axis ferromagnet in the bias field *H* [72]:

$$\zeta^2 = \frac{\omega^2}{\omega_{me}^2} = \frac{H}{H + H_A + H_{me}}, \tag{1.21}$$

wher ω is the magnetoelastic gap, ω_{me} is the magnetoelastic contribution to this gap, H_A - magnetic anisotropy field, $H_{me} = B^2/(CM_0)$ - magnetostriction field, B – constant of magnetoelastic coupling, M_0 – magnetization of saturation, *C* is elastic constant . For typical magnets ($M_0 \sim 10^2\ Gs$, $C \sim 10^{12}\ erg/cm^3$, $B \sim 10^7\ erg/cm^3$, $H_A \sim 10^2\ Oe$) the value of this parameter is of the order $\zeta^2 \sim 10^{-4} - 10^{-3}$.

Such a weak coupling makes significant contributions to the spectrum branches behavior only in the point of intersection (during magnetoacoustic resonance) in the hypersound band. Observation of MAR at the ultrasound frequencies that are more appealing for practical applications is limited due to dipole-dipole interaction in ferrites that does not allow lowering the external magnetic field in single domain state. Real life applications and scientific research of non-resonance effects requires media with much higher interaction.

Some materials with more complicated magnetic ordering like antiferromagnets have a higher coupling between magnetic and elastic subsystems because of different energy

hierarchy. In ferromagnets relativistic and dipole-dipole interaction energies dominate magnetoelastic energy, while in antiferromagnets their contribution is suppressed, bringing the magnetoelastic energy on the first place. Pioneering theoretical studies on magnetoelastic waves in antiferromagnets with easy-axis anisotropy were done in work [73] and for easy plane anisotropy (AFEP) in [74]. It was found that specific participation of the exchange interaction in easy plane antiferromanets extremely increases the value of coupling magnetoelastic coefficient [72, 75, 76]:

$$\zeta_{AFM}^2 = \frac{H_E H_{me}}{H^2 + H_E H_{me}}, \tag{1.22}$$

where H is external magnetic field, H_E is exchange field and H_{me} is magnetoelastic field. As a result, for easy plane antiferromagnets in fields that are much greater than the field of mono-domainisation of the crystal, the values of coupling coefficient can be close to 1 (to simplify the comparison H_D is considered to be equal to zero). The spectrum of magnetoelastic excitations in AFEPs Ω_k is determined by the equation [76]:

$$\left(\omega_{fk}^2 - \Omega_k^2\right) + \sum_{S=1}^{3} \frac{\zeta_{Sk}^2 \omega_{fk}^2 \omega_{Sk}^2}{\Omega_k^2 - \omega_{Sk}^2} = 0, \tag{1.23}$$

where ω_{Sk} is the partial frequency of specific (S = 1, 2, 3) elastic mode with the wave vector k, ω_{fk} is the partial frequency of ferromode and ζ_{Sk}^2 is magnetoelastic coupling coefficient. The term "partial" means that the frequencies are calculated with fixed other coupled subsystems, so ω_{fk} is calculated for a "frozen" lattice.

1.5.2 The frozen lattice (magnetoelastic gap) effect in magnetic materials

The frozen lattice (or alternatively - magnetoelastic gap) effect in quasi-magnon branch of coupled magnetoelastic waves was noticed in several works on antiferromagnetic resonance in easy plane antiferromagnet – iron hematite α-Fe_2O_3 above the temperature of Morin transition [77, 78]. The frequency ω of the low-frequency antiferromagnetic resonance mode could not be fully described by the known at that time contributions to the ω caused by

magnetic anisotropy and external magnetic field *H*. If both these contributions are described byω_M^2, then:

$$\omega^2 = \omega_M^2 + \omega_{me}^2, \tag{1.24}$$

where the second term presents the discovered frozen lattice effect. This term does not depend on the direction of bias field H in the easy plane, so it was not connected with the anisotropy. It was suggested that this term ω_{me}^2 is connected with spontaneous magnetostriction [79]. It makes the crystal stretch or contract in the direction of the antiferromagnetic vector, which creates an additional effective anisotropy field for spin oscillations. The important part is that these spontaneous deformations of the lattice do not follow the magnetization oscillations that are created by the AFMR, they get "frozen" [80]. Strong frozen lattice effect was predicted in rare earth ferromagnets with easy plane anisotropy (dysprosium and terbium) that was experimentally proven later on [81]. The effect of frozen lattice was subsequently studied in other magnets: similar easy plane antiferromagnetic crystal of iron borate $FeBO_3$ [82-84], cubic antiferromagnetic garnets [85, 86] and other crystals. It was shown that the effect of frozen lattice is common for all the magnets [87], however the effect is usually hidden by magnetic anisotropy. That's why this effect was mostly observed on easy plane antiferromagnets, where in plane crystallographic anisotropy is relatively small.

Further research showed that magnetoelasic gap represents only one side of the phenomenon. The gap is caused by the influence of the elastic subsystem on magnetic one, but there is also an opposite influence of magnetic system on elastic one. On the waves spectra of magnetoelastic oscillations this is reflected as strong interaction of phonon and magnon branches between each other. Not only magnetoelastic gap gets added to the quasimagnon branch of the spectrum, but also quasiacoustic branch of the spectrum gets deformed, and dispersion law in the small wave number values transforms from linear to square nature. Experimentally this is observed as decrease of the sound speed with the decrease of resonance frequency that can be achieved by bias field, temperature or pressure change. In this case it is said that the quasi-phonon branch softens [88, 89, 72]. Together with the decrease of the speed of sound the relaxation time can decrease [90, 91]. Sound speed variation has been observed in a number of magnetically ordered materials, the highest ones were noticed in easy plane antiferromagnets: hematite [92, 93] and iron borate [92], also in terbium [94] and erbium orthoferrite [95].

1.5.3 Spectra of magnetoelastic excitations in easy plane antiferromagnet

Spectra of magnetoelastic excitations in easy plane antiferromagnet crystals (1.23) depend on the Neel temperature and Debye temperature relations. The AFEPs with the Neel temperature below Debye temperature $T_N < T_D$ (like $MnCO_3$, $CoCO_3$, $CsMnF_3$) are called "low temperature antiferromagnets". The spectrum of these AFEPs is presented in Figure 1.5 (right). The speed of spin waves is lower than the speed of sound, so the branches of pure elastic $\omega_S k$ and magnetic $\omega_f k$ waves overlap, and the highest coupling occurs in the resonance region near the point where they cross.

Easy plane antiferromagnets with the Neel temperature above Debye temperature $T_N > T_D$ (like α-Fe_2O_3 and $FeBO_3$) are called "high temperature antiferromagnets". The spectrum of magnetoelastic excitations in these crystals is presented in Figure 1.5 (left). The speed of spin waves is higher than the speed of sound and the branches of pure elastic $\omega_S k$ and magnetic $\omega_f k$ waves never overlap, so the coupled waves in these antiferromagnets are always either elastic-like or spin-like ones. The highest coupling in high temperature AFEPs occurs in the long-wavelength band of the spectrum.

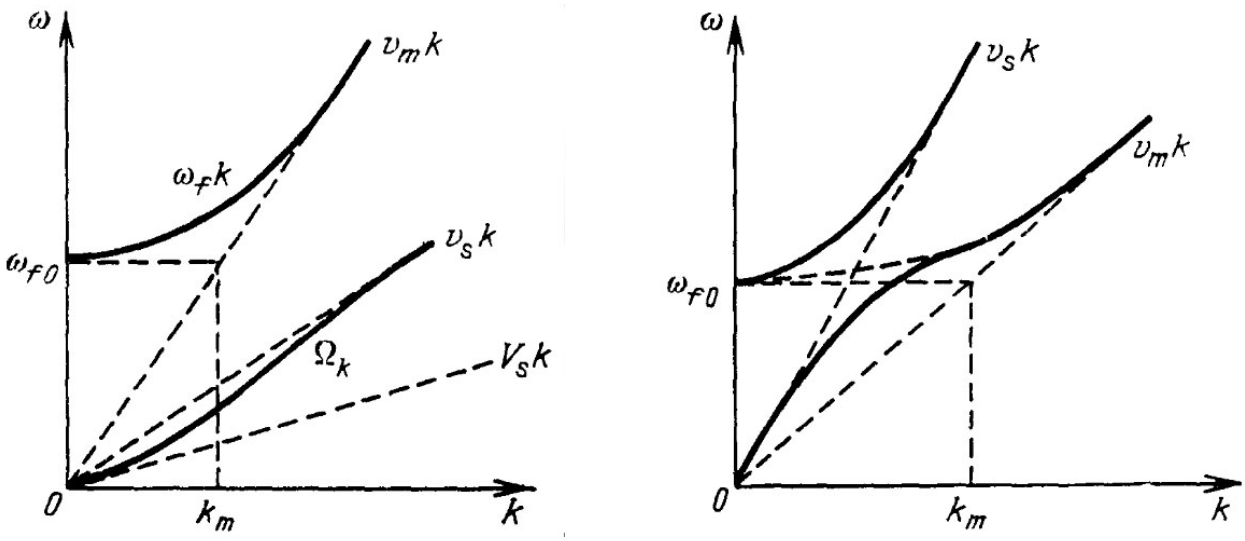

Figure 1.5. Spectra of coupled magnetoelastic waves (solid lines) in the high temperature AFEP crystals (right) and low temperature AFEP crystals (left). w_{f0} shows magnetoelastic gap [76].

One of the main methods of experimental magnetoelastic coupling coefficient study is measurement of the sound speed dependence from the bias field *H*. Magnetoelastic coupling coefficient can be determined from the sound speed as [76]:

$$V_{Sk}(H) = v_{Sk}(1 - \zeta_{Sk}^2(H))^{1/2} \tag{1.25}$$

All the factors discussed above make iron borate and hematite attractive model objects for magnetoacoustic research and applications. Their unprecedented magnetoelastic coupling in the band of widespread ultrasound frequencies is combined with high Neel temperatures (T_N = 970 K for α-Fe_2O_3 and T_N = 348 K for $FeBO_3$) well above room temperature meaning that they do not require any cryogenic systems for experiments and applications (unless some specific temperature dependencies are searched). This interaction is organized in a wide range of bias fields $0 < H(H + H_D) \leq 2H_E H_{ms}^{(0)}$ and the magnitude of this interaction depends on the bias magnetic field $\zeta_{Sk}^2(H)$.

1.5.4 Magnetoelastic coupling of critical resonator modes

A great scientific and applied value is presented by the acoustic modes, that satisfy the condition of the limiting strong coupling $\zeta_{S,k\to 0}(H \to 0) \to 1$. The existence of such modes in a crystal with an easy plane magnetic symmetry is possible due to the lack of stability of equilibrium state to slow rotations of the magnetization in the *xy* easy plane (with a corresponding change in the spontaneous deformation) [88, 98]; this situation is similar to the orientation phase transition [72].

Contour shear mode of a resonator shaped as a disk is of an interest for magnetoelastic research as according to the calculations this mode satisfies the criterion of limiting strong coupling. The field dependency of its frequency is described by a relationship similar to the one of the travelling waves [76]:

$$\Omega(H) = \Omega(\infty)\left(1 - \frac{2H_E H'_{ms}}{\bar{\omega}_{f0}^2 \gamma^{-2}}\right)^{\frac{1}{2}}, \tag{1.26}$$

where H'_{ms} is effective magnetostriction gield. However in this case the frequency of quasiferromagnetic resonance mode $\bar{\omega}_{f0}$:

$$\bar{\omega}_{f0} = \gamma[H(H + H_D) + 2H_E H'_{ms}]^{1/2} \tag{1.27}$$

differs from the experimentally measured frequency of AFMR because of the magnetoelastic gap, renormalized by the plate elastic boundary conditions [99]. The structure of the contour shear mode of a thin disc resonator is presented in Figure 1.6. The arrows are proportional to the total displacements at the corresponding points at the apex of the oscillations. The model was created with the help of FemLab® Comsol Multiphysics™ software.

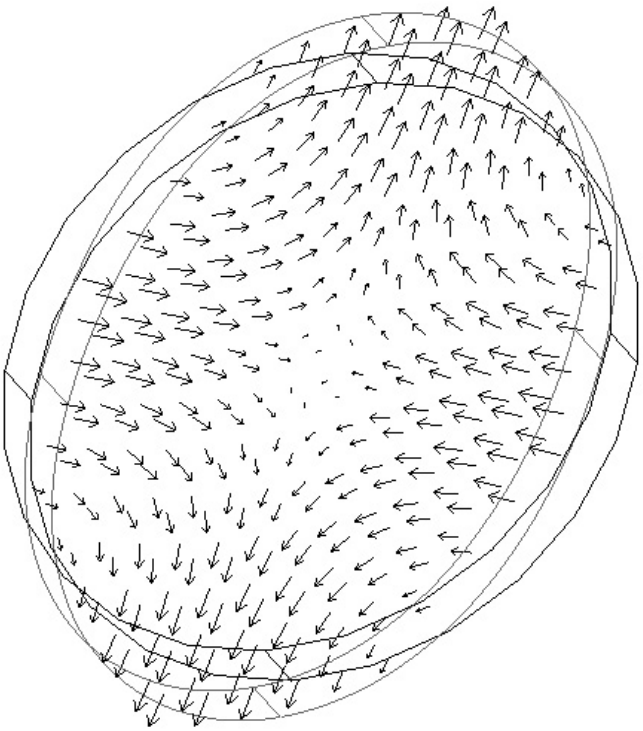

Figure.1.6. Structure of the contour shear mode of a disk resonator. Total displacements at the apex of the oscillations are shown with arrows. The shape of the deformed resonator is shown in grey.

1.6 Parametric excitation of magnetoelastic waves in easy plane antiferromagnets

Parametric instability of magneto-elastic waves in antiferromagnets was first discovered in hexagonal low temperature AFEP $CsMnF_3$ [100], and in rhombohedral AFEPs $MnCO_3$ and $CoCO_3$ [101 - 103]. In these works, like in the first works on ferrites, parametric instabilities were excited near the conditions of magnetoacoustic resonance.

Theoretically the threshold amplitude $h_{c||}$ of the parametric excitation with parallel pumping ($hcos\omega_p t \,||\, H$) was calculated in paper of Ozhogin and Yakubovskii [101]:

$$\gamma_k = V_{||} h_c \,,$$
$$\gamma_k = 2\pi\eta = 1/(2\tau), \tag{1.28}$$
$$V_{||} = \gamma^4 H_D H_\Delta^2 \omega_{ph}/4\omega_e^4$$

Here, $V_{||}$ is the coefficient representing the coupling of phonons at the frequency ω_{ph} with the pump field at the frequency ω_p: $\omega_{ph} = \omega_p/2$, τ is the lifetime of the excited phonons, γ_k is dissipation parameter, h_c is the amplitude of pumping field.

In high temperature AFEPs parametric instability of elastic waves excited with perpendicular pumping was first observed in 1978 on a α-Fe_2O_3 resonator via elastic moduli modulation [104] in continuous mode. When a high frequency alternating magnetic pumping field h is applied homogeneously throughout the resonator the threshold of the amplitude of pumping field with h_c the frequency ω is:

$$h_c = Q_n^{-1}\Omega_\mathrm{n}/\frac{\partial\Omega}{\partial\mathrm{H}}, \tag{1.29}$$

where Q_n^{-1} is resonator quality factor, Ω_n is pumping frequency, H is bias magnetic field. When it is reached a parametric instability of magnetoacoustic waves manifests itself on the frequency $\Omega_\mathrm{n} = \omega/2$. The formula describes that for parametric instability the critical depth of modulation has to compensate the dissipation of magnetoelastic oscillations.

Experimental field dependence of the parallel threshold pumping field for the thickness shear mode of a hematite disk acoustic resonator (C_3 axis is perpendicular to the basal plane) is shown in Figure 1.7 with dots [104]. The pumping and recording of the instability were performed by an induction method. The line in Figure 1.7 shows results of theoretical calculations for the resonator by formula (1.29) based on the data obtained from separate measurements of $Q(H)$ and $\Omega(\mathrm{H}) = \Omega(\infty)(1-\zeta^2(H))^{1/2}$. Parametric excitations of magnetoelastic excitations of travelling waves have been also observed [105].

Wettling and Jantz in their work [106] have first observed parametric excitation of short-wavelength phonons ($k \approx 10^4 - 10^5\ cm^{-1}$) in another high temperature AFEP $FeBO_3$.

They used perpendicular transverse pumping at the frequency 9.2 GHz. The excited phonons were recorded using Brillouin light scattering, however the threshold was not determined.

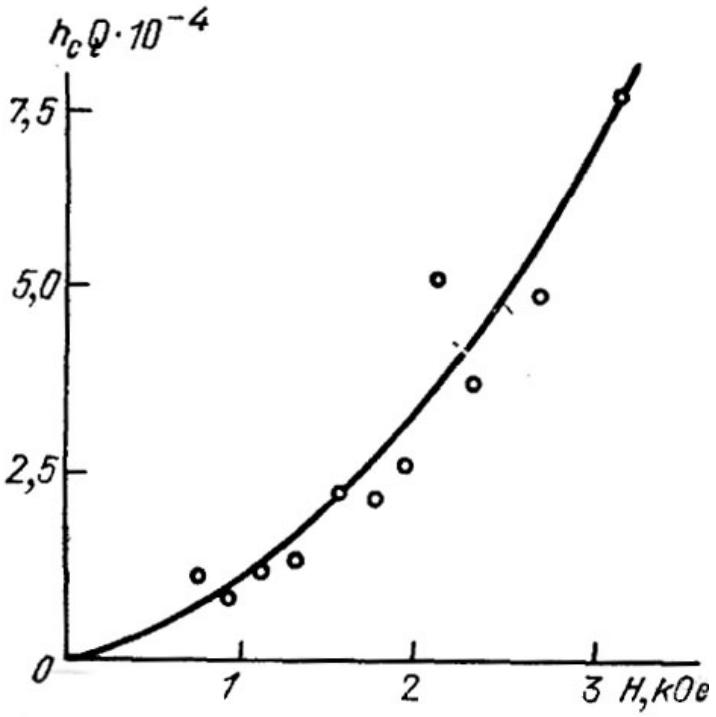

Figure 1.7. Dependence of the amplitude of threshold parallel pumping field from the bias magnetic field [104].

Later Kotyuzhanskii and Prozorova [103] have determined the threshold field $h_{c\perp}$ dependence on the magnitude of bias field H with pumping frequency 35.4 GHz. In their work they have developed the theory from [107] for the first-order Suhl instability and compared it to the experimental results. Figure 1.8 shows experimental dependence of the shear pumping threshold field h_c on the static field H of the parametric quasiphonon generation at T = 90 K, ω_p = 35.0 GHz observed by Katyuzhansky and Prozorova in $FeBO_3$.

Parametric instability with parallel excitation on $FeBO_3$ was experimentally observed by Andrienko and Poddyakov [108, 109] in a wide range of frequencies. In [109] parametric excitation of phonons in different orientations of pumping field h and bias field H is investigated. The experimental dependence of the threshold amplitude of the parallel pumping field on the static magnetic field for ω_p= 1140 MHz at T = 77 K is presented on Figure 1.9

Despite the difference in the mechanisms in the magnetoelastic waves parametric generation under perpendicular and parallel pumping, in the limiting case when $\omega_p \ll \omega_{fk}$

and $H \ll H_D$ the thresholds of the parametric instabilities are determined by the dissipation forces and magnetoelastic interaction.

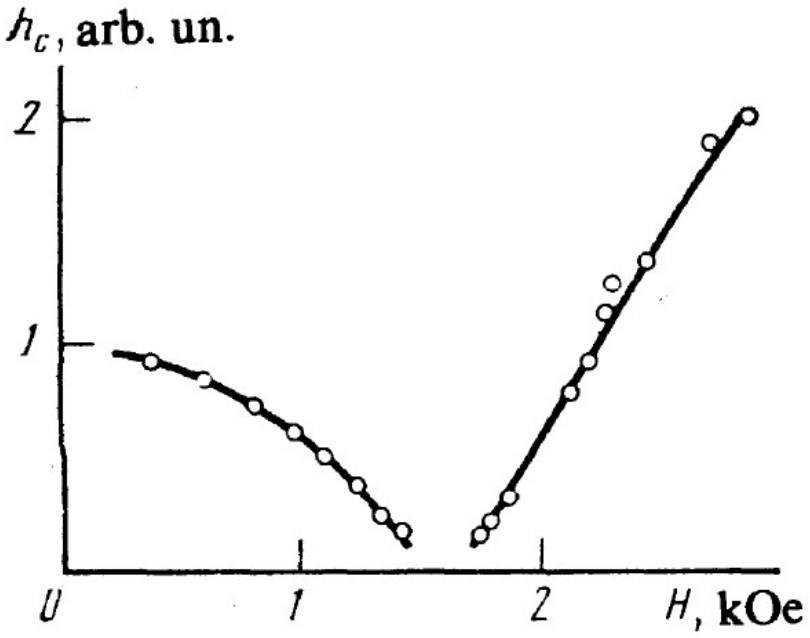

Figure 1.8. Dependence of the threshold amplitude of the parallel pumping field on the static magnetic field of the parametric quasiphonon generation in $FeBO_3$ at T = 77 K [105].

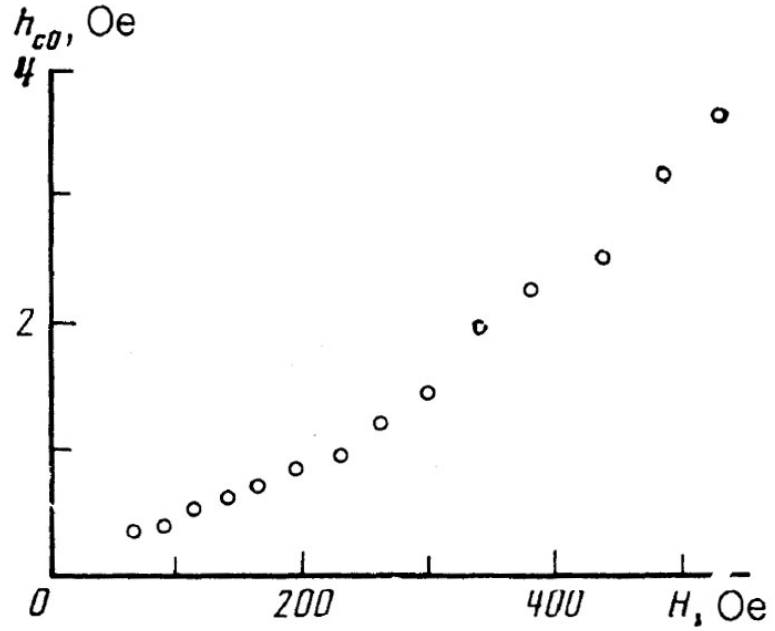

Figure 1.9. Amplitude dependence of the shear pumping threshold field h_c on the static field H of the parametric quasiphonon generation in $FeBO_3$, T = 90 K, ω_p=35.0 GHz [109].

Beyond the thresholds of parametric excitation nonlinear effects manifest themselves limiting the amplitudes of generated waves and oscillations. Just like in the ferrites these effects come from two different mechanisms. The first one is nonlinear-self-action of acoustic modes resulting in difference of the values of the frequency detuning ($\Delta\omega = \omega_p - 2\Omega_n$) with respect to the parametric resonance at which sound generation arises and disappears. The second one is nonlinear damping of the oscillations at high amplitudes. Due to a high magnetoelastic coupling coefficient in AFEPs nonlinear effects manifest themselves much brighter even at lower oscillation amplitudes.

Easy plane antiferromagnets have also been studied as an active media to use in wave phase conjugation. Parametric amplification of 35 dB at a frequency of 30 MHz was achieved in an antiferromagnetic hematite single crystal [110]. However real life applications of PCs with AFEP is problematic as easy plane antiferromagnetic monocrystals are usually relatively small, as it is hard to grow a big and pure crystal, so the active zone of phase conjugator based on AFEP is very short, limiting the amplification that can be achieved. Also easy plane crystal structure of hematite limits the angles at which the waves can enter in the active zone.

1.7 Giant effective anharmonicity of easy plane antiferromagnets

Nonlinear acoustic effects in solids are very diverse and serve as a powerful tool for scientific research, but their observation is usually problematic or requires very high amplitudes [111]. The reason for that lies in the elastic moduli values. The elastic potential energy density of a solid can be written in a power series:

$$F_e = \frac{1}{2}\hat{C}^{(2)}\hat{u}\hat{u} + \frac{1}{3!}\hat{C}^{(3)}\hat{u}\hat{u}\hat{u} + \frac{1}{4!}\hat{C}^{(4)}\hat{u}\hat{u}\hat{u}\hat{u} \ldots \tag{1.30}$$

The possibility of such representation is justified by usually very small displacements of the lattice atoms compared to the distance between them $|u| \ll 1$, and relatively low variations of their magnitude with the increase of their order: $C^{(n+1)}/C^{(n)} \approx 1 - 10$. The second order elastic moduli are responsible for linear acoustic effects, the third and higher orders moduli describe nonlinear ones. As the values of dynamic deformations are $u \approx 10^{-5}$ the contribution of nonlinear components is usually weak.

In magnetically ordered crystals elastic modules for low frequency quasi-elastic oscillations are changing due to magnetoelastic interaction. Acoustic waves are exciting spin waves that are adding anharmonicity to the elastic oscillations. In AFEP a giant effective anharmonicity is observed due to typical for AF exchange interaction participation in long wave oscillations and is particularly interesting due to its strong dependency on the magnetic field.

This anharmonicity changes the effective elastic modules of the magnets, so that $\hat{C}_{eff}^{(n)} = \hat{C}^{(n)} + \Delta\hat{C}^{(n)}$. Linear coupling of the elastic subsystem can be presented as a change of second-order dynamic moduli of elasticity. In AF with anisotropy of the "easy plane" type (AFEP), such as α-Fe_2O_3 and $FeBO_3$, the experimental values of $\Delta\hat{C}^{(2)}/\hat{C}^{(2)}$ amount to tens of percent [92,112]. Modulation of the contribution $\Delta\hat{C}^{(2)}$ by alternating magnetic field generates parametric excitations discussed in the previous section.

Ozhogin and Preobrazhensky have calculated the third order elastic moduli magnetoelastic contributions $\Delta\hat{C}^{(3)}$ in AFEP crystals [113]. It was shown that the contribution is by several orders of magnitude higher than regular third-order elastic moduli in solids [111] and $\hat{C}^{(3)} \approx \Delta\hat{C}^{(3)}$. These unprecedented values of nonlinear moduli corrections in AFEPs are responsible for giant effective anharmonicity. Some nonlinear effects were predicted [113] and later experimentally observed based on the effective anharmonicity model. These effects are discussed later in this chapter. A number of important nonlinear effects require consideration of higher orders elastic moduli. Effective moduli of the fourth order are determined are responsible for the cubic acoustic nonlinearity. Preobrazhensky et al. have showed the contributions of the magnetoelastic interaction to the fourth order elastic moduli [114]. Anharmonic approximation model of AFEP is discussed in details in the Second chapter.

1.8 Over-threshold nonlinearity of parametric magnetoelastic waves and excitations in antiferromagnets

There are a number of nonlinear over-threshold effects that manifest themselves in easy plane antiferromagnets due to giant effective anharmonicity of the crystals. Some are caused by the effective anharmonic moduli of the third order, some are caused by the cubic

magnetoelastic nonlinearity (fourth order modules). These over-threshold effects observed in AFEPs are discussed in this section.

1.8.1 Nonlinear effects due to the third order effective anharmonicity

Some nonlinear effects caused by the effective anharmonicity of the third-order elastic modules were theoretically described by Ozhogin and Preobrazhensky [113], including: parametric generation of sound by sound, doubling of the sound frequency and acoustic detection. The effects were later observed experimentally proving the suggested anharmonicity model.

Doubling of the sound frequency and acoustic detection of modulated acoustic wave were experimentally observed in α-Fe_2O_3 in the work [115]. Magnetoelastic wave of 37 MHz was excited on one end of the sample and resulting oscillations at the double frequency 74 MHz were registered on the other end. The dependencies of the second harmonic power on the square of initial wave power at different bias magnetic fields are presented in Figure 1.10 (left).

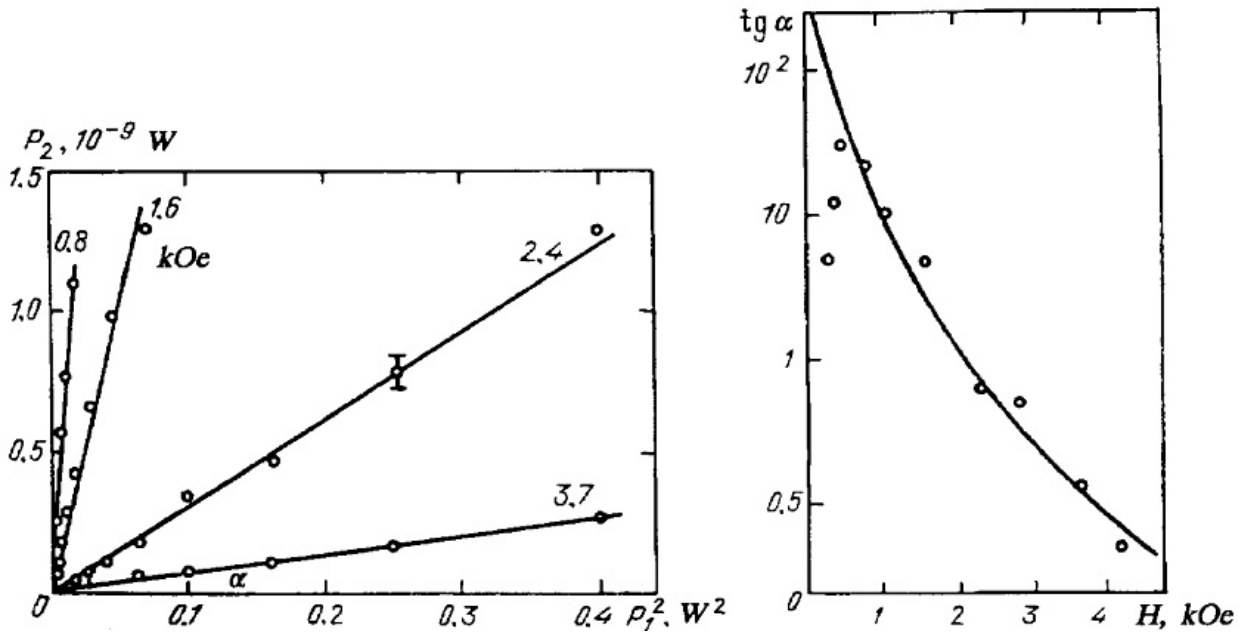

Figure 1.10. Dependencies of the second harmonic power on the square of initial wave power at different bias magnetic fields (left). Dependence of the effectiveness of sound wave transformation on the bias magnetic field (right) [115].

The dependencies appear to be linear. Bias field strength is written for every line in kOe. The power of the second harmonic has a clear square dependence on the initial signal power. Tangent of the angle between the lines and the *x* axis that characterizes the effectiveness of the sound transformation is plotted in Figure 1.10 (right) as a dependence from bias magnetic field showing the magnetoelastic nature of the effect. The effectiveness of the second harmonic generation observed in the experiment was by two orders of magnitude higher compared to regular solids.

The effect of acoustic detection by travelling waves was experimentally observed in hematite when the incident wave at 34 MHz was modulated with the frequency 390 kHz [115] and the resulting signal was registered at the modulation frequency. The power of detected signal also has linear dependencies on the square of the power of the incident wave. Generation of the second acoustic harmonic of a surface magnetoelastic wave was reported in [116].

The first generation of sound by sound in antiferromagnet predicted in [113] was reported in [117]. Stimulated combination scattering of running magnetoelastic wave with the frequency ω_p and wave vector k_p parallel to the trigonal axis was observed. This threshold process is generating of backwardrunning magnetoelastic waves (ω_1, k_1) and (ω_2, k_2) so that:

$$\omega_1 + \omega_2 = \omega_p, \;\; k_1 + k_2 = k_p \tag{1.31}$$

The diagram of this process is presented in Figure 1.11 (left). The pumping wave has polarization $e_p \perp H \parallel y$ and has no linear coupling with the magnetoelastic subsystem. However due to nonlinear interaction it scatters into two waves k_1 and k_1 that have polarization $e_{1,2} \parallel H \parallel y$ and are linearly coupled with magnetic subsystem, so their frequencies depend on the magnetic field. Dependencies of the frequencies f_1 and f_1 on the bias field *H* are presented in Figure 1.11 (right).

The magnitude of the deformation threshold for the stimulated combination scattering according to the calculations [113] is:

$$u_p^c = \pi \frac{2|B_{14}|}{C_{44}} \frac{(1-\zeta^2)^{3/2}}{k_p L \zeta^5} \tag{1.31}$$

$$\zeta^2 \equiv \frac{H_E}{M_0}\frac{(2B_{14}\gamma)^2}{\omega_{f0}^2 C_{44}} \tag{1.32}$$

where L is the length of the specimen, B_{14} is magnetoelastic tensor compoent, C_{44} is elastic tensor component, ζ is magnetoelastic coupling coefficient, γ is gyromagnetic constant, k_p is . For the experimental conditions H = 0.5 kOe the threshold is $\left(u_p^c\right) \approx (3.5 \pm 1.5) \cdot 10^{-7}$.

For the nonlinear effects discussed above induced by third anharmonic modules the strain thresholds are about $\varepsilon_0 \sim 10^{-6}$ and are easily reached with piezoceramic transducers.

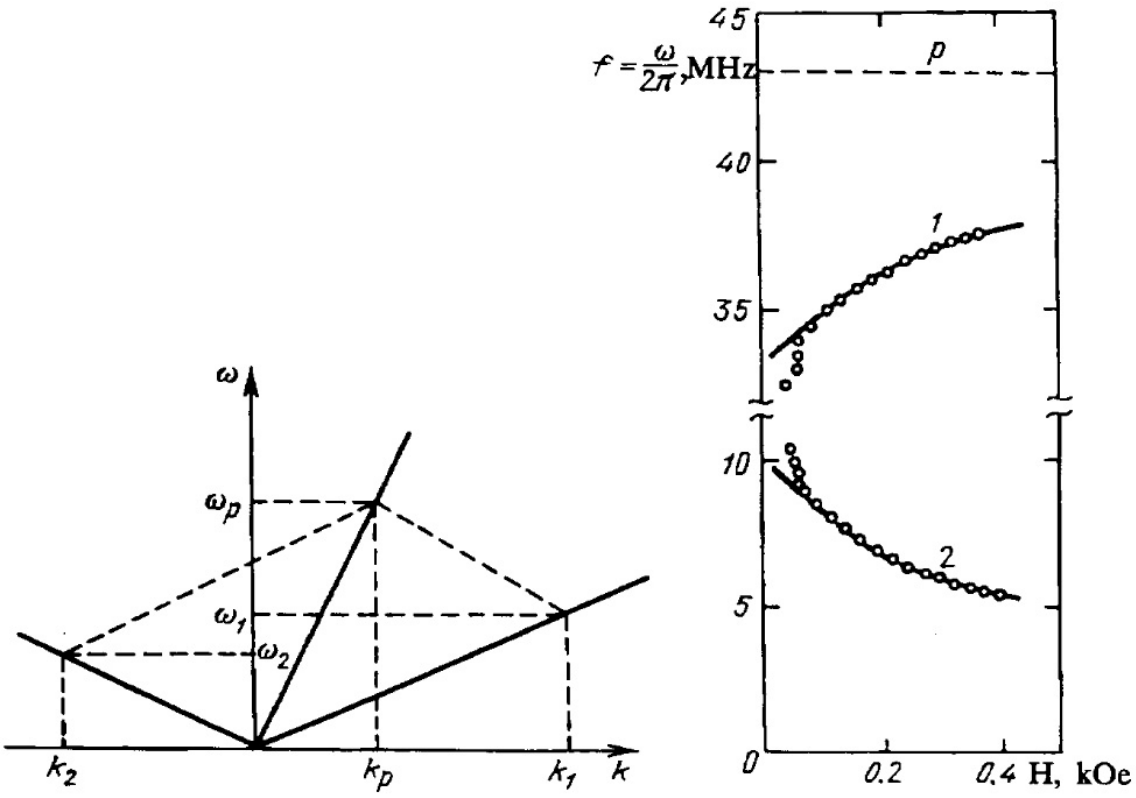

Figure 1.11. Diagram of stimulated combination scattering of magnetoelastic wave with frequency ω_p (left). Dependencies of the resulting frequencies f_1 and f_2 on the bias field H (right) [117].

1.8.2 Cubic nonlinearity in antiferromagnets

Cubic nonlinearity introduced by the fourth order anharmonic modules also provokes various nonlinear effects, including sound waves self-action, nonlinear frequency shift, double parametric resonance, etc [114].

Acoustic wave's self-action and nonlinear misphasing is the main amplitude limitation mechanism during parametric excitations in antiferromagnets that were discussed earlier in this chapter. When amplitude of a wave grows, nonlinear misphasing changes the phase of excited phonons and limits the amplitudes of excitations. In case of a resonator it manifests itself as nonlinear frequency shift of the magnetoacoustic resonance mode first observed in [114]. Figure 1.12 shows experimental amplitude frequency spectra of magnetoacoustic resonance at different oscillation amplitudes in bias field H = 0.53 kOe [118]. The frequency of the mode increases and the resonance line gets distorted as the oscillation amplitude goes up from 0.3 mV (1) to 2.7 mV (2), 4.9 mV (3) and 8.7 mV (4). The inset on the figure shows normalized frequency shift for two values of the oscillation amplitude: 3.3 mV (bottom) and 12 mV (top).

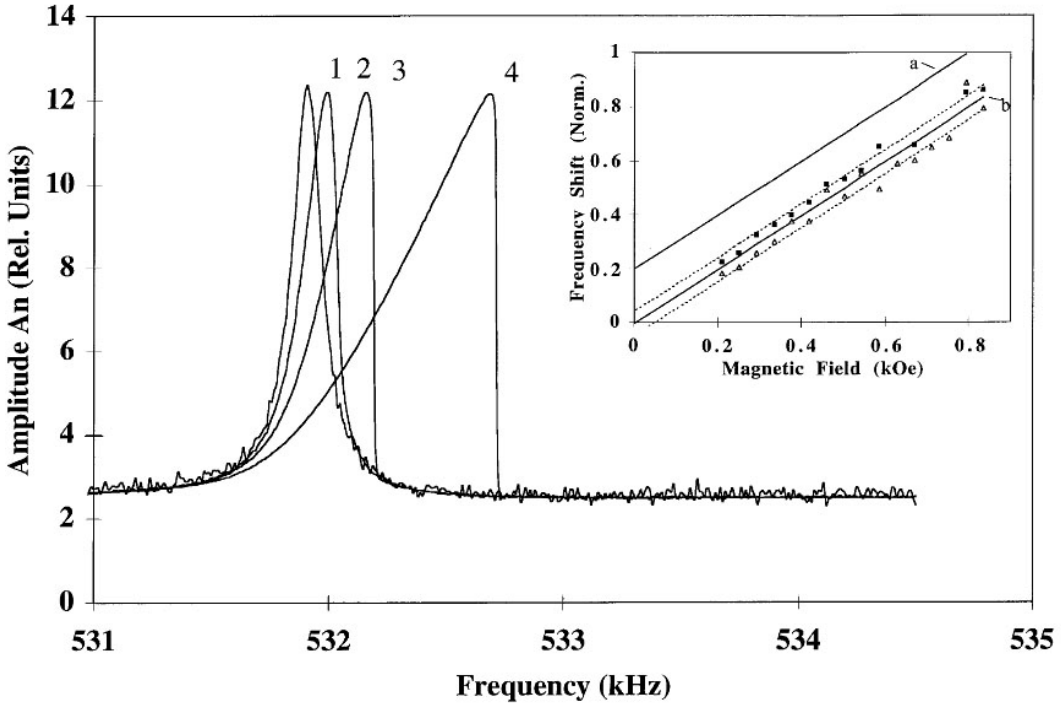

Figure 1.12 Amplitude frequency spectra of nonlinear magnetoacoustic oscillations at different amplitude of: 0.3 mV (1), 2.7 mV (2), 4.9 mV (3), 8.7 mV (4). Inset shows normalized frequency shift for two values of the oscillation amplitude: 3.3 mV (bottom) and 12 mV (top) [118].

Strong field dependence of the nonlinear frequency shift confirms that sound waves self-action is determined by the magnetoelastic interaction.

Fourth order elastic modules induce double parametric resonance of quasiacoustic waves that was experimentally observed in [119]. The sample was excited with parallel alternating field h_p at double frequency of the resonance mode and a modulating field h_m at low frequency of about 1 kHz. Modulating excitation caused excitations of parametric nature that had a clear threshold. In agreement with theoretical calculations, nonlinear frequency shift of the oscillations was negative.

1.9 Multi-boson nonlinear effects in magnetic materials. Three waves coupling

In quantum physics magnetoelastic waves are interpreted by their quasi-particles – quasi-phonons. These quasiparticles contain magnetic and elastic components and can be excited by either alternating magnetic field or elastic vibrations. An act of parametric excitation results in conversion of one photon to two elementary excitations corresponding to oscillations of the magnetic (magnons) or elastic (photons) systems.

As it has been discussed earlier, in the chapter magnetic materials, especially easy plane antiferromagnets, are very appealing objects from the acoustics point of view. Unprecedented coupling of elastic system with magnetic system completely changes its acoustic properties, especially the nonlinear ones. What is even more important, this coupling can be changed with the help of magnetic field in wide range. Strong nonlinearity in magnetic materials is limiting the oscillations at higher amplitudes, but the dependence of the nonlinearity on external field creates a new family of parametrical processes that result in multi-boson coupling. Multi-boson processes are of an interest not only for acoustics, but for fundamental physics in general as well. The diagram of a simple multi-boson process is shown on the Figure 1.13. The diagram shows decay of a pumping phonon with the frequency ω_p and wave vector $k_p \sim 0$ that creates three quasi-phonons with the frequencies ω_1, ω_2, ω_3 and wave vectors k_1, k_2, k_3. In comparison with a diagram of two-boson parametric process presented in the Figure 1.3 in 2D space, three-boson process is presented in 3D space.

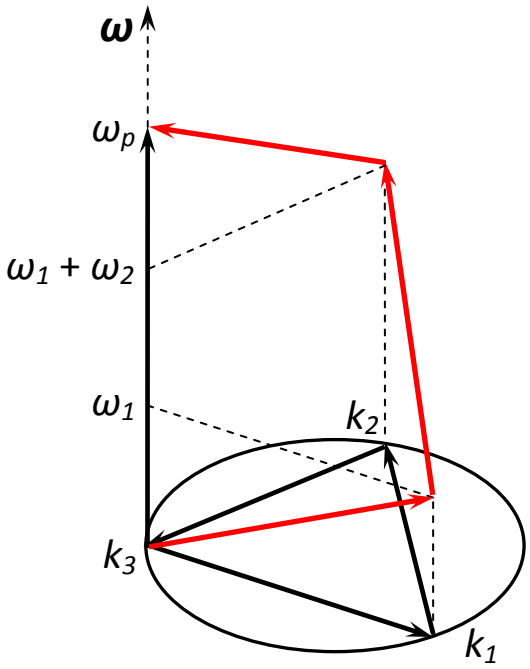

Figure 1.13. Vector diagram of energy and impulse conservation laws for phonon interactions with pumping for three quasi-phonon process.

The energy conservation laws for three-phonon process are:

$$\omega_p = \omega_1 + \omega_2 + \omega_3$$
$$k_1 + k_2 + k_3 = 0 \qquad (1.32)$$

Recently three-boson coupled excitations were predicted and observed in single-mode excitations in magnetoelastic AFEP resonator α-Fe_2O_3 under homogeneous perpendicular RF pumping [120]. Large single-crystals of high temperature AFEPs are hard to produce [122], so single-mode three phonon excitations are more experimentally appealing than three travelling waves coupling as smaller crystals can be used for the experiments. Symmetry analysis shows that single-mode three phonon excitations can be induced only with perpendicular pumping, while travelling waves can be coupled with both perpendicular and parallel pumping. Theoretical studies showed that three-boson coupling is also possible for travelling waves [121].

Parametric instabilities arising from modulation of nonlinear parameters of the system have also been recently experimentally detected in MEMS structures [138,139]. Nonlinear coupling between an array of nonlinearly coupled microcantilevers was modulated with alternating electric field resulting in subharmonic instabilities formation.

In comparison with three-boson equilibrium bound states ([123,124] and references within) non equilibrium three quasi-phonon excitations possess some specific dynamic features. Theoretically in both single-mode [120] and travelling mode [121] excitations demonstrate explosive instability. In the supercritical regime the amplitude of oscillations tends to infinity in the finite time. Three travelling waves coupling also demonstrates spatial localisation of quasi-phonon triads [121]. Explosive instabilities of nonlinear wave systems usually involve so-called "negative energy" waves for which an increase of amplitude causes a decrease of energy. Because of energy conservation law it is generally considered that explosive instability is impossible in a system with only positive or only negative waves [125-127]. In a mixed system, amplitudes of positive and negative waves can increase in an explosion manner due to their interaction when one wave gains energy from the other. Many works have been published with theoretical models of negative and positive waves interaction however only few experimental observations of this process have been reported. Most of the known experiments were done in plasma [128, 129]. Recent theoretical approaches [120, 121] showed that the explosive instability of a system with only positive waves is possible.

These multi-boson processes are new for both magnetoacoustics and for nonlinear physics as well. It was shown that in contrast with parametric generation of quasi-phonon pairs [76], the threshold of three-boson instability depends not only on intensity of pumping field but also on initial number of bosons [120]. In case of bi-phonon parametric excitations process second order elastic modules are modulated, thus the speed of waves in the crystal serves as a parameter for energy flow, and the threshold of the depth of modulation only depends on the dissipation. During the three phonon process third order elastic moduli that are responsible for the interaction between magnetic and elastic subsystems are modulated. The physics of parametric three-phonon excitations will be discussed in detail in Chapter II.

The manifestations of explosive supercritical dynamics in real AFEP crystals are usually smoothed over by higher order nonlinear effects and first of all by nonlinear phase or frequency shift of magnetoelastic waves [76,130]. Due to the nonlinear frequency shift theoretically predicted explosive supercritical dynamics in solids has never been experimentally achieved. The effect itself is important from both the scientific point of view as well as from the applied side. It can find important practical applications in various magnetoelastic devices that currently already use parametric excitation, like wave phase conjugators discussed in this chapter as explosive instabilities is a more attracrive

amplification process in comparison with exponential growth of the parametrical amplification. Thus research of the compensations methods for nonlinear frequency shift to observe explosive instability of three-phonon excitations is of a great interest.

1.10 Chapter I conclusion

State of the art analysis in parametric magnetoacoustics shows that currently supercritical dynamics of multi-boson processes is among the most topical research problems. Recently discovered theoretically the new family of multi-boson nonlinear parametric processes possesses some unique features like explosive amplitude growth and space localization. High temperature AFEPs are the most suitable media for the supercritical dynamics research as they demonstrate unprecedented magnetoelastic coupling and their dynamic and nonlinear properties can be widely changed with the help of magnetic field. Three quasi-phonon coupling has been experimentally achieved in single-mode regime in α-Fe_2O_3 single crystal. It was theoretically predicted that the oscillations could interact and gain energy from electromagnetic homogeneous pumping and blow up in a finite time, however this singularity has not been experimentally observed because of nonlinear effects of higher orders. Parametric coupling of three travelling waves in the medium without nonlinear frequency shift was also theoretically shown for perpendicular pumping but is yet to be experimentally observed.

All these factors have defined the scope and goals of the present research that consist of theoretical and experimental studies of supercritical explosive instabilities of magnetoelastic waves. The first major goal of the present work was development and theoretical approbation of the compensation methods of nonlinear frequency shift to observe explosive supercritical dynamics of single-mode three quasi-phonon excitations in AFEP α-Fe_2O_3. Theory development and approbation was based on the anharmonic approximation model previously suggested for stationary triads coupling.

The second major goal was application of the developed methods for experimental supercritical single-mode quasi-phonon excitations in α-Fe_2O_3 and explosive dynamics research. Theoretical and experimental approbation of the developed methods on another crystal with different properties was also important. Iron borate $FeBO_3$ is a perfect candidate

due to strong magnetoelastic interaction yet different from hematite characteristic fields. Unlike hematite, iron borate does not have Morin spin reorientation transition at lower temperatures, so it is possible to decrease experiments temperature to lower elastic system dissipations. Experimental and theoretical research of three quasi-phonon excitations supercritical dynamics in iron borate at different temperatures was thus also a goal of the present work. Explosive instability research in $FeBO_3$ also required investigation of cubic nonlinearity of the crystal that had not been previously reported for this crystal. This research was necessary to find its compensation laws.

Strong nonlinearity of AFEP required development of a complete theory of three-phonon single-mode coupling that takes into account magnetoelastic nonlinearities outside of anharmonic approximation. Development of such theory for quantitative description of the explosive process for α-Fe_2O_3 and $FeBO_3$ was the third major goal of the present research.

The fourth major goal of the research was creation and analysis of a model of three travelling magnetoelastic waves parametric coupling in a real AFEP crystal. The model had to include strong cubic nonlinearity. Two models under perpendicular pumping and also parallel pumping that has easier experimental geometry were developed. Cubic nonlinearity compensation methods for travelling waves were suggested. Numerical simulations of the developed models for real life crystals were performed with and without compensation methods to compare the behaviour and thresholds of instabilities for further possible experiments.

Chapter II

Single Mode Three Quasi-Phonon Excitations and Supercritical Dynamics in Effective Anharmonicity Model

2.1 Chapter II introduction

Recently predicted three quasi-phonon parametric instability features explosive supercritical dynamics [120, 121]. However, experimentally the singular behavior has not been observed due to strong cubic nonlinearity that breaks the process [120]. The main goal of the research presented in the Second Chapter is analysis of the mechanisms that affect explosive supercritical dynamics manifestation and development of techniques that can compensate these mechanisms.

Theoretical investigation of the supercritical dynamics of three quasi-phonon parametric instability in an antiferromagnetic resonator is performed on the basis of the single-mode excitations effective anharmonicity model limited to the forth order terms. Cubic nonlinearity compensation technique via proper phase modulation law of the pumping field is suggested.

The equations for amplitude and phase in three quasi-phonon excitation process are numerically solved with and without the suggested phase modulation law to verify the performance of the compensation method. Explosive supercritical dynamics clearly manifests itself when the parameters of the modulation correspond to the cubic nonlinearity of the resonator.

2.2 Anharmonicity model of three quasi-phonon excitations

Nonlinear dynamics of hybrid magnetoelastic excitations in an easy plane antiferromagnetic crystal can be described with the help of free energy density that can be presented as a sum of corresponding densities of magnetic energy F_m, elastic energy F_e and magnetoelastic energy F_{me}:

$$F = F_m + F_e + F_{me} \tag{2.1}$$

It has been shown [76, 120] that for vibrations at frequencies much lower than the resonance frequency of antiferromagnetic mode $\omega << \omega_{a0} = \gamma\sqrt{2H_E H_A + H_D(H + H_D)}$, where H_{ms} is the effective magnetostriction field, H is the external bias field, H_D is

Dzyaloshinsky field and H_E is exchange field, the dynamics of magnetic system can be described only with one variable $\varphi = \varphi(\hat{u}, h_\perp(t))$ that is the angle between the antiferromagnetic vector $l = (M_1 - M_2)/2M_0$ and direction, perpendicular to the external magnetization field H in the basal plane. M_1 and M_2 are magnetizations of antiferromagnet sublattices and M_0 is net magnetization.

Geometry of the magnetic system of AFEP is presented in the Figure 2.1 showing normalized magnetization of sublattices M_1/M_0 and M_2/M_0, ferromagnetic vector $m = (M_1 + M_2)/2M_0$, antiferromagnetic vector l, dynamic angle φ, external magnetization field H, hard direction C_3 and binary axis U_2.

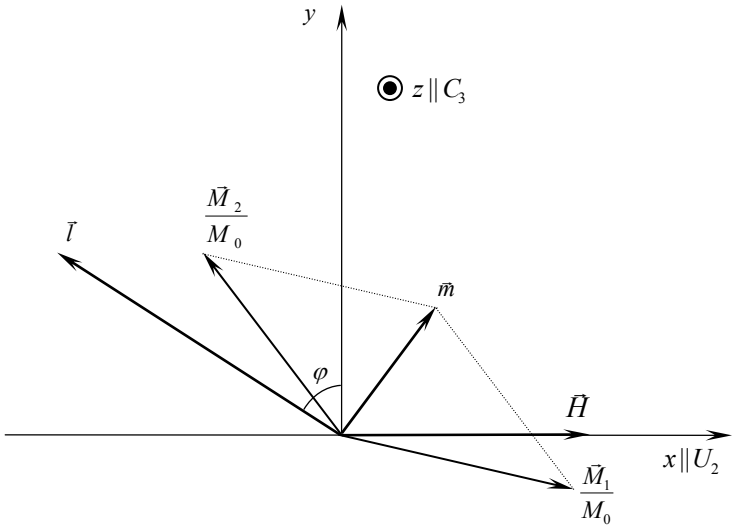

Figure 2.1. Magnetizations of the sublattices in an AFEP crystal and the angles that determine their configuration.

By solving the equation of motion for the angle φ that depends on the deformations and alternating electromagnetic field it is possible to describe the free energy density of the system (2.1) via the free energy density of quasi-phonons. Homogenous in-plane alternating pumping field $h_\perp(t)$ applied in the basal plane perpendicular to bias magnetic field H can be used as a coupling mechanism for nonlinear interaction of quasi-phonons. In this case, up to the fourth order terms, quasi-phonons energy can be presented as [120]:

$$F = \sum_{m=2}^{4} \frac{1}{m!} \hat{C}_{eff}^{(m)}(H)\hat{u}^m + h_\perp(t)\hat{\Psi}(H)\hat{u}^3 , \qquad (2.2)$$

where $\hat{C}_{eff}^{(m)}(H) = \hat{C}^{(m)} + \Delta\hat{C}^{(m)}(H)$ are the effective anharmonicity moduli renormalized by magnetoelastic coupling, $\hat{u}$ is deformations tensor and $\hat{\Psi}(H)$ is the three quasi-phonon interaction coefficient calculated for perpendicular alternating magnetic field $h_{\perp}(t)$. The value of the linear magnetoelastic contribution in second order moduli is [76]:

$$\Delta\hat{C}^{(2)} = -\frac{H_E}{M_0}\left(\frac{2\gamma\hat{B}_2}{\omega_{fk}}\right)^2, \tag{2.3}$$

where γ is gyromagnetic ratio and $\hat{B}_2$ is the tensors of magnetoelastic constants. The lowest order nonlinearity of the acoustic branch excitation comes mostly from the nonlinearity of magnetoelastic interaction. Magnetoelastic energy density is defined as:

$$F_{me} = \left(\hat{B}_1 cos2\varphi + \hat{B}_2 sin2\varphi\right)\hat{u}\,, \tag{2.4}$$

where $\hat{B}_1$ and $\hat{B}_2$ are the tensors of magnetoelastic constants. Their convolutions with deformation tensor are given by:

$$\begin{aligned}\hat{B}_1\hat{u} &= -\frac{1}{2}(B_{11} - B_{12})\left(u_{xx} - u_{yy}\right) - B_{14}u_{yz}\\ \hat{B}_2\hat{u} &= -(B_{11} - B_{12})u_{xy} - 2B_{14}u_{xz}\end{aligned} \tag{2.5}$$

B_{ij} and u_{ij} are corresponding components of the tensors. The expansion of the magnetoelastic energy density in a power series in the amplitude φ of the spin oscillations contains the anharmonic term:

$$F_{me}^{(3)} = -2\hat{B}_1\hat{u}\varphi^2 \tag{2.6}$$

That describes the process of interaction of one sound wave and two spin waves. Taking into account spin oscillations that are produced by sound waves $\varphi = -\frac{2H_E}{M_0}\frac{\hat{B}_2\hat{u}}{(\omega_{f0}/\gamma)^2}$ [76] the contribution to the third elasticity moduli can be derived as:

$$\Delta\hat{C}^{(3)} = -6\left(\frac{H_E}{M_0}\right)^2 \frac{(2\hat{B}_1)(2\hat{B}_2)^2}{(\omega_{f0}/\gamma)^4} \tag{2.7}$$

For α-Fe_2O_3 (considering $B \sim 10^7$ erg/cm^3; $H_E \sim 10^7$ Oe, $M_0 \sim 10^3$ G) in the bias field H of about 1 kOe magnetoelastic gap is $(\omega_{f0}/\gamma)^2 \sim 30$ kOe^2, the relative correction to the elastic modulus is $\Delta\hat{C}^{(2)}/C_{44} \approx 25\%$. Modulation of the second order elastic moduli results in bi-phonon parametric instabilities with exponential amplitude growth.

As mentioned in the First Chapter, magnetoelastic contribution to the third order elastic moduli is several orders higher than the acoustic subsystem nonlinearity, so $\hat{C}^{(3)} \approx \Delta\hat{C}^{(3)} \sim 10^{15}$ - 10^{16} erg/cm^3. Equation (2.7) describes the process of interaction of three acoustic waves. Parametric modulation of this interaction in AFEP with alternating electromagnetic field $h_\perp(t)$ is causing three quasi-phonon coupling that results in explosive instability [120].

Effective cubic nonlinearity moduli corrections are formed by three main mechanisms: four-wave interactions of non-resonance excitation spin waves, magnetoelastic interaction of a sound wave and three non-resonance spin waves:

$$\Delta\hat{C}^{(4)} = -12\left(\frac{H_E}{M_0}\right)^3 \frac{(2\hat{B}_2)^4}{(\omega_{f0}/\gamma)^6}\left(1+\frac{1}{4}\frac{\gamma^2 H H_D}{\omega_{f0}^2}\right) - 48\left(\frac{H_E}{M_0}\right)^3 \frac{\left(2\hat{B}_2\right)^2\left(2\hat{B}_1\right)^2}{\left(\omega_{f0}/\gamma\right)^6} \tag{2.8}$$

Similar to third order elastic moduli, cubic nonlinearity of acoustic subsystem in AFEP is negligible in comparison to magnetoelastic contribution and $\hat{C}^{(4)} \approx \Delta\hat{C}^{(4)}$. For hematite at H ≈ 0.5 kOe, $\Delta\hat{C}^{(4)} \approx 10^{20}$ erg/cm^3.

2.3 Three quasi-phonon interaction coefficient in perpendicular pumping geometry

The energy density (2.2) term $h_\perp(t)\hat{\Psi}(H)\hat{u}^3$ represents the energy of three quasi-phonon coupling. In order to derive the coupling coefficient $\hat{\Psi}(H)$ stress tensor caused by the

magnetoelastic interaction has to be considered. It is defined as $\hat{\sigma}_{me} = \partial F_{me}/\partial(\frac{\partial u_i}{\partial x_k})$, leaving only the terms of magnetoelastic energy density F_{me} (2.4) that depend on u:

$$\hat{\sigma}_{me} = \hat{B}_1 cos2\varphi + \hat{B}_2 sin2\varphi \tag{2.9}$$

In low frequency regime the angle can be approximated as a sum of three terms up to the third order of value relatively to deformation $\hat{u}$ and pumping field h_p:

$$\varphi \sim \varphi_1 + \varphi_2 + \varphi_3; \tag{2.10}$$

The components can be defined as:

$$\varphi_1 = \frac{1}{(\omega_{s0}/\gamma)^2}\left(-\frac{H_E}{M_0}\left(2\hat{B}_2\hat{u}\right) + (H + H_D)h_\perp\right) \tag{2.11}$$

$$\varphi_2 = \frac{H_E}{M_0}\left(2\hat{B}_1\hat{u}\right)2\varphi_1 \tag{2.12}$$

$$\varphi_3 = \left(\frac{2}{3} - \frac{HH_D}{2(\omega_{s0}/\gamma)^2}\right)\varphi_1^3 - \frac{1}{(\omega_{s0}/\gamma)^2}\left(\begin{array}{c}\frac{(H_D + 4H)h_\perp\varphi_1^2}{2} + \\ \left(\frac{H_E}{M_0}\right)\left(\left(2\hat{B}_1\hat{u}\right)2\varphi_2 + 2\left(2\hat{B}_2\hat{u}\right)\varphi_1^2\right)\end{array}\right) \tag{2.13}$$

To the third order terms, it can be approximated that $\sin2\varphi = \varphi - 2\varphi^3/3$ and $\cos2\varphi = -\varphi^2$. The stress tensor is then defined as:

$$\begin{gathered}\hat{\sigma}_{me} = -2\hat{B}_1\varphi^2 + 2\hat{B}_2(\varphi - 2\varphi^3/3\,) \\ \varphi^2 = \varphi_1^2 + 2\varphi_1\varphi_2;\;\; \varphi^3 = \varphi_1^3\end{gathered} \tag{2.14}$$

Using equations (2.10 - 2.13) the following strain tensor equation can be finally obtained from (2.13):

$$\hat{\sigma}_{me} = \left(\frac{H_E}{M_0}\right)^2 \frac{(H + H_D)h_\perp}{(\omega_{s0}/\gamma)^6}\left\{8(2\hat{B}_1\hat{u})^2(2\hat{B}_2\hat{u})\left(2\hat{B}_1\right) + (2\hat{B}_1\hat{u})^2\left(2\hat{B}_2\right)(4 - 3\Xi/2)\right\}, \tag{2.15}$$

where Ξ is defined as:

$$\Xi = \frac{3H_D + 4H}{H_D + H} + \frac{HH_D}{(\omega_{s0}/\gamma)^2} \tag{2.16}$$

From where the amplitude $\hat{\Psi}$ of nonlinear quasi-phonons interaction with transverse alternating field can be found as the antiderivative of stress tensor $\hat{\sigma}_{me}$:

$$\hat{\Psi} = \left(\frac{H_E}{M_0}\right)^2 \frac{(H + H_D)h_0}{(\omega_{s0}/\gamma)^6}\left\{4(2\hat{B}_1)^2(2\hat{B}_2) - \Xi(2\hat{B}_2)^3/2\right\} \tag{2.17}$$

The three quasi-phonon coupling coefficient is linearly proportional to the amplitude of alternating pumping field h_0 and also proportional to $1/(\omega_{s0}/\gamma)^6$. The square of magnetoelastic coupling coefficient ζ^2 is defined as [76]:

$$\zeta^2 = \frac{4H_E B_{14}^2}{M_0 C_{44}} \frac{1}{(\omega_{s0}/\gamma)^2}, \tag{2.17}$$

meaning that three quasi-phonon coupling is also proportional to ζ^6. For this reason observations of three quasi-phonon coupling is preferable for systems that satisfy the condition of the limiting strong coupling $\zeta_{S,k\to 0}(H \to 0) \to 1$.

2.4 Single mode three quasi-phonon excitations model

Single mode three quasi-phonon excitations in magnetoacoustic resonators are easier to observe experimentally in comparison with travelling waves coupling. In resonator case, the wavelength is comparable with the crystal size, so smaller samples can be used. Resonator quality factor also helps to achieve higher amplitudes of oscillation. The condition of single-mode three quasi-phonon coupling is that the alternating electromagnetic pumping has to be applied at the triple eigenfrequency ω_n of the resonance mode:

$$\begin{gathered} h_\perp(t) = h_p \cos(\omega_p t + \psi), \\ \omega_p = 3\omega_n \end{gathered} \tag{2.18}$$

The eigenmode frequency depends on the bias magnetic field H and is determined by the linear magnetoelastic coupling:

$$\omega_n = \omega_{n0}\sqrt{1-\zeta_n^2(H)} \tag{2.19}$$

In the case of excitations with a wavelength comparable with the crystal size it is enough to provide non-zero mean value of volume energy of interactions between three quasi-phonons and alternating magnetic field.

The elastic deformations can be presented as a superposition of quasi-phonon modes:

$$\hat{u}(r,t) = \sum A_n(t)\hat{u}_n(r), \tag{2.20}$$

where $A_n(t)$ is amplitude of corresponding mode and $\hat{u}_n(r)$ is its deformations tensor. In this case volume integral of the free energy takes the form of the energy of interacting nonlinear oscillators. In the case of selective single-mode excitations, the free energy of the resonator can be described as:

$$\int drF = \frac{1}{2}M_n\omega_n^2A_n^2 + \Phi_n^{(4)}(H)A_n^4 + h_\perp(t)\chi_n(H)A_n^3\,, \tag{2.21}$$

where:

$$M_n = \int dr\rho u_n^2,\ \ \Phi_n^{(4)}(H) = \frac{1}{4!}\int dr\hat{C}_n^{(4)}(H)\hat{u}_n^4,\ \ \chi_n = \int dr\hat{\Phi}_{\mathrm{n}}(H)u_n^3 \tag{2.22}$$

Let $A_n(t) = \frac{1}{2}a_n(t)e^{i\omega_n t} + c.c.$ Then the three quasi-phonon excitations can be described by the following equations of motion for the amplitude a_n and phase ψ of the three phonon correlator $G = |a_n|e^{i\psi}$ [120]:

$$\begin{aligned} &\frac{\partial|a_n|^2}{\partial t} + 2\delta_n|a_n|^2 - \kappa_n h_p|a_n|^3\sin\psi = 0\,; \\ &\frac{\partial\psi}{\partial t} - 3\beta_n|a_n|^2 - \frac{3}{2}\kappa_n h_p|a_n|\cos\psi = 0 \end{aligned} \tag{2.23}$$

Here δ_n is the mode attenuation coefficient, $\kappa_n = 3\chi_n / 4M_n\omega_n$ is the three-phonon coupling constant, and $\beta_n = 3\Phi_n^{(4)} / 2M_n\omega_n$ is the mode's nonlinear frequency shift constant induced by cubic nonlinearity.

2.5 Threshold of the three quasi-phonon parametric instability

In the sections (2.5 – 2.6) some particular cases of three quasi-phonon dynamics are considered given by V. Preobrazhensky et al. [120] and O. Bou Matar.

Let $n = |a_n|^2$ and $V = \kappa_n h_p$, then the system becomes:

$$\begin{aligned} &\frac{\partial n}{\partial t} + 2\delta_n n - Vn^{3/2}\sin\psi = 0\,; \\ &\frac{\partial \psi}{\partial t} - 3\beta_n n - \frac{3}{2}Vn^{1/2}\cos\psi = 0 \end{aligned} \tag{2.24}$$

Determining the threshold of the three quasi-phonon parametric instability at low initial intensity $n << 1$ it is possible to neglect the nonlinear frequency shift $\beta_n = 0$ as its contribution starts to dominate the process only when the amplitude reaches certain levels that will be discussed later in this chapter. If the phase ψ is set to the optimal value of $\frac{\pi}{2}$ the system simplifies to one equation:

$$\frac{\partial n}{\partial t} + 2\delta n - Vn^{3/2} = 0 \tag{2.25}$$

Since $n << 1$, then $\frac{\partial n}{\partial t} \cong -2\delta n\left(1 - \frac{Vn_0^{1/2}}{2\delta}\right)$ where $n_0^{1/2}$ is magnitude of the oscillations amplitude at the instant of the pumping start.

The solution of this equation, corresponding to the onset of the instability process, is given by $n = Ae^{\Gamma' t}$, where

$$\Gamma' = 2\delta_n\left(\frac{Vn_0^{1/2}}{2\delta_n} - 1\right) = 2\delta_n(\Gamma - 1)\,, \tag{2.26}$$

where Γ is the supercriticality parameter [120]:

$$\Gamma = \frac{Vn_0^{1/2}}{2\delta} = \frac{\kappa_n h_p |a_n| Q_n}{\omega_n}\,, \tag{2.27}$$

where $Q_n = \omega_n/2\delta_n$ is the mode's quality factor and a_{n0} is the initial amplitude of oscillations. The intensity of oscillations n increases from the initial value n_0 when $\Gamma' > 0$, that condition is met when $\Gamma > 1$, which acts as a threshold condition of the instability. Substituting κ_n the threshold of explosive instability Γ can be defined as:

$$\Gamma = \frac{9}{16} Q_n \frac{\zeta_n^4}{1-\zeta_n^2}\left(\frac{\gamma}{\omega_{f0}}\right) H_D h_0 a_{n0} > 1 \tag{2.28}$$

Required condition of the superthreshold process observation is that Γ > 1, or $h_p a_{n0} > (h_p a_{n0})_{th}$.

After certain time of the process development the approximation *n << 1* is not fulfilled any more. To determine the system behavior at higher amplitudes the system needs to be solved without this simplification.

2.6 Explosive behavior of the parametric instability without higher order nonlinearity

In this section supercritical behavior of the system under three quasi-phonon instability excitations is analyzed. If cubic nonlinearity is not taken into account then the nonlinear frequency shift is $\beta_n = 0$. In case when attenuation is considered $\delta_n = 0$ the system of equations (2.24) becomes:

$$\frac{\partial n}{\partial t} - Vn^{3/2} sin\psi = 0 \tag{2.29}$$

$$\frac{\partial \psi}{\partial t} - \frac{3}{2} V n^{1/2} cos\psi = 0$$

Letting $y = n^{3/2} \sin\psi$:

$$\begin{aligned} \frac{\partial n}{\partial t} &= -Vy \\ \frac{\partial y}{\partial t} &= \frac{3}{2} V n^2 \end{aligned} \tag{2.30}$$

Combining these two equations:

$$\frac{\partial^2 y}{\partial t^2} = \frac{3}{2} V^2 n^2 \tag{2.31}$$

Looking for the solution in the form of $n = A\left(t - t_0\right)^{-2}$ final solution can be obtained:

$$n = \frac{4}{V^2} \frac{1}{\left(t - \frac{2}{V n_0^{1/2}}\right)}, \tag{2.32}$$

where the characteristic $2/Vn_0^{1/2} = 2/\kappa_n h_\perp \mid a_n \mid_0 = t_0$ is the time when singularity arises. If the attenuation is considered $\delta_n \neq 0$, then the system of equations becomes:

$$\begin{aligned} \frac{\partial n}{\partial t} &= -2\delta_n n + Vy \\ \frac{\partial y}{\partial t} &= \frac{3}{2} V n^2 - 3\delta_n \end{aligned} \tag{2.33}$$

It can be combined to:

$$\frac{\partial^2 n}{\partial t^2} + 5\delta_n \frac{\partial n}{\partial t} + 6\delta_n^2 n = \frac{3}{2} V^2 n^2 \tag{2.34}$$

Looking for the solution in the form of $n = \left(A - Be^{\delta_n t}\right)^{-2}$ finally the result presented in [120] can be obtained:

$$n(t) = \frac{n_0}{(\Gamma - (\Gamma - 1)e^{\delta_n t})^2} \tag{2.35}$$

As can be seen in this case for reasonable attenuation levels the amplitude growth is not stabilized by the attenuation and the solution becomes singular at a finite time t_0' which is determined by the relation:

$$t_0' = \frac{1}{\delta_n} \ln\left(\frac{\Gamma}{\Gamma - 1}\right) \tag{2.36}$$

The time $t_0' \to t_0$ when $\delta_n \to 0$.

2.7 Influence of cubic nonlinearity on the parametric instability

Since the attenuation is not able to break the explosive instability process, let's neglect it $\delta_n = 0$ and consider the nonlinear frequency shift $\beta_n \neq 0$. Letting $z = n^{3/2}\cos\psi$ we obtain the following system of equations:

$$\begin{aligned} \frac{\partial z}{\partial t} &= -3\beta_n n^{5/2} \sin\psi \\ \frac{\partial n}{\partial t} &= V n^{3/2} \sin\psi - 3\delta_n \end{aligned} \tag{2.37}$$

That gives $\frac{\partial z}{\partial t} = -\frac{3\beta_n n}{V}$ with the following solution:

$$z = -\frac{3\beta_n}{2V} n^2 + C \tag{2.38}$$

Where C is chosen to be 0. This gives $\cos\psi = -3\beta_n n^{1/2} / 2V$ and the second equation from the system becomes:

$$\frac{\partial n}{\partial t} = \pm V(n^3 - \eta n^4)^{1/2} \tag{2.39}$$

Where $\eta = 9\beta_n^2 / 4V^2$. This equation can be rewritten as:

$$\frac{1}{2}\left(\frac{\partial n}{\partial t}\right)^2 + \pi(n) = 0, \tag{2.40}$$

where $\pi(n) = V^2\left(\eta n^4 - n^3\right)$. Solution of this equation is given by:

$$n(t) = \frac{1}{\left(\eta + \frac{V^2}{4}(t_1 - t)^2\right)}, \tag{2.41}$$

where

$$t_1 = \frac{1}{V n_0^{\frac{1}{2}}}(1 - \eta n_0)^{1/2} \tag{2.42}$$

is the time of the amplitude growth stabilization. The maximum value of the amplitude after the stabilization is determined by the following equation:

$$n_{max} = \frac{4V^2}{9\beta_n^2} \tag{2.43}$$

Since $n = |a_n|^2$ and $V = \kappa_n h_\perp$ finally we obtain:

$$|a_n|_{max} = \frac{3}{2}\frac{V}{\beta_n} = \frac{2\kappa_n h_\perp}{3\beta_n} \tag{2.44}$$

In real AFEPs cubic nonlinearity is anomalously strong and in the superthreshold conditions the intensity and the respected number of generated quasi-phonon triads is limited first of all by the nonlinear frequency shift (NFS) of the mode. This limitation does not allow observation of explosive supercritical dynamics without special methods of NFS compensation. The NFS compensation by application of the pumping with a proper law of phase modulation is proposed below.

2.8 Compensation of the cubic nonlinearity in single mode three quasi-phonons excitations

Cubic nonlinearity in a resonator manifests itself as nonlinear frequency shift $\Delta\omega_n$ of the magnetoacoustic resonance mode as discussed in the first chapter. It was shown [188] that this eigenmode frequency of critical contour shear mode has a square dependence on the amplitude of oscillations $\Delta\omega_n = \alpha |\, a_n \,|^2$ where α is a constant. Let's consider a situation when the effect of cubic nonlinearity on the three quasi-phonon coupling is somehow completely compensated, this will mean that the square of the amplitude of oscillations is described by the law (2.35), which gives us the law at which the frequency of the oscillations would change:

$$\omega_n(t) = \omega_{n0} + \Delta\omega_n = \omega_{n0} + \frac{\alpha n_0}{(\Gamma - (\Gamma - 1)e^{\delta_n t})^2}, \tag{2.45}$$

where $\Delta\omega_n$ represents the nonlinear frequency shift and ω_{n0} is eigenfrequency of the mode in the selected bias magnetic field. If the pumping field frequency would change with the oscillations amplitude increase to follow this eigenmode's frequency shift, the effect of nonlinear frequency shift can be completely compensated and the amplitude of the oscillations would tend to infinity in a finite time τ_c demonstrating the explosive instability of purely positive waves. For this frequency adjustment the pumping field phase modulation has to be applied:

$$h_\perp(t) = h_0 \cos\big(3\omega_n t + \psi(t)\big), \tag{2.46}$$

where $\psi(t)$ was found as antiderivative of equation (2.43):

$$\psi(t) = \frac{\alpha Q}{\Gamma}\left(\frac{(\Gamma - 1)\big(1 - e^{-\delta_n t}\big)}{1 - \Gamma(1 - e^{-\delta_n t})} - \frac{\ln\Big(1 - \Gamma\big(1 - e^{-\delta_n t}\big)\Big)}{\Gamma}\right) + \psi_0 \tag{2.47}$$

is the time-varying singular phase modulation that provides desired frequency shift. This law of phase modulation for an eigenmode at 350 kHz is presented in the Figure 2.2 with the experimentally obtainable parameters: Γ = 2.7, α = 0.014, Q = 1000, $\psi_0 = \pi$ and τ_c shows phase singularity time.

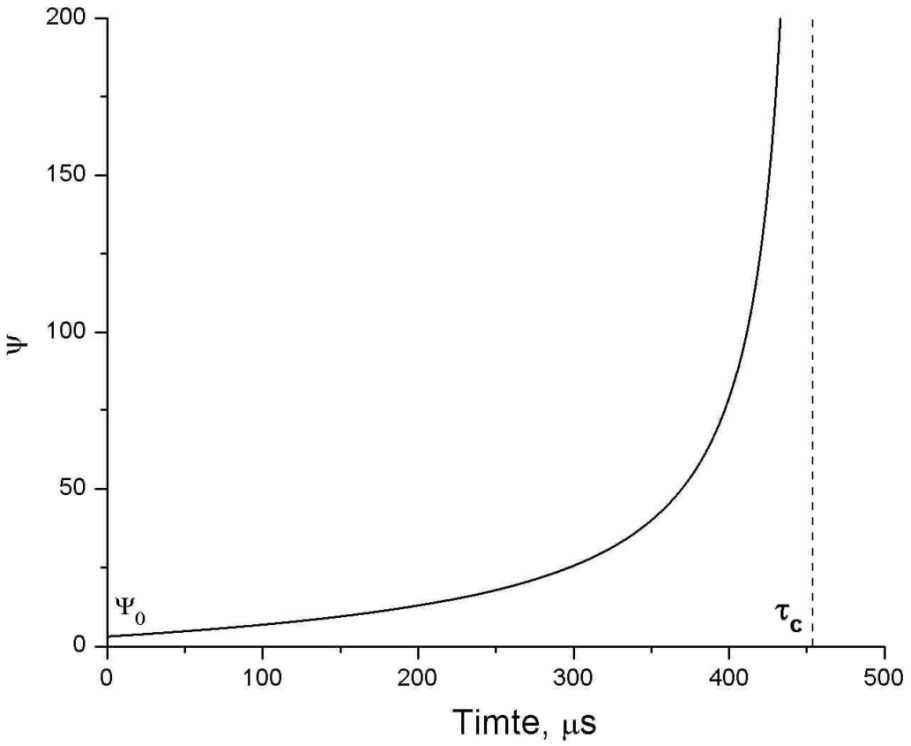

Figure 2.2. Pumping phase modulation law that compensates nonlinear frequency shift. At the time τ_c the phase reaches singularity.

2.9 Numerical simulations of the three quasi-phonon excitations using anharmonicity model

Following the formulae (2.18 – 2.23) the oscillations of a magnetoelastic resonator under three quasi-phonon excitations have been modeled with the help of the following equation of an anharmonic damped resonator driven by a time dependent parametric force that is produced by excitation electromagnetic pumping:

$$\ddot{a}_n + \dot{a}_n/Q_n + a_n + \beta a_n^3 - \vartheta a_n^2 h_\perp(t) G(t) = 0\,, \tag{2.48}$$

where a_n is oscillations amplitude, $Q_n = \omega_n/2\delta_n$ is n^{th} mode quality factor, $\beta = \alpha\left(\zeta^6/(1-\zeta^2)\right)$ is cubic nonlinearity coefficient, $\vartheta = \varepsilon\left(\zeta^6/(1-\zeta^2)\right)H_D\left(H + H_{ms}^{(2)}\right)^{-1}$ is the coupling coefficient, α and ε are corresponding proportionality constants. Pumping field $h_\perp(t)$ was modeled according to equations (2.44) and (2.45). $G(t)$ is an m^{th} order Gaussian

envelope used to wrap the pumping field to avoid excitations of other harmonics by step function:

$$G(t) = e^{-\left(\frac{t-\tau_a}{\tau_b}\right)^m}, \tag{2.49}$$

where τ_a and τ_b are constants defining the position of wrapping envelope. Second order differential equation (2.46) was rewritten as a system of first order equations and solved numerically with the help of Mathcad software using fourth order fixed-step Runge – Kutta method.

The parameters were assumed according to the experimental conditions of three quasi-phonon excitations on a real α-Fe_2O_3 single crystal resonator that are discussed in detail in the Third Chapter: H = 60 Oe, ζ_n = 0.78, h_0 = 9 Oe, Γ = 2.7, α = 0.024, Q = 1000. The initial amplitude was taken equal to a_{n0} = 0.17 that corresponds to initial pulse amplitude 330 mOe for its duration 20μs used in the further experiments, the pumping starts at the time $\tau = 100\,\mu s$. Initial phase shift of the pumping is $\psi_0=\pi$. Calculated oscillation waveforms were processed using Hilbert transform to plot their envelopes that are presented in the figures. The results of numerical simulation are presented in Figure 2.3. Initial amplitude is normalized in the figure to 0.1 for better presentation. When the frequency of the pumping pulse is modulated with proposed law (2.47) (Figure 2.3 (a)) the amplitude of oscillations tends to infinity within finite time. The amplitude gain at the end of the pumping pulse calculated as $G = 10\log(a/a_{n0})$ was found to be about 10.8 dB.

When the frequency modulation of pumping pulse is turned off, no explosive amplification was obtained (Figure 2.3(b)). If the initial excitation is set to a_{n0} = 0, three-phonon excitations were not observed neither with, nor without frequency modulation (Figure 2.3(c)). Dashed line shows theoretical explosive amplitude growth in case when $\beta = 0$ that reaches singularity at the time τ_c. The results of numerical simulation show clear explosive instability process development when the pumping magnetic field is modulated with proposed self-consistent phase modulation law. In the anharmonic model the oscillations amplitude growth during explosive instability process depends on the pumping field amplitude. Figure 2.4 shows development of the process under different pumping amplitudes: (a) 9 Oe, (b) 18 Oe and (c) 36 Oe.

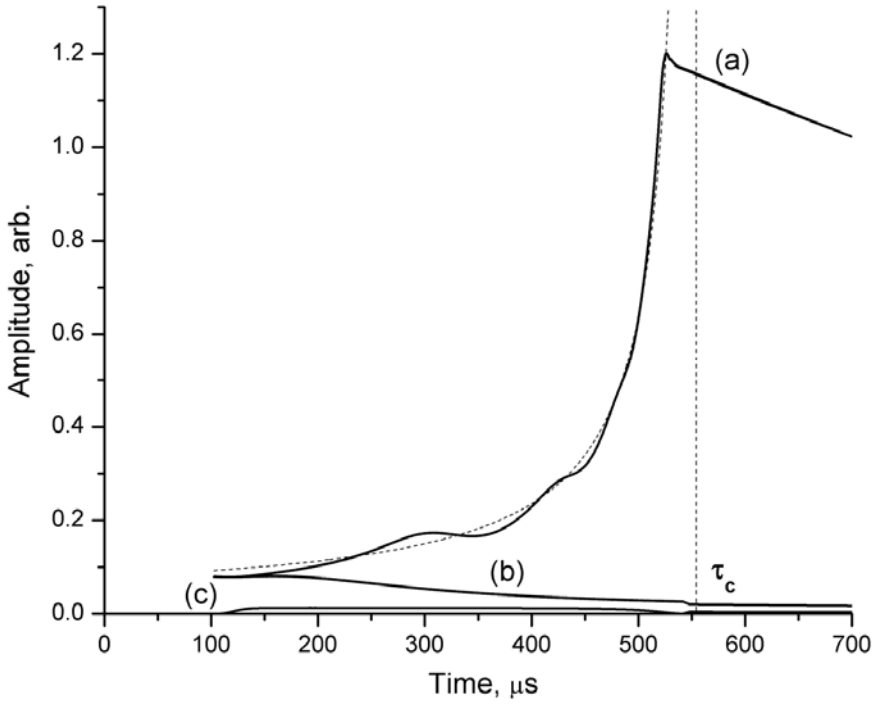

Figure 2.3. Calculated time dependencies of magnetoelastic oscillations amplitude under electromagnetic pumping in α-Fe_2O_3 resonator (a) with proposed phase modulation law, (b) without frequency modulation, (c) without initial excitation $a_{n0} = 0$; dashed line shows theoretical explosive amplitude growth when $\beta = 0$ that reaches singularity at the time τ_c

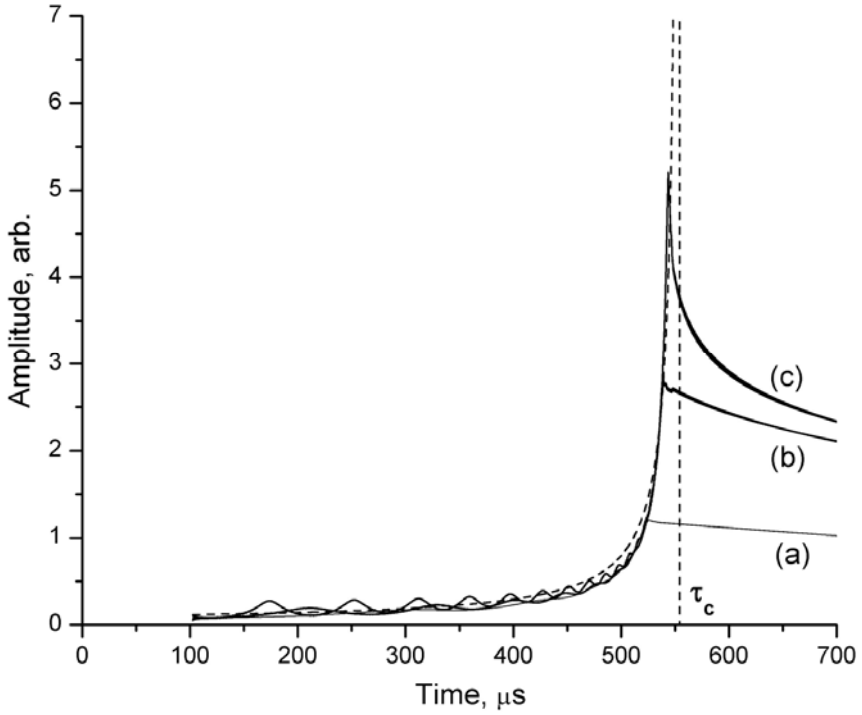

Figure 2.4. Calculated time dependencies of amplitude of α-Fe_2O_3 resonator oscillations under electromagnetic pumping for different values of h_p: (a) 9 Oe, (b) 18 Oe and (c) 36 Oe.

Figure 2.4 shows that increase of the pumping amplitude makes supercritical excitations closed to the ideal explosion. The reason of that lies in the nonlinear frequency shift compensation law that is following the amplitude growh, but is not perfectly matched with it. Minimal misphasings that is negligible at the beginning of explosive process at high amplitudes dominates the process and breaks explosive dynamics development. Higher pumping amplitude postpones the time of the process break.

2.10 Chapter II conclusion

The analysis of effective anharmonicity model of quasi-phonons single-mode excitations in easy plane antiferromagnet resonator showed that the main mechanism of supercritical explosive instability development limitation comes from the fourth order (cubic nonlinearity) energy term. In a resonator, this mechanism manifests itself as a nonlinear frequency shift. Attenuation is not able to break instability development process.

The threshold of three quasi-phonons instability depends not only on intensity of the pumping field, but also on initial amplitude of oscillations. As cubic nonlinearity contributions are considerably large beyond the threshold, explosive supercritical dynamics does not manifest itself without special methods of nonlinearity compensation.

In order to compensate the nonlinear frequency shift an advanced technique has been proposed. Based on the fact that the shift has a square dependence on the amplitude of oscillations, a proper pumping consistent time-varying singular phase modulation law has been applied.

Numerical solutions of the equation of motion for the magnetoelastic resonator under electromagnetic pumping with the parameters of real hematite α-Fe_2O_3 confirmed that the threshold of three-boson parametric instability depends on the initial amplitude. When the threshold conditions are met and pumping field is applied without phase modulation explosive behavior is not observed. When the pumping field is modulated with the proposed phase modulation law, the nonlinear frequency shift gets compensated and supercritical explosive dynamics of the process manifests clear explosive behavior with quasi-singular amplitude of oscillations.

Chapter III

Experimental Studies of Supercritical Explosive Dynamics of Single Mode Three Quasi-Phonon Instability

3.1 Chapter III introduction

The Third Chapter focuses on the studies of single-mode supercritical dynamics of three quasi-phonon excitations in easy plane antiferromagnetic resonators of α-Fe_2O_3 and $FeBO_3$. The main subject of presented investigation is the first experimental observation and investigation of the explosive instability behavior in real life crystals that has not been reported before. A new technique is proposed for experimental observation of the supercritical dynamics. The nonlinear frequency shift compensation method suggested in the Second chapter is applied for the electromagnetic pumping field modulation.

The first part of the chapter presents results of magnetoelastic characteristics study and three quasi-phonon excitations in hematite. The research of magnetoelastic characteristics was necessary to obtain certain characteristics of the resonators required for the instability excitation and select proper operating point. These parameters are obtained with the help of studies of magneto-elastic spectra of the samples, measurements of contour shear modes' frequency dependencies on the bias magnetic field, nonlinear frequency shifts of the modes and quality factor studies.

In the second part the results of characteristics measurement and supercritical dynamics research in iron borate resonator are presented. In contrast with hematite, this crystal features favorable conditions for three quasi-phonon excitations at lower temperatures, where the dissipations in elastic subsystem decrease. Experiments on iron borate are carried out at the temperature range 77 K – 293 K at which magnetoelastic parameters vary essentially.

3.2 Easy plane antferromagnetic resonators of α-Fe_2O_3 and $FeBO_3$

The experiments were carried out on two high temperature easy plane antiferromagnetic single crystal samples shaped as a disk: hematite α-Fe_2O_3 and iron borate $FeBO_3$. The samples were used as resonators in which different magneto-acoustic modes could be excited.

The α-Fe_2O_3 resonator had diameter of 5.5 mm and was 0.5 mm thick. The plane of the disk was parallel to the basal plane. The sample was placed in an organic glass frame with

two perpendicular coils wound around it. The sample could freely oscillate inside the frame. One of the coils was used as a pumping coil to excite the resonator and the other one was used as a detection coil to register the resonator oscillations. For hematite the pumping coil contained 28.5 turns of rectangular shape 10.4 mm by 3.2 mm. Detection coil contained 29.5 turns also of rectangular shape 10.6 mm by 2.7 mm.

The $FeBO_3$ single crystal sample was shaped as a 0.1 mm thick disk with a diameter of 3mm. Basal plane of the crystal was also parallel to the plane of the sample. It was placed in a similar but smaller frame as the hematite sample, with 2 perpendicular coils wound around it for excitation and signal detection. Iron borate pumping coil had 19.5 turns of a rectangular shape 6.6 mm by 1.8 mm. Iron borate detection coil had 20.5 turns of a rectangular shape 6.9 mm by 1.3 mm.

A picture of the hematite resonator and organic glass frame with pumping and detection coils is presented in the Figure 3.1. Iron borate resonator was placed in a similar frame.

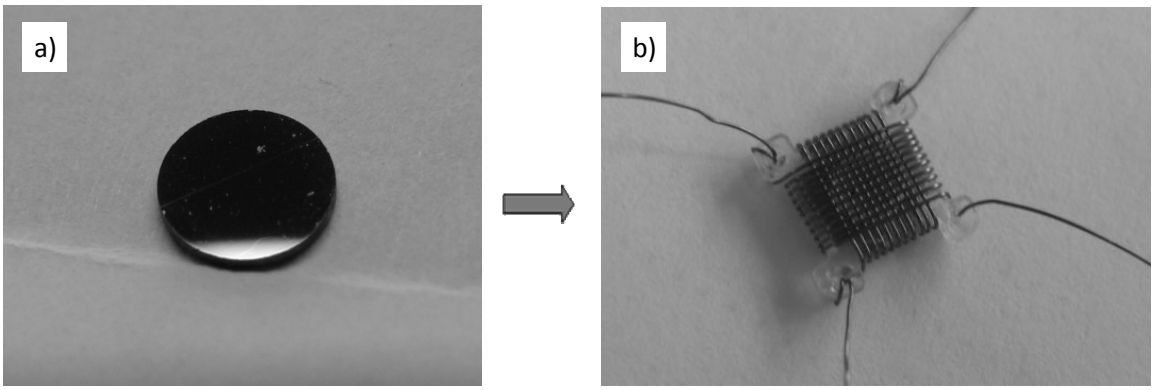

Figure 3.1. Picture of α-Fe_2O_3 single crystalline resonator (a) and a frame with sample inside and two perpendicular coils wound around it (b).

The coils were aligned at 90 degrees, so that their mutual induction was close to zero. In this case if a harmonic signal was applied to the pumping coil, it was not visible at the receiving coil. However if the pumping frequency was close to the frequency of magneto-elastic mode of the resonator in selected bias magnetic field, the sample was oscillating and generated signal in the detection coil by projection of vibrating magnetic moment.

3.3 Experimental setup for the studies of magnetoelastic properties

Magneto-elastic characteristics of α-Fe_2O_3 and $FeBO_3$ resonators were measured as they are required for studies of single mode three quasi-phonon instability. For each sample a proper mode that satisfies the condition of theoretically limiting strong coupling $\zeta_{S,k\to 0}(H \to 0) \to 1$ had to be found and studied. Nonlinear frequency shift and attenuation coefficient of this mode had to be determined. The scheme of experimental setup for magneto-elastic properties studies is presented in the Figure 3.2. Pumping and detection coils were connected to Hewlett Packard 4195A Network Analyzer that was sweeping the frequency of the excitation signal and measuring sample spectra at different frequency ranges and amplitudes. Network analyzer was operated by the computer via GPIB interface. All acquired spectra were also sent to the computer via GPIB for further processing.

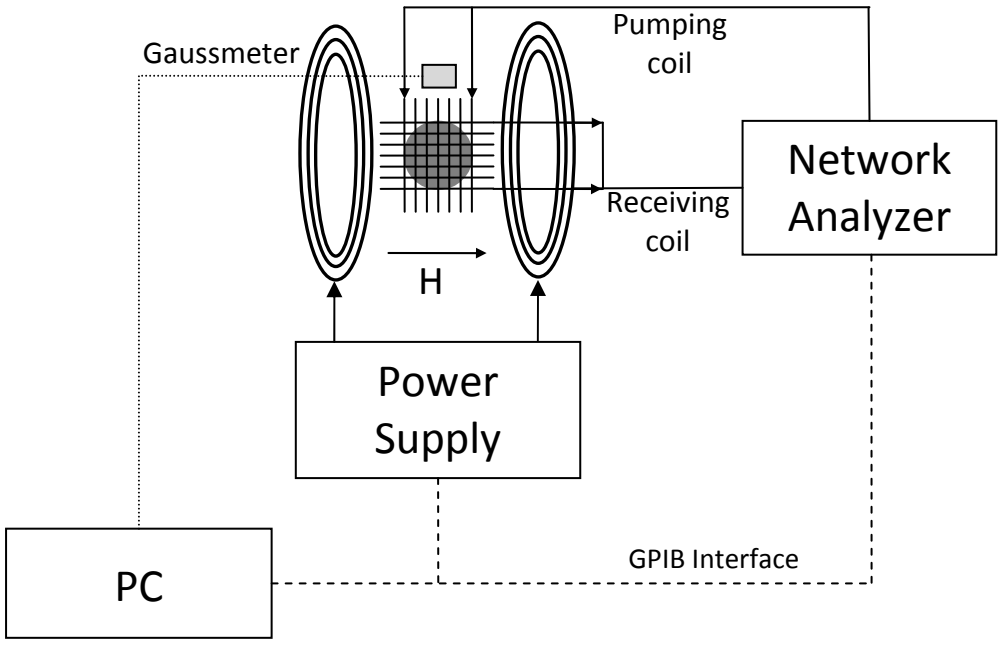

Figure 3.2. Scheme of the experimental setup for magneto-elastic characteristics measurement.

A sample in the frame was placed inside Helmholtz coils that provided bias magnetic field *H* in the range 0 - 140 Oe. It was applied in the basal crystalline plane at the angle of 45° with respect to alternating field $\vec{h}_{\perp}$ created by the pumping coil. Helmholtz coils were

powered by programmable Power Supply unit TTi TSX 1820P that was operated by PC via GPIB interface. The magnitude of the field was controlled with the help of serial port gaussmeter MI 2010T that was connected to the computer via COM port.

All the measurements were managed by a custom Labview virtual instrument that was created for magnetoelastic characteristics measurement. Bias magnetic field, spectra frequency ranges and sweeping signal amplitude were automatically changed by the computer with the help of this program via GPIB. Acquired data were processed and saved on PC by this program too.

3.4 Magneto-elastic characteristics of α-Fe_2O_3 resonator

Hematite has Morin spin reorientation transition at T_M = 256 K and below that temperature antiferromagnetic ordering is reorganized from being aligned perpendicular to the C_3 axis to be aligned parallel to the C_3 axis. This reorientation dramatically lowers magnetoelastic coupling coefficient making observations of explosive parametric instability at low temperatures impossible at experimentally available excitation amplitudes. All experiments with hematite presented in this chapter were conducted at room temperature of 293 K.

3.4.1 Spectrum of magneto-elastic coupled oscillations of a-Fe_2O_3

The research of magneto-elastic oscillations spectra was performed in order to determine the magneto-acoustic modes of the resonators, their frequencies and structures. Based on the results obtained it was possible to select a mode that is most optimal for further three quasi-phonon excitations.

The spectrum of coupled magneto-elastic oscillations in the frequency range 0.3 MHz – 1.2 MHz is presented in the Figure 3.3; no magneto-elastic modes were found in the frequencies below 0.3 MHz. Power of the input signal was -30 dBm.

The spectra were acquired in different bias magnetic fields. Here the spectrum in the field H = 60 Oe is shown, that corresponds to the operating point selected for single mode

three-boson coupling. The factors that determined operating point selection are discussed further in this chapter.

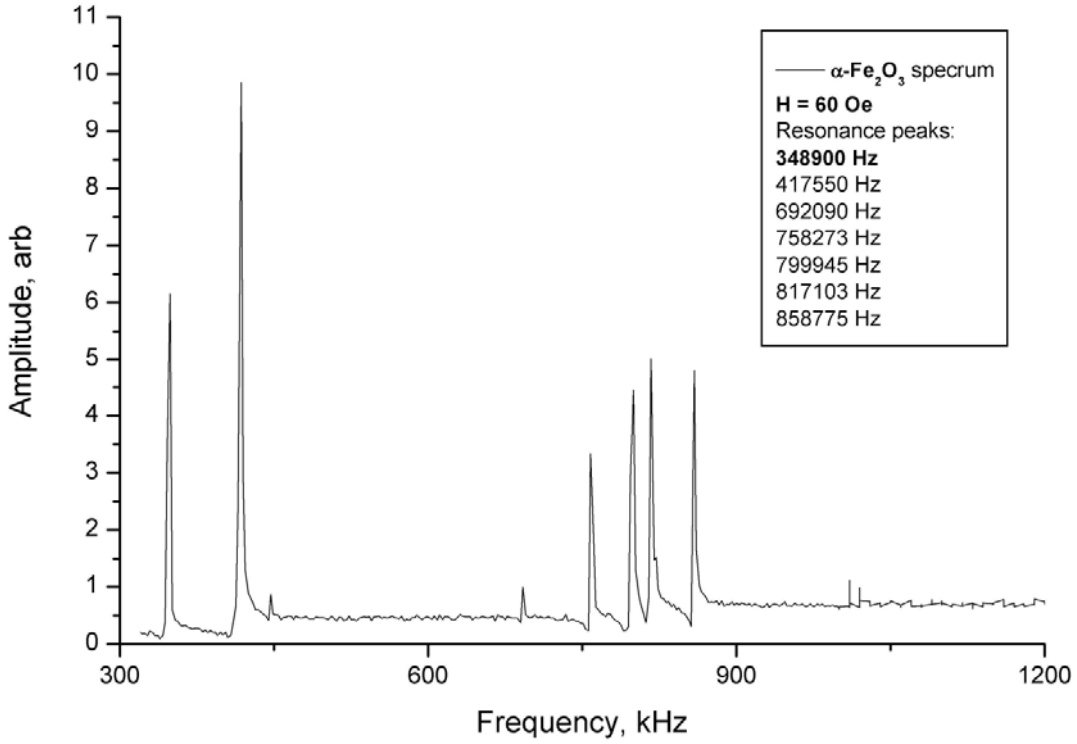

Figure 3.3. Spectrum of magnetoelastic oscillations of α-Fe_2O_3 resonator in the bias magnetic field H = 60 Oe.

The peaks on the spectrum represent magneto-elastic modes of the resonator. Exact frequencies of the seven most prominent modes are indicated in the legend. It was shown [93, 118] that the resonance mode found at the frequency 348.9 kHz is a contour shear mode that satisfies the condition of limiting strong coupling as discussed in the first chapter. The structure of this mode is presented in the Figure 1.6. Anomalously strong magnetoelastic coupling of this mode, sufficient distance in frequency between it and other modes and absence of any harmonics at the double or triple frequencies make it suitable for supercritical three quasi-phonon excitations.

3.4.2 Dynamic properties of hematite contour shear mode

The dynamic parameters of the resonator and optimal operation point for three-boson instability were determined by measuring the bias magnetic field dependence of the contour

shear mode resonance frequency. Results of the measurements in hematite resonator at room temperature are presented in the Figure 3.4 by circles.

Dependence of the magneto-elastic coupling coefficient of the mode $\zeta_n(H)$ on the frequency of the mode can be described as:

$$\omega_n = \omega_{n0}\sqrt{1-\zeta_n^2(H)}\,, \tag{3.1}$$

where ω_{n0} is the mode resonance frequency in saturating bias field at selected temperature. From the formulae (1.26) and (1.27) we obtain:

$$\omega_n = \omega_{n0}\left(1-\frac{2H_E H_{me}^{(1)}}{H(H+H_D+2H_E H_{me}^{(2)})}\right)^{1/2}, \tag{3.2}$$

where $H_{me}^{(1,2)}$ are the values of the magneto-elastic fields renormalized by the selected mode's boundary conditions [93]. Renormalized magnetoelastic gap for the mode can be written as $H_{ms}^{(2)} = 2H_E H_{me}^{(2)} / H_D$ and the first magnetoelastic field can be presented as a parameter $H_{ms}^{(1)} = 2H_E H_{me}^{(1)} / H_D$. If $H << H_D$ as in present research the term H^2 / H_D can be neglected and we obtain:

$$\omega_n = \omega_{n0}\sqrt{1-\frac{H_{ms}^{(1)}}{H+H_{ms}^{(2)}}} \tag{3.3}$$

Values of the fields $H_{ms}^{(1,2)}$ and the frequency ω_{n0} for the sample were calculated by fitting the theoretical formula (3.3) on the experimental results. Theoretical calculation of the mode frequency dependence is presented in the Figure 3.4 with a solid line. For hematite it was found that $H_{ms}^{(1)} = 124.8$ Oe, $H_{ms}^{(2)} = 146.0$ Oe and $\omega_{n0} = 550$ kHz. The dependence of magneto-elastic coupling coefficient on bias field *H* was calculated using the formula:

$$\zeta_n^2(H,T) = \frac{H_{ms}^{(1)}(T)}{H+H_{ms}^{(2)}(T)} \tag{3.4}$$

The results of the dependence calculation for hematite's contour shear mode are presented in Figure 3.5.

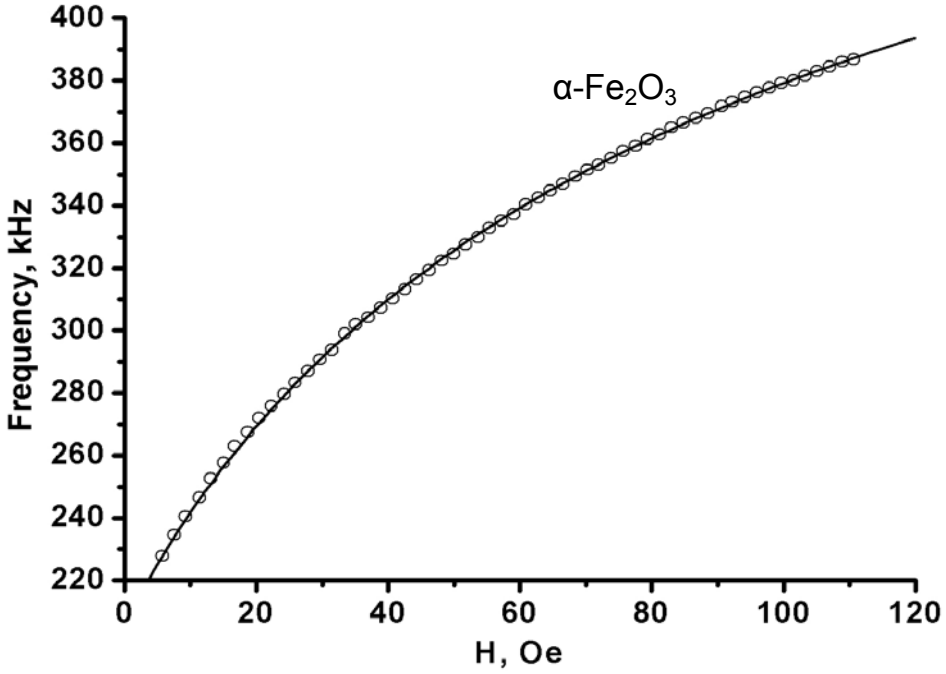

Figure 3.4. Experimental (dots) and theoretically approximated (line) bias magnetic field dependence of the contour shear mode eigenfrequency in hematite resonator.

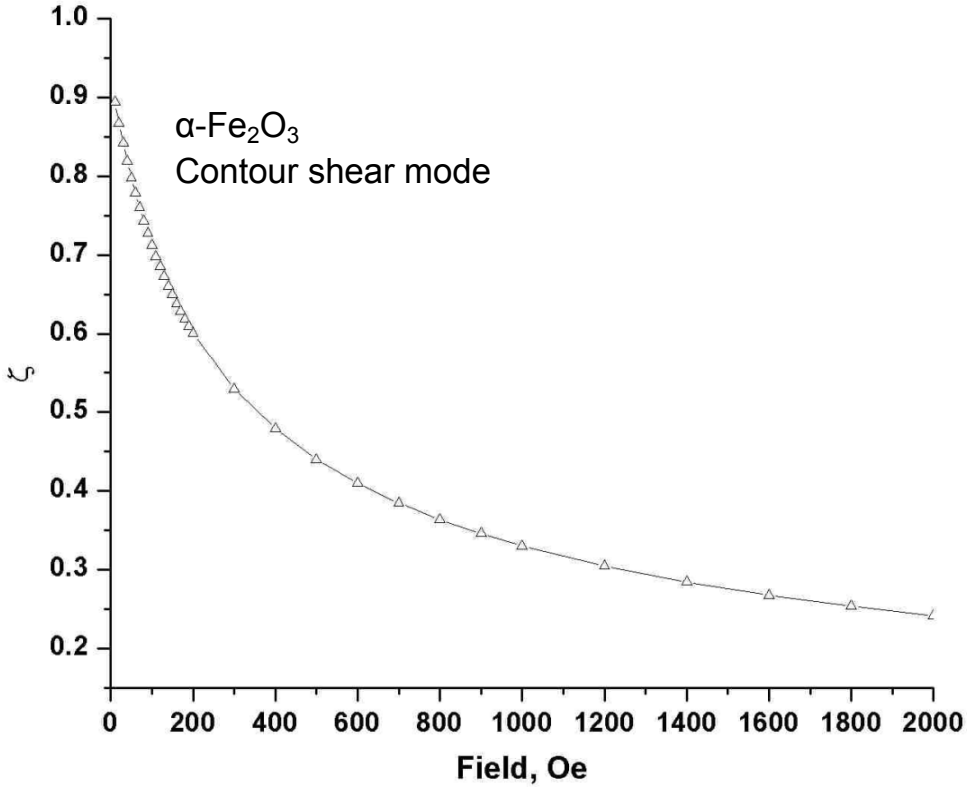

Figure 3.5. Dependence of the contour shear mode magneto-elastic coupling coefficient on bias magnetic field H in hematite resonator.

The operating point for three quasi-phonon excitations in the resonator had to be selected in the most optimal conditions, when the bias magnetic field is not too low for the defects to form the domains and break the process yet not too high to avoid decreasing the magneto-elastic coupling coefficient. Another thing considered was the amplitude of the contour shear mode oscillations as the threshold of explosive instability depends on the initial number of quasi-phonons. The bias field dependence of contour shear resonance amplitude is presented in the Figure 3.6. The maximum amplitude was achieved at the field H = 40 Oe and then the amplitude starts decreasing.

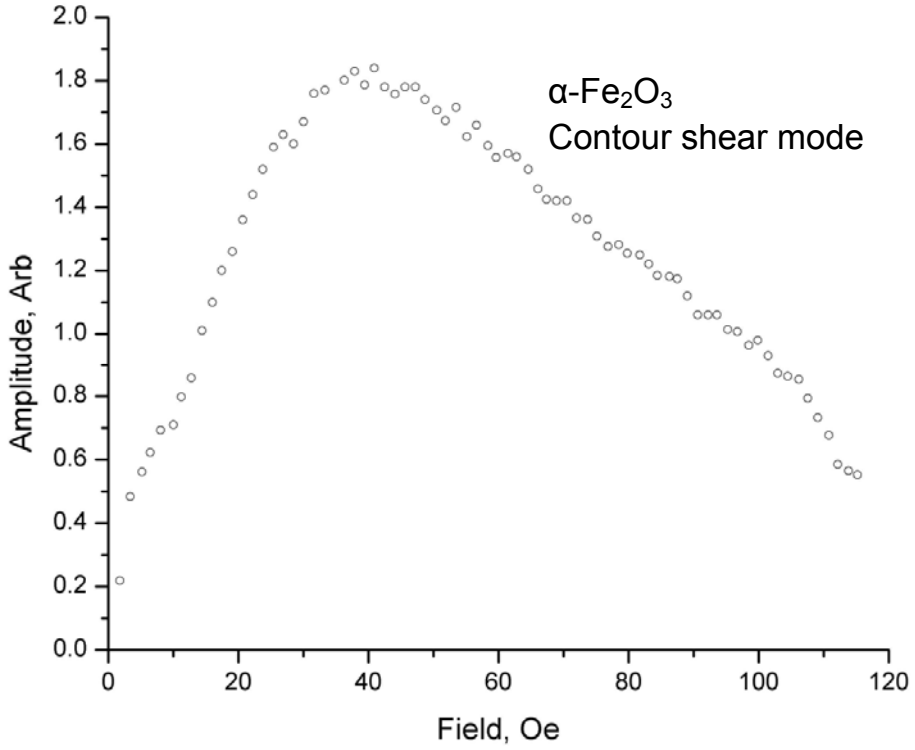

Figure 3.6. Bias field dependence of the amplitude of contour shear magneto-elastic mode.

The operating point was chosen at the bias field of H = 60 Oe. This point corresponds to eigenfrequency of $\omega_n/2\pi$ = 340 kHz, high enough coupling coefficient of ζ_n = 0.78 and sufficient amplitude of oscillations.

3.4.3 Nonlinear frequency shift of the magneto-elastic mode

Due to strong magnetoelastic interaction hematite sample acts as a nonlinear resonator. Resonance mode demonstrates strong nonlinear frequency shift (NFS) of the resonance as the

amplitude of oscillations increases. A study of this shift in hematite [118] showed that resonance frequency has linear dependence on the square of oscillations amplitude. Analysis of the anharmonic expansion (2.2) shows that NFS is caused by the cubic nonlinearity that are described by the fourth order energy terms:

$$F^{(4)} = -12\left(\frac{H_E}{M_0}\right)^3 \frac{(2\hat{B}_2\hat{u})^4}{(\omega_{f0}/\gamma)^6}\left(1+\frac{1}{4}\frac{\gamma^2 H H_D}{\omega_{s0}^2}\right) \tag{3.5}$$

To measure NFS the resonance lines of the selected mode were registered at different oscillation amplitudes. Sweeping frequency signal was applied to the pumping coil at different amplitudes. The frequency and amplitude of magnetic oscillations accompanying elastic vibration were registered with the detection coil. The Figure 3.6 shows dependence of the mode's resonance frequency on the square of oscillations amplitude at the bias field H = 60 Oe that demonstrates expected nearly linear behavior.

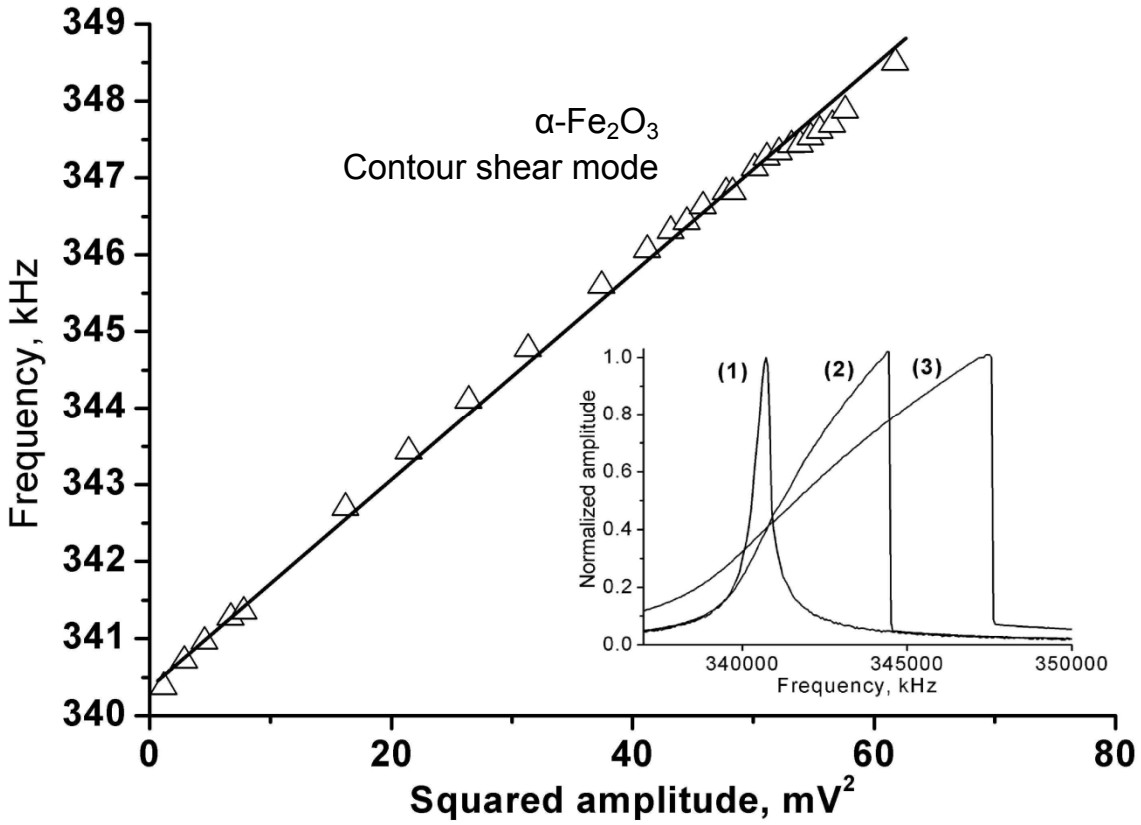

Figure. 3.7. Nonlinear frequency shift dependence on the square of oscillations amplitude. Inset: magneto-elastic resonance lines at different amplitudes of oscillations: 1.9 mV (1), 6.7 mV (2), 7.2 mV (3).

Resonance frequency increases as the amplitude goes up. The inset in the Figure 3.6 shows the resonance lines at different amplitudes of exciting magnetic field that correspond to registered oscillations of 1.9 mV (1), 6.7 mV (2), 7.2 mV (3). At low amplitudes (1) the shape of the resonance remains similar to the shape of linear resonance. As the amplitude of oscillations increases, the shape of nonlinear resonance gets distorted (2), (3) manifesting as so-called foldover effect.

3.4.4 Attenuation of contour shear mode in hematite resonator

Attenuation of nonlinear contour shear resonance was determined via the quality factor of the mode. Quality factor was calculated by the width of the resonance curve at half the maximum power value ($1/\sqrt{2}$ of the amplitude value) at low amplitude of oscillations to minimize the influence of nonlinear frequency shift:

$$Q_n = \frac{f_0}{2\Delta f}, \tag{3.6}$$

where $2\Delta f$ is the width of the resonance curve at half maximum power value ($1/\sqrt{2}$ of the amplitude value) and f_0 is the resonance frequency.

For hematite the shape of contour shear resonance line at low amplitudes is presented in the inset in Figure 3.7 (1). The quality factor of contour shear oscillations was measured to be $Q_n \approx 10^3$.

At higher amplitudes the quality factor of the resonator was measured with the help of relaxation method. Amplitude of a free oscillating resonator at the time *t* can be described as $a = a_0 e^{-\delta_n t}$, where a_0 is the start amplitude of oscillations. Then the quality factor can be determined as:

$$Q_n = \frac{\omega_0}{2\delta_n} = \frac{\pi f_0 t}{\ln(a_0/a)}, \tag{3.7}$$

Resonator was excited by a short pulse at the resonance mode frequency $\omega = \omega_n$ with a pumping coil and oscillations of the sample were recorded with detection coil. The pulse was

applied at the time $t = 10\mu s$ and its duration was $\tau = 20\mu s$. After the pulse, the sample would continue to oscillate as a damped resonator. The envelopes of obtained waveforms at different excitation pulse amplitudes are presented in the Figure 3.8.

The amplitudes of excitation magnetic field were (1) h = 330 mOe , (2) h = 660 mOe, (3) h = 1.32 Oe, (4) h = 2 Oe, (5) h = 3.3 Oe. At high levels of excitation (4), (5) magnetoelastic relaxation of hematite resonator demonstrates accelerated behavior before it reaches certain level due to high order nonlinearities. After it reaches this level it attenuates exponentially with close quality factors of $Q_n \approx 1090$ (1), $Q_n \approx 1080$ (2), $Q_n \approx 1050$ (3-5). Logarithm of the oscillations amplitude demonstrates linear behavior confirming that the resonator attenuates at a nearly constant quality factor. Thus the quality factor of the hematite contour shear resonance mode for further calculations was taken as $Q_n \approx 10^3$.

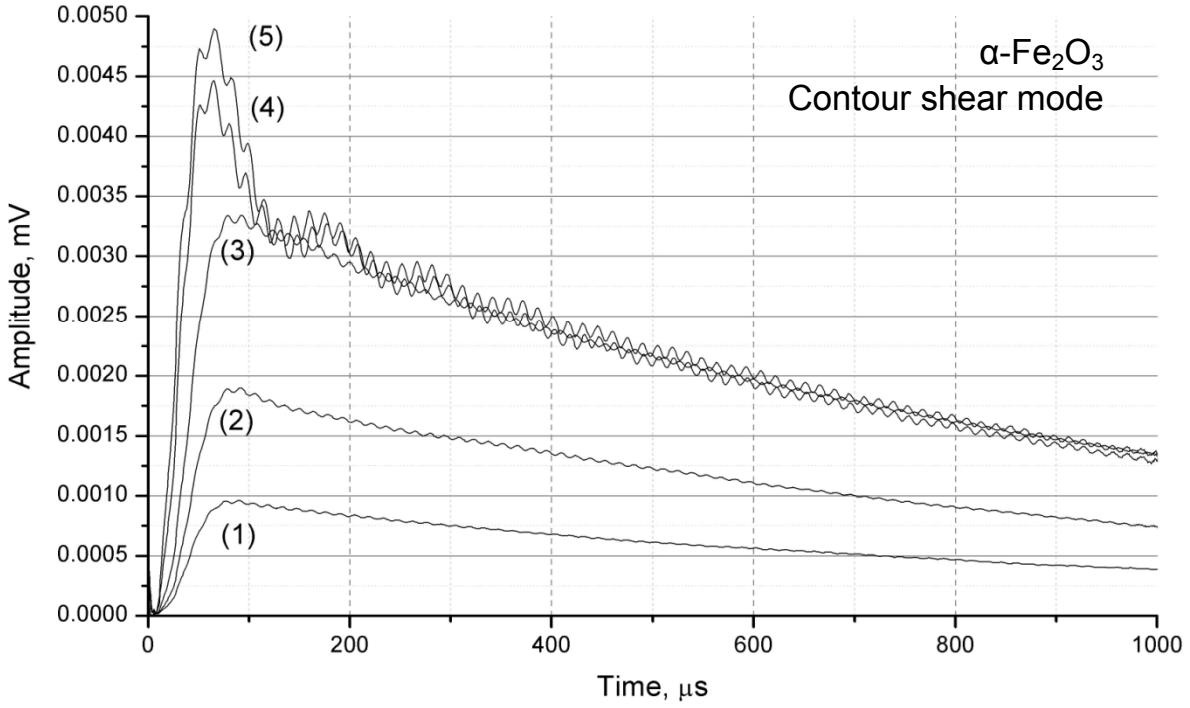

Figure 3.8 Free relaxation of magneto-elastic oscillations amplitude of hematite resonator after an excitation pulse at the eigenfrequency ω_n = 340 kHz that stopped at $t = 30\mu s$. Pulse amplitude was: (1) h = 330 mOe , (2) h = 660 mOe, (3) h = 1.32 Oe, (4) h = 2 Oe, (5) h = 3.3 Oe.

3.5 Experimental technique of supercritical three quasi-phonon instability research

A new custom technique was developed for experimental research of three quasi-phonon excitations in supercritical regime. This technique was used to reveal the behavior of contour shear mode amplitude under electromagnetic pumping. This section will explain main principles of the technique and describe the developed Labview virtual instrument used for the experiments.

3.5.1 Geometry of the three quasi-phonon experiment

Following the theory described in the second chapter, a phase-modulated pumping described by the formula (2.47) at sufficient amplitude had to be applied on the resonator, which already was excited to initial threshold amplitude a_0 for experimental research of supercritical three quasi-phonon dynamics. The pumping h_p had to be applied in the basal plane of the crystal, approximately perpendicular to the bias magnetic field.

Selected geometry of the experiment is presented in the Figure 3.9. Three quasi-phonon coupling was observed by applying two different subsequent pulses using same pumping coil.

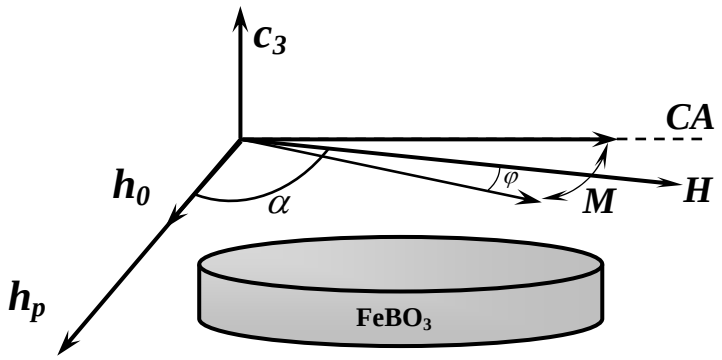

Figure 3.9.Geometry of the experiment. H is the bias magnetic field, h_0 and h_p are the initial excitation and the pumping fields respectively, M is ferromagnetic vector. Detection coil axis CA is perpendicular to the h_p.

The first pre-pumping pulse was a sinusoidal burst h_0 at the contour shear mode frequency ω_n that was used to excite initial threshold oscillations of amplitude a_0 in the resonator. The second pumping pulse h_p was applied at the pumping frequency ω_p with modulated phase.

External bias magnetic field H was applied in the basal crystalline plane of the sample at an angle α of about 80 degrees with respect to the alternating magnetic field of the pumping coil. Small declining from perpendicular geometry was used to provide induction in the detecting coil from ferromagnetic moment oscillations.

3.5.2 Resonator excitation for three quasi-phonon instability observation

Since the pulses had to be applied one after another using the same pumping coil, and the phase of the second pulse had to be modulated, an arbitrary waveform generator was used for the experiments. Experiments were managed by a custom Labview program created especially for supercritical three quasi-phonon instability research. This program was generating the waveforms in point-by-point mode based on the input parameters in the formula (2.47) and some technical parameters like waveform length in points, generator clock frequency, pulses length, etc. To improve the quality of the experiments a minimum of 36 points per oscillation period was used in waveforms generation. Generated waveforms were uploaded to the arbitrary waveform generator. The scheme of a typical three quasi-phonon coupling excitation waveform is presented in the Figure 3.10.

The scheme shows the two pulses used in the excitation. Experimental waveforms had more oscillation periods in each pulse. Presented figure is a demonstration that shows principles of generation. In the figure τ_1 represents duration of the first initial excitation pulse and τ_2 is duration of the pumping pulse that was applied about 10 μs after the first one. To avoid the noises created by the Gibbs effect due to step-like increase of amplitude of the bursts, the first pulse and the rising edge of the second pulse were shaped using Gaussian-like envelopes. The phase of the second pulse was modulated with proposed singular law and the duration was limited by the achievement of the singularity point of this law.

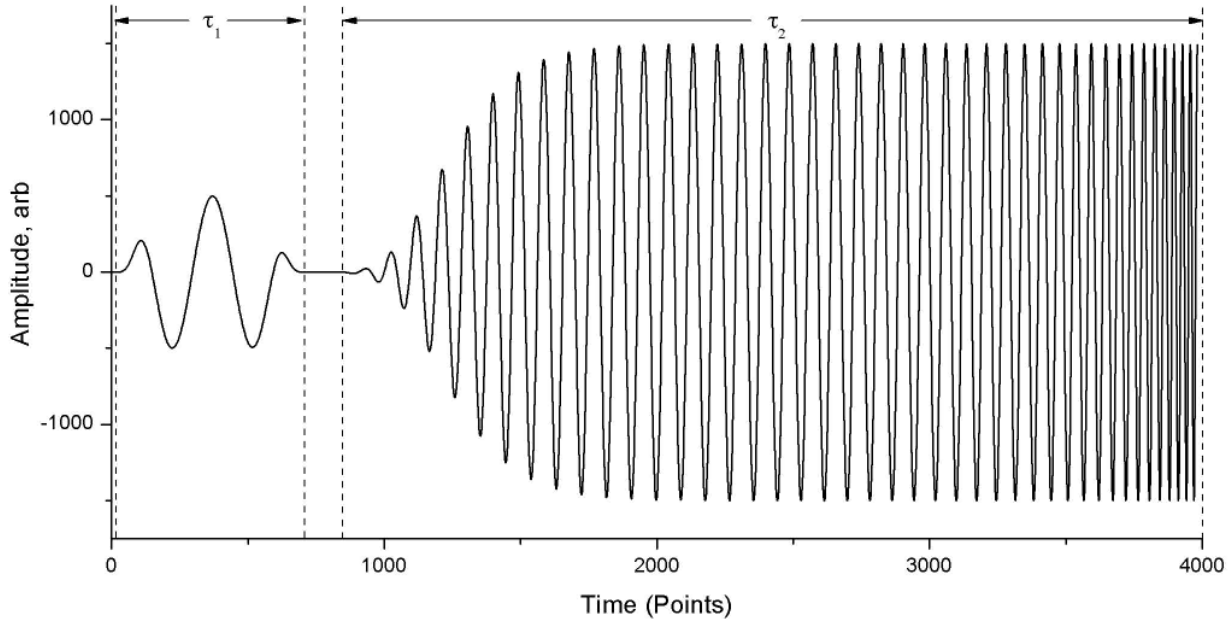

Figure 3.10 Scheme of the three quasi-phonon instability excitation waveform; τ_1 shows duration of the first initial excitation pulse, τ_2 shows duration of the pumping pulse. Pulses have Gaussian envelopes. Pumping pulse phase is modulated resulting in frequency shift.

3.5.3 Experimental setup for the explosive instability research

The scheme of experimental setup for three quasi-phonon excitations research is presented in the Figure 3.9. The heart of the setup was Labview virtual instrument program that managed the experiments. This program was generating the waveforms and uploading them to arbitrary waveform generator Tektronix AWG 2020 via GPIB interface. Generator was sending excitation pulses to the pumping coil via linear Amplifier SCD 30 dBm that was providing required pulses amplitude.

Receiving coil of the resonator assembly was connected directly to digital oscilloscope Tektronix TDS 5052 that was capturing the waveforms and sending them back to the Labview program via GPIB. Arbitrary waveform generator and oscilloscope were triggered with the clock pulse generator Tekelec TE 10 that was set to the frequency 10 Hz to provide enough time for the sample oscillations decay between pulses. Resonator assembly was placed inside Helmholtz coils that were used to bring the sample to the desired operating point with optimal magnetoelastic parameters. The coils were powered with programmable Power Supply unit

TTi TSX 1820P connected to the PC via GPIB interface. The magnitude of the field was controlled with the help of serial port gaussmeter MI 2010T that was connected to the computer via COM port.

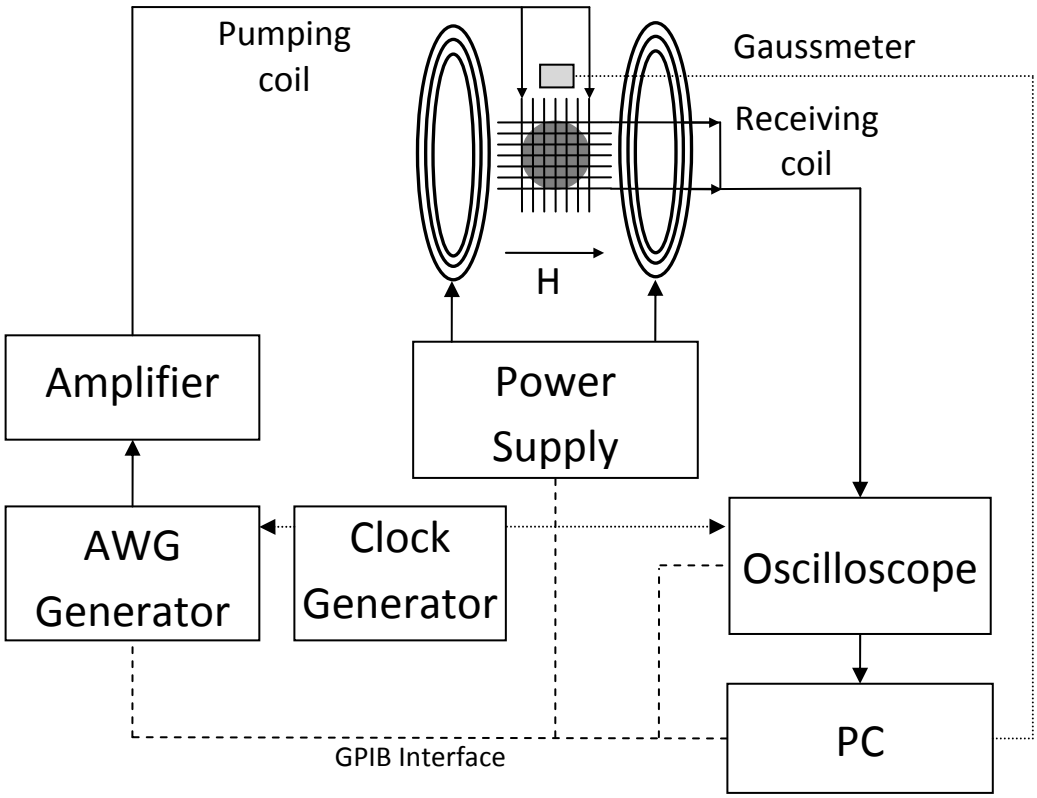

Figure 3.11 Experimental setup for the explosive instability research

Front panel of the program is presented in the Figure 3.12. Labview program was also responsible for acquired waveforms processing. A bandwidth of 100 kHz around selected resonance mode frequency was filtered with the help of Butterworth filter to delete pumping pulse from it.

Resulting waveforms were processed with Hilbert transform to create an envelope of the signal. Such approach allowed registering time dependence of the resonance mode amplitude during a relatively strong electromagnetic pumping pulse without interferences with it. Acquired envelopes were saved to a separate data file with a graph and experimental parameters including initial excitation and pumping frequencies, amplitudes, phase modulation coefficients, etc.

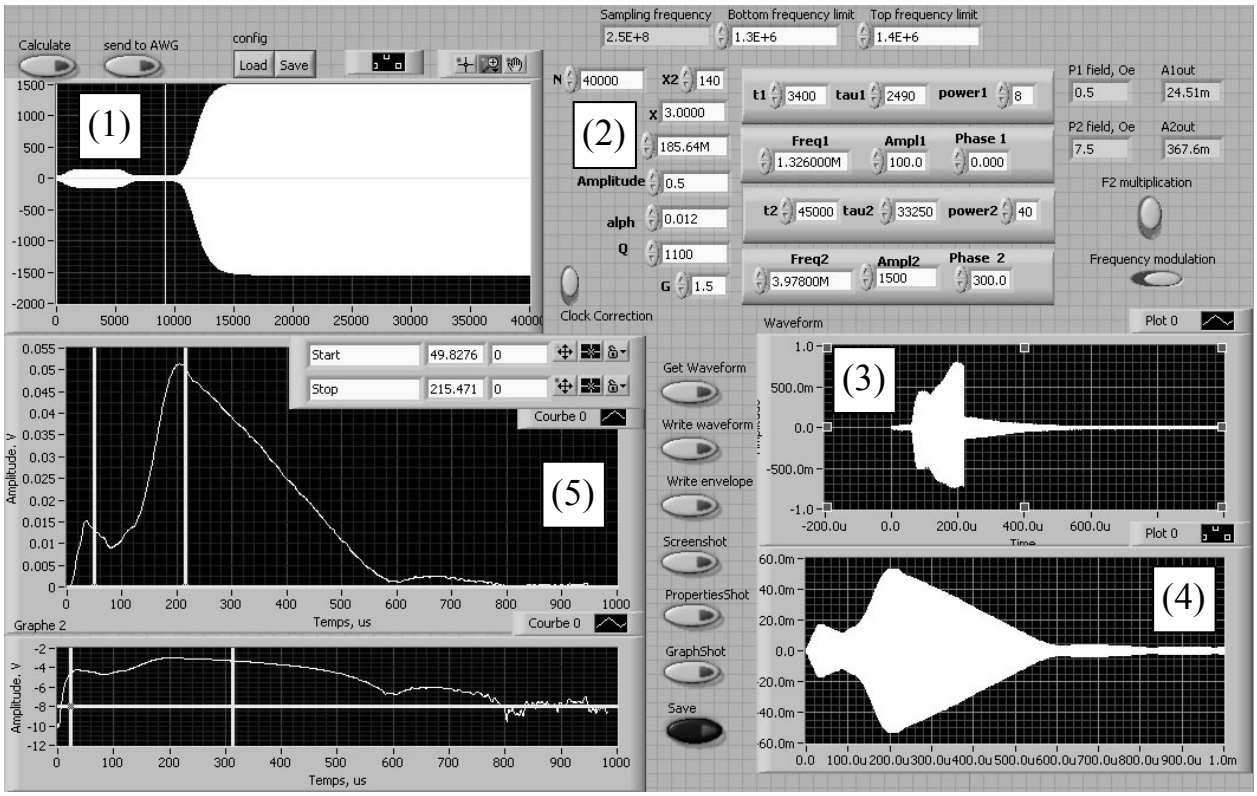

Figure 3.12 Front panel of the Labview program showing generated excitation waveform (1) based on the input parameters (2), acquired waveform (3), filtered for the resonance frequency (4) and plotted envelope (5) in linear (top) and logarithmic (bottom) scales.

3.6 Supercritical single mode three quasi-phonon excitations in α-Fe_2O_3

As the explosive instability threshold in a crystal depends on two factors that are the initial level of excitation and the pumping field strength, the amplitudes of the first and second pulses were selected high enough to exceed the threshold of instability. Hematite resonator was placed in selected operating point of bias magnetic field H = 60 Oe. The first excitation pulse was at the frequency of contour shear mode $\omega_n = 340\ kHz$, had the length τ_1 = 20 μs and amplitude h_p = 330 mOe that corresponds to initial amplitude of a_{n0} = 0.17 that was used in theoretical calculations in the second chapter. Then 10 μs later the second pumping pulse at frequency $\omega_p = 3\omega_n$ was applied. The duration of this pumping pulse was τ = 370 μs and its amplitude was h_p = 9 Oe. To compensate nonlinear frequency shift of the mode, the pumping frequency was modulated by phase shift during the pulse according to the law (2.47) with Γ = 2.7, α = 0.024 and Q_n = 1000. The results of excitations are presented in the Figure 3.13. When the sample was excited with two subsequent pulses and the phase of the pumping

pulse was modulated by the selected law (2.47), the pumping frequency followed the nonlinear frequency shift of the eigenmode of the sample and an explosive amplification of the magnetoelastic oscillations was observed (curve (a)). At the same pumping but without modulation of the pumping pulse no amplification was observed (curve (b)). Only partial compensation of attenuation was possible. When the first pulse was not applied, no signal at the eigenfrequency was detected under the pumping neither with, nor without, modulation (curve (c)).

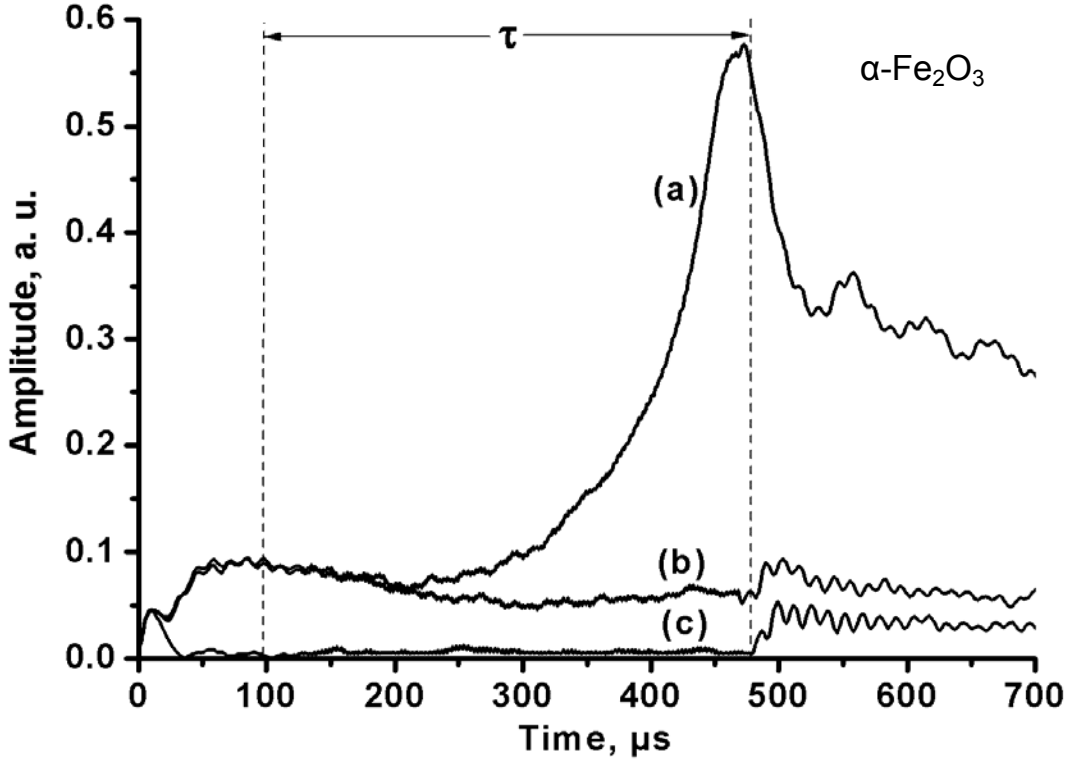

Figure 3.13. Experimental time dependence of amplitude of the eigenmode oscillations under electromagnetic pumping $\omega_p = 3\omega_n$ with (a) and without (b) frequency modulation; no signal at the frequency ω_n is detected in absence of initial excitation (c).

Such behavior of the system is one of the specific features of three-boson parametric coupling. The initial amplitude of excitation has to be strong enough to satisfy the threshold condition (2.28). That is why amplification of triads from the level of thermal quasi-phonons is impossible for realistic levels of pumping.

The parameters used in the experiment correspond to the ones used in theoretical modulation of three quasi-phonon process in hematite using anharmonicity model. Results of the modulation are presented in Figure 2.3 in the second chapter. Registered amplitude gain

was 7.5 dB, which is somewhat lower than the 10.8 dB gain that anharmonic model anticipated. Theoretically expected gain level was not achieved because with the increase of amplitude of the oscillations, contribution of higher orders nonlinearities also increases and they distort the process. These nonlinearities are not taken into account in anharmonicity model so they are not reflected in the modeling. A complete model of the process that considers higher order nonlinearities is discussed in the Fourth Chapter.

The amplitude behavior in the time region after the pumping is switched off reflects specificity of magnetoelastic relaxation of the crystal at a high level of excitation (as can be seen in the Figure 3.8, curve (5)). Increase of the eigenmode oscillations amplitude after the pumping had been turned off (Figure 3.13, curves (b) and (c)) took place because descending edge of the pumping pulse was a step function.

3.7 Magnetoelastic characteristics of $FeBO_3$ resonator

Unlike hematite, iron borate does not experience Morin transition and preserves easy plane antiferomagnetic ordering in low temperatures. Elastic subsystem characteristics and magneto-elastic coupling of the crystal strongly depend on the temperature. This dependence change the conditions of three quasi-phonon coupling. For this reason the studies on $FeBO_3$ resonator were performed at the temperature range 77 K – 293 K. For the experiments at 77 K the frame with the crystal was placed directly in liquid nitrogen. For the experiments in intermediary temperatures the frame was cooled down in nitrogen vapor with the help of cryogenic system form vibration magnetometer. The temperature of each measurement on iron borate is indicated in the text and in figure descriptions.

3.7.1 Spectrum of magnetoelastic coupled oscillations of iron borate resonator

Spectra of magnetoelastic oscillations of the $FeBO_3$ resonator in the frequency range 1 MHz – 4 MHz are presented in the Figure 3.14 at the temperatures of 293 K (top) and 77 K (bottom). The frequencies of the two most prominent resonance peaks are indicated in the legends. No magneto-elastic modes were found in the frequencies below 1 MHz. The frequency band of the spectrum has shifted compared to hematite as iron borate resonator is smaller in size and maximum sound velocity is higher in $FeBO_3$. The spectra were registered

in bias magnetic field H = 20 Oe that corresponds to the selected operating point for $FeBO_3$ at 293 K. Power of the input signal was -30 dBm. At 77 K resonance line of the first mode dramatically widens, decreasing mode's quality factor and making three quasi phonon excitations problematic, as discussed later in this chapter. That's why operating point for low temperature studies was selected at higher biasing field.

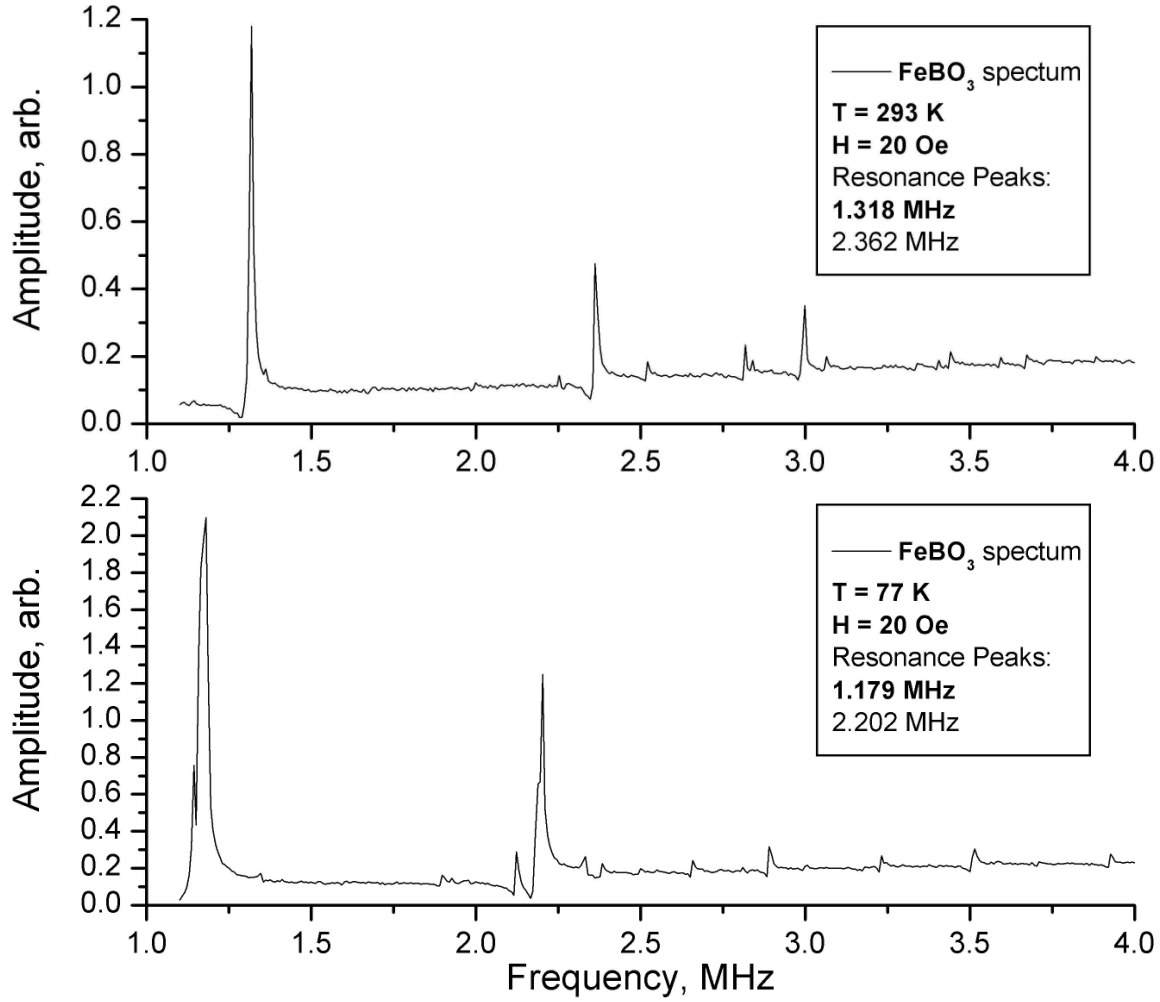

Figure 3.14. Spectra of magnetoelastic oscillations of $FeBO_3$ resonator in the bias magnetic fields H = 20 Oe at the temperatures of 293 K (top) and 77 K (bottom).

Numerical modeling of the iron borate resonator eigenmodes with the help of Comsole Multiphysics software showed that the magneto-acoustic mode found at the frequencies of 1.318 MHz at 293 K and 1.179 Mhz at 77 K is also a contour shear mode thus it was selected for further experimental research of three quasi-phonon coupling in iron borate at 293 K.

Spectra of magnetoelastic oscillations in iron borate at the biasing field H = 70 Oe are presented in the Figure 3.15 in the same scale as spectra in the Figure 3.14, at the temperatures of 293 K (top) and 77 K (bottom). Power of the input signal was -30 dBm. The spectra show that at this biasing field at 293 K magnetoelastic coupling coefficient decreases making the resonance amplitude too low for instability studies. However as the temperature is lowered the magnetoelastic coupling coefficient increases, improving the amplitude of the resonance.

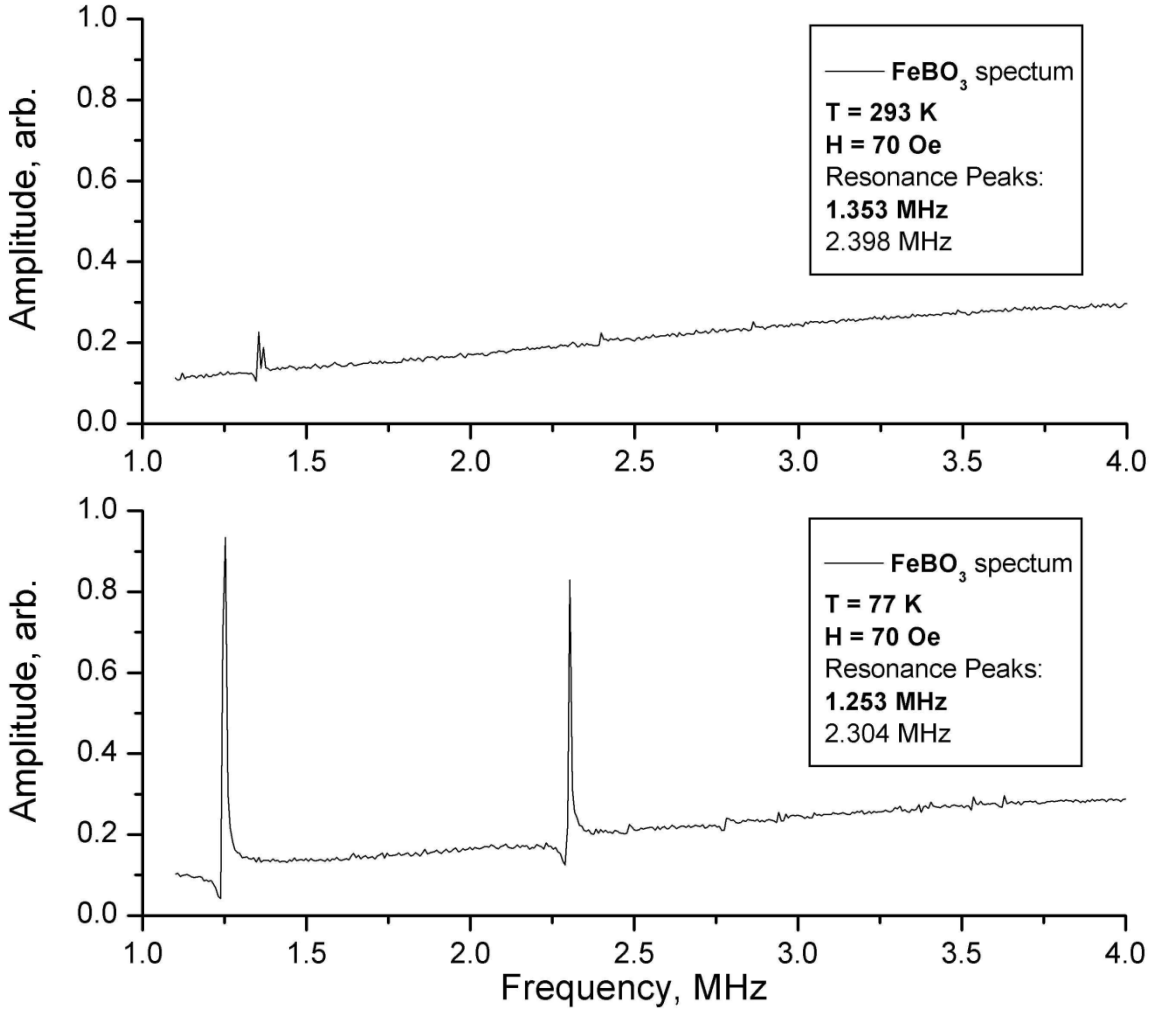

Figure 3.15. Spectra of magnetoelastic oscillations of $FeBO_3$ resonator in the bias magnetic fields H = 70 Oe at the temperatures of 293 K (top) and 77 K (bottom).

The width of the resonance line also decreases and the conditions become favorable for experiments quasi-phonon triads generation. The bias magnetic field H = 70 Oe was selected as operating point for $FeBO_3$ at 77 K. At low temperature and higher biasing field

most of the harmonics in the sample are suppressed making its spectrum cleaner which also benefits the studies by lowering the number of harmonics that are getting excited.

3.7.2 Dynamic properties of contour shear mode in $FeBO_3$

Dynamic parameters of iron borate resonator were determined by measuring the bias magnetic field dependences of the contour shear mode resonance frequency at different temperatures. Results of experimental measurements are presented in the Figure 3.16 with symbols at the temperatures of 293 K, 253 K, 227 K,197 K, 177 K, 137 K and 77 K.

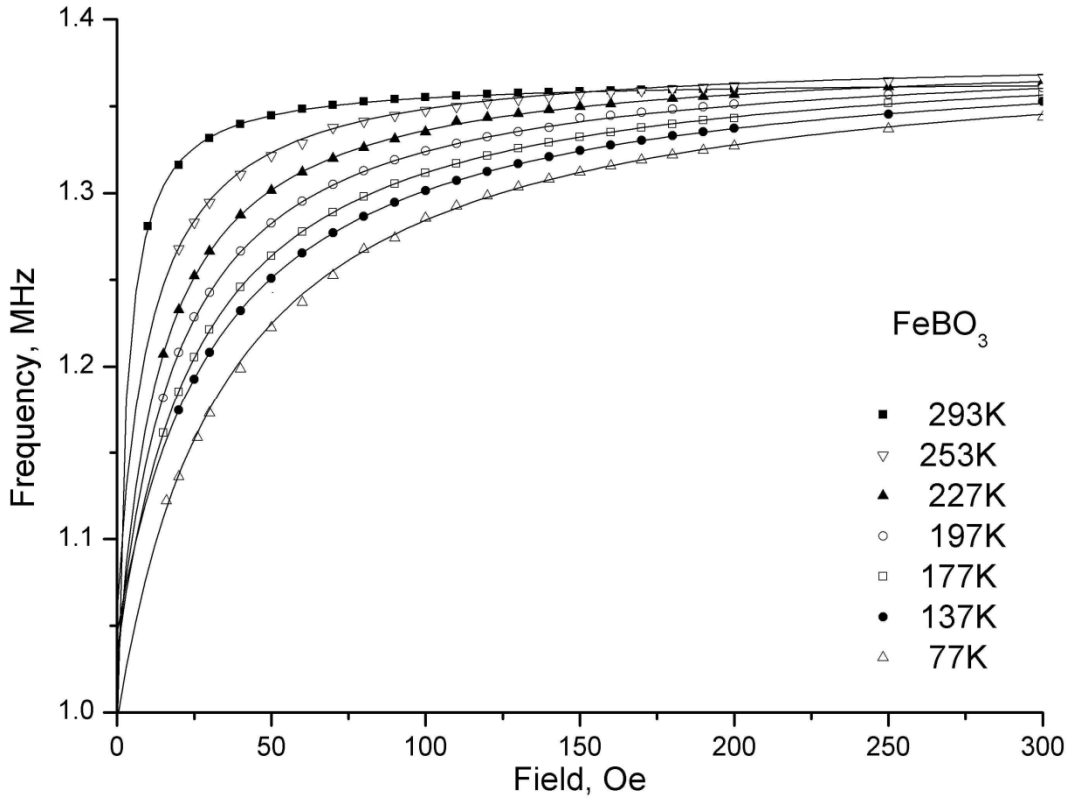

Figure. 3.16. Experimental (dots) and theoretically approximated (line) dependences of the contour shear mode eigenfrequency on bias magnetic field in iron borate resonator at different temperatures of 293 K, 253 K, 227 K,197 K, 177 K, 137 K and 77 K.

Registered frequency dependences differ as the values of magneto-elastic fields $H_{ms}^{(1,2)}(T)$ and saturated frequencies $\omega_{n0}(T)$ also depend on the temperature and thus magnetoelastic coupling coefficient $\zeta_n(H,T)$ changes.

As a result from the formula (3.3) the equation for contour shear mode frequency in iron borate resonator for different temperatures is:

$$\omega_n(H,T) = \omega_{n0}(T)\sqrt{1 - \frac{H_{ms}^{(1)}(T)}{H + H_{ms}^{(2)}(T)}} \tag{3.8}$$

Values of the fields $H_{ms}^{(1,2)}(T)$ and the frequencies $\omega_{n0}(T)$ for the samples were calculated by fitting the theoretical formula (3.8) on the experimental results for every temperature. The results of calculations are presented in Table 3.1. Theoretical curves of the mode frequency dependences at different temperatures are presented in the Figure 3.16 with solid lines.

Bias magnetic field dependences of magneto-elastic coupling coefficient for iron borate's contour shear mode at different temperatures were calculated with the help of formula (3.4) using corresponding values of magneto-elastic fields for every temperature. The results of calculations are presented in the Figure 3.17. The graph shows that at room temperature in the same bias field the value of magneto-elastic coupling coefficient of contour shear mode in iron borate resonator is much lower than it is in hematite.

Parameter\Temp	**293 K**	**253 K**	**227 K**	**197 K**	**177 K**	**137 K**	**77 K**
$\omega_{n0}/2\pi$, MHz	1.377	1.379	1.380	1.382	1.384	1.385	1.388
$H_{ms}^{(1)}$, Oe	1.7	4.9	7.4	10.1	13.2	16.1	26.6
$H_{ms}^{(2)}$, Oe	4.1	11.9	16.5	22.8	29.7	37.4	57.1

Table 3.1. The values of $H_{ms}^{(1,2)}$ and $\omega_{n0}(T)$ calculated for $FeBO_3$ resonator for different temperatures.

Small values of coupling coefficient forced to move the operating point for explosive instability research to lower biasing fields. In the bias fields below 20 Oe defects in the crystal and parasite harmonics affected resonance line shape and make it impossible to work in that region. Like with hematite, amplitudes of the mode oscillations were also taken into account. The spectra presented in the Figures 3.14 and 3.15 show that amplitude of oscillations decreases with the bias field increase.

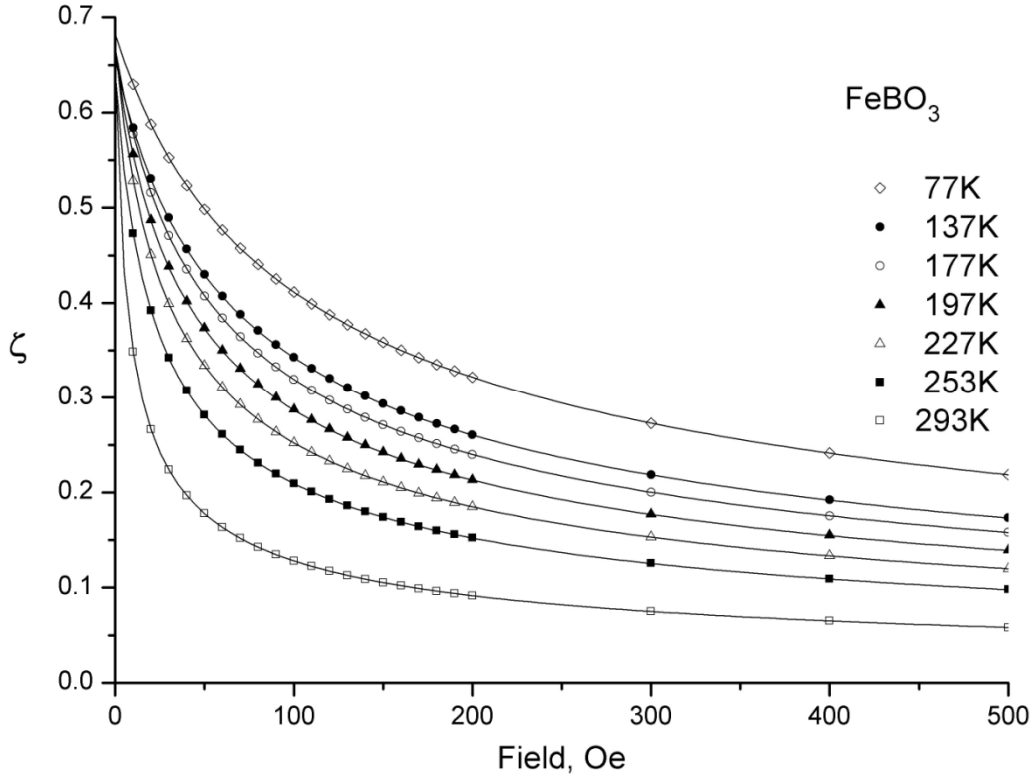

Figure. 3.17. Dependences of the contour shear mode magneto-elastic coupling coefficient on bias magnetic field H in iron borate resonator at different temperatures.

As a result of the measurements bias field H = 20 Oe was chosen as operating point for three phonon explosive instability research at room temperature. That corresponds to the value of magnetoelastic coupling coefficient of $\zeta_n = 0.24$. Since the amplitude of three quasi phonon interaction (2.17) is proportional to the ζ_n^6, such a dramatic drop of coupling compared to hematite increases the threshold values of the instability. Further examination of magnetoelastic spectrum of the sample at the bias field of 20 Oe revealed some parasite harmonics near the resonance mode and around double and triple frequencies. As it will be shown later in this chapter, these harmonics can get excited because of nonlinear frequency shift of the operating mode and affect the process. Results presented in the Figure 3.17 suggested that a better operating point for three-phonon explosive instability observation could be found at lower temperatures.

Decrease of the temperature enhances the eigenfrequency sensitivity to the bias field variation due to the increase of the coupling coefficient ζ. The growth of magnetoelastic

coupling also causes increase of magnetoelastic contribution to the energy dissipation processes in the sample thus lowering the acoustic quality factor as it is shown later in the chapter. As a result biasing field of H = 70 Oe was chosen as operating point for further experiments in liquid nitrogen temperatures that corresponds to a higher coupling coefficient of $\zeta = 0.46$.

3.7.3 Nonlinear frequency shift of the magneto-elastic mode

Iron borate resonator demonstrated behavior of a nonlinear oscillator with the frequency of mode depending on the amplitude of oscillations. Nonlinear frequency shift of contour shear resonance mode was measured the similar way as in hematite at two different temperatures of 293 K and 77 K. As the amplitude of mode oscillations increased, the form of resonance lines was getting distorted. Shapes of magnetoelastic resonance lines at different amplitudes of exciting magnetic field (Oe): (a) 0.1, (b) 1.0, (c) 1.7, (d) 2.0, (e) 2.7, (f) 3.0 in bias field H = 70 Oe, T = 77 K are presented in Figure 3.19.

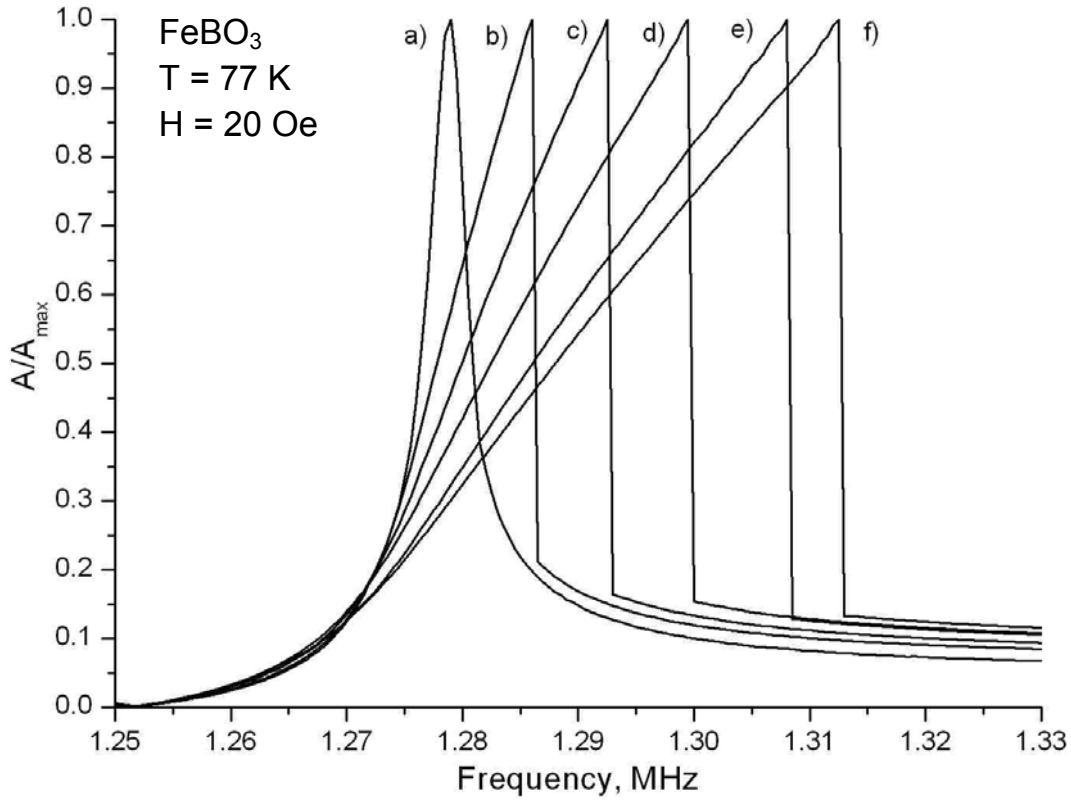

Figure. 3.19. Magnetoelastic resonance lines of contour shear mode in $FeBO_3$ crystal at different amplitudes of exciting magnetic field (Oe): (a) 0.1, (b) 1.0, (c) 1.7, (d) 2.0, (e) 2.7, (f) 3.0

in bias field H = 70 Oe, T = 77 K.

In higher biasing fields at a constant temperature nonlinear frequency shift decreases. It happens because of the decrease of the magnetoelastic coupling coefficient that lowers fourth order energy terms (3.5).

Experimental nonlinear frequency shift dependence at different biasing fields at room temperature is presented in Figure 3.20.

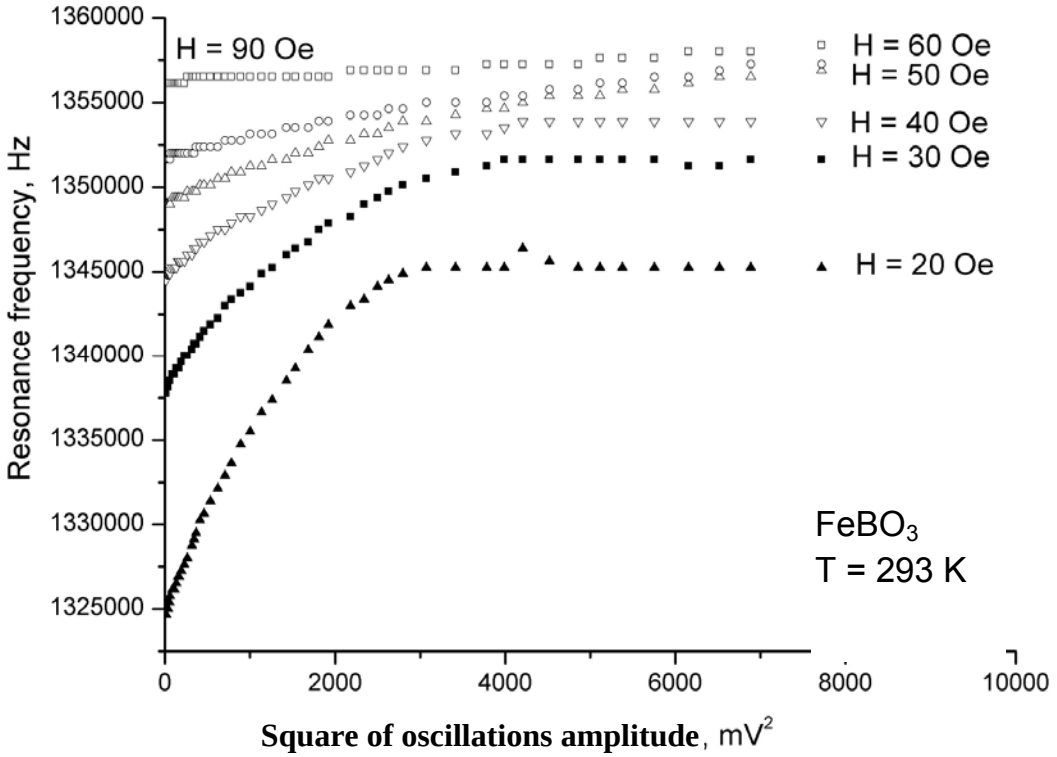

Figure 3.20. Nonlinear frequency shift of contour shear resonance frequency at different biasing fields H in $FeBO_3$ crystal at 293 K.

The Figure 3.21 shows dependence of the mode's resonance frequency on the square of oscillations amplitude at operating points at 293 K, H = 20 Oe and at 77K, H = 70 Oe. The room temperature dependence was registered at the bias field H = 20 Oe and the liquid nitrogen dependence was measured at the operating point H = 70 Oe.

At the room temperature at low oscillation levels the shift demonstrates near linear behavior. The maximum shift of resonator's frequency at 293 K was registered to be 21.6

kHz, or 1.6%. At this level the shift became saturated and further increase of excitation field was not changing the frequency of oscillations. At liquid nitrogen temperature nonlinear frequency shift was demonstrating near-linear behavior at the whole range of obtainable excitation levels. The dependence was not as steep as at room temperature operating point. The shift of the frequency at maximum amplitude was 34.3 kHz that corresponds to 2.7%.

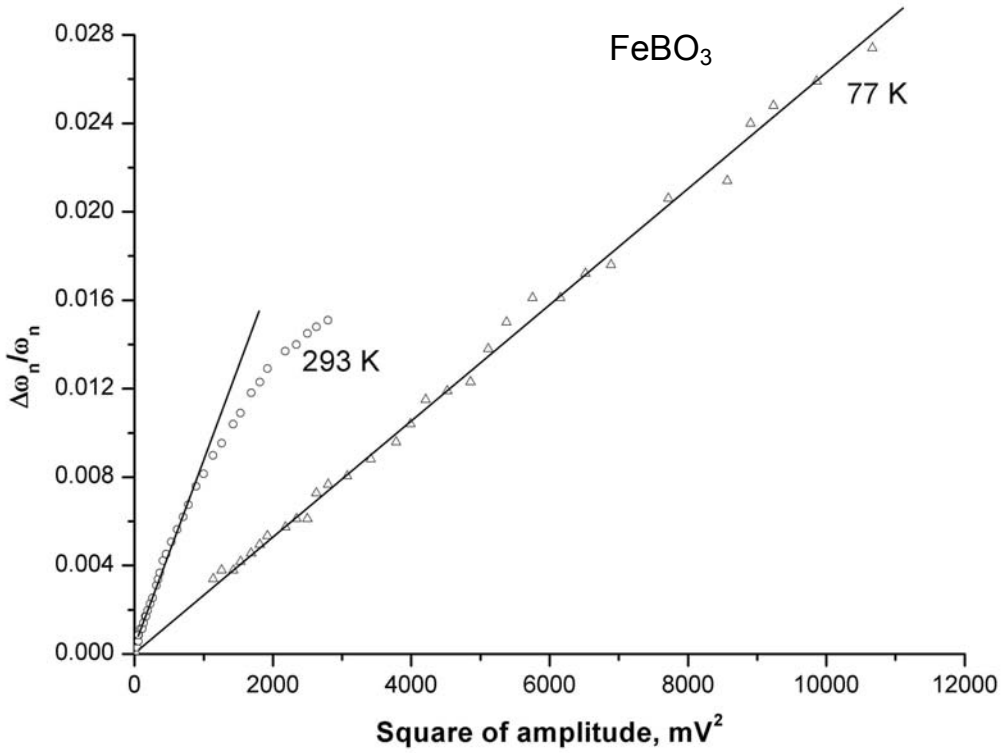

Figure 3.20. Nonlinear frequency shift dependences on the square of oscillations amplitude in $FeBO_3$ crystal at operating points at 293K and at 77K.

The reason for stronger dependence of the NFS on the vibration intensity at 293 K compared to the same dependence at 77K is that the magnetic moment of iron borate at 293K is 0.508 times smaller than at 77K. The difference in bias magnetic fields of room temperature and liquid nitrogen temperature operating points also changed the nonlinear frequency shift behavior. As a result the same output voltage induced on the receiving coil corresponds to much higher amplitude of elastic deformations and higher angular displacements of the magnetic moments. Thus it corresponds to stronger nonlinearity of the vibrations.

Square dependence of the nonlinear frequency shift on the amplitude of oscillations makes it logical to use the same frequency modulation law (2.47) that was suggested for hematite to compensate the cubic nonlinearity in iron borate during three quasi-phonon excitations.

The studies of nonlinear frequency shift of the resonances were performed only in the frequency sweep up mode, meaning it was changing from its minimum to maximum. If the results are compared with the sweep down data, the effect of acoustic bistability can be observed above certain threshold amplitude.

Bistability manifests itself as hysteresis-like dependence of the amplitude of resonator oscillations on the frequency so that two stable levels of amplitude are possible at the same exciting signal. Amplitude bistability is also accompanied by phase bistability that has the same threshold conditions. The effect was observed in hematite magnetoacoustic resonator earlier [104], as well as in the present research; it was thoroughly investigated [130].

In the present research acoustic bistability was also experimentally observed on iron borate magneto-elastic resonator. The boundary frequencies $f_{1,2}$ of bistability region can be defined as [130]:

$$f_{1,2} = \frac{2(f - f_0) \pm \sqrt{(f - f_0)^2 - 3(\Delta f)^2}}{3B}, \tag{3.9}$$

where f_0 is the resonance frequency in low-amplitude linear mode, Δf is the resonance curve width and B is nonlinear coefficient. The results of $FeBO_3$ nonlinear magnetoacoustic resonator excitations with different sweep directions are presented in the Figure 3.22.

Dependences were registered in the bias magnetic field H = 20 Oe at room temperature. Curve (a) corresponds to excitations with alternating magnetic field of h = 0.1 Oe in both sweep-up and sweep-down mode. The amplitude of oscillations was below bistability threshold so no hysteresis was observed.

When the resonator was excited with high alternating electromagnetic field (h = 3 Oe) that made oscillations amplitude exceed the threshold, bistability was observed when the sample was excited in sweep up mode (b) and sweep down mode (c).

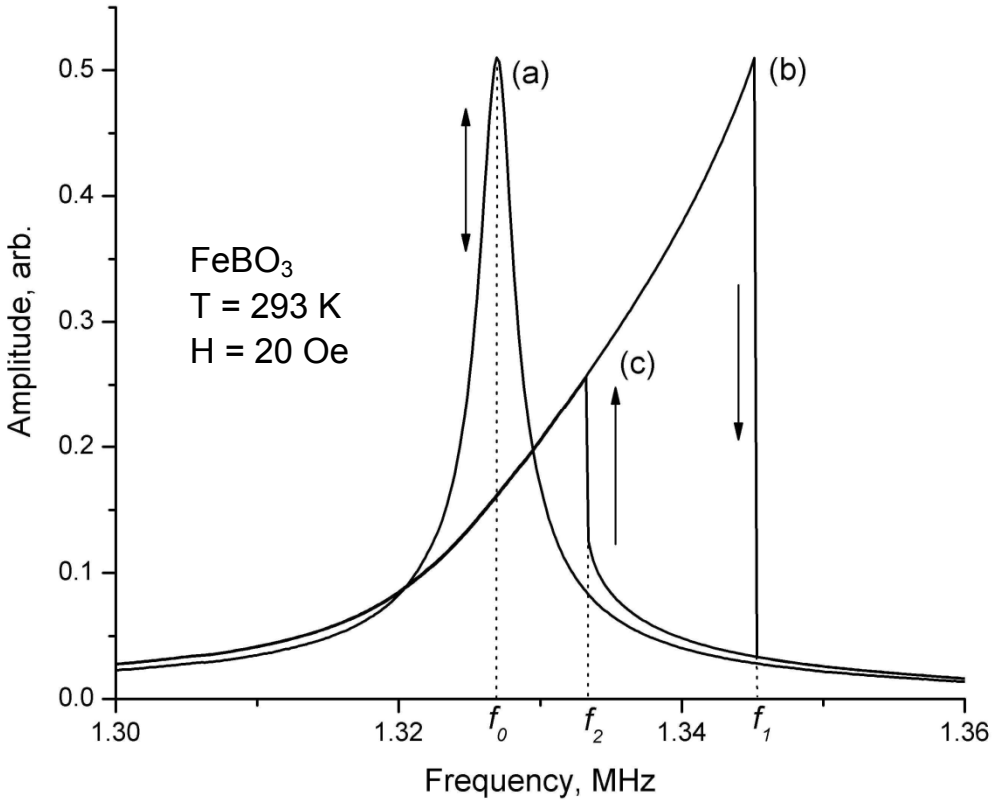

Figure 3.22. Bistability of iron borate resonator at 293 K. Below the threshold (a) no hysteresis is observed. In high amplitudes bistability manifests itself (b), (c).

3.7.4 Attenuation of contour shear mode oscillations in iron borate resonator

Quality factor of the contour shear mode of iron borate resonator in linear mode at room temperature operating point was calculated according to the formula (3.6) and was found to be $Q_n \approx 7 \cdot 10^2$. At higher oscillation amplitudes and lower temperatures the relaxation method was used to analyze free relaxation of the resonator and determine its quality factor.

The envelopes of free relaxation waveforms of iron hematite crystal at 293 K and at bias field $H = 20$ Oe are presented in the Figure 3.23.

Similar to the measurements on hematite, iron borate resonator was excited with a short pulse $\tau = 10\,\mu s$ of different amplitude at the resonance mode frequency $\omega = \omega_n$ with a pumping coil, and free relaxation oscillations of the sample were recorded with detection coil. When the resonator was excited with a strong pulse, it was oscillating with wobbles.

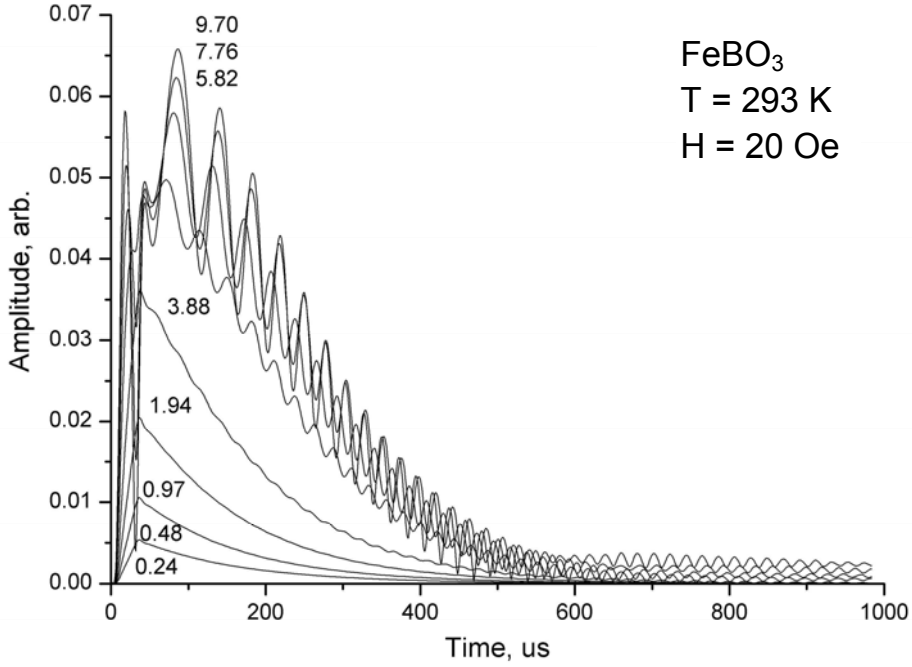

Figure. 3.23. Envelopes of free relaxation oscillations of iron borate resonator magneto-elastic oscillations after pulse excitation at the eigenfrequency ω_n = 1.350 kHz with different amplitudes of 0.24 – 5.82 Oe at T = 293 K.

At high oscillation amplitudes due to nonlinear frequency shift the contour shear resonance mode found at the frequency 1.315 MHz was also exciting another harmonic at the frequency 1.365 MHz. Fast Fourier transform of the captured relaxation waveform after 9.7 Oe pulse excitation is presented in Figure 3.24. Two resonance peaks can be clearly seen.

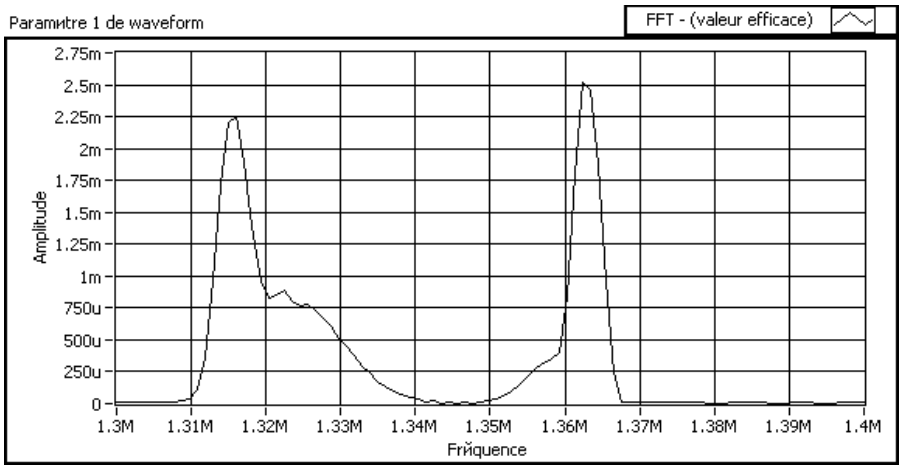

Figure. 3.24. Fast Fourier transform of the obtained free relaxation waveform of iron borate resonator after sinusoidal burst excitation with h = 9.7 Oe.

The quality factor of the resonator for different pumping amplitudes was calculated with the help of formula (3.7) and appeared to be $Q_n \approx$ 645-710 for different excitation amplitudes. Thus the quality factor of the iron borate contour shear resonance mode at room temperature operating point for further calculations was taken as $Q_n \approx 7 \cdot 10^2$. Similar envelopes of free relaxation waveforms of iron borate resonator at the low temperature T = 77 K are presented in Figure 3.25.

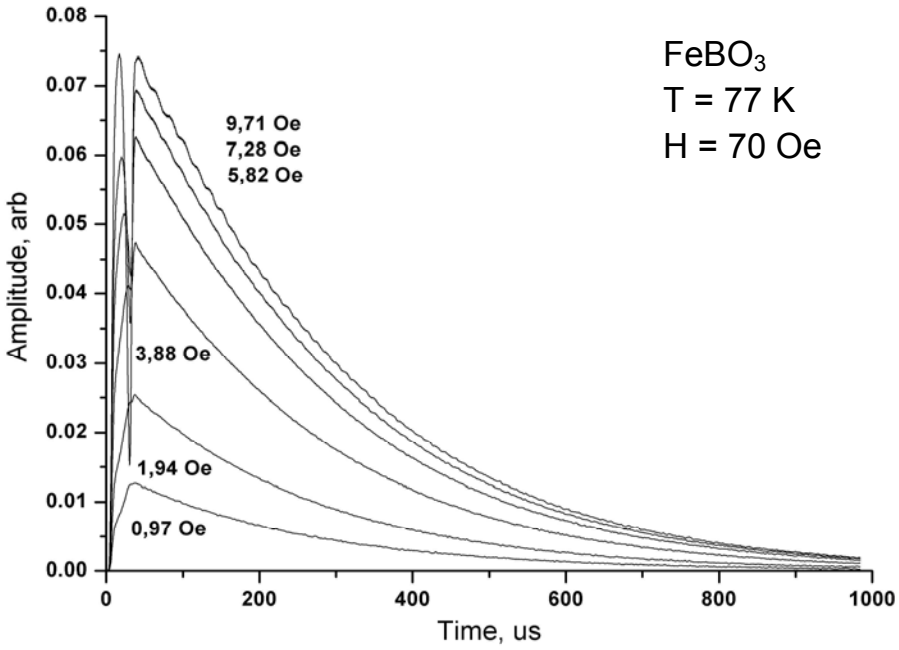

Figure. 3.25. Envelopes of free relaxation oscillations of iron borate resonator after pulse excitation at the eigenfrequency ω_n = 1.270 kHz with different amplitudes 0.97 Oe – 9.71 Oe at T = 77 K.

They were captured at corresponding operating point with biasing H = 70 Oe. At low temperature operating point most of the parasite harmonics are suppressed with higher constant field, so even at high excitation amplitudes the resonator was attenuating practically without wobbles. The quality factor was measured to be $Q_n \approx 940 - 1030$. The quality factor of the iron borate contour shear resonance mode at liquid nitrogen temperature was taken as $Q_n \approx 10^3$ for further numerical modeling.

3.7.5 Peculiarities of low temperature dynamics of $FeBO_3$ resonator

In solids decrease of the temperature lowers purely elastic subsystem contributions to dissipation and usually increases quality factor. However it was shown that in iron borate magnetoelastic coupling increases with the temperature drop. This increase augments dissipation of oscillations in magnetic system lowering total quality factor of the resonator. For the contour shear mode the quality factor at 293K and bias field H = 20 Oe was measured to be $Q = 7 \cdot 10^2$, but at 77 K it dropped down to $Q = 10^2$ in the same field. Such a dramatic decrease makes problematic the supercritical coupling of three quasi-phonons. Only at the bias field H = 70 Oe the quality factor of $Q = 10^3$ was compatible with the high enough coupling coefficient equal to $\zeta = 0.45$ so this biasing was selected as operating point at 77 K.

Experimentally measured dependences of the attenuation coefficient Q^{-1} on the bias field for different temperatures are presented in the Figure 3.26. This figure demonstrates behavior of the attenuation in lower fields. Behavior of the attenuation at higher fields is presented in Figure 3.27 as bias field dependences of quality factor Q at different temperatures.

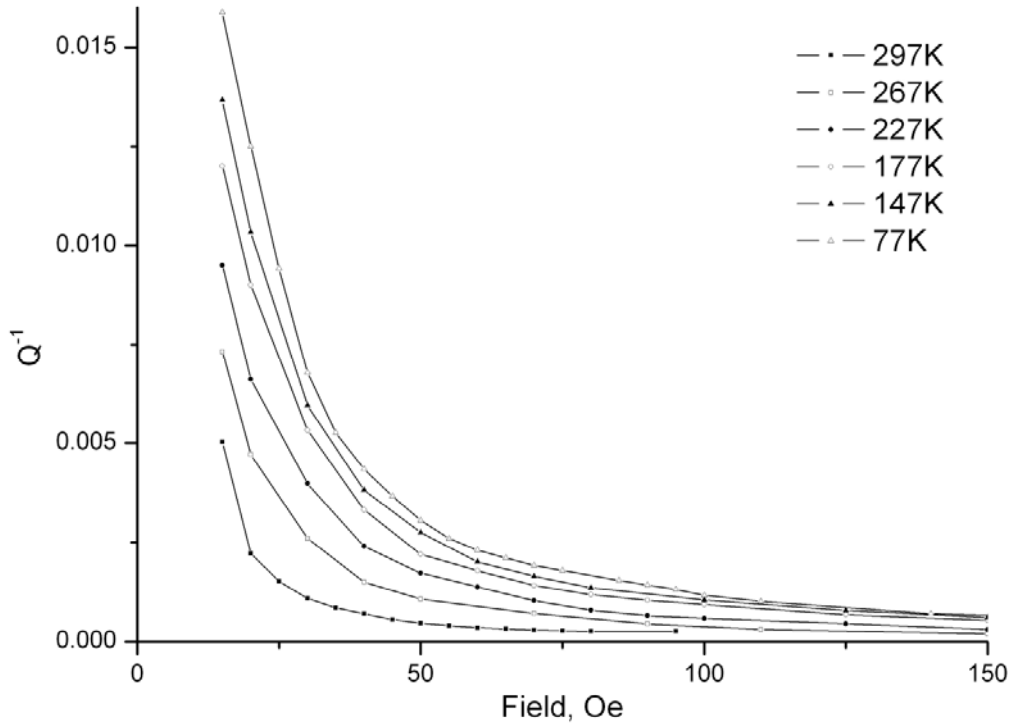

Figure 3.26. Dependences of attenuation coefficient of magneto-elastic mode on bias field H in $FeBO_3$ crystal at different temperatures 77 K – 293 K.

Bias field dependencies of contour shear mode attenuation were measured with the help of free relaxation method. Resonator was excited with the mode's resonance frequency and quality factor was determined analyzing the acquired attenuation waveform. Resonance frequency of excitation pulse at selected bias field and temperature was set according to the measurements presented in the Figure 3.16.

Figures 3.26 and 3.27 show that with the temperature decrease at the same bias field the quality factor was also decreasing dramatically.

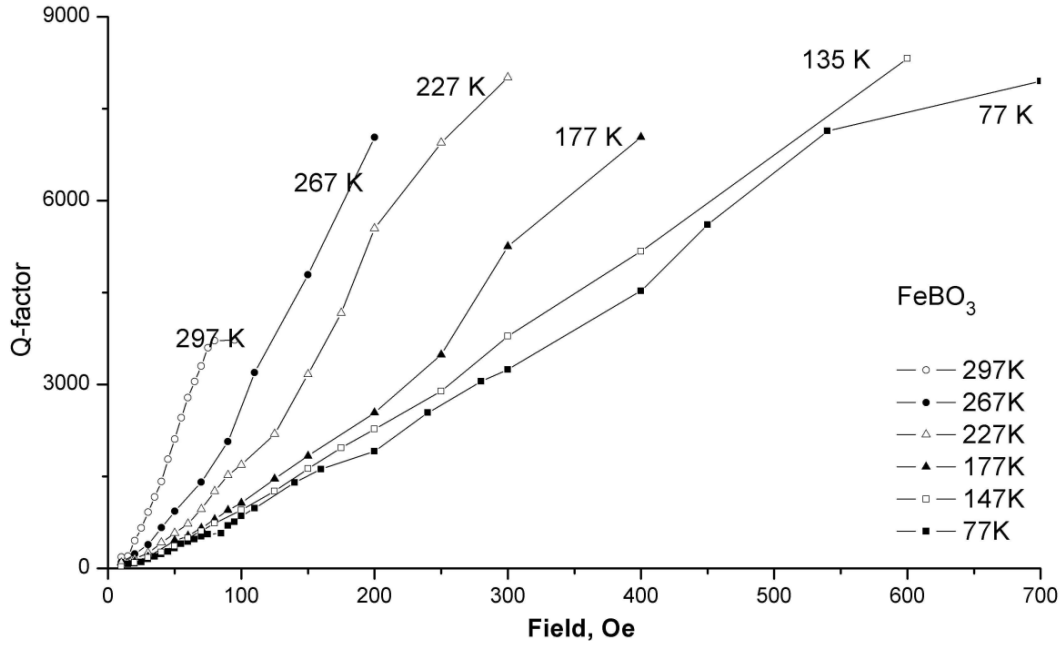

Figure 3.27. Dependences of the quality factor of magneto-elastic mode on bias field H in $FeBO_3$ crystal at different temperatures 77 K – 293 K.

In higher biasing fields the oscillations were getting suppresses due to the decrease of magnetoelastic coupling. In Figure 3.27 the dependences for each temperature stop at corresponding points where resonance oscillations were too weak to be measured. The lower was the temperature, the higher was the limit of bias field for the resonance observation.

Experimental dependence of the attenuation coefficient Q^{-1} on the magnetoelastic coupling at different temperatures is presented in the Figure 3.28 with symbols. It was reconstructed from the data of Figures 3.26 and 3.16. There are two main contributions to the dissipation in nonlinear magnetoelastic crystal that are caused by the magnetoelastic coupling. The first contribution comes from the dissipations in the magnetic subsystem of the crystal

and is proportional to ζ^4. It can be presented as $B(T)\zeta^4$ where $B(T)$ is proportionality coefficient that depends on the temperature. The second contribution comes from the dislocations resulting from non-ideal structure of the crystal and it is proportional to ζ^8 [131] and can be similarly presented as $C(T)\zeta^8$. There is also a pure elastic subsystem contribution that does not depend on the magnetoelastic coupling coefficient but has strong temperature dependence and can be presented as $A(T)$. Hence the dissipation coefficient of magnetoelastic resonator Q^{-1} can be approximated with the help of the following equation:

$$Q^{-1} = A(T) + B(T)\zeta^4 + C(T)\zeta^8 \tag{3.10}$$

The results of theoretical approximations with the help of formula (3.10) at the temperatures 77 K – 293 K are presented in the Figure 3.28 with solid lines. Proportionality coefficients are presented in the figure legend.

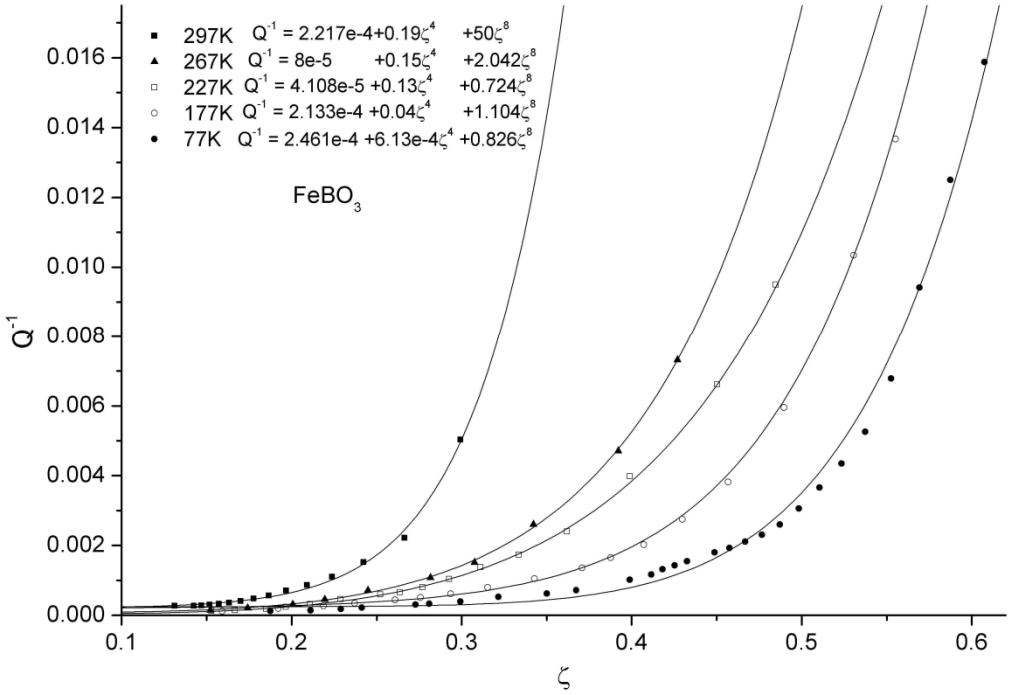

Figure 3.28. Experimental (symbols) and theoretical (lines) dependences of attenuation of magneto-elastic mode in $FeBO_3$ crystal on the magneto-elastic coupling coefficient at different temperatures 77 K – 293 K.

Theoretical fittings demonstrate good agreement with experimentally obtained results. Contribution to dissipations that is introduced by the magnetic subsystem represented by the

coefficient *B* steadily decreases with the temperature, while dislocations contribution above 293 K presents close values.

3.8 Supercritical single mode three quasi-phonon excitations in $FeBO_3$

Similar technique described for hematite was used to study supercritical behavior of three quasi-phonon coupling in iron borate. The sample was excited with two subsequent electromagnetic pulses applied to the one of the crossed coils. Geometry of the experiment was as presented in the Figure 3.9. Amplitudes of the first and second pulses were selected high enough to exceed the threshold of instability (2.26) for iron borate. Oscillation waveforms were acquired with the help of oscilloscope connected to the receiving coil. The obtained data were filtered to select the signal in the frequency band between 1.3 MHz and 1.4 MHz for the experiments at 293 K. For low temperature experiments the frame with the sample was placed in liquid nitrogen. As the temperature shifted the resonance frequency, data obtained at 77 K were filtered in the frequency band 1.2 MHz – 1.3 MHz. The results of experimental studies at 293 K are presented in Figure 3.29.

The parameters for observation of three quasi-phonon explosive instability at room temperature were used as following: the first pulse frequency was $\omega_n /2\pi$= 1.322 MHz with duration τ_1 = 25 μs and amplitude h_0 = 0.9 Oe. For the second pulse at the beginning the frequency was equal to $\omega_{p0} = 3\omega_n$ and then it was modulated with the proposed law (2.47) with the following parameters: Q_n = 700, Γ = 1.5, α = 0.012. Duration of the second (pumping) pulse was τ_2 = 220 μs and the amplitude of pumping field was h_p = 15 Oe. Acquired envelope of the explosive development of three quasi-phonon process is presented on Figure 3.29 (a). Explosive growth of the oscillations amplitude is limited by the nonlinearities of higher orders. Registered amplitude gain was 7.5 dB. The beats that are observed after the end of the second pulse during relaxation process were caused by interaction of the selected mode with another one found at the frequency 1.361 MHz.

The latter one was getting excited due to NFS of the selected mode at high amplitude of oscillations. When the sample was excited by the same two pulses, but the frequency of the second pulse remained constant $\omega_{p0}/2\pi$=3.966 MHz throughout the pulse, no explosive

amplification was observed (Figure 3.29 (b)). If the second pumping pulse was not applied the sample was relaxing as a resonator with quality factor Q=700 (Figure 3.29 (c)). As can be seen on Figure 3.29 (d), if the first pulse was not applied no amplification was observed at all because the system was in the sub threshold state. A small rise of oscillations amplitude at the end of pumping pulse can be observed due to step-like falling edge of the pumping pulse.

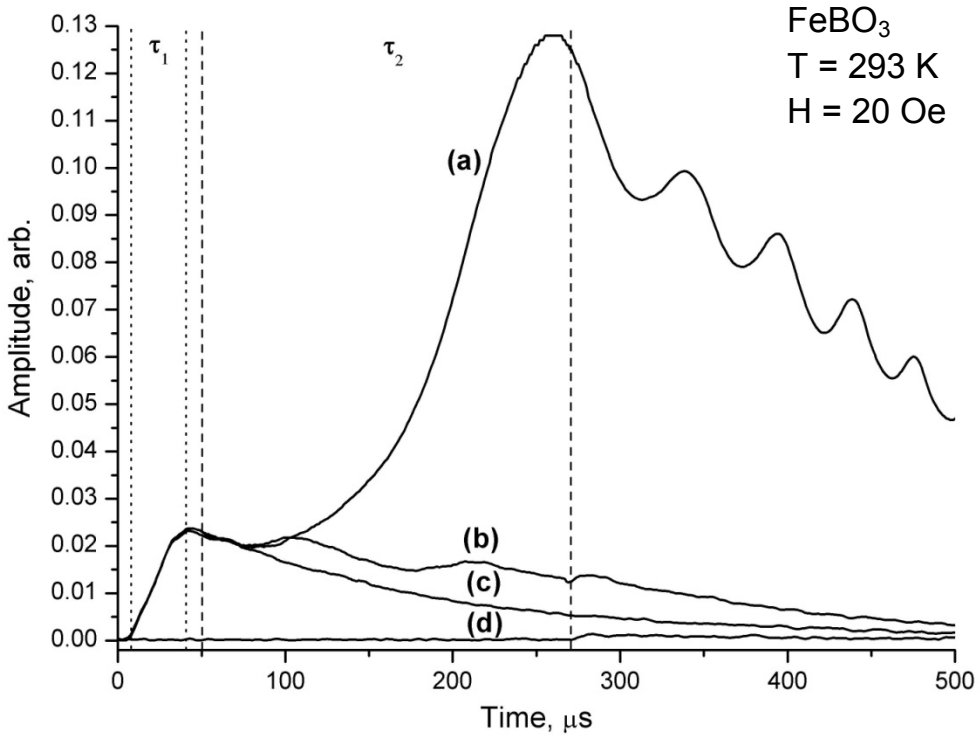

Figure 3.29. Experimental time dependences of amplitude of magneto-elastic oscillations under electromagnetic pumping in $FeBO_3$ crystal at 293K: (a) with pumping frequency modulation (h_p=15 Oe) (b) without frequency modulation (h_p=15 Oe) (c) without applied pumping (h_p=0), (d) without initial pulse (a_{n0}=0); τ_1 and τ_2 are the durations of initial exciting pulse and pumping pulse respectively.

The supercritical behavior of magnetoelastic excitations at low temperatures 77 K was studied when the sample was placed in a chamber filled with liquid nitrogen. The following parameters were used to observe three quasi-phonon explosive instability in this case: first pulse frequency $\omega_n/2\pi$ = 1.272 MHz, duration τ_1 = 25 μs and amplitude h_0 = 1.3 Oe. For the second pulse starting frequency was $\omega_{p0}/2\pi$= 3.816 MHz, duration of the pumping pulse was τ_2 = 150 μs and the amplitude was h_p = 20 Oe. Acquired envelope of the explosive three quasi-phonon process is presented in Figure 3.30 (a). Registered amplitude gain at 77 K was 5.5 dB. The pumping pulse was modulated with the law (2.47) with the following parameters:

Q_n = 1000, Γ = 2.2, α = 0.003. When the sample was excited by the same two pulses, but the frequency of the second pulse remained constant $\omega_{p0}/2\pi$ = 3.816 MHz throughout the pulse, no explosive amplification was observed as shown in Figure 3.30 (b).

Magnetoelastic relaxation process, when the sample was only excited with the first pulse and the second pumping pulse was not applied, is presented on Figure 3.30 (c). If the first pulse was not applied, no excitation was observed even with frequency modulated second pulse as can be seen on Figure 3.30 (d).

The main difference between explosive dynamics at 293K and 77K is manifested in values of the time interval of development of explosion equals to 220 μs and 160 μs respectively and in the gain that is two times higher at 293K. The ratio of the pumping and the bias fields used in the experiment at 77K was smaller compared to the one used at room temperature. Nevertheless the rising and saturation times of supercritical excitations are notably shorter at 77K than at 293K because of stronger magneto-elastic coupling and higher supercriticality parameter at low temperature

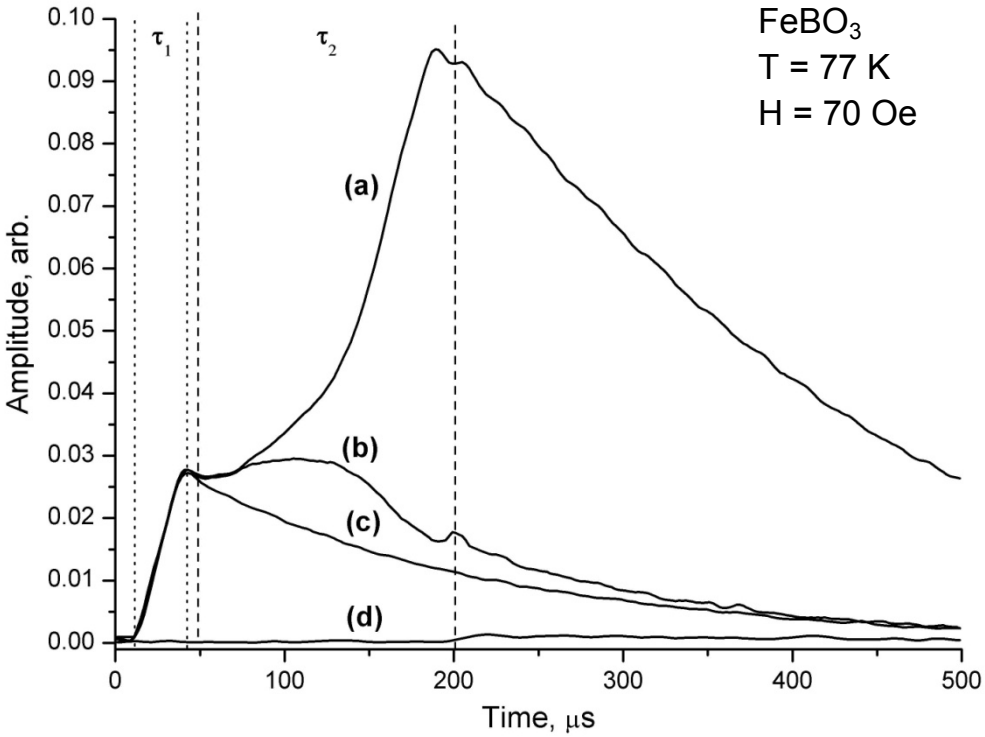

Figure 3.30. Experimental time dependences of the amplitude of magneto-elastic oscillations under electromagnetic pumping in $FeBO_3$ crystal at 77K. (a) with pumping frequency modulation (h_p=20 Oe), (b) without frequency modulation (h_p=20 Oe) (c) without applied pumping (h_p=0), (d) without initial pulse (a_{n0}=0); τ_1 and τ_2 are the durations of initial exciting pulse and pumping pulse respectively.

Stronger low-temperature coupling coefficient favors higher amplitude gains at stronger pumping fields. The results of three quasi-phonon excitations with pumping field of h_p = 40 Oe are presented in the Figure 3.31. Initial oscillations pulse was applied at the frequency $\omega_n/2\pi$ = 1.272 MHz, had duration τ_1 = 25 μs and amplitude h_0 = 1.5 Oe. For the pumping pulse, starting frequency was $\omega_{p0}/2\pi$= 3.816 MHz and frequency modulation parameters were: Q_n = 1100, Γ = 2.5, α = 0.012. Duration of the pumping pulse was τ_2 = 110 μs. Acquired envelope of the explosive development of three quasi-phonon process under phase-modulated pumping that is presented in Figure 3.31 (a) demonstrates amplitude gain of 7.9 dB. No explosive amplification was observed without phase modulation (Figure 3.31 (b)) and no three quasi-phonon coupling was registered without initial excitation pulse no explosive amplification was observed (Figure 3.31 (d)). Free oscillations of the resonator after initial excitation pulse without pumping pulse are presented in Figure 3.31 (c).

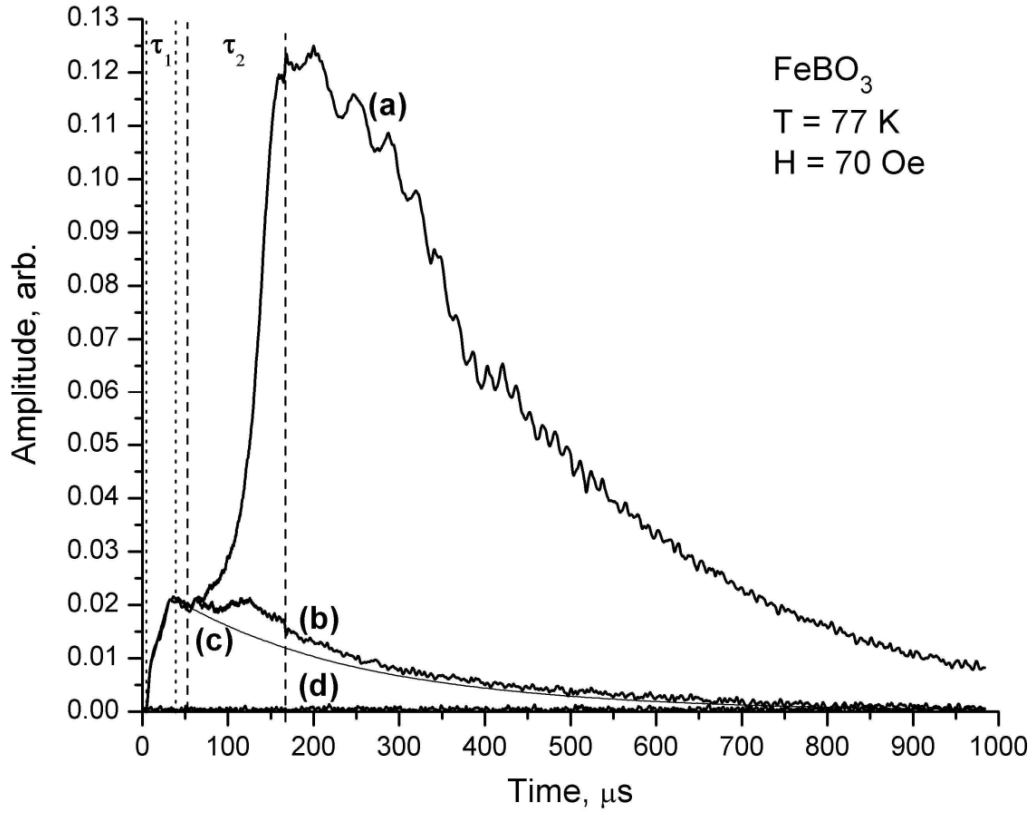

Figure 3.31. Experimental time dependences of amplitude of magneto-elastic oscillations under electromagnetic pumping in $FeBO_3$ crystal at 77K. (a) with pumping frequency modulation (h_p=40 Oe), (b) without frequency modulation (h_p=40 Oe) (c) without applied pumping (h_p=0), (d) without initial pulse (a_{n0}=0); τ_1 and τ_2 are the durations of initial exciting pulse and pumping pulse respectively.

Logarithmic representation of the oscillations amplitude evolution from the Figure 3.31 (a) and (c) is presented in the Figure 3.32 with corresponding curves (a) and (c). The graph (a) shows amplitude behavior under phase-modulated pumping and curve (c) presents amplitude behavior in the absence of pumping pulse. During the pumping pulse τ_2 oscillations amplitude demonstrates explosive behavior with faster-than-linear growth. This behavior is one of the key differences of three quasi-phonon processes and conventional parametric instabilities of quasi-phonon pairs, where amplitude growth would be linear in the logarithmic plot. Exponential relaxation plot (c) is presented for comparison showing linear logarithmic amplitude decay.

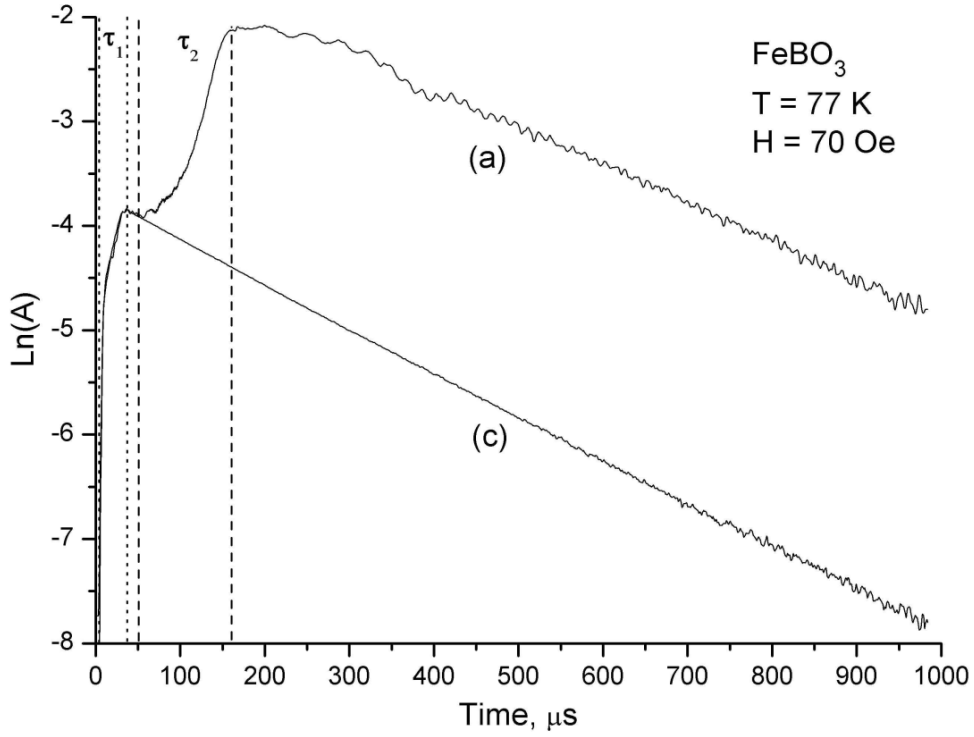

Figure 3.32. Logarithmic representation of the experimental amplitude evolution of magneto-elastic oscillations under electromagnetic pumping in $FeBO_3$ crystal at 77K. (a) with pumping frequency modulation (h_p=40 Oe), (c) without applied pumping (h_p=0), τ_1 and τ_2 are the durations of initial exciting pulse and pumping pulse respectively.

3.9 Chapter III conclusion

For the first time supercritical parametric amplification of coupled triads of magneto-elastic waves in single mode regime was experimentally studied. Investigation was performed in two AFEP single crystal resonators with different magnetoelastic properties: α-Fe_2O_3 and $FeBO_3$. The studies on hematite were performed at room temperature and on iron borate they were performed at the temperature range 77 K - 293 K. New experimental method has been developed that allows arbitrary pumping pulse frequency modulation and continuous amplitude monitoring of magnetoelastic oscillations under electromagnetic pumping.

Study of the nonlinear frequency shift of contour shear mode in $FeBO_3$ resonator showed linear dependence of the sample oscillations on the intensity. It made possible application of a similar pumping pulse phase modulations law that was used for hematite. When the law was applied with iron borate resonator parameters, nonlinear frequency shift was compensated and explosive behavior of the instability was observed. Explosive amplification of quasi-phonons in $FeBO_3$ at low temperatures was also registered but required optimal choice of the bias magnetization allowing compromise between strong enough magnetoelastic interaction and magnetic contribution to the absorption of elastic excitations.

Operating points for the instability research and cubic nonlinearity compensation laws were selected based on the results obtained from research of magnetoelastic characteristics of the resonators. The law of modulation for hematite was chosen based on the fact that nonlinear frequency shift of contour shear mode in hematite has a square dependence on the amplitude of the oscillations. Obtained results correlate with theoretical analysis of the process presented in the second chapter. The instability threshold condition depends on pumping amplitude as well as on the intensity of initial excitation and the amplification of triads develops as an explosive instability. The supercritical gain is limited in the beginning of the amplification process by nonlinear frequency shift of quasi-phonons. When this mechanism of limitation is compensated by the proper phase modulation of transverse pumping field the further limitations are determined by the high order nonlinearities of magneto-elastic system.

Anharmonic model does not take into account higher order nonlinearities so amplitude gains predicted by the model in the Second Chapter did not completely correlate with experimental results at high amplitudes for hematite. The magneto-elastic coupling

coefficient of iron borate crystal at room temperature was relatively small, so achievement of supercritical mode required high enough initial amplitude of deformations (bigger than spontaneous magnetostriction) and pumping of the same order of value as the bias magnetic field. In such conditions anharmonic model presented in the second chapter cannot be applied and strongly nonlinear model had to be developed. Strongly nonlinear model of three quasi-phonon excitations is developed and analyzed in the Fourth Chapter.

Chapter IV

Strongly Nonlinear Model of Three Quasi-Phonon Excitations in AFEPs. Numerical Simulations

4.1 Chapter IV introduction

Anharmonic approximation presented in the Second Chapter describes the process of three quasi-phonon excitations up to the fourth order terms. The model clearly shows contributions of each term to the energy of the system and allows deep analysis of the limitations of explosive instability. However as the amplitude of magnetoelastic oscillations increases, the nonlinearities that are beyond anharmonic approximation start affecting the process. As a result, theoretically predicted levels of amplification are not reached. Theoretical modeling of the explosive instability with anharmonic approximation for hematite resonator anticipates amplitude gain of about 10.8 dB but experimental results show an amplification of only 8.5 dB. Experimental pumping fields for supercritical three quasi-phonon excitations in iron borate were of the same order of value as the bias magnetic field leading to even stronger contributions of nonlinearities of higher orders. Theoretical description of the resonator description at high amplitudes of magnetic oscillations requires development of a complete theoretical model of three quasi-phonon supercritical excitations in magnetoelastic resonator that would take into account magnetoelastic nonlinearities of higher orders.

In the Fourth Chapter strongly nonlinear model of three quasi-phonon supercritical excitations in magnetoelastic resonator is developed. It takes into account magneto-elastic nonlinearities that are beyond anharmonic approximations. Supercritical behavior of hematite and iron borate resonators in three quasi-phonon excitations process is modeled with the help of strongly nonlinear theory. Obtained results are compared with the solutions based on anharmonic approximation and experimental data. Comparison shows that developed model describes three quasi-phonon excitations with sufficient precision proving validity of developed theory.

4.2 Strongly nonlinear model of three quasi-phonon excitations in a magnetoelastic AFEP resonator

Magnetoelastic oscillations in an antiferromagnet in two sublattices model in general case can be described phenomenologically with a following system of coupled nonlinear

equations of precession of the sublattices' magnetization vectors M_1 and M_2 and elasticity equations:

$$-\gamma^{-1}\dot{M}_n = [M_n H_n], \qquad (n = 1, 2);$$
$$\rho\ddot{U}_i = \frac{\partial \sigma_{ij}}{\partial x_j}, \qquad (i, j = 1, 2, 3), \tag{4.1}$$

where $H = -\delta\int FdV / \delta M_n$ is the effective field acting on the n^{th} sublattice, U_i is displacement vector, $\sigma_{ij} = \delta F / \delta\left(\partial U_i / \partial x_j\right)$ is the tensor of mechanical stress and F is crystal energy density.

In high temperature antiferromagnets exchange field H_E is much bigger than Dzyaloshinsky field H_D, magnetic anisotropy field H_A and external field H (for hematite $H_E \approx 10^7$ Oe, $H_D \approx 2 \cdot 10^4$ Oe, $H_A \approx 2 \cdot 10^2$ Oe) which helps to simplify significantly the equations approximating H, $H_{D,A}/H_E << 1$ and the system of equations can be brought to only one motion equation of the antiferromagnetic vector l [113].

For the ultrasound frequency oscillations that are much lower than the frequency of antiferromagnetic branch activation $\omega << \omega_{a0} = \gamma\sqrt{2H_E H_A + H_D(H + H_D)}$ and generally weak magnetostriction fields $H_{me} << H_A$ oscillations of the antiferromagnetic vector outside of the basal plane can be neglected, so $l_z \approx 0$. Following the strong nonlinear model of AFEP low frequency dynamics described in [88] the system of the precession equations can be brought to an equation of oscillation motion of only the antiferromagnetic vector l:

$$\gamma^{-2}\left[l\left(\ddot{l} - v_s^2\nabla^2 l\right)\right]_z = (Hl)([Hl]_z + H_D) + 2H_E[lH_{me}]_z + \gamma^{-1}\dot{H}_z \tag{4.2}$$

With the module of the antiferromagnetic vector being a constant $| l | = 1$, the only dynamic variable in the equation (4.2) is the angle φ between the antiferromagnetic vector $l = (M_1 - M_2)/2M_0$ and external magnetization field H in the basal plane. Following the Second Chapter a homogenous in-plane alternating pumping field $h_\perp(t) = h_p \cos(3\omega_n t + \psi(t))$ is applied in the basal plane perpendicular to bias magnetic field H to excite three wave coupling. The phase of the field oscillations is modulated by the law (2.47) to compensate cubic nonlinearity effect in the system. The new variable allows

presenting the free energy of long wave spin excitations F_m and magnetoelastic interaction F_{me} as:

$$F_m = -\frac{M_0}{2H_E}(H_D + H\cos\varphi + h_\perp \sin\varphi)^2 \tag{4.3}$$

$$F_{me} = \left(\hat{B}_1 cos2\varphi + \hat{B}_2 sin2\varphi\right)\hat{u} \tag{4.4}$$

where $\hat{B}_1$ and $\hat{B}_2$ are the tensors of magnetoelastic constants. Their convolutions with deformation tensor are given by:

$$\begin{aligned} \hat{B}_1\hat{u} &= -\frac{1}{2}(B_{11} - B_{12})\left(u_{xx} - u_{yy}\right) - B_{14}u_{yz} \\ \hat{B}_2\hat{u} &= -(B_{11} - B_{12})u_{xy} - 2B_{14}u_{xz} \end{aligned} \tag{4.5}$$

The elastic energy can be presented as:

$$F_e = \frac{1}{2}\hat{C}^{(2)}\hat{u}^2 \tag{4.6}$$

For frequencies much smaller than quasiferromagnetic resonance frequency $\omega << \omega_{f0} = \gamma\sqrt{H(H+H_D)+2H_E H_{ms}}$ The magnetic variable $\varphi = \varphi\,(\hat{u}, h_\perp(t))$ can be found as a solution of quasi-static equation:

$$\frac{\partial(F_m + F_{me})}{\partial\varphi} = 0 \tag{4.7}$$

Following reference [140] elastic deformations can be presented as a superposition of quasi-phonon modes: $\hat{u}(r,t) = \sum A_n(t)\hat{u}_n(r)$. As a result the potential energy of vibrations can be expressed as:

$$F = \sum_n \left(\frac{1}{2}M_n\omega_{n0}^2 A_n^2 + A_n \int d\vec{r}\left(\hat{B}_2\hat{u}_n\right)\sin 2\varphi\right), \tag{4.8}$$

where $M_n = \int d\vec{r}\rho u_n^2$ and $\vec{u}_n(\vec{r})$ are effective mass and displacement vector of the mode, ρ is density of the crystal, ω_{n0} is the eigenfrequency of pure elastic mode in absence of magnetoelastic interaction.

The equation of motion for amplitude A_n(t) is similar to one for oscillator:

$$M_n\left(\ddot{A}_n + 2\delta_n\dot{A}_n\right) = -\frac{\partial F}{\partial A_n}, \tag{4.9}$$

where δ_n is an attenuation coefficient. The equation (4.7) is expressed as:

$$HH_D \sin\varphi + \left(\frac{\omega_{f0}^2}{\gamma^2} - HH_D\right)\sin 2\varphi - h_\perp(t)H_D\cos\varphi + \frac{H_E}{M_0}\sum_n A_n\left(2\hat{B}_2\hat{u}_n\right)\cos 2\varphi = 0 \tag{4.10}$$

For definition of the scale of amplitudes it is convenient to normalize deformation A_n(t) = $\varepsilon_n a_n(t)$ on the value ε_n related to spontaneous magnetostrictive deformations:

$$\varepsilon_n = \int d\vec{r}\left(\hat{B}_2\hat{u}_n\right) / \int d\vec{r}\left(\hat{C}^{(2)}u_n^2\right) \tag{4.11}$$

In order to reduce the integral-differential equation (4.9) to an ordinary equation in the model we substitute real spatial structure of a mode by its mean value of deformations. In a single mode assumption the equation for normalized amplitude can be found from (4.9) and (4.10) as:

$$\ddot{a}_n + 2\delta_n\dot{a}_n + \omega_{n0}^2(a_n + \sin 2\varphi) = 0 \tag{4.12}$$

For numerical integration of the system (4.10) and (4.12) it is convenient to transform nonlinear equation (4.10) in the form of differential equation:

$$\dot{\varphi} = \frac{\left(-\frac{\omega_{f0}^2}{\gamma^2}\zeta_n^2\frac{1}{2}a_n\cos 2\varphi + H_D\dot{h}_\perp(t)\cos\varphi\right)}{\left(HH_D\cos\varphi + \left(\frac{\omega_{f0}^2}{\gamma^2} - HH_D\right)\cos 2\varphi - h_\perp(t)H_D\sin\varphi - \frac{\omega_{f0}^2}{\gamma^2}\zeta_n^2 a_n\sin 2\varphi\right)} \tag{4.13}$$

System of the equations (4.12) and (4.13) describes the behavior of magnetoelastic mode in an AFEP magnetoelastic resonator in bias magnetic field H and perpendicular

alternating magnetic field $h_{\perp}$. The equations were derived without any oscillation amplitude limitations so they can be used to describe strongly nonlinear effects.

At low oscillation amplitudes the contribution of nonlinearities higher than the cubic one is relatively small. Anharmonic approximation and strongly nonlinear model demonstrate similar behavior and the threshold of explosive instability can be described by the same equation:

$$\Gamma = \frac{9}{16} Q_n \frac{\zeta_n^4}{1-\zeta_n^2} \left(\frac{\gamma}{\omega_{f0}}\right) H_D h_0 a_{n0} > 1\,, \tag{4.14}$$

where a_{n0} is the initial amplitude of oscillations and h_0 is the pumping field amplitude.

4.3 Numerical simulations of single mode three quasi-phonon excitations in iron borate

Theoretical simulation of the quasi-phonon triads' excitation in iron borate was performed using both presented models. Following experimental conditions, the process was modeled at two different temperatures: 293 K and 77 K. Experimental pumping fields for supercritical three quasi phonon excitations in iron borate were of the same order of magnitude as the bias magnetic field, so a bigger than in hematite difference between the models behavior was expected.

4.3.1 Instability simulation for $FeBO_3$ resonator using anharmonic approximation

Simulation of the supercritical three quasi-phonon excitations in iron borate using anharmonic approximation was performed by solving numerically the equation 2.48 with the help of Mathcad software and fourth-order Runge-Kutta fixed-step method using corresponding parameters of the AFEP resonator. Pumping field was modulated according to the formulae 2.46 and 2.47. The results of simulation at two different temperatures of 293 K and 77 K are presented in the Figure 4.1 and Figure 4.2 respectively.

According to the experiments on iron borate resonator discussed in the Third Chapter, the following parameters were used for calculations at 293 K : bias magnetic field H = 20 Oe, magnetoelastic coupling coefficient ζ = 0.24. Used contour shear mode resonance frequency was ω_n = 1.35 MHz, mode's quality factor Q_n = 700. Pumping pulse amplitude was h_P = 15 Oe and the phase of pumping pulse was modulated with the law (2.47) with the following parameters: Γ = 1.8, α = 0.012, Q_n = 700. Initial amplitude of oscillations a_{n0} = 6.5 (that value is normalized in the figure to 0.2 for easier comparison with experimental results) and phase equal to $\psi_0 = \pi/2$. Following the experiment pumping started at the time $\tau = 50\mu s$.

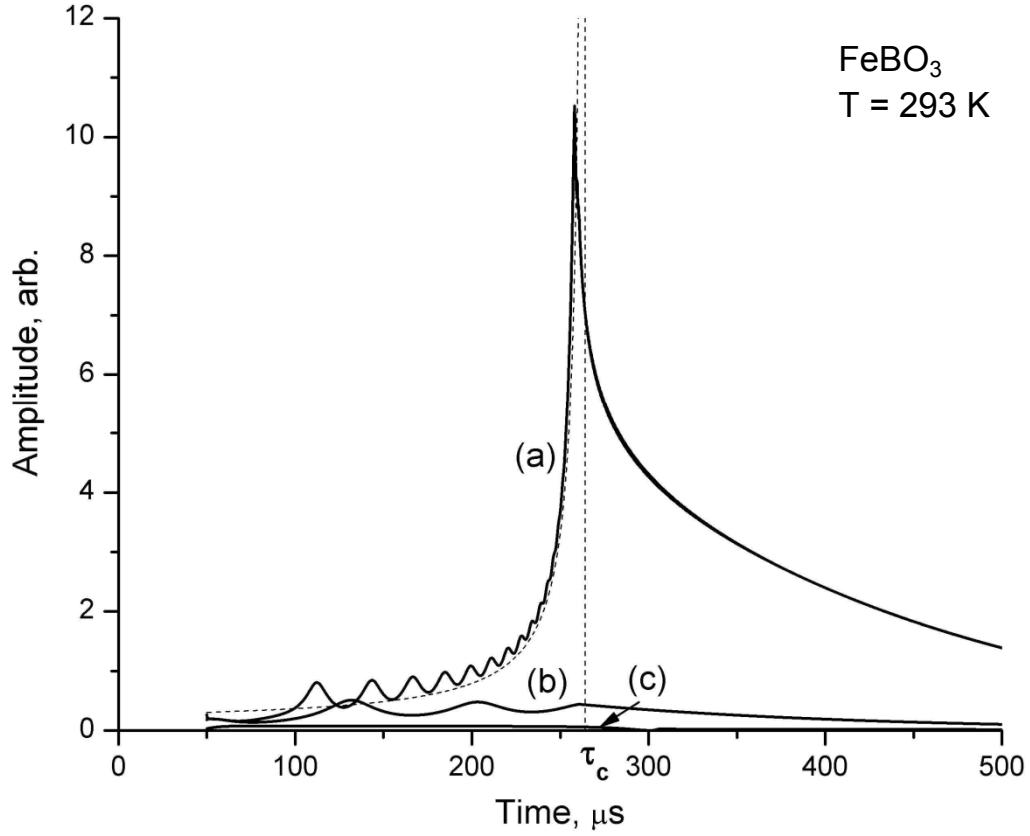

Figure 4.1. Calculated time dependencies of magnetoelastic oscillations amplitude under electromagnetic pumping in $FeBO_3$ resonator at 293 K (a) with proposed phase modulation law, (b) without frequency modulation, (c) without initial excitation $a_{n0} = 0$; dashed line shows theoretical explosive amplitude growth when $\beta_n = 0$ that reaches singularity at the time τ_c.

Similar to the results obtained on hematite, an explosive amplification is observed when the frequency of the second pulse is modulated with proposed law (2.47) (Figure 4.1(a)). Theoretical amplification of the amplitude was about 17 dB with the parameters that correspond to the experimental conditions at 293 K. When the frequency modulation of

pumping pulse was turned off, no explosive amplification was obtained (Figure 4.1(b)). If the initial excitation was set to $a_{n0} = 0$, three-phonon coupling was not observed neither with, nor without frequency modulation (Figure 4.1(c)).

For calculations corresponding to the temperature of 77 K the following parameters were used: $\omega_n = 1.27$ MHz, $Q_n = 10^3$, $\Gamma = 2.2$, $\alpha = 0.03$, $\zeta = 0.45$, $H = 70$ Oe, $h_\perp = 20$ Oe, initial amplitude $a_{n0} = 1.7$ (that value is normalized in the figure to 0.3 for easier comparison with experimental results) and phase equal to $\psi_0 = \pi/2$. The results of low temperature calculations are presented in the Figure 2.6. The pumping starts at the time $\tau = 50\mu s$.

Like at the room temperature, an explosive amplification of oscillations amplitude was observed when the pumping pulse frequency was modulated with the proposed law (2.47) (Figure 4.2(a)).

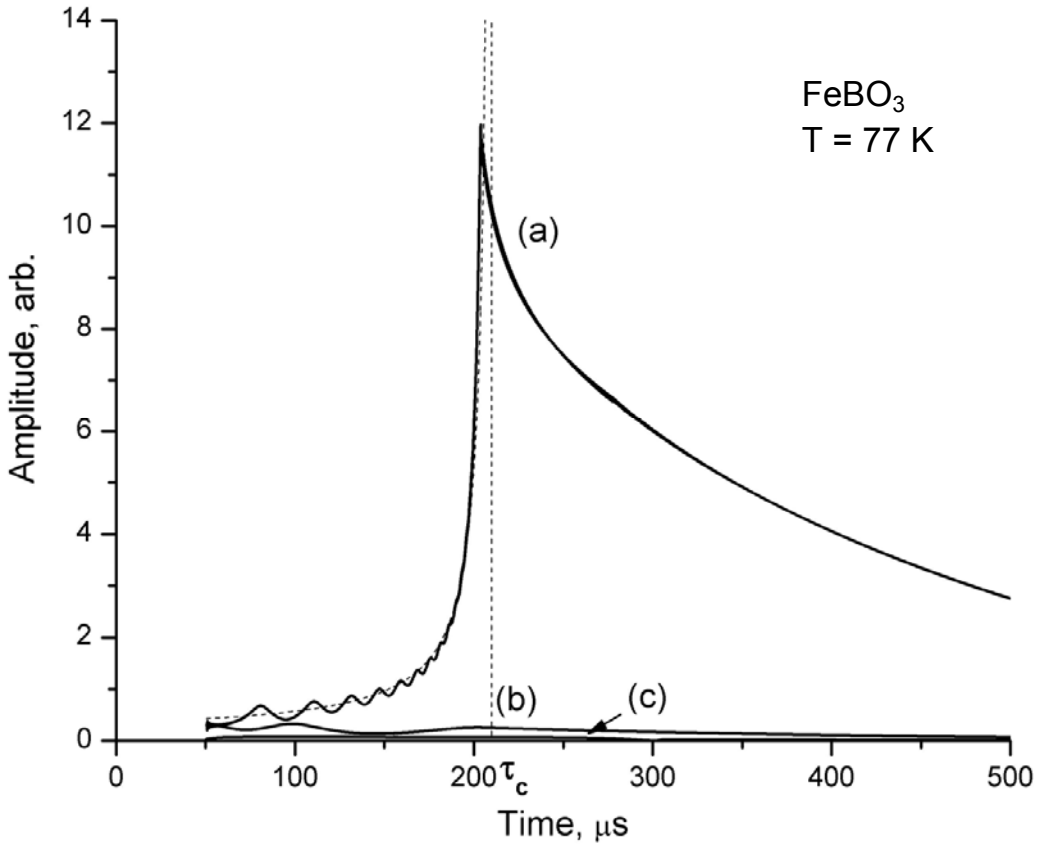

Figure 4.2. Calculated time dependencies of magnetoelastic oscillations amplitude under electromagnetic pumping in $FeBO_3$ resonator at 77 K (a) with proposed phase modulation law, (b) without frequency modulation, (c) without initial excitation $a_{n0} = 0$; dashed line shows theoretical explosive amplitude growth when $\beta_n = 0$ that reaches singularity at the time τ_c.

Calculated amplification was about 16 dB with the parameters that correspond to the experimental conditions a 77 K. If the frequency modulation was turned off, no explosive amplification was observed (Figure 4.2(b)). When the initial oscillations level was set to zero no amplification was registered at all (Figure 4.2(c)).

In agreement with experimental data, theoretical simulation of the three quasi-phonon excitations in iron borate with experimental parameters using anharmonic approximation demonstrated supercritical explosive instability dynamics when the pumping pulse is modulated with the suggested compensation law. However theoretically obtained amplitude gains of 17 dB at 293 K and 16 dB a 77 K are much higher than the experimental results.

4.3.2 Instability simulation for $FeBO_3$ resonator using strongly nonlinear model

For explosive instability modeling in iron borate resonator the system of differential equations (4.12), (4.13) with the pumping field (2.46) and the phase modulation (2.47) was solved numerically with corresponding experimentally obtained magneto-elastic parameters. The results of simulations of time dependence of the amplitude of magnetoelastic oscillations for the temperatures 293 K and 77 K are presented in the Figure 4.3 and Figure 4.4 respectively.

According to the experimental conditions the following parameters were used for calculations at 293 K. Biasing magnetic field was H = 20 Oe and magneto-elastic coupling coefficient ζ = 0.24. The quality factor of the sample was taken Q_n = 700, H_D = 62 kOe, H_E = 38 · 10^2 kOe. The parameters were used for pumping pulse phase modulation were : Γ = 1.5, α = 0.012, Q_n = 700. The amplitude of the pumping was h_P = 15 Oe, initial oscillations amplitude a_{n0} = 3.5 and phase equal to $\psi_0 = \pi/2$.

In agreement with experimentally obtained results, an explosive amplification is observed when the frequency of the second pulse is modulated with proposed law (4) (Figure 4.3(a)). Calculated amplitude gain was about 8.1 dB. When the frequency modulation of pumping pulse was turned off, no explosive amplification was obtained (Figure 4.3(b)). If the initial excitation was set to a_{n0} = 0, explosive instability was not observed neither with, nor without frequency modulation (Figure 4.3(c)).

For calculations corresponding to the temperature of 77 K the following magneo-elastic parameters were used. Biasing magnetic field was H = 70 Oe and magneto-elastic coupling coefficient ζ = 0.45. The quality factor of the sample was taken $Q_n = 10^3$, $H_D = 10^2$ kOe, $H_E = 71 \cdot 10^2$ kOe. The parameters were used for pumping pulse phase modulation were: $\Gamma = 1.5$, $\alpha = 0.012$, $Q_n = 1000$. The amplitude of the pumping was $h_P = 20$ Oe, initial oscillations amplitude $a_{n0} = 0.17$ and phase equal to $\psi_0 = \pi/2$.

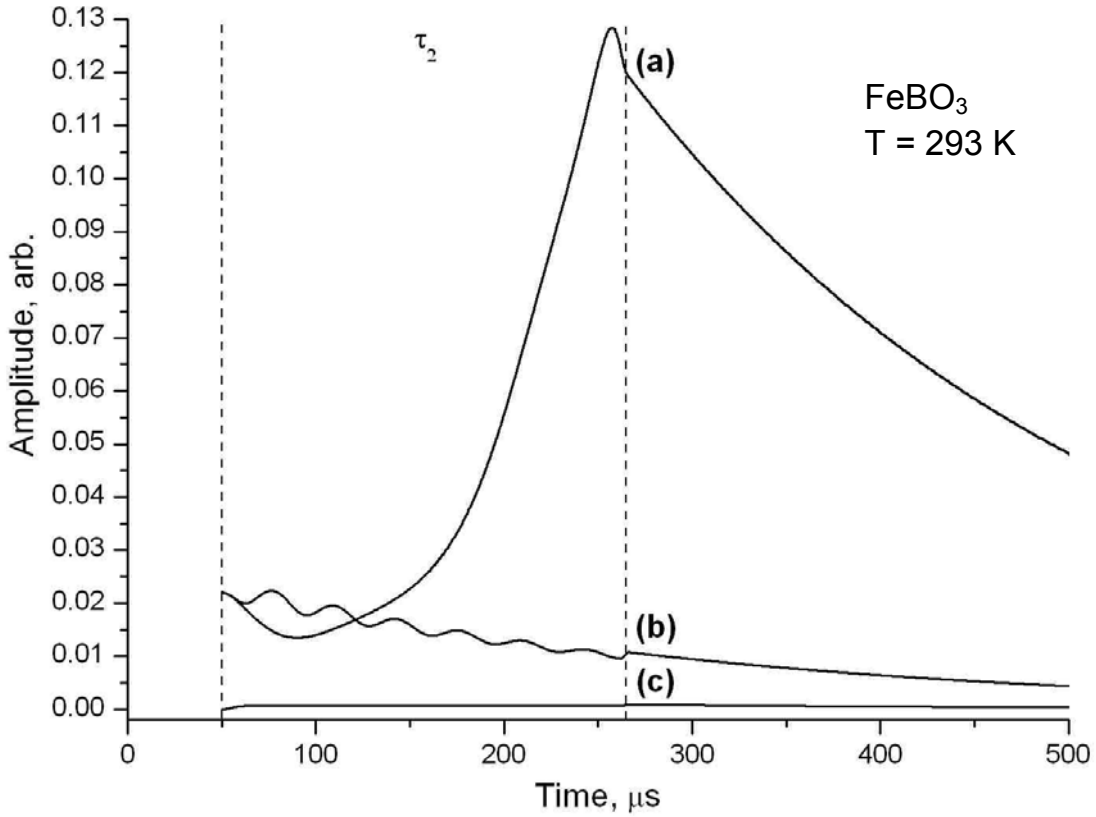

Figure 4.3. Calculated time dependencies of amplitude of magnetoelastic oscillations under electromagnetic pumping in $FeBO_3$ resonator at 293 K: (a) with phase modulation, (b) without frequency modulation and (c) without initial excitation; τ_2 indicates the pumping pulse duration.

The results of low temperature calculations are presented on the Figure 4.5. Similar to the results obtained at 293 K, an explosive amplification of oscillations amplitude was observed when the pumping pulse frequency was modulated with the proposed law (4) (Figure 4.4(a)). Resulting amplitude gain was about 5.5 dB. If the frequency modulation was turned off, no explosive amplification was observed. (Figure 4.4(b)). When the initial oscillations level was set to zero no amplification was registered at all (Figure 4.4(c)).

The results of numerical simulations presented on Figure 4.3 and Figure 4.4 are in good agreement with the experimental data presented respectively on Figure 2.8 and Figure 2.9. Theoretical amplitude gain yielded from strongly nonlinear model at 293 K was 8.1 dB during 220 μs pumping pulse which is close to the experimental gain of 7.8 dB gain during the same pumping duration. Theoretical gain at 77 K was 5.5 dB with 160 μs pumping which also is in good agreement with the experimental value of 5.4 dB.

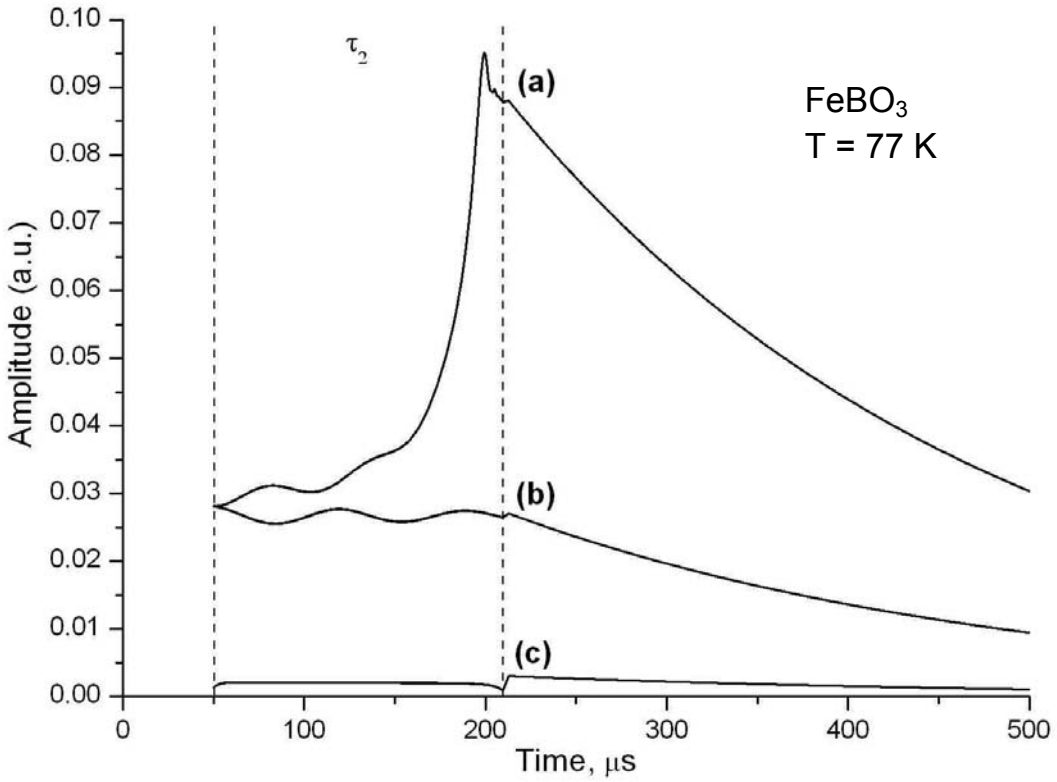

Figure 4.4. Calculated time dependencies of amplitude of magnetoelastic oscillations under electromagnetic pumping in $FeBO_3$ resonator at 77 K. (a) with phase modulation, (b) without frequency modulation and (c) without initial excitation; τ_2 indicates the pumping pulse duration.

The main difference between explosive dynamics at 293 K and 77 K is manifested in values of the time interval of development of explosion equals to 220 μs and 160 μs respectively and in the gain that is two times higher at 293 K. The ratio of the pumping and the bias fields used in the experiment at 77 K was smaller comparing to one used at room temperature. Nevertheless the rising and saturation times of supercritical excitations are notably shorter at 77 K than at 293 K because of stronger magneto-elastic coupling and higher supercriticality parameter at low temperature.

4.4 Numerical simulations of single mode three quasi phonon excitations in hematite

4.4.1 Instability simulation for a-Fe_2O_3 resonator using anharmonic approximation

Simulation of the supercritical three quasi-phonon excitations in hematite using anharmonic approximation was performed by solving numerically the equation 2.48 with the parameters of hematite resonator. Pumping field was modulated according to the formulae 2.46 and 2.47. Results of the modeling are presented and discussed in the Second Chapter in Figure 2.3. The parameters used in the equations correspond to the experimental ones. Obtained amplitude gain with the frequency modulation was 10.8 dB during 370 μs pumping pulse.

4.4.2 Instability simulation for a-Fe_2O_3 resonator using strong nonlinear model

To simulate single mode three quasi-phonon excitations in α-Fe_2O_3 using strong nonlinear model the equations (4.12), (4.13) were rewritten as a system of first order differential equations and solved numerically with the help of Mathcad software. Magneto-elastic characteristics of hematite and parameters taken from the experiments on hematite resonator presented in the Third Chapter were used in the equations. Envelopes of the obtained amplitude oscillations were plotted with the help of Hilbert transformation.

The results of calculations are presented in the Figure 4.5. Calculations were performed for the parameters in selected operating point with bias field H = 60 Oe that corresponds to magneto elastic coupling coefficient of $\zeta_n = 0.78$. The quality factor of the sample was taken $Q_n = 10^3$, H_D = 22 kOe, $H_E = 9 \cdot 10^3$ kOe. Following the experiment, pumping pulse starts at the time t = 100 μs and has the duration of $\tau \approx 370$ μs.

Similar to experimental conditions the rising edge of the pumping pulse had Gaussian-shaped envelope. The envelope (a) in the Figure 4.5 depicts explosive dynamics of supercritical regime of the three quasi-phonon coupling process when the phase of pumping pulse with amplitude $h_\perp$ = 9 Oe was modulated according to the equation (2.47) with the following parameters: $Q_n = 10^3$, $\Gamma = 2.7$, $\alpha = 0.024$.

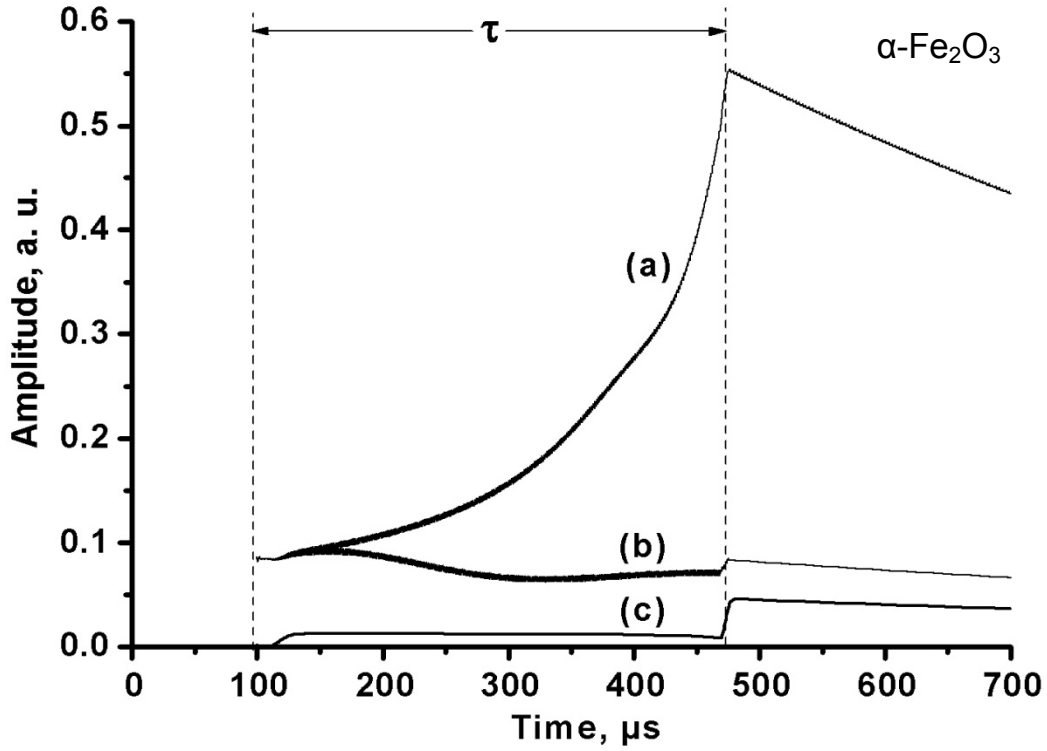

Figure 4.5. Numerical solution of equations (8), (9) with following parameters of α-Fe_2O_3 resonator: $Q_n = 10^3$, $H_D = 22$ kOe, $H_E = 9 \cdot 10^3$ kOe under electromagnetic pumping $\omega_p = 3\omega_n$, (a) with frequency modulation, (b) without frequency modulation and (c) without initial excitation.

The initial amplitude was taken equal to $a_{n0} = 0.17$ that corresponds to initial pulse amplitude 330 mOe for its duration $\tau_1 = 20$ μs. The initial phase shift of the pumping was set to $\psi_0 = \pi$. Obtained amplitude gain in the numerical solution was about 8 dB.

Envelope of the process modulation with the same parameters but without pumping pulse phase modulation is presented in the Figure 4.5 (b). In the beginning of pumping at 100 – 150 μs the amplitude of oscillations starts growing but as it increases the nonlinear frequency shift misphases the contour shear mode and the pumping. Explosive supercritical behavior is not manifested.

If the initial excitation was set to $a_{n0} = 0$, explosive instability was not observed neither with, nor without frequency modulation as shown in the Figure 4.5 (c). An increase of the amplitude oscillations at the end of the pumping pulse of the curves (b) and (c) is due to step-like descending edge of the pumping pulse.

The results of the supercritical dynamics modulation in hematite using the strongly nonlinear model demonstrate good agreement with the experimentally obtained results presented in the third chapter in the Figure 3.13. Explosive process development time in the model and in the experiment is about 370 μs and the amplitude gain is about 7.5 dB.

Modeling results show that strongly nonlinear model gives better description of the three quasi-phonon supercritical dynamics of hematite resonator in comparison to anharmonic approximation. For hematite the anharmonic approximation anticipated faster development of the process with an amplification of 10.8 dB that has not been reached in the experimental conditions due to higher order nonlinearities beyond anharmonic approximation.

4.5 Explosive instability gain dependence on the initial phase of pumping pulse

One of the typical peculiarities of three quasi-phonon coupling that is strong dependence of the process on the phase shift between first and second pulse ψ_0. Experimental and theoretical graphs of explosive instability supercritical dynamics presented earlier were registered with the values of initial phase optimal for quasi-phonon coupling. Figure 4.6 illustrates the envelopes of the contour shear mode amplitude in iron borate at different values of the pumping pulse initial phase $\psi_0 = \pi/2$ (a), $2\pi/3$ (b), $13\pi/18$ (c), $7\pi/9$ (d), $8\pi/9$ (e), π (f).

The envelopes were acquired at the temperature 77 K in bias magnetic field H = 70 Oe. The pumping pulse of the amplitude $h_\perp$ = 22 Oe and duration τ_2 = 150 μs was modulated with the law (2.47) using the following parameters: Q_n = 1100, Γ = 2.2, α = 0.003.

The curve (g) in Figure 4.6 is the envelope of contour shear mode free relaxation oscillations in the absence of the pumping pulse. Comparison of the oscillation amplitudes at the end of pumping pulse with the free relaxation amplitude at the same time shows that three quasi-phonon coupling can either amplify initial oscillations (curves a – d) or attenuate them (curves f – e) depending on the initial phase of the pumping pulse.

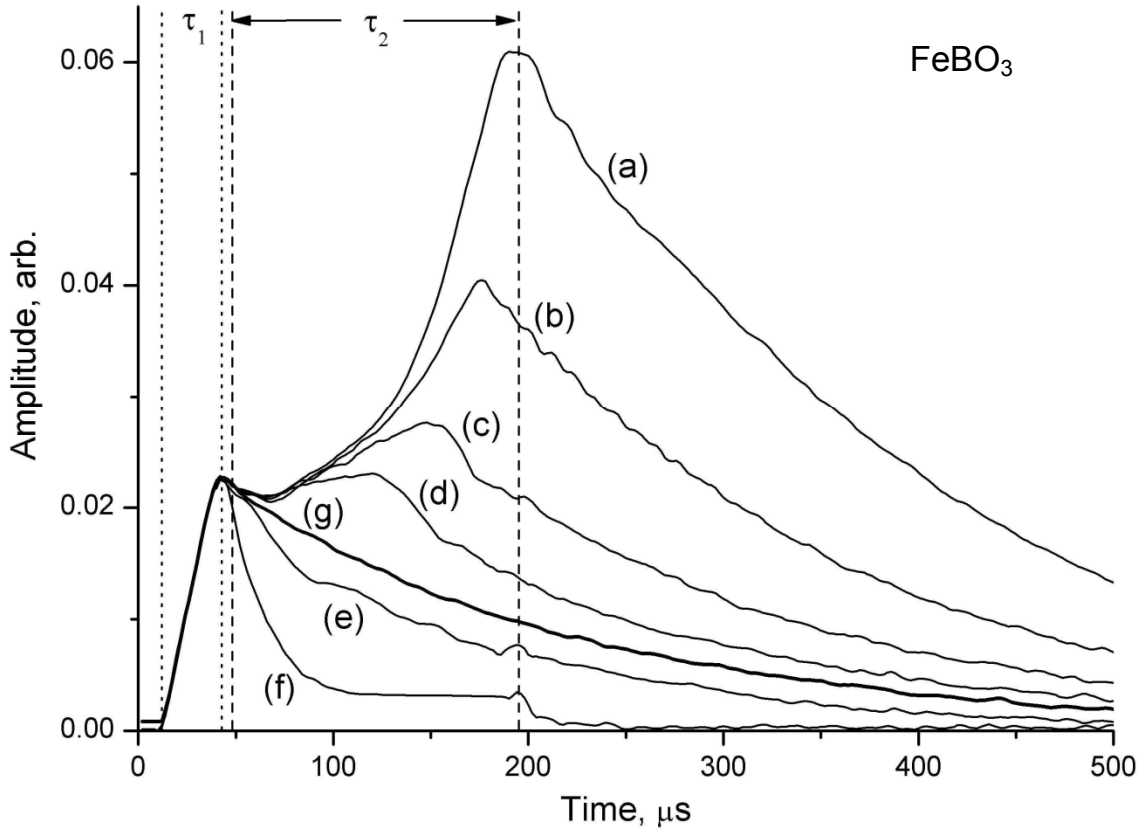

Figure 4.6. Experimental time dependences of amplitude of magneto-elastic oscillations in iron borate at 77K at different values of the pumping pulse initial phase $\psi_0 = \pi/2$ (a), $2\pi/3$ (b), $13\pi/18$ (c), $7\pi/9$ (d), $8\pi/9$ (e), π (d).

Polar dependences of the three quasi-phonon coupling amplitude gain on the initial phase shift of the pumping pulse ψ_0 at the temperatures of 293 K (1) and 77 K (3) are presented in the Figure 4.7. The graph is normalized on the level of amplitude in absence of the pumping (the dashed circle) and plotted in decibels. The gains were registered at the end of the pumping pulse. Theoretical dependence of the amplitude gain on the phase is presented in the Figure 4.7 (2).

Theoretical dependence was calculated using strongly nonlinear model. It represents the gain of resonator oscillations amplitude after the pumping pulse compared to the amplitude of oscillations at the same time when the pumping was set to $h_p = 0$ Oe.

Theoretically calculated gain dependence is in good agreement with experimentally obtained results. Explosive instability brightly manifests itself in pumping pulse initial phase range from +100 to -40 degrees showing maximum amplification of oscillations. When the initial pumping pulse phase value is in the vicinity of 180 degrees ($\pm$45 degrees) the pumping

pulse is attenuating the oscillations and the amplitude at the end of pumping pulse is even less than it would have been without pumping. In the region 180 – 350 degrees experimental and theoretical results have some differences with experimental amplitudes appearing to be more attenuated compared to strongly nonlinear model results.

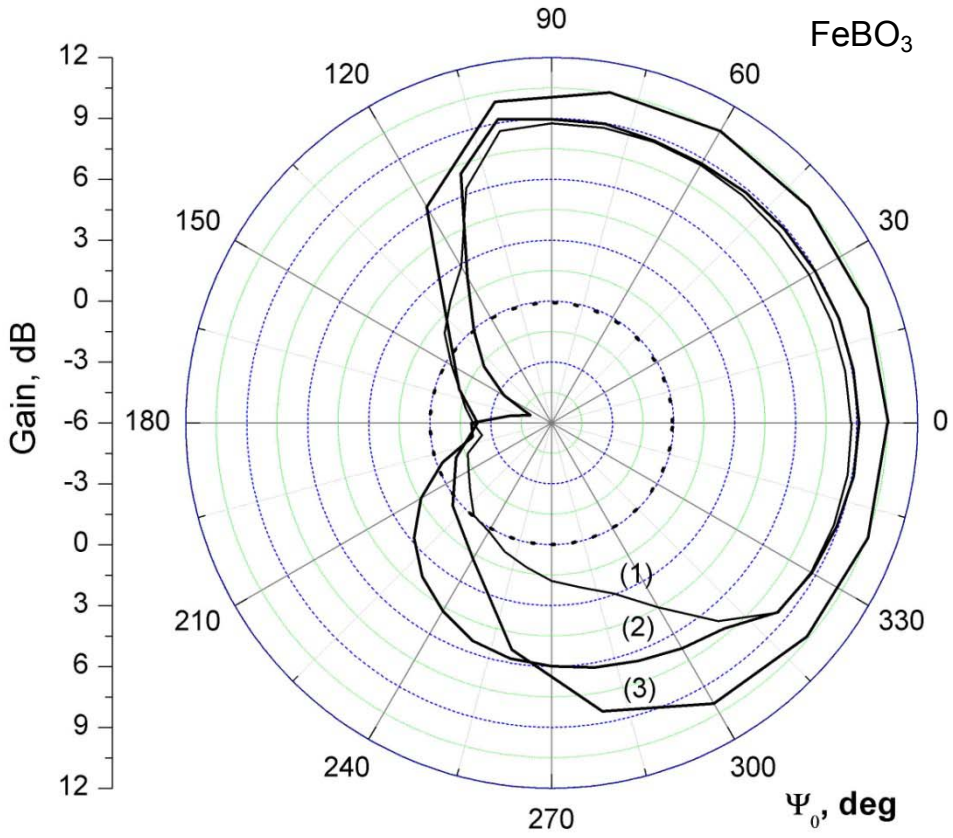

Figure 4.7 Polar phase diagram of three quasi-phonon amplification in $FeBO_3$ resonator at the temperatures 293K (1) and 77K (3) compared with numerical calculations at 293K (2).

4.6 Chapter IV conclusion

Strongly nonlinear model of single mode three quasi-phonon excitations in easy plane antiferromagnetic resonator has been developed that takes into account magnetoelastic nonlinearities outside of anharmonic approximations. The results of numerical simulations with the help of developed model for hematite at 293 K and for iron borate at 293 K and 77 K

demonstrate good agreement with the experiments. Similar to the experiment, strong nonlinear model demonstrates explosive supercritical dynamics when transverse pumping phase follows suggested singular modulation law.

Strongly nonlinear model and anharmonic approximation demonstrate similar behavior at low oscillation amplitudes where contribution of higher order nonlinearities is relatively low. Explosive instability threshold analytically derived in the Second Chapter for anharmonic approximation can be applied for the calculations in strongly nonlinear model as well as it is located in low amplitudes region. Anharmonic approximation allows deeper analysis of the supercritical amplitude limitation mechanism as the model clearly shows contribution of each term to the total energy. The model allowed separation of the cubic nonlinearity term responsible for the nonlinear frequency shift for further compensation law suggestion. However in the supercritical mode of three quasi phonon generation as the oscillations amplitude increases higher order nonlinearities affect the explosive development of the process. Anharmonic approximation is no longer able to accurately describe the process and the use of strongly nonlinear model is required to simulate the behavior of hematite and iron borate resonators is in a good agreement with experimental results even at high amplitude of oscillations.

Experimental supercritical three quasi-phonon excitations in hematite resonator give amplitude gain of 7.5 dB during 370 μs of pumping. Theoretical simulation of the process with the help of anharmonic approximation with the experimental parameters is qualitatively in agreement with the experiments but yielded amplification of 10.8 dB which is considerably higher. Process modeling with the help of strongly nonlinear theory gave amplification of 8 dB which is in good agreement with the experimental results.

The differences between the amplitude gains anticipated by the two models are even more for iron borate simulations. At 293 K experimentally obtained amplitude gain was 7.8 dB during 220 μs pumping pulse and the anharmonic modeling yielded a much higher gain of 17 dB. Process simulation using strongly nonlinear model showed reasonable 8.1 dB gain that closely correlates with the experimental results. Similarly at 77 K experimentally obtained amplification was 5.5 dB, anharmonic approximation gave 16 dB and the strongly nonlinear model results gave more realistic gain of 5.4 dB.

Experimentally obtained gain dependencies on the phase of the pumping pulse show that three quasi-phonon excitations can either amplify or damp initial amplitude of oscillations. Comparison of the results with the numerical simulations using strongly nonlinear model also demonstrate a good agreement of the experiment and theory. Thus presented strongly nonlinear model gives a very close description of the explosive dynamics in antiferromagnetic resonators.

Chapter V

Explosive Dynamics and Spatial Localization of Coupled Travelling Magnetoelastic Wave Triads

5.1 Chapter V introduction

The Fifth Chapter is devoted to the studies of three travelling magnetoelastic waves coupling under electromagnetic pumping. Interaction of the waves is investigated in strongly nonlinear easy plane antiferromagnetic crystal medium.

The studies are performed on the basis of developed anharmonic approximation models that take into account cubic nonlinearity of real AFEP crystals. Two models are developed for both geometries with perpendicular and parallel electromagnetic pumping.

Numerical simulations for the models are performed in time and space domain using a custom program that was written in Fortran language. Dynamic magnetoelastic parameters of available α-Fe_2O_3 crystal are experimentally determined and used in the simulations.

Results of the simulations for parallel pumping and perpendicular pumping models show that nonlinear three-wave coupling features explosive dynamics and spatial localization in supercritical mode. The thresholds of explosive instability are determined and compared for both of the models.

Introduction of cubic nonlinearity limits singular behaviour of the system. Pumping field modulation techniques are suggested that compensate nonlinear phase shift and expose explosive instability.

5.2 Nonlinear three-wave parametric coupling in magnetoelastic system

It has been recently shown [121] that three magnetoelastic waves can nonlinearly interact under electromagnetic pumping in magnetic media with square nonlinearity. A model has been developed for wave triads' interaction in strongly nonlinear antiferromagnetic medium with "easy plane" anisotropy and D_{3d}^{6} symmetry. That model is presented in this section as it is further used for development of anharmonic models with parallel pumping and perpendicular pumping that consider strong cubic nonlinearity of real AFEP crystals.

As discussed in the Fourth Chapter, the dynamics of magnetic system in easy plane antiferromagnet at the frequencies lower than the activation of so-called antiferromagnetic branch can be described by motion of the angle of rotation $\varphi(t, \boldsymbol{r})$ of the antiferromagnetic vector *l* in the basal plane. Following the model presented in [121] Lagrangian density *L* of the AFEP crystal can be presented as a sum of elastic L_e, magnetic L_m and magnetoelastic L_{ME} components:

$$L = L_e(\dot{\vec{u}}, \hat{u}) + L_m(\dot{\varphi}, \varphi, \nabla\varphi) + L_{ME}(\hat{u}, \varphi), \tag{5.1}$$

where elastic Lagrangian density component is the difference between kinetic and potential energy:

$$L_e = \frac{1}{2}\rho\dot{\vec{u}}^2 - \frac{1}{2}\hat{C}^{(2)}\hat{u}^2\,, \tag{5.2}$$

and magnetic and magnetoelastic components are taken as:

$$L_m = \frac{M_0}{2H_E}[\gamma^{-2}(\dot{\varphi}^2 - v_m^2(\nabla\varphi)^2) + (H_D + Hcos\varphi + h_\perp(t)sin\varphi)^2] \tag{5.3}$$

$$L_{ME} = (\hat{B}_1\hat{u})cos2\varphi + (\hat{B}^2\hat{u})sin2\varphi \tag{5.4}$$

Here ρ is crystal density, v_m is spin wave velocity, and other notations are similar to the ones used in the Fourth Chapter.

The Lagrangian (5.1) creates system of coupled equations:

$$\frac{dy}{dx}\frac{\partial L}{\partial\dot{\vec{\xi}}} - \frac{\delta}{\delta\vec{\xi}}\int d\vec{r}\,L = 0\,, \tag{5.5}$$

where $\vec{\xi} = (\vec{u}, \varphi)$ is the four-dimensional dynamic variable, and $\delta/\delta\vec{\xi}$ is a functional derivative.

For the ultrasound frequencies much lower than the antiferromagnetic resonance frequency of quasiferromode $\omega \ll \omega_{f0} = \gamma\sqrt{H(H + H_D) + 2H_E H_{ms}}$ the system (5.5) can be

resolved relatively to magnetic variable $\varphi = \varphi[\hat{u}, h_\perp(t)]$ and reduced to only one equation for hybridized mode of magnetoelastic waves:

$$\rho\ddot{\vec{u}} = -\frac{\delta}{\delta\vec{u}}\int d\vec{r}\, F^{eff} = 0, \tag{5.6}$$

where F^{eff} is the effective potential energy density describing three-wave parametric interaction under perpendicular electromagnetic pumping. It can be factorized in linear and nonlinear parts $F^{eff} = F^L + F^{NL}$, where linear part can be presented as:

$$F^L = \frac{1}{2}\hat{C}^{(2)}_{eff}(H)\hat{u}^2, \tag{5.7}$$

where $\hat{C}^{(2)}_{eff}(H) = \hat{C}^{(2)} + \Delta\hat{C}^{(2)}(H)$ is the effective tensor of elastic moduli, renormalized by magnetoelastic interaction (2.3). Nonlinear part up to third order terms can be presented as:

$$F_1^{NL} = h_\perp(t)\hat{\Psi}\hat{u}^3, \tag{5.8}$$

where $h_\perp(t)$ is applied electromagnetic pumping field and $\hat{\Psi}$ is three-wave coupling coefficient. A parametric coupling of three shear waves in the crystal is considered. The crystal is placed in bias field $H \parallel x$ with the z axis parallel to the hard direction C_3 and the waves are propagating in the (y,z) plane with polarization $\vec{u}_n \parallel \vec{x}$. For the waves with wave vectors $k_{1,2,3}$ and frequencies $\omega_{1,2,3}$ the following pulse conservation law applies:

$$\vec{k}_1 + \vec{k}_2 + \vec{k}_3 = 0 \tag{5.9}$$

Scheme of the considered model and vector diagram of pulse conservation law are presented in the Figure 5.1. Active layer is limited by the crystal size ($0 < z < L$). Alternating electromagnetic pumping field $h_\perp(t) = h_0\cos\omega_p t$ aligned along the hard direction can be used to couple the three waves, where ω_p is the pumping frequency that meets the following phase synchronizm condition:

$$\omega_p = \omega_1 + \omega_2 + \omega_3 \tag{5.10}$$

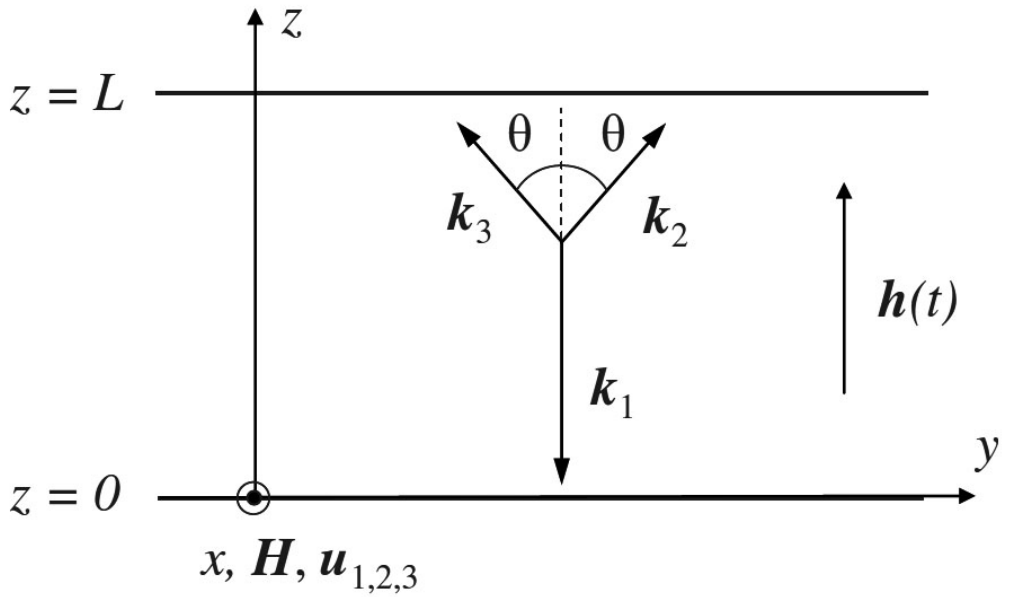

Figure 5.1. Scheme of the interaction model with perpendicular electromagnetic pumping and vector diagram of the pulse conservation law [121].

Fulfilling the conditions (5.9, 5.10) the system of equations for slowly varying amplitudes for the three waves $A_{1,2,3}(t, z)$ can be obtained from (5.6):

$$\begin{cases} \omega_1 \left(\dfrac{\partial A_1}{\partial t} + v_1 \dfrac{\partial A_1}{\partial z} \right) = \Psi \varepsilon_{321} A_2^* A_3^* \\ \omega_2 \left(\dfrac{\partial A_2}{\partial t} + v_2 \dfrac{\partial A_2}{\partial z} \right) = \Psi \varepsilon_{231} A_1^* A_3^* \\ \omega_3 \left(\dfrac{\partial A_3}{\partial t} + v_3 \dfrac{\partial A_3}{\partial z} \right) = \Psi \varepsilon_{123} A_1^* A_2^* \end{cases}, \tag{5.11}$$

where ε is completely antisymmetric tensor, Ψ is the three-wave parametric interaction coefficient that depends on the pumping field geometry. It is proportional to the cube of magnetoelastic coupling, cube of wave vector and pumping field amplitude:

$$\Psi \sim \zeta^3 v_\infty^2 k_B^3 h_0 \tag{5.12}$$

In (5.11) $v_{1,2,3}$ is the correspomding wave's group velocity projection on the z axis that depends on he wave vector projections and can be calculated as:

$$v_n = \frac{C_{44}(H)}{\rho\omega_n} k_{nz} + \frac{C_{14}(H)}{\rho\omega_n} k_{ny}\,, \tag{5.13}$$

and $\omega_{1,2,3}$ is the corresponding wave frequency determined as:

$$\omega_n = \sqrt{(C_{44}(H)k_{nz}^2 + C_{66}(H)k_{ny}^2 + 2C_{14}(H)k_{ny}k_{nz})/\rho} \tag{5.14}$$

The components of effective elastic tensor $\hat{C}_{eff}^{(2)}$ in AFEP depend on the bias magnetic field can be determined according to formula (2.3):

$$C_{44}(H) = C_{44} - \frac{4H_E}{M_0}\left(\frac{\gamma}{\omega_{f0}}\right)^2 B_{14}^2 \tag{5.15}$$

$$C_{14}(H) = C_{14} - \frac{2H_E}{M_0}\left(\frac{\gamma}{\omega_{f0}}\right)^2 B_{14}(B_{11} - B_{12}) \tag{5.16}$$

$$C_{66}(H) = C_{44} - \frac{H_E}{M_0}\left(\frac{\gamma}{\omega_{f0}}\right)^2 (B_{11} - B_{12})^2 \tag{5.17}$$

Numerical simulations of this model for perpendicular pumping showed that when the initial wave amplitudes $A_{02}\,A_{03}$ together with the pumping field amplitude h_0 are high enough, an explosive instability is anticipated when the amplitudes of all three waves blow up in finite time [121]. Statinary solutions defined the threshold of the instability:

$$\Gamma = \left|\frac{\Psi\sqrt{A_{02}A_{03}}}{\omega_1 v_1}\right| \sqrt{2}L > 0.663\,, \tag{5.18}$$

where Γ is the supercriticality parameter of the system. Equations (5.18) and (5.17) show that the threshold of the explosive instability depends on the amplitudes of incident waves, the length of pumping zone, generated wave frequency, its speed, and magnetoelastic coupling coefficient. Calculations suggested that for conditions that are close to the experiment, pumping field threshold is within tens of oersted, which is quite feasible. However, the model did not take into account strong cubic nonlinearity that is very large in real life easy plane antiferromagnets. As it has been shown in the Second Chapter, for single-mode three quasi-

phonon excitations cubic nonlinearity manifests itself as nonlinear frequency shift and is the main mechanism that affects supercritical explosive dymanics. In the next section dynamic properties of experimentally available hematite crystal are studied for further development of anharmonic models that consider fourth order terms.

5.3 Dynamic properties of experimental hematite crystal

Various techniques can be used for the growth of hematite single crystals, including hydrothermal, vapor transport, flux and optical floating zone furnace methods. Crystals with the size of 55mm in the hard direction and diameter of 5 mm have been reported [132]. Available sample of iron hematite was shaped as a rectangular parallelepiped. Dimentions of the sample were measured with the help of a micrometer. The length was found to be l = 13.16 mm, with the width of 4.93 mm and the height of 4.37 mm.

Crystal faceting was such that the hard direction C_3 of magnetic subsystem was along the long side of the crystal. One of the three binary axes U_2 was directed along the 4.93 mm side of the sample. Applying the geometry discussed in the previous section, the axis z was set along the hard ditection in the crystal that corresponds to the longer side of the sample, giving about 13 mm of active zone for three wave coupling. Picture of the sample is presented in the Figure 5.2 with selected coordinate axes.

Magnetoelastic properties of the crystal were measured by determining the transverse sound velocity dependences on the bias magnetic field. The coupling of a transverse acoustic wave with magnetic system strongly depends on its polarization [76]. One of the normal modes with the polarization $e_1 \perp x \parallel H$ perpendicular to the binary axis in perfect crystal has no linear interation with magnetic system and travels at the speed $v_\infty = \sqrt{C_{44}/\rho}$. The second normal mode with polarization parallel to the U_2 axis $e_2 \parallel x \parallel H$ features strong linear coupling with magnetic system.

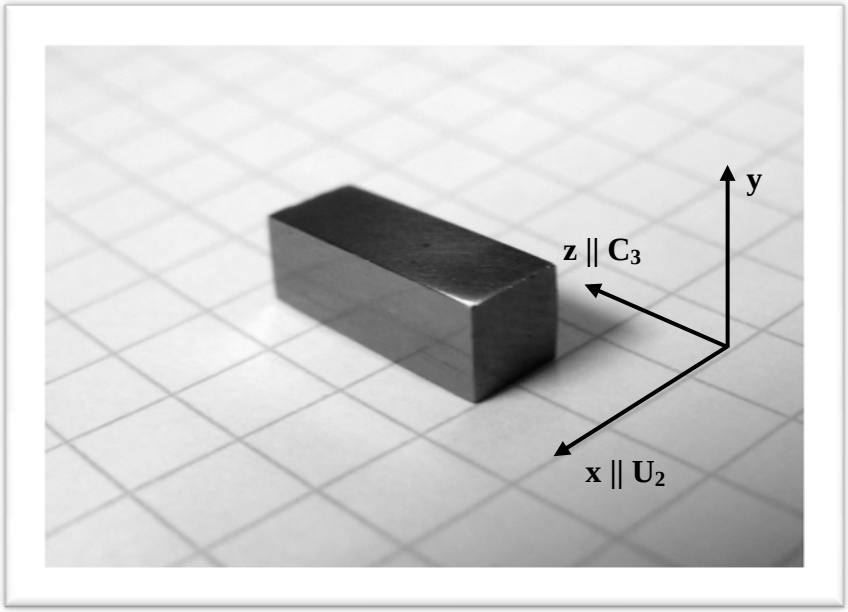

Figure 5.2. Picture of α-Fe_2O_3 sample, its magnetic axis and chosen coordinate axis. The axis z is selected parallel to the hard direction C_3 of the crystal. The axis x is aligned parallel to one of the binary axis U_2. Each line represents 5 mm.

Phase velocity of a wave with such polarization $\upsilon_\perp(H)$ strongly depends on the value of magnetoelastic coupling coefficient $\zeta(H)$ thus it depends on the bias magnetic field:

$$\upsilon_\perp(H) = \upsilon_\infty \sqrt{(1-\varsigma^2(H))} \tag{5.19}$$

Magnetoelastic coupling coefficient can be presented as (3.4), yielding:

$$\upsilon_\perp(H) = \upsilon_\infty \sqrt{1-\frac{H_{ms}^{(1)}}{H+H_{ms}^{(2)}}} \tag{5.20}$$

The dependences of transversal sound velocity with different polarizations in the hematite crystal was measured with the help of ultrasonic pulse method [133]. A transverse sound transducer was attached to one of the surfaces of the crystal that are parallel to the basal plane. It was excited with a short pulse with the help of Sofranel pulser/receiver 5077PR. The pulse would travel to the opposite side, reflect from it, and return back at the transducer. The pulse travel time τ was measured as a function of bias field H and sound velocity was determined as $\upsilon_\perp(H) = 2l/\tau$. The experiment was performed with a help of a custom Labview program that was automaticaly changing bias magnetic field and aquiring the waveforms from

the oscilloscope. Aquired waveforms were then analyzed with another Labview program that calculated and plotted dependence of the sound speed $v_{\perp}(H)$ on bias field H. Experimental results of the sound velocity measurements for the two modes with different polarizations are presented in the Fugure 5.3 with dots. The results are normalized on the maximum sound velocity value which was measured to be about 3900 m/s. Due to dipole-dipole interaction at lower fields multiple domains form in the crystal causing modes mixing. At this situation absolute separation of the modes is impossible and experimentally observed are mostly coupled and mostly non-coupled normal modes. At the fields lower than 300 Oe it becomes impossible to detemine the speed correctly. Theoretical fittings of the the formula (5.20) on the dependences are presented in the same Figure with solid lines. The values of effective fields for mostly-coupled mode were found to be $H_{ms}^{(1)}$ =564.8 Oe, $H_{ms}^{(2)}$ =934.0 Oe and v_{∞} = 3912 m/s. The results of magnetoelastic coupling coefficient calculations based on the formula (3.4) are presented in the Figure 5.4.

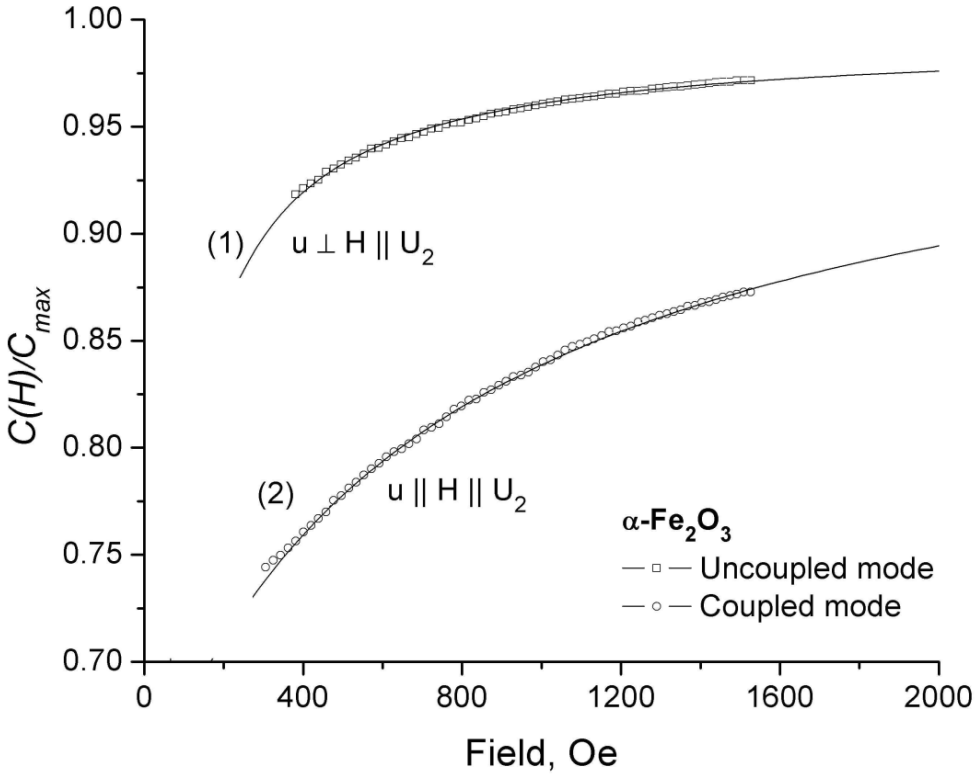

Figure 5.3. Experimental (symbols) and theoretical (lines) dependences of normalized sound velocities on bias magnetic field in α-Fe_2O_3 for shear waves with different polarizations: (1) $u \perp H \parallel U_2$ and (2) $u \parallel H \parallel U_2$.

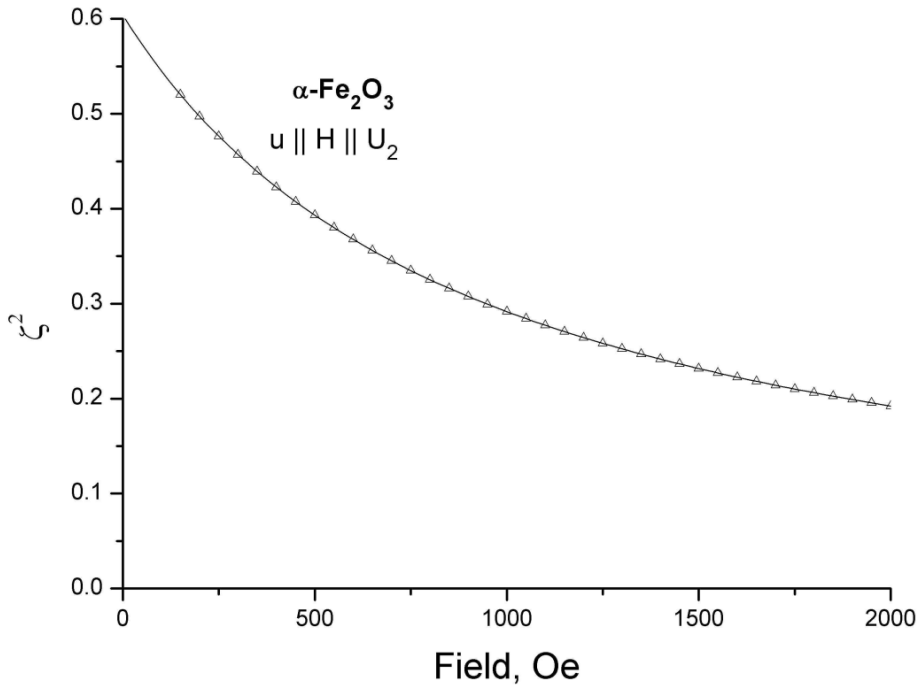

Figure 5.4. Dependence of the magneto-elastic coupling coefficient of shear mode with polarization $u \parallel H \parallel U_2$ on bias magnetic field H in hematite.

As a result of the hematite sample studies, the most optimal operating point on this crystal was found in the bias field H = 300 Oe that corresponds to high value of magnetoelastic coupling coefficient $\zeta^2 = 0.46$. The length of available active zone in the crystal is L = 1.3 cm. These parameters were used for further numerical simulations of developed three-wave coupling models.

5.4 Anharmonic model of three travelling waves coupling with parallel electromagnetic pumping

5.4.1 Three waves coupling under parallel electromagnetic pumping

In this section an anharmonic model of three-wave nonlinear interaction is developed that takes into account cubic nonlinearity of real life AFEP crystals. The case when two incident waves with identical wave vectors are propagating along the z axis is considered to simplify the calculations. Following the notations in the previous section $\vec{k}_2 = \vec{k}_3$. In this section a new variable is introduced to describe the projections of the wave vectors on the z axis $k_A = k_{2z} = k_{3z}$. The projection of generated wave's vector is described by another new

variable k_B, following pulse conservation law (5.9) $k_B = k_{1z} = 2k_A$. Alternating electromagnetic pumping field $h_\perp(t) = h_0 \cos\omega_p t$ is used to couple the three waves. The condition of phase synchronism determines the frequency of pumping ω_p:

$$\omega_p = 2\omega_A + \omega_B \tag{5.22}$$

The energy density of easy plane antiferromagnet crystal is given by:

$$F_{me} = \left(\hat{B}_1 cos2\varphi + \hat{B}_2 sin2\varphi\right)\hat{u}\,, \tag{5.23}$$

where $\hat{B}_1$ and $\hat{B}_2$ are the tensors of magnetoelastic constants. Their convolutions with deformation tensor are given by:

$$\begin{aligned} \hat{B}_1\hat{u} &= -\frac{1}{2}(B_{11} - B_{12})\left(u_{xx} - u_{yy}\right) - B_{14}u_{yz} \\ \hat{B}_2\hat{u} &= -(B_{11} - B_{12})u_{xy} - 2B_{14}u_{xz} \end{aligned} \tag{5.24}$$

In the first order of approximation the angle φ of non-resonant rotations of antiferromagnetic vector is given by:

$$\varphi = -\frac{2H_E}{M_0}\left(\frac{\gamma}{\omega_{f0}}\right)^2 \left(\hat{B}_2\hat{u}\right) \tag{5.25}$$

To the third order terms, it can be approximated that in (5.23) $\sin 2\varphi = \varphi - 2\varphi^3/3$ and $\cos 2\varphi = -\varphi^2$. In this case magnetoelastic energy of three-wave interactions of transverse waves is determined only by $\hat{u}\varphi^2$ term and can be written as:

$$F_{me} = -2\left(\frac{2H_E}{M_0}\right)^2 \frac{1}{(\omega_{s0}/\gamma)^4}(2B_{14})^3 u_{yz}u_{xz} = C_{eff}^{(3)} u_{yz}u_{xz}^2\,, \tag{5.26}$$

where $C_{eff}^{(3)}$ is anharmonic elastic module (2.7), u_{yz} and u_{xz} are shear displacements. Equation (5.26) shows that two transverse waves with polarization *xz* and one transverse wave with polarization *yz* interact nonlinearly in AFEP crystal. Polarization *xz* corresponds to linearly coupled magnetoelastic waves and polarization *yz* corresponds to an uncoupled wave.

Corresponding components of magnetoelastic stress tensor can be presented as $(\hat{\sigma}_{me})_{xz} = C^{(3)}u_{yz}u_{xz}$ and $(\hat{\sigma}_{me})_{yz} = C^{(3)}u_{xz}^2/2$ and magnetoelastic nonlinear interaction creates a system of coupled equations of motion for the waves:

$$\begin{cases} \rho\ddot{u}_x = C_{44}(H)\dfrac{\partial^2 u_x}{\partial z^2} + \dfrac{1}{4}C^{(3)}\dfrac{\partial}{\partial z}\left(\dfrac{\partial u_x}{\partial z}\dfrac{\partial u_y}{\partial z}\right) \\ \rho\ddot{u}_y = C_{44}(\infty)\dfrac{\partial^2 u_y}{\partial z^2} + \dfrac{1}{8}C^{(3)}\dfrac{\partial}{\partial z}\left(\dfrac{\partial u_x}{\partial z}\right)^2 \end{cases} \tag{5.27}$$

Three waves interaction can be excited via modulation of the nonlinear module $C_{eff}^{(3)}$. In case of parallel pumping the alternating magnetic field directly modulates $C_{eff}^{(3)}$:

$$C^{(3)} = \frac{\partial C^{(3)}}{\partial H} h_0 \sin\left(\omega_p t + \psi\right), \tag{5.28}$$

Looking for the solution of the system (5.27) in the form:

$$\begin{aligned} u_x &= Ae^{i(\omega_A t - k_A z)} + c.c \\ u_y &= Be^{i(\omega_B t - k_B z)} + c.c \end{aligned} \tag{5.29}$$

and substituting the derivatives in the system of equations (5.27):

$$\begin{aligned} \frac{\partial u_x}{\partial z}\frac{\partial u_y}{\partial z} &= A^* B^* e^{i(\omega_A+\omega_B)t + i(k_A - k_B)z} k_A k_B + c.c \\ \left(\frac{\partial u_x}{\partial z}\right)^2 &= (A^*)^2 e^{-i(2\omega_A t) + i(2k_A z)}(-k_A^2) + c.c \\ \ddot{u}_x &= \left(-\omega_A^2 A + 2i\omega_A \frac{\partial A}{\partial t}\right) e^{-i(\omega_A t) + i(k_A z)} + c.c \\ \ddot{u}_y &= \left(-\omega_B^2 B + 2i\omega_B \frac{\partial B}{\partial t}\right) e^{-i(\omega_B t) + i(k_B z)} + c.c \end{aligned} \tag{5.30}$$

It can be resolved to a system of equations for slowly variable amplitudes:

$$\begin{cases} \omega_1\left(\dfrac{\partial A}{\partial t}+v_\perp(H)\dfrac{\partial A}{\partial z}\right)=-2\Psi A^*B^*+F_A \\ \omega_2\left(\dfrac{\partial B}{\partial t}-v_\infty\dfrac{\partial B}{\partial z}\right)=-\Psi(A^*)^2+F_B \end{cases}, \tag{5.31}$$

where F_A and F_B are corresponding nonlinear phase shift contributions to the motion equations of incident wave A and generated wave B. Ψ is the amplitude of three-wave interaction under parallel pumping that is given by:

$$\Psi=\frac{1}{8\rho}k_A^3\frac{\partial C^{(3)}}{\partial H}h_0=2\zeta^4v_\infty^2k_A^3\left(\frac{C_{44}}{2B_{14}}\right)\frac{2H+H_D}{(\omega_{s0}/\gamma)^2}h_0 \tag{5.32}$$

5.4.2 Nonlinear phase shift of ultrasonic triads under parallel pumping

Nonlinear contributions F_A and F_B of the coupled magnetoelastic waves described by the system (5.31) come mainly from the cubic nonlinearity that can be characterised by effective elastic moduli $\hat{C}_{eff}^{(4)}$ (2.8). They can be calculated from the energy density of the fourth order terms $F^{(4)}=\hat{C}_{eff}^{(4)}\hat{u}^4$:

$$F^{(4)}=\frac{1}{2}\left(\frac{H_E}{M_0}\right)^3\frac{1}{\left(\omega_{f0}/\gamma\right)^6}\left(\left(1+\frac{1}{4}\frac{\gamma^2HH_D}{\omega_{f0}^2}\right)\left(2\hat{B}_2\hat{u}\right)^4-4\left(2\hat{B}_2\hat{u}\right)^2\left(2\hat{B}_1\hat{u}\right)^2\right) \tag{5.33}$$

Leaving only related tensor convolution components that correspond to shear waves that propagate along z axis $\left(\hat{B}_1\hat{u}\right)=2B_{14}u_{yz}$, $\left(\hat{B}_2\hat{u}\right)=2B_{14}u_{xz}$ the energy reduces to:

$$F^{(4)}=\frac{1}{2}\left(\frac{H_E}{M_0}\right)^3\frac{1}{\left(\omega_{f0}/\gamma\right)^6}(4B_{14})^4\left(\left(1+\frac{1}{4}\frac{\gamma^2HH_D}{\omega_{f0}^2}\right)u_{xz}^4-4u_{xz}^2u_{yz}^2\right) \tag{5.34}$$

Introducing the new variables:

$$\eta=\frac{1}{2}\left(\frac{H_E}{M_0}\right)^3\frac{1}{\left(\omega_{f0}/\gamma\right)^6}(4B_{14})^4 \tag{5.35}$$

$$\xi = 1 + \frac{1}{4}\frac{\gamma^2 H H_D}{\omega_{f0}^2}$$

the corresponding shear components of the stress tensor can be written as:

$$\begin{gathered}\left(\sigma_{me}^{(4)}\right)_{xz} = \eta\left(2\xi u_{xz}^3 - 4u_{xz}u_{yz}^2\right) \\ \left(\sigma_{me}^{(4)}\right)_{yz} = \eta\left(-4u_{xz}^2 u_{yz}\right)\end{gathered} \tag{5.36}$$

Displacement components u_x, u_y are defined as (5.29). They can be calculated as:

$$\begin{aligned} u_{xz}u_{yz}^2 &= \frac{1}{4}(-ik_A)k_B^2|B|^2 A e^{i(\omega_A t - k_A z)} + c.c \\ u_{xz}^3 &= \frac{3}{8}(-ik_A^2)A|A|^2 A e^{i(\omega_A t - k_A z)} + c.c \\ u_{yz}u_{xz}^2 &= \frac{1}{4}(ik_B)k_A^2|A|^2 B e^{i(\omega_B t - k_B z)} + c.c \end{aligned} \tag{5.37}$$

And finally the cubic nonlinearity contributions to the system of coupled waves (5.31) are given by:

$$\begin{gathered}\frac{\partial\left(\sigma_{me}^{(4)}\right)_{xz}}{\partial z} = 2\eta k_A^4\left(-\frac{3}{8}\xi|A|^2 + 2|B|^2\right)A e^{i(\omega_A t - k_A z)} + c.c \\ \frac{\partial\left(\sigma_{me}^{(4)}\right)_{yz}}{\partial z} = \eta k_A^2 k_B^2 |A|^2 B e^{i(\omega_B t - k_B z)} + c.c\end{gathered} \tag{5.38}$$

Taking into account that $k_B^2 = 4k_A^2$ the contributions of the cubic nonlinearity to the phase shift can be obtained as:

$$\begin{gathered}F_A^{(4)} = i2\eta k_A^4\left(\frac{3}{8}\xi|A|^2 + 2|B|^2\right)A/\rho \\ F_B^{(4)} = -i\eta k_A^4|A|^2 B/\rho\end{gathered} \tag{5.39}$$

In the second order of the perturbations theory square nonlinearity also contributes to the nonlinear phase shift and total contribution in the system of equations (5.31) can be presented as:

$$F_A = F_A^{(4)} + F_A^{(3)}, \quad F_B = F_B^{(4)} + F_B^{(3)} \tag{5.40}$$

Square nonlinearity contributions can be calculated by taking into account non-resonance contributions u_x' and u_y' from of square nonlinearity in the solutions of the equations of motion (5.26):

$$\begin{aligned} u_x &= Ae^{i(\omega_A t - k_A z)} + c.c + u_x' \\ u_y &= Be^{i(\omega_B t - k_B z)} + c.c + u_y' \end{aligned} \tag{5.41}$$

The equations of motion for non-resonance contributions are defined by the force that comes from square nonlinearity:

$$\begin{aligned} \ddot{u}_x' - V_\perp^2(H)\frac{\partial u_x'}{\partial z^2} &= \frac{1}{\rho}\left(\sigma_{me}^{(3)}\right)_{xz} \\ \ddot{u}_y' - V_\infty^2\frac{\partial u_y'}{\partial z^2} &= \frac{1}{\rho}\left(\sigma_{me}^{(3)}\right)_{yz} \end{aligned} \tag{5.42}$$

In (5.42) $\left(\sigma_{me}^{(3)}\right)_{xz}$ and $\left(\sigma_{me}^{(3)}\right)_{xz}$ are corresponding components of square nonlinearity magnetoelastic tensor that are defined by the energy density $F^{(3)} = C^{(3)}\frac{1}{8}\left(\frac{\partial u_y}{\partial z}\right)\left(\frac{\partial u_x}{\partial z}\right)^2$ that comes from the square nonlinearity:

$$\begin{aligned} \left(\sigma_{me}^{(3)}\right)_{yz} &= C^{(3)}\frac{1}{8}\left(\frac{\partial u_x}{\partial z}\right)^2 \\ \left(\sigma_{me}^{(3)}\right)_{xz} &= C^{(3)}\frac{1}{4}\left(\frac{\partial u_y}{\partial z}\right)\left(\frac{\partial u_x}{\partial z}\right) \end{aligned} \tag{5.43}$$

Solving the system of equations (5.42) the non-resonance contributions u_x' and u_y' can be found as:

$$u_x' = \frac{C_{eff}^{(3)}}{4\rho}\left(\begin{array}{c} \frac{-2ik_A}{4V_\infty(V_\perp + V_\infty)}ABe^{i(\omega_A+\omega_B)t+i(k_B-k_A)z} + \\ + \frac{6ik_A}{4(V_\infty^2 - V_\infty V_\perp - 2V_\perp^2)}A^*Be^{i(\omega_A+\omega_B)t+i(k_B+k_A)z} + c.c \end{array}\right) \tag{5.45}$$

$$u_y' = \frac{C_{eff}^{(3)}}{16\rho}\frac{ik_A}{(V_\infty^2 - V_\perp^2)}A^2 e^{2i(\omega_A t - k_A z)} + c.c$$

Whence the square nonlinearity contributions can be found as:

$$F_A^{(3)} = \frac{C_{eff}^{(3)}}{4\rho}\frac{\partial}{\partial z}\left(\frac{\partial u_x'}{\partial z}\frac{\partial u_y}{\partial z} + \frac{\partial u_x}{\partial z}\frac{\partial u_y'}{\partial z}\right)$$
$$F_A^{(3)} = \frac{1}{2}\frac{C_{eff}^{(3)}}{4\rho}\frac{\partial}{\partial z}2\left(\frac{\partial u_x}{\partial z}\frac{\partial u_x'}{\partial z}\right) \tag{5.46}$$

Substituting the partial derivatives values in (5.44) and introducing new variables

$$\mho = \frac{1}{(1 + V_\perp/V_\infty)} + \frac{9}{(1 - V_\perp/V_\infty - 2V_\infty^2/V_\perp^2)}$$
$$\chi = \frac{1}{2(1 - V_\perp^2/V_\infty^2)}, \quad \varepsilon = \frac{1}{2V_\infty^2}\left(\frac{C_{eff}^{(3)}}{4\rho}\right) \tag{5.47}$$

the square nonlinearity corrections can be obtained:

$$F_A^{(3)} = i\varepsilon k_A^4(\chi|A|^2 + \mho|B|^2)A$$
$$F_B^{(3)} = i\varepsilon k_A^4\chi|A|^2 B \tag{5.48}$$

Introducing the obtained values of square and cubic nonlinearity contributions to the phase shift in (5.31) the system of equations becomes:

$$\begin{cases} \omega_A\left(\dfrac{\partial A}{\partial t} + v_\perp(H)\dfrac{\partial A}{\partial z}\right) = -2\Psi A^* B^* + i\varepsilon k_A^4(\chi|A|^2 + \mho|B|^2)A \\ \qquad\qquad +i2\eta k_A^4\left(\dfrac{3}{8}\xi|A|^2 + 2|B|^2\right)A/\rho \\ \omega_B\left(\dfrac{\partial B}{\partial t} - v_\infty\dfrac{\partial B}{\partial z}\right) = -\Psi(A^*)^2 + i\varepsilon k_A^4\chi|A|^2 B - i\eta k_A^4 \end{cases} \tag{5.49}$$

Regrouping the nonlinear contributions the system can be brought to:

$$\begin{cases} \omega_A \left(\dfrac{\partial A}{\partial t} + v_\perp(H) \dfrac{\partial A}{\partial z} \right) = -2\Psi A^* B^* + i[\alpha_1 |A|^2 + \alpha_2 |B|^2] A \\ \omega_B \left(\dfrac{\partial B}{\partial t} - v_\infty \dfrac{\partial B}{\partial z} \right) = -\Psi (A^*)^2 + i\alpha_2 |A|^2 B \end{cases}, \tag{5.50}$$

where α_1, α_2 are nonlinear phase shift coefficients given by:

$$\begin{aligned} \alpha_1 &= \zeta^6 \left(\frac{C_{44}}{2B_{14}} \right)^2 v_\infty^2 k_b^4 \left(\frac{3}{4} \frac{\gamma^2 \mathrm{HH_D}}{\omega_{s0}^2} + 4 \right) \\ \alpha_2 &= -8\zeta^6 \left(\frac{C_{44}}{2B_{14}} \right)^2 v_\infty^2 k_b^4 \left(\frac{\left(1 + \sqrt{1-\zeta^2}\right)^2}{2\sqrt{1-\zeta^2} - 1} \right) \end{aligned} \tag{5.51}$$

If the nonlinear coefficients are set to 0, the system of equations (5.50) describes the process of three-wave interaction in coupled magnetoelastic system without nonlinear phase shift.

The hard direction of the crystal is set along the *z* axis and the circular frequency of shear wave with wave vector *k* is determined by its polarization. For incident linearly-coupled magnetoelastic waves with *xz* polarization the value of circular frequency ω_A is given by:

$$\omega_A = \sqrt{\frac{C_{44}(H)}{\rho}} |k_A| \tag{5.52}$$

And for the linearly-uncoupled generated wave with *yz* polarization the value of circular frequency ω_B is given by:

$$\omega_B = \sqrt{\frac{C_{44}}{\rho}} |k_B| \tag{5.53}$$

In case of parallel pumping following phase synchronism condition (5.22) frequency of pumping is determined by equation:

$$\omega_\mathrm{p} = 2\omega_A + \omega_B = 2\sqrt{\frac{C_{44}(H)}{\rho}} |k_A| + 2\sqrt{\frac{C_{44}}{\rho}} |k_A| \tag{5.54}$$

Equation (5.54) shows that for parallel geometry the frequency of pumping depends of the value of effective linear elastic module $C_{44}(H)$ that is determined by bias magnetic field. For the hematite crystal in bias magnetic field H = 300 Oe pumping frequency is $\omega_p \approx 4.6\omega_A$.

5.5 Numerical simulations program

A custom computer program was written in Fortran language for numerical simulations of the three waves coupling process in easy plane antiferromagnet. This program was created by modifying the code that was originally written by O. Bou Matar et al. [134, 135] for numerical solutions of ordinary differential equations with the help of 4th order Adams Bashforth method. That code was later modified for numerical simulation of the three wave coupling model described in [121].

The program uses a Fourier pseudospectral time domain method to calculate the partial spatial derivatives in the equations. Specral methods are widely used for partial differential equation solutions in heat conduction, fluid flow, and sound propagation. The idea of the method is to use fast Fourier transform to write the solution in trigonometrical series to calculate the derivatives in the frequency domain, and then substitute this series it in the original system using inverse Fourier transform to get an ordinary differential equation. After such substitution an ordinary equation can be easily solved using ordinary time-stepping method like Adams Bashforth's or Runge-Kutta's one.

To circumvent wraparound inherent to fast Fourier-based pseudospectral method, the boundaries of calculation region were wrapped with perfectly matched layers (PLM). PML is an artificial layer that was developed for wave equations in 1994 [136] as a layer that does not reflect any incident waves at the interface. This property allows absorption of all the waves travelling from the computational region and simplifies solutions. A complex frequency-shifted (CFS) PML, also called convolution PML (CPML) [137] was implemented for the calculations due to its high effectiveness at absorbing evanescent waves and waves of long time signature.

For numerical solution of ordinary differential equations of the created models Adams Bashforth 4th order numerical method was used in the program. This linear multi-step method was selected as it provides higher efficiency in the solutions by using the information from

previous steps instead of discarding as like it is usually done in one-step methods like Runge-Kutta. It was selected to provide sufficient accuracy within reasonable calculation time.

Adams Bashforth method is an explicit linear method, meaning that the variable at the time step t_{i+1} is calculated based on the time derivatives of the variable at the previous time points (for the 4th order method the values at times t_i, t_{i-1}, t_{i-2} and t_{i-3} are used). This method is optimized for the slow-varying amplitudes equations.

Combination of these advanced numerical methods allowed optimization of the code so that numerical simulations could be performs on a standard PC computer in time and space domain in reasonable timings. Results of each step calculations were saved in text files and then post-processed with the help of MathWorks® MatLab™ 7.0 for graph plotting or video visualization of the process.

Presented simulation results were obtained using the parameters of the experimentally available hematite crystal described in the section 5.3. For numerical simulations AFEP crystal was presented as a 1D model with $f = 512$ points. The number of points had to be a multiple of the power of two for correct Fast Fourier transformations work. The scheme of selected crystal model is presented in the Figure 5.5.

Axiz z was selected parallel to hard direction of the crystal. The crystal (white) was surrounded by CPML perfectly matched layers (grey) that were completely absorbing waves leaving the crystal. The layers were located at the regions $0 - p_1$ and $p_2 - f$. Incident wave was introduced at the point z_1 and was travelling in the positive direction of the axis z. Eectromagnetic pumping field was applied in the Active Zone region $z_1 - z_2$. Nonlinear interaction of the waves was generating a wave propagating backwards.

In presented calculations $z_1 = 100$ pts, $z_2 = 400$ pts, $p_1 = 48$ pts, $p_2 = 464$ pts. Time step of the calculations was 1.0803 ns, spatial step was 0.0433 mm. Selected spatial step determined the size of active zone that corresponds with the size of experimentally available hematite crystal $L_s = 1.299\,cm \approx L$. Inside the Active Zone in the Figure 5.5 a typical supercritical distribution of Incident and Generated wave amplitudes is shown, with incident wave travelling to the right and generated wave travelling to the left.

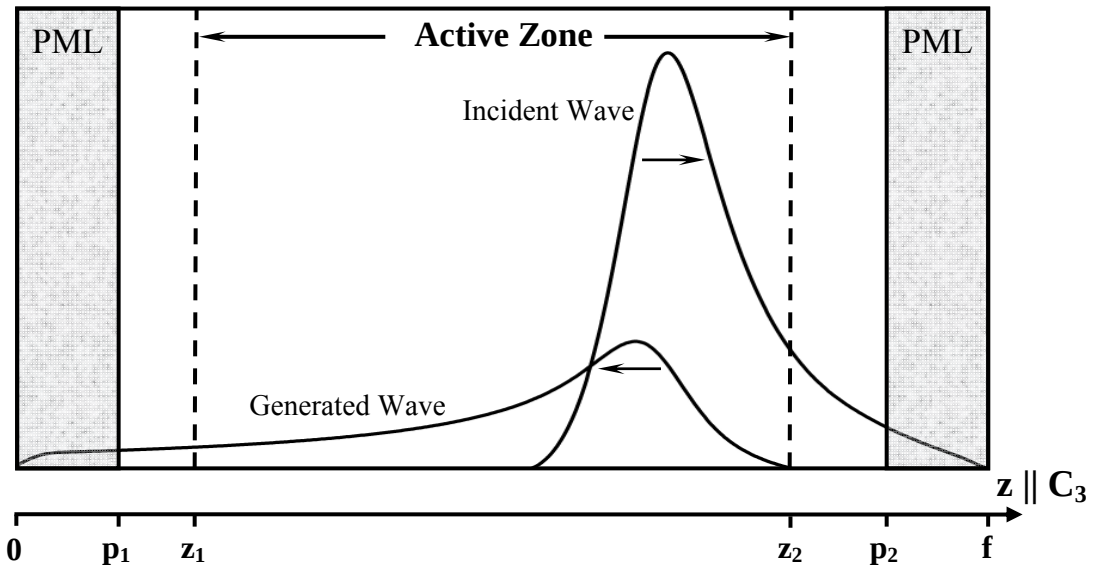

Figure 5.5. Scheme of the theoretical crystal model used for numerical simulations. The axis z was directed along hard direction. The crystal (white) was surrounded with two PML perfectly matched layers (grey). Incident wave was introduced at the point z_1 and was travelling in the positive direction of z axis. Electromagnetic pumping was applied in the Active Zone region. Nonlinear interaction was generating a wave that was travelling in the opposite direction.

The form of slowly variable amplitude of incident waves was one period of cosine function applied as $A_{z1} = \frac{1}{2}\left(1 - \cos\frac{2\pi t}{T}\right)$, with the duration of pulse $T = 10\ \mu s$. In experimental conditions such wave can be excited by a shear wave transducer attached to one of the easy plane surfaces of the crystal. Input signal on the base frequency has to be modulated with the frequency $f = 100$ kHz.

5.6 Numerical simulations of three travelling waves coupling model with parallel pumping

For numerical simulations of three waves coupling the system of equations (5.50) the real and imaginary parts in the equations were separated and equations were reorganized to have time derivatives in the right hand side:

$$\begin{cases} \dfrac{\partial A_r}{\partial t} = -v_\perp(H)\dfrac{\partial A_r}{\partial z} - \dfrac{2\Psi}{\omega_1}[A_r B_r - A_i B_i] - \dfrac{A_i}{\omega_1}[\alpha_1(A_r^2 + A_i^2) + \alpha_2(B_r^2 + B_i^2)] \\ \dfrac{\partial A_i}{\partial t} = -v_\perp(H)\dfrac{\partial A_i}{\partial z} + \dfrac{2\Psi}{\omega_1}[A_i B_r - A_r B_i] - \dfrac{A_r}{\omega_1}[\alpha_1(A_r^2 + A_i^2) + \alpha_2(B_r^2 + B_i^2)] \\ \dfrac{\partial B_r}{\partial t} = v_\infty \dfrac{\partial B_r}{\partial z} - \dfrac{\Psi}{\omega_2}[A_r^2 + A_i^2] - \dfrac{B_i}{\omega_2}\alpha_2(A_r^2 + A_i^2) \\ \dfrac{\partial B_i}{\partial t} = v_\infty \dfrac{\partial B_i}{\partial z} + \dfrac{\Psi}{\omega_2}[2A_r A_i] + \dfrac{B_r}{\omega_2}\alpha_2(A_r^2 + A_i^2) \end{cases} \quad (5.55)$$

Nonlinearity coefficients α_1 and α_2 are the same and are described by (5.51), A_r, B_r and A_i, B_i represent real and imaginary pars of the wave amplitudes respectively. Obtained system of equations (5.55) was numerically solved with the help of developed Fortran program in time and space domains.

5.6.1 Numerical solutions of parallel geometry model in subthreshold mode

The value of three-wave interaction coefficient under parallel electromagnetic pumping (5.32) was found to be $|\Psi| = 2.2 \cdot 10^{21} \times h_0$ using the following variables: $\zeta^2 = 0.46$, $k_A = 2.1 \cdot 10^4\ m^{-1}$, $v_\infty = 4 \cdot 10^3\ m^{-1}$. The value of wave vector k_A was determined according to selected incident waves ultrasound frequencies of $\frac{\omega_A}{2\pi} = 10$ MHz. The amplitude of incident waves was selected as $A_0 = 10^{-10}\ m$. Low value of the amplitude was chosen to minimize nonlinear phase shift contributions.

For the research of model dynamics in subthreshold conditions the pumping field with amplitude $h_0 = 50$ Oe was used. Supercriticality parameter (5.18) with these conditions was calculated to be $\Gamma = 0.31$, which is well below the supercritical threshold value of 0.663.

The results of numerical simulations of the system of equations (5.55) with the nonlinear phase shift calculated according to the coefficients (5.51) are presented in the Figure 5.6. The figure demonstrates spatial distributions incident and generated wave amplitudes A/A_0, B/A_0 normalized on the value of the initial incident amplitude A_0. The incident wave is introduced at the border of active zone (AFEP crystal) at coordinate z = 4.33 mm in the calculations region during three waves coupling process under parallel pumping. A_0 is the value of initial incident wave amplitude.

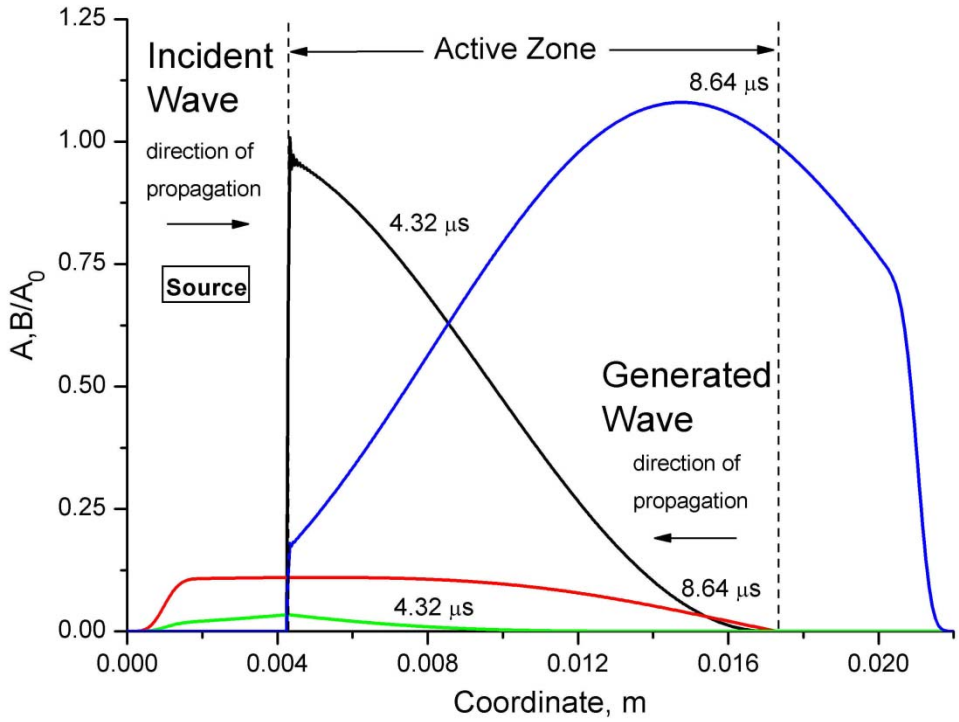

Figure 5.6. Spatial distributions of normalized incident and generated wave amplitudes A/A_0, B/A_0 during three waves coupling process under parallel pumping with subthreshold conditions. Distributions are presented at two time moments for incident (black) and generated (green) waves at 4.32 μs and for incident (blue) and generated (red) waves at 8.64 μs. $A_0 = 1 \cdot 10^{-10}$, $h_0 = 50$ Oe.

Amplitudes of the waves were obtained from the calculated imaginary and real parts as $A = \sqrt{A_r^2 + A_i^2}$, $B = \sqrt{B_r^2 + B_i^2}$. Distributions are presented for two time moments: at 4.32 μs and at 8.64 μs after the start of incident wave introduction. Below the threshold no explosive amplification was observed. The incident wave amplitude distribution at 4.32 μs (black line) travels to the right to the distribution at 8.64 μs (blue line) with slight amplification. Cosine shape of the incident wave slowly varying amplitude can be observed. Generated wave distribution at 4.32 μs (green line) travels in the opposite direction to the distribution at 8.64 μs (red line). At the borders the effect of introduced CPML layers can be observed. The incident wave gets absorbed by the right layer and the generated wave is absorbed by the left layer. Numerical simulations without nonlinear phase shift in subthreshold mode demonstrate similar behaviour as presented in the Figure 5.6. At low oscillation amplitudes introduction of cubic nonlinearity does not change the process development.

5.6.2 Numerical solutions of parallel geometry model in supercritical mode

To analyze the effect of nonlinear phase shift on the three waves coupling process under parallel pumping in the supercritical mode the system of equations (5.55) was numerically solved with the values of nonlinear coefficients (5.51) set to zero and the results were compared with the solutions of the same system with the real crystal coefficient values.

To achieve supercritical mode of three-wave coupling supercriticality parameter value (5.18) had to be raise above 0.663. Pumping field $h_0 = 50$ used in subthresold simulations was already quite high and hard to achieve experimentally. For that reason it was left unchanged and at first the amplitude of incident waves was tripled to the value $A_0 = 3 \cdot 10^{-10}\ m$ with the same pumping field amplitude $h_0 = 50$ Oe. These values correspond to supercriticality parameter of $\Gamma = 0.93$ that moved the system to supercritical mode.

Time evolution of spatial distribution of the incident wave normalized amplitudes A/A_0 in supercritical regime without nonlinear phase shift is presented in the Figure 5.7. Distributions of the incident wave amplitude are presented at the time t = 4.32 μs (black line), 5.54 μs (blue line), 7.56 μs (green line), 8.64 μs (red line), 9.37 μs (purple line). Maximum amplitude amplification at the time 9.37 μs is A/A_0 = 182, reaching infinity and blowing up at the time 9.39 μs. The effect of spatial localization clearly manifests itself as the maximum amplitude amplification is only observed in a small part of incident pulse.

Time evolution of spatial distribution of normalized incident wave amplitudes A/A_0 at the same supercritical conditions but with real crystal nonlinear phase shift is presented in the Figure 5.8. Distributions are presented at the same time moments using the same colors. When the strong cubic nonlinearity of AFEP crystals was taken into account explosive behavior of coupled magnetoelastic three-wave interaction was not manifested.

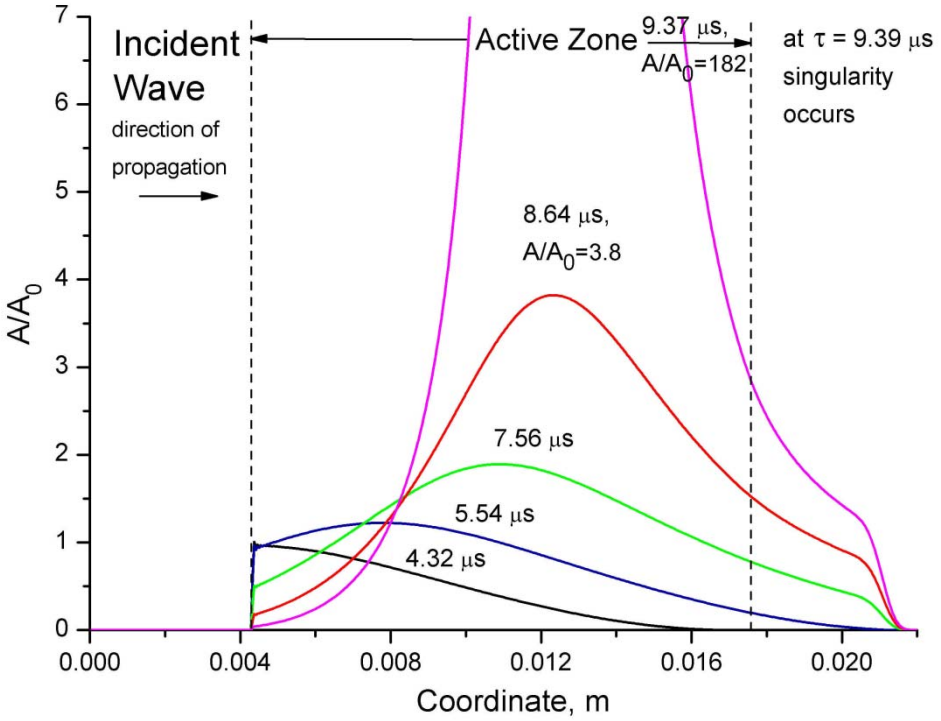

Figure 5.7. Supercritical time evolution of spatial distribution of normalized incident wave amplitude A/A_0 during three waves coupling process under parallel pumping without nonlinear phase shift. Distributions are shown for time moments: 4.32 μs (black), 5.54 μs (blue), 7.56 μs (green), 8.64 μs (red), 9.37 μs (purple). At t = 9.39 μs singularity occurs. $A_0 = 3 \cdot 10^{-10}$, $h_0 = 50$ Oe, $\Gamma = 0.93$.

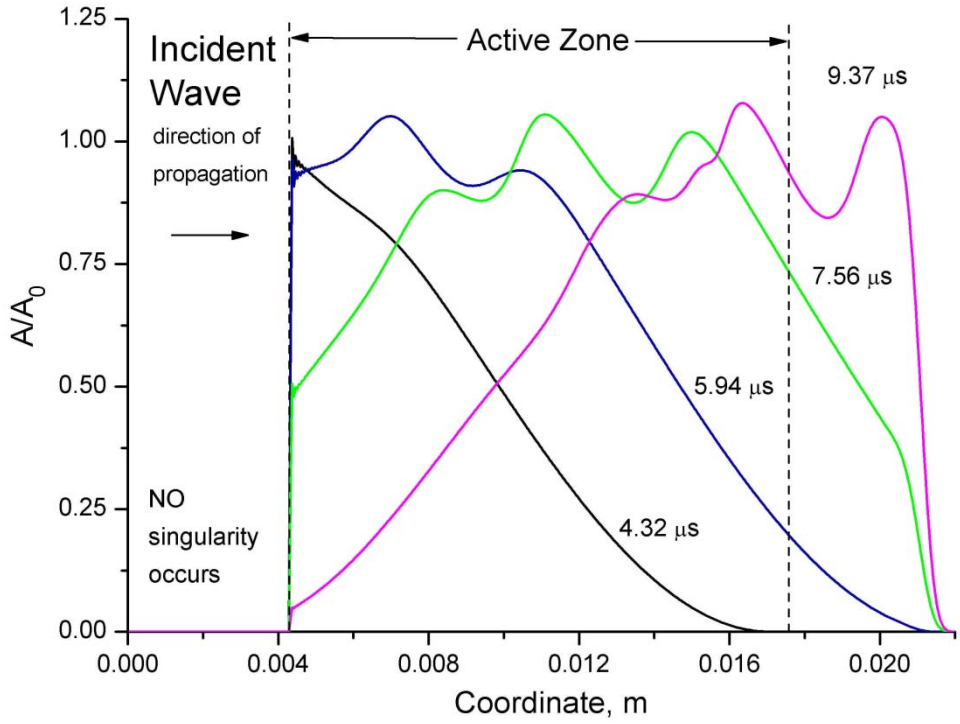

Figure 5.8. Supercritical time evolution of spatial distribution of normalized incident wave amplitude A/A_0 during three waves coupling process under parallel pumping with nonlinear phase shift. Distributions are shown for time moments: 4.32 μs (black), 5.54 μs (blue), 7.56 μs (green), 8.64 μs (red), 9.37 μs (purple). No singularity is observed. $A_0 = 3 \cdot 10^{-10}$, $h_0 = 50$ Oe, $\Gamma = 0.93$.

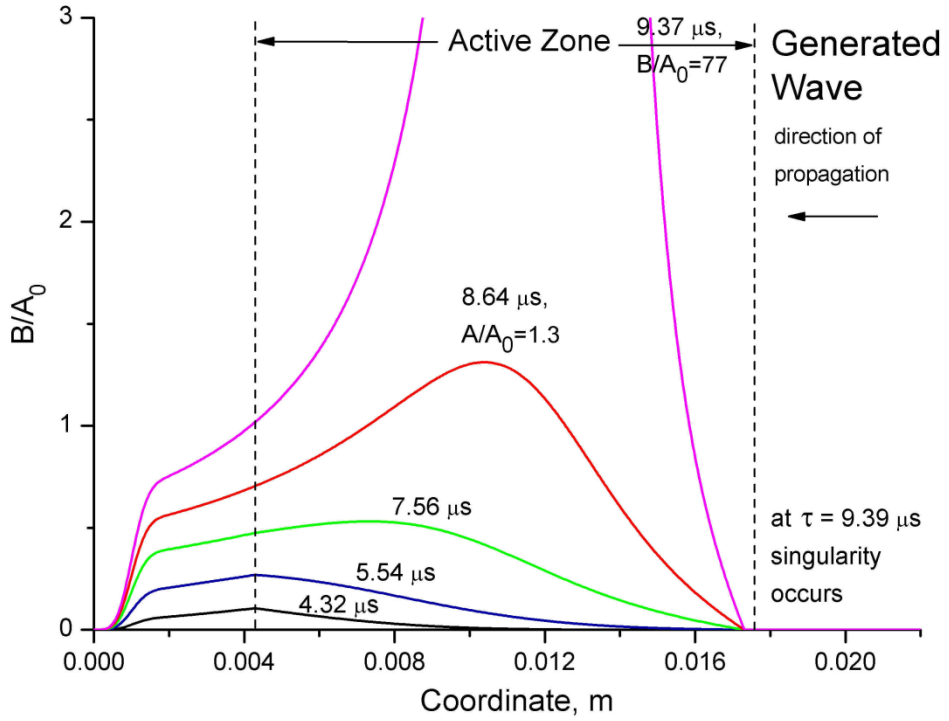

Figure 5.9. Supercritical time evolution of spatial distribution of normalized generated wave amplitude B/A_0 during three waves coupling process under parallel pumping without nonlinear phase shift. Distributions are shown for time moments: 4.32 μs (black), 5.54 μs (blue), 7.56 μs (green), 8.64 μs (red), 9.37 μs (purple). At 9.39 μs singularity occurs. $A_0 = 3 \cdot 10^{-10}$, $h_0 = 50$ Oe, $\Gamma = 0.93$.

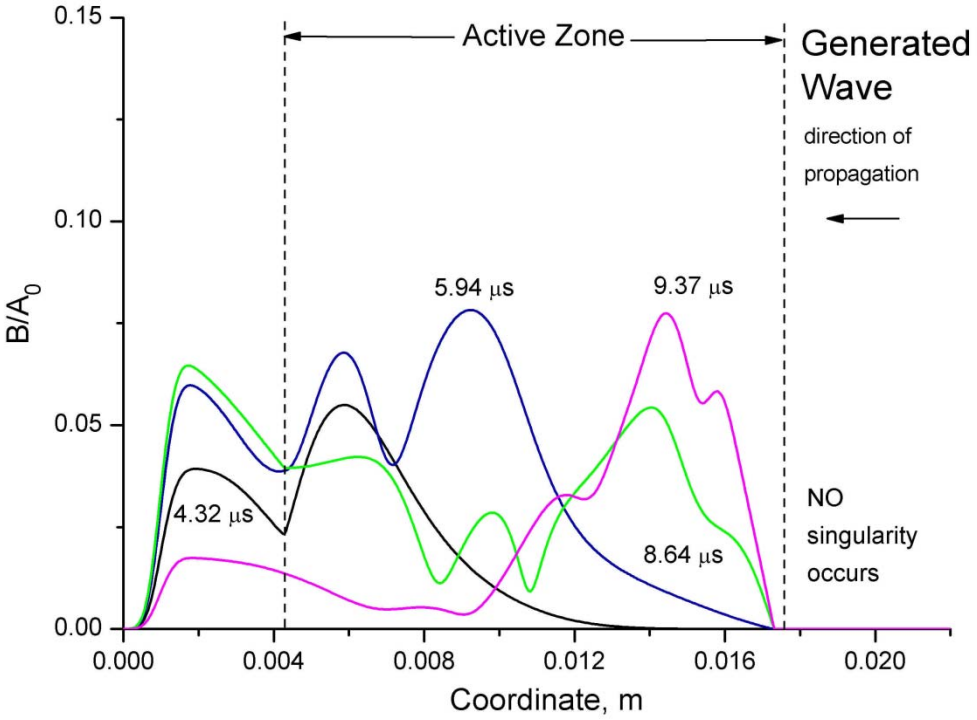

Figure 5.10. Supercritical time evolution of spatial distribution of normalized generated wave amplitude B/A_0 during three waves coupling process under parallel pumping with nonlinear phase shift. Distributions are shown for time moments: 4.32 μs (black), 5.54 μs (blue), 7.56 μs (green), 8.64 μs (red), 9.37 μs (purple).Singularity is not observed. $A_0 = 3 \cdot 10^{-10}$, $h_0 = 50$ Oe, $\Gamma = 0.93$.

Nearly no amplification of incident waves pulse was observed and the shape of the pulse got distorted by the coupling. Initial amplitude of the incident pulse was too high and nonlinear phase shift was misphasing the coupling process. Obtained time evolution of normalized amplitude distribution for generated wave B/A_0 in supercritical regime without cubic nonlinearity are presented in the Figure 5.9. Distributions of generated wave are presented at the same time moments as distributions of the incident waves. Maximum amplitude amplification at the time 9.37 μs was B/A_0 = 77. Similar to incident wave, the amplitude of generated wave afterwards demonstrates singular behavior and blows up at the time $\tau = 9.39\,\mu s$. Time evolution of spatial distributions for the generated wave in the case when nonlinear phase shift is taken into account is presented in the Figure 5.10. Due to severely distorted incident wave pulse generated wave amplitude was oscillating in the medium and the growth was very limited. Generated wave amplitude has not even reached one tenth of the value of incident waves amplitudes.

Threshold equation of the explosive instability (5.18) suggests that the threshold condition has linear dependence on the amplitude of incident wave in case $A_{02} = A_{03}$ and on the pumping field amplitude h_0. Nonlinear phase shift has square dependence of the amplitude of oscillations as presented in the system of equations (5.50). This means that for example if the amplitude of initial oscillations is lowered by the factor of 3 and the pumping field amplitude is increased threefold, supercritical condition will be preserved, but nonlinear phase shift will be nine times less at the beginning of the process. This fact was used to simulate the process of three waves coupling in supercritical conditions with lower effective nonlinear phase shift. The value of incident wave amplitude was selected as $A_0 = 1 \cdot 10^{-10}\,m$ m and pumping field amplitude was selected at $h_0 = 150$ Oe. Numerical simulations of the process with neglected nonlinear phase shift yielded same result as presented in the Figures 5.7 and 5.9 as the supercriticality parameter has not changed and remained at Γ = 0.93. Time evolutions of amplitude distributions for the case when square nonlinearity and cubic nonlinearity phase shift were taken into account are presented in the Figure 5.11 and 5.12 for incident and generated wave respectfully. Lowering of the initial amplitude helped to reduce the influence of nonlinear phase shift on the instability development process. Initial pulse amplifications up to 3 times were obtained. Values of applied alternating pumping field h_0 = 150 Oe that were required for supercritical mode with these amplitudes are very hard to achieve experimentally. In the following paragraph perpendicular pumping field geometry is considered that provides more favourable conditions for supercritical three waves coupling.

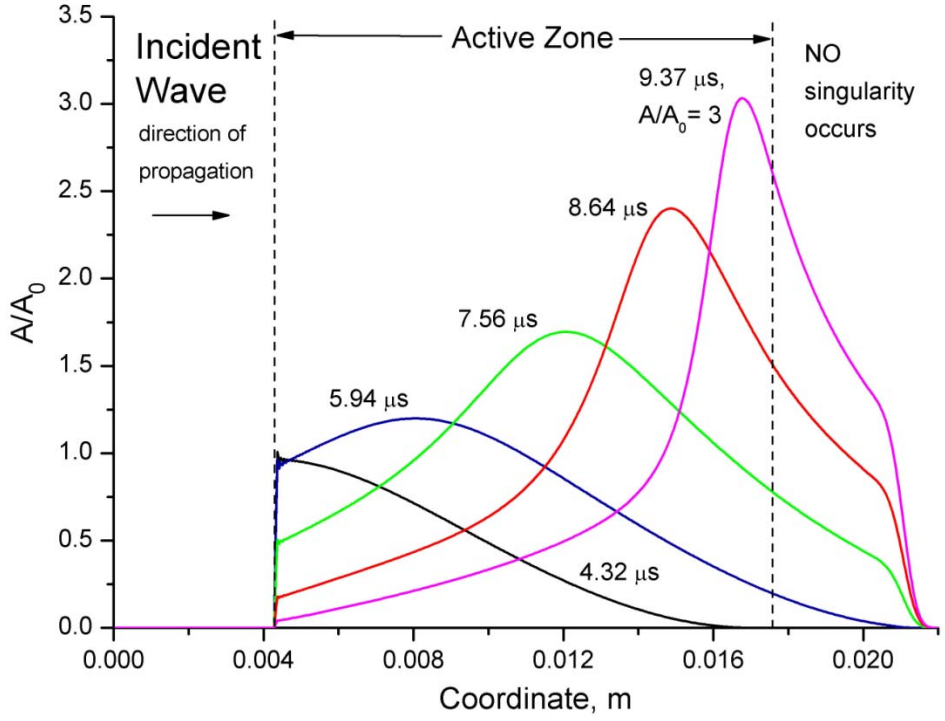

Figure 5.11. Supercritical time evolution of spatial distribution of normalized incident wave amplitude A/A_0 during three waves coupling process under parallel pumping with nonlinear phase shift. Distributions are shown for time moments: 4.32 μs (black), 5.54 μs (blue), 7.56 μs (green), 8.64 μs (red), 9.37 μs (purple). Singularity is not observed. $A_0 = 1 \cdot 10^{-10}$, $h_0 = 150$ Oe, $\Gamma = 0.93$.

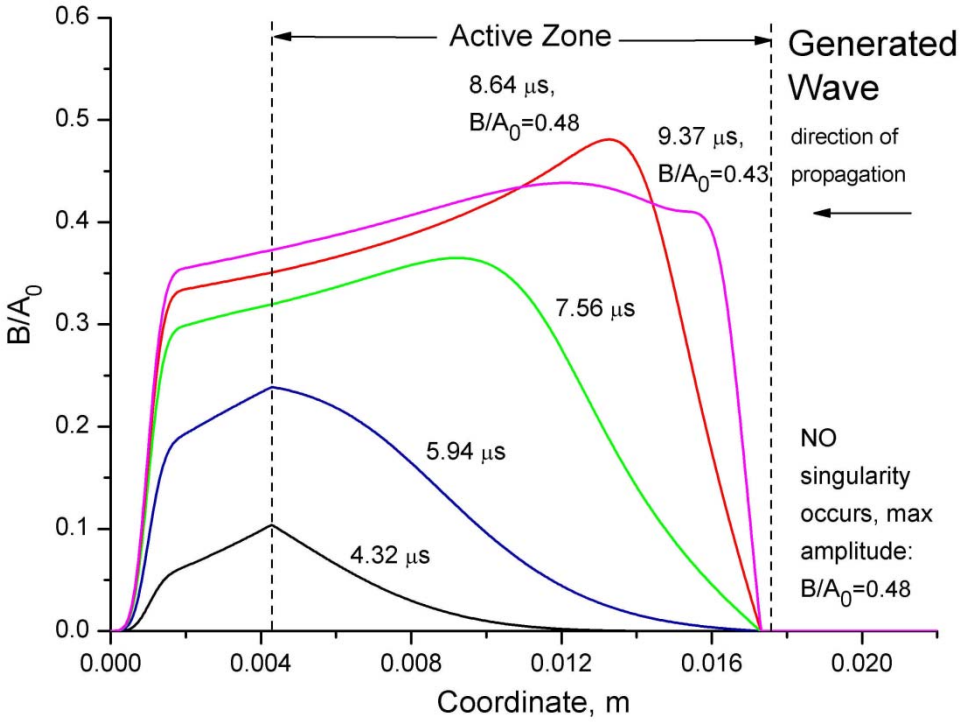

Figure 5.12. Supercritical time evolution of spatial distribution of normalized incident wave amplitude A/A_0 during three waves coupling process under parallel pumping with nonlinear phase shift. Distributions are shown for time moments: 4.32 μs (black), 5.54 μs (blue), 7.56 μs (green), 8.64 μs (red), 9.37 μs (purple). Singularity is not observed. $A_0 = 1 \cdot 10^{-10}$, $h_0 = 150$ Oe, $\Gamma = 0.93$.

5.7 Anharmonic model of three travelling waves coupling under perpendicular electromagnetic pumping

5.7.1 Three waves coupling under perpendicular electromagnetic pumping

In this section the model of nonlinear three waves interaction in easy plane antiferromagnetic crystal under perpendicular electromagnetic pumping is developed. As it has been shown in the Section 2.3 of the Second Chapter, the parametric interaction coefficient between three the waves is given by:

$$\hat{\Psi} = \left(\frac{H_E}{M_0}\right)^2 \frac{(H + H_D)h_0}{(\omega_{s0}/\gamma)^6}\left\{4(2\hat{B}_1)^2(2\hat{B}_2) - \Xi(2\hat{B}_2)^3/2\right\}, \tag{5.56}$$

where Ξ is defined as:

$$\Xi = \frac{3H_D + 4H}{H_D + H} + \frac{HH_D}{(\omega_{s0}/\gamma)^2} \tag{5.57}$$

The terms $(2\hat{B}_1)^2(2\hat{B}_2)$ represent coupling of two waves with polarization u_{yz} and one wave with polarization u_{xz}. The term $(2\hat{B}_2)^3$ represents coupling of three waves with polarization u_{xz}. Since a case when the wave vectors of two incident waves are identical is considered, their coupling is only possible if they have polarization u_{xz}. The density of magnetoelastic energy of coupling is expressed as:

$$F_{me} = \left(\hat{\Psi}\hat{u}^3\right) = \Phi h_\perp (2B_{14})^3 u_{xz}^3 , \tag{5.58}$$

where $u_{xz} = \frac{1}{2}\frac{\partial u_x}{\partial z}$. Looking for the solution in the form of the waves:

$$u_x = Ae^{i(\omega_A t - k_A z)} + Be^{i(\omega_B t - k_B z)} + c.c. , \tag{5.59}$$

considering that the component u_{xz} of the magnetoelastic stress tensor is given by:

$$(\sigma_{me})_{xz} = \frac{3}{8}\Phi h_\perp (2B_{14})^3 \left(\frac{\partial u_x}{\partial z}\right)^2 \tag{5.60}$$

and following similar calculation steps as presented for the three wave coupling model with parallel pumping the following system of equations of slowly varying amplitudes can be obtained:

$$\begin{cases} \omega_A \left(\dfrac{\partial A}{\partial t} + v_\perp(H) \dfrac{\partial A}{\partial z} \right) = -2\Psi_\perp A^* B^* + F_A \\ \omega_B \left(\dfrac{\partial B}{\partial t} - v_\perp(H) \dfrac{\partial B}{\partial z} \right) = -\Psi_\perp (A^*)^2 + F_B \end{cases} \tag{5.61}$$

Where $\Psi_\perp$ is the three wave coupling amplitude under perpendicular pumping that is given by:

$$\Psi_\perp = -6\zeta^4 V_\infty^2 k_A^3 \left(\frac{C_{44}}{2B_{14}} \right) \frac{(H + H_D)\left(HH_D + \frac{3}{2} H_E H_{ms} \right)}{(\omega_{s0}/\gamma)^4} h_0 \tag{5.62}$$

The components F_A, F_B are nonlinear contributions responsible for the nonlinear phase shift.

5.7.2 Nonlinear phase shift of three waves coupling under perpendicular pumping

Similar to the case with parallel pumping, nonlinear contributions F_A and F_B of the coupled magnetoelastic waves described by the system (5.61) come mainly from the cubic nonlinearity that can be characterised by effective elastic moduli $\hat{C}_{eff}^{(4)}$ (2.8). They can be calculated from the energy density of the cubic nonlinearity $F^{(4)}$ (5.33). In the case of perpendicular pumping, considering only the terms with u_{xz}^3 the corresponding component of magnetoelastic stress tensor can be described as:

$$\left(\sigma_{me}^{(4)} \right)_{xz} = \eta \xi 2 u_{xz}^3 \tag{5.63}$$

Substituting η and ξ defined by (5.35) and $u_{xz}^3 = \frac{1}{8} \frac{\partial^3 u_x}{\partial z^3}$ the component can be presented as:

$$\left(\sigma_{me}^{(4)}\right)_{xz} = \frac{3}{4}\eta\xi(-k_A^3)\begin{pmatrix}(|A|^2+8|B|^2)Ae^{i(\omega_A t-k_A z)}-\\-2(-4|A|^2-8|B|^2)Be^{i(\omega_B t+k_B z)}\end{pmatrix}+c.c. \tag{5.64}$$

Whence the contribution can be calculated as

$$\frac{\partial\left(\sigma_{me}^{(4)}\right)_{xz}}{\partial z} = \frac{3}{4}\eta\xi(-k_A^4)\begin{pmatrix}(|A|^2+8|B|^2)Ae^{i(\omega_A t-k_A z)}+\\+8(|A|^2-2|B|^2)Be^{i(\omega_B t+k_B z)}\end{pmatrix}+c.c \tag{5.65}$$

Whence the contributions can be calculated as:

$$\begin{aligned}F_A^{(4)} &= -\frac{3}{8i\rho}\xi\eta k_A^4(|A|^2+8|B|^2)A\\ F_B^{(4)} &= -\frac{3}{8i\rho}\xi\eta k_A^4 k_B(|A|^2+8|B|^2)B\end{aligned} \tag{5.66}$$

The second major contribution to the nonlinear phase shift comes from the second order of the perturbations theory square nonlinearity and total contribution in the system of equations (5.61) can be presented as a sum of square nonlinearity contribution and cubic nonlinearity contribution (5.40). The contribution of the square nonlinearity for the waves with *xz* polarization comes from the corresponding term in the tensor of magnetoelastic stress $\left(\sigma_{me}^{(3)}\right)_{xz} = C_{eff}^{(3)}\frac{1}{4}\left(\frac{\partial u_y}{\partial z}\right)\left(\frac{\partial u_x}{\partial z}\right)$. The component has both u_y and u_x contributions. Calculating these contributions in the same way as described for the case with parallel pumping the final contributions to of the cubic nonlinearity can be obtained as:

$$\begin{aligned}F_A^{(3)} &= -iV_\infty^2\zeta^8\left(\frac{C_{44}}{2B_{14}}\right)^2\frac{C_{44}}{\rho}k_A^4\left(|A|^2A\frac{1}{V_\infty^2-V_\perp^2}+8|B|^2A\left(\frac{1}{V_\infty^2-9V_\perp^2}+\frac{1}{9V_\infty^2-V_\perp^2}\right)\right)\\ F_B^{(3)} &= -iV_\infty^2\zeta^8\left(\frac{C_{44}}{2B_{14}}\right)^2\frac{C_{44}}{\rho}k_A^3k_B\left(|B|^2B\frac{1}{V_\infty^2-V_\perp^2}+8|A|^2B\left(\frac{1}{V_\infty^2-9V_\perp^2}+\frac{1}{9V_\infty^2-V_\perp^2}\right)\right)\end{aligned} \tag{5.67}$$

Substituting the square nonlinearity contributions (5.67) and cubic nonlinearity contributions (5.66) in the original system of equations (5.61) and regrouping the terms final equations of motion for incident and generated waves can be written as following system for slowly varying amplitudes:

$$\begin{cases} \omega_A\left(\dfrac{\partial A}{\partial t}+v_\perp(H)\dfrac{\partial A}{\partial z}\right)=-2\Psi A^*B^*+i[\alpha_{11}|A|^2+\alpha_{12}|B|^2]A \\ \omega_B\left(\dfrac{\partial B}{\partial t}-v_\perp(H)\dfrac{\partial B}{\partial z}\right)=-\Psi(A^*)^2+i[\alpha_{22}|B|^2+\alpha_{12}|A|^2]B \end{cases} \tag{5.68}$$

Where $\alpha_{11},\alpha_{22},\alpha_{12}$ are cubic nonlinearity coefficients described as:

$$\alpha_{11}=\zeta^6\left(\frac{C_{44}}{2B_{14}}\right)^2 v_\infty^2 k_A^4(3\vartheta-1)$$

$$\alpha_{22}=\zeta^6\left(\frac{C_{44}}{2B_{14}}\right) v_\infty^2 k_A^4 2(3\vartheta-1) \tag{5.69}$$

$$\alpha_{12}=\zeta^6\left(\frac{C_{44}}{2B_{14}}\right) v_\infty^2 k_A^4 8\left(3\vartheta-\zeta^2\left(\frac{9}{8+\zeta^2}-\frac{1}{8-9\zeta^2}\right)\right)$$

where $\vartheta=1+\frac{1}{4}\frac{HH_D}{HH_D+2H_EH_{ms}}$ and Ψ is the three waves interaction amplitude defined b:

$$\Psi=-6\zeta^4 v_\infty^2 k_A^3\left(\frac{C_{44}}{2B_{14}}\right)\frac{H+H_D}{HH_D+2H_EH_{ms}}h_0\frac{2HH_D+3H_EH_{ms}}{2(HH_D+2H_EH_{ms})} \tag{5.70}$$

For linearly-coupled magnetoelastic waves with *xz* polarization circular frequency has following dependence on the wave vector:

$$\omega_A=\sqrt{\frac{C_{44}(H)}{\rho}}|k_A| \tag{5.71}$$

The circular frequency of the pumping field ω_p can be determined from the condition of phase synchronism (5.53) and the fact that $2k_A=-k_B$:

$$\omega_p=2\omega_A+\omega_B=4\omega_A=4\sqrt{\frac{C_{44}(H)}{\rho}}|k_A| \tag{5.72}$$

Thus in the perpendicular geometry model the pumping has to be applied at the frequency four times higher than the incident wave frequency.

5.8 Numerical simulations of three travelling waves coupling model with perpendicular pumping

Numerical simulations of the three waves coupling model under perpendicular pumping in time and space domains were conducted with the help of the same Fortran program that was used for simulations of the model with parallel pumping. The real and imaginary parts of the equations (5.68) were separated and the terms were regrouped:

$$\begin{cases} \frac{\partial A_r}{\partial t} = -v_\perp(H)\frac{\partial A_r}{\partial z} - \frac{2\Psi}{\omega_1}[A_r B_r - A_i B_i] - \frac{A_i}{\omega_1}[\alpha_{11}(A_r^2 + A_i^2) + \alpha_{12}(B_r^2 + B_i^2)] \\ \frac{\partial A_i}{\partial t} = -v_\perp(H)\frac{\partial A_i}{\partial z} + \frac{2\Psi}{\omega_1}[A_i B_r - A_r B_i] - \frac{A_r}{\omega_1}[\alpha_{11}(A_r^2 + A_i^2) + \alpha_{12}(B_r^2 + B_i^2)] \\ \frac{\partial B_r}{\partial t} = v_\perp(H)\frac{\partial B_r}{\partial z} - \frac{\Psi}{\omega_2}[A_r^2 + A_i^2] - \frac{B_i}{\omega_2}[\alpha_{22}(B_r^2 + B_i^2) + \alpha_{12}(A_r^2 + A_i^2)] \\ \frac{\partial B_i}{\partial t} = v_\perp(H)\frac{\partial B_i}{\partial z} + \frac{\Psi}{\omega_2}[2A_r A_i] + \frac{B_r}{\omega_2}[\alpha_{22}(B_r^2 + B_i^2) + \alpha_{12}(A_r^2 + A_i^2)] \end{cases} \quad (5.73)$$

System of equations (5.71) was directly solved with the help of the program.

5.8.1 Perpendicular geometry model numerical solutions in subthreshold mode

Calculations of the three-wave coupling coefficient under perpendicular pumping defined by the equation (5.70) at the selected operating point show the value of $|\Psi| = 5.68 \cdot 10^{21} \times h_0$ using the same values of variables as were used for parallel pumping: $\zeta^2 = 0.46$, $k_A = 2.1 \cdot 10^4\ m^{-1}$, $v_\infty = 4 \cdot 10^3\ m^{-1}$. Its value is 2.58 times higher than the coefficient value under parallel pumping. Such a considerable increase creates better conditions for supercritical experimental observation as lower amplitudes of incident waves and pumping field need to be applied to go beyond the threshold. The value of incident waves ultrasound frequencies was selected as $\frac{\omega_A}{2\pi} = 10$ MHz. The amplitude of incident waves was selected as $A_0 = 10^{-10}\ m$.

Sub-threshold behaviour of perpendicular pumping model for three-wave coupling under was numerically simulated the pumping field amplitude $h_0 = 20$ Oe. According to the

threshold condition (5.18) this corresponds to the supercriticality parameter $\Gamma = 0.42$ which is below the instability threshold.

The results of numerical simulation of the system of equations (5.73) with the nonlinear phase shift defined by the coefficients (5.69) are presented in the Figure 5.13. Two incident waves with identical wave vector are introduced at the border of active zone and propagate to the right. As a result of the nonlinear three-wave interaction, a wave with double value of wave vector is generated that propagates to the left. The amplitude of incident waves also increases during the process, but as the system is in subthreshold mode no explosive instability is observed.

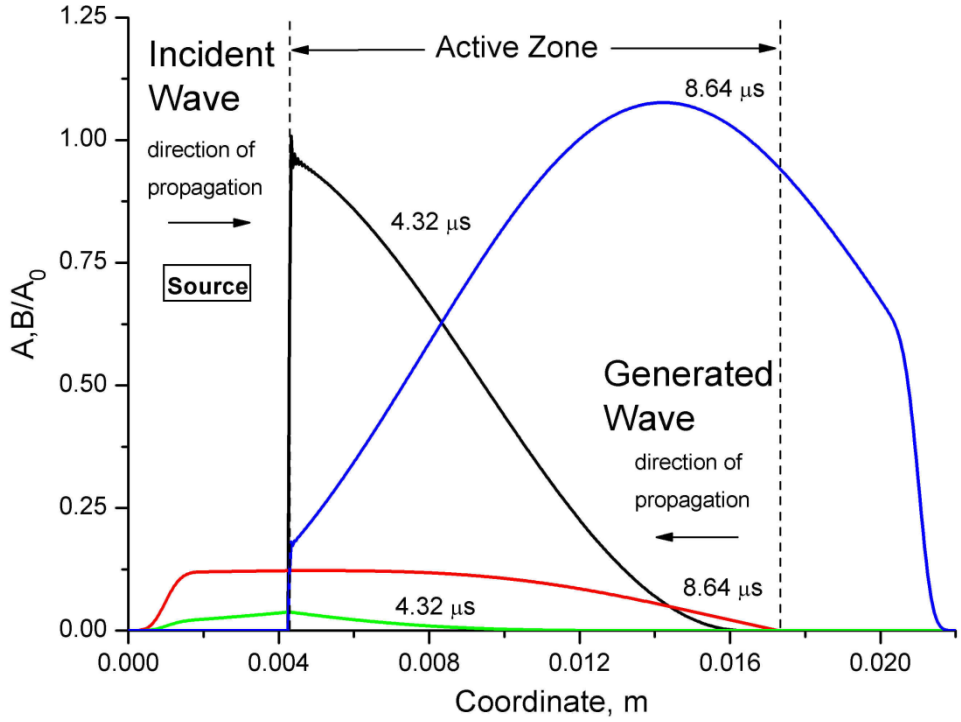

Figure 5.13. Supercritical time evolution of spatial distribution of normalized incident and generated wave amplitudes A/A_0, B/A_0 during three waves coupling process under perpendicular pumping with subthreshold conditions. Distributions are presented at two time moments for incident (black) and generated (green) waves at 4.32 μs and for incident (blue) and generated (red) waves at 8.64 μs. $A_0 = 10^{-10}$ $h_0 = 20$ Oe., $\Gamma = 0.42$.

If the nonlinear phase shift is neglected and coefficients values (5.69) are set to zero the system demonstrates similar behaviour as presented in the Figure 5.13, as in subthreshold mode and low displacement amplitudes phase shift has a little effect on coupling process.

5.7.2 Perpendicular geometry model numerical solutions in supercritical mode

Higher value of the nonlinear three-wave coupling coefficient Ψ in the perpendicular pumping geometry creates favourable conditions for supercritical mode investigation at lower pumping fields compared to parallel pumping geometry. If the amplitude of incident waves is left the same at $A_0 = 1 \cdot 10^{-10}\ m$ and the value of pumping magnetic field is increased to $h_0 = 50$ Oe corresponding value of supercriticality parameter becomes $\Gamma = 1.04$. This pumping field value was used for supercritical numerical simulations of developed three waves coupling anharmonic model under perpendicular pumping. The effect of nonlinear phase shift in the model in supercritical mode was analyzed comparing simulations of the system of equations (5.73) with the real values of the coefficients (5.69) and with the values of coefficients set to zero.

Time evolution of spatial distributions of the incident waves in supercritical regime without nonlinear phase shift is presented in the Figure 5.14. Distributions of the incident wave amplitude are presented at the time t = 4.32 μs (black line), 5.54 μs (blue line), 7.56 μs (green line), 8.64 μs (red line), 9.31 μs (purple line). Maximum amplitude amplification at the time 9.37 μs is A/A_0 = 130, reaching infinity and blowing up at the time 9.37 μs. Similar to the parallel pumping model the effect of spatial localization clearly manifests itself as the maximum amplitude amplification is only observed in a small part of incident pulse. Time evolution of spatial distributions of the incident waves at the same supercritical conditions but with real crystal nonlinear phase shift is presented in the Figure 5.15. Distributions are presented at the same time moments as in Figure 5.14 using the same colors. When the strong cubic nonlinearity of AFEP crystals was taken into account explosive behavior of coupled magnetoelastic three-wave interaction was limited. However maximum observed incident wave amplitude amplification was A/A_0 = 14 times which is much higher than amplification of 3 times obtained in parallel pumping model. The shape of the incident pulse also got distorted. Obtained time evolutions of normalized amplitude distributions for generated wave in supercritical regime without and with nonlinear phase shift are presented in the Figures 5.16 and 5.17 respectfully.

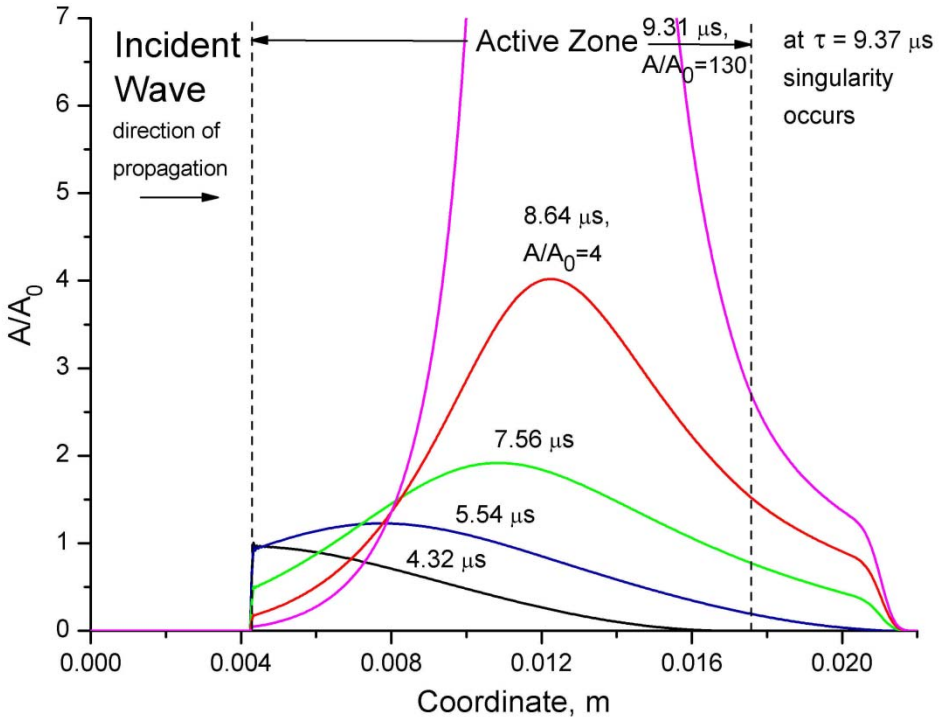

Figure 5.14. Supercritical time evolution of spatial distribution of normalized incident wave amplitude A/A_0 during three waves coupling process under parallel pumping without nonlinear phase shift. Distributions are presented at the time moments: 4.32 μs (black), 5.54 μs (blue), 7.56 μs (green), 8.64 μs (red) and 9.31 μs (purple). At τ = 9.37 μs singularity occurs. $A_0 = 10^{-10}$, $h_0 = 50$ Oe, $\Gamma = 1.04$.

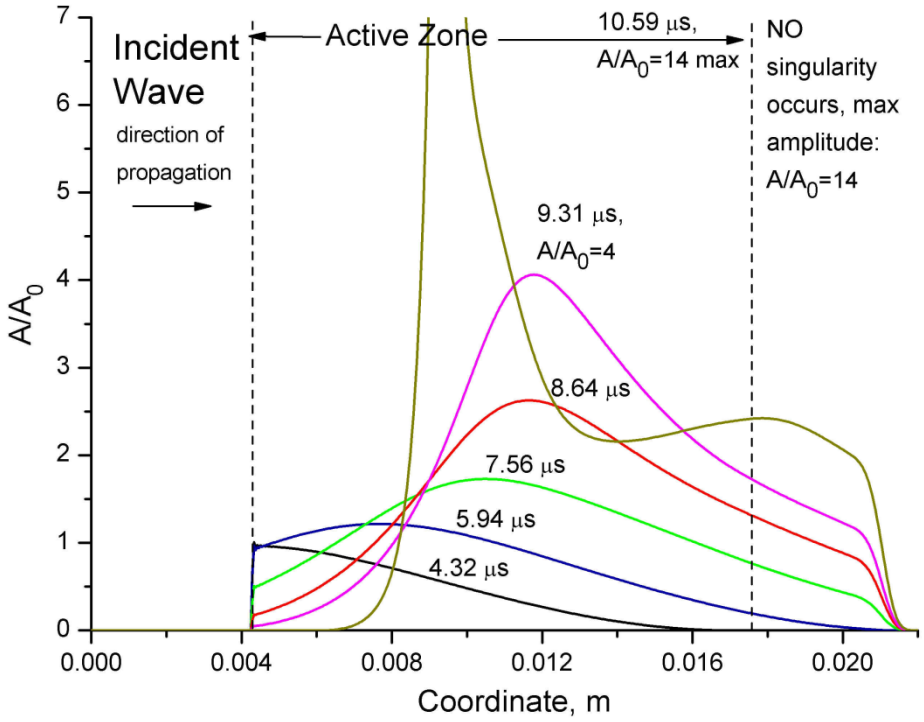

Figure 5.15. Supercritical time evolution of spatial distribution of incident wave amplitude A/A_0 during three waves coupling process under parallel pumping with nonlinear phase shift. Distributions are shown for time moments: 4.32 μs (black), 5.54 μs (blue), 7.56 μs (green), 8.64 μs (red) and 9.31 μs (purple)) and 10.59 μs (khaki). At τ = 9.37 μs singularity occurs. $A_0 = 10^{-10}$, $h_0 = 50$ Oe, $\Gamma = 1.04$.

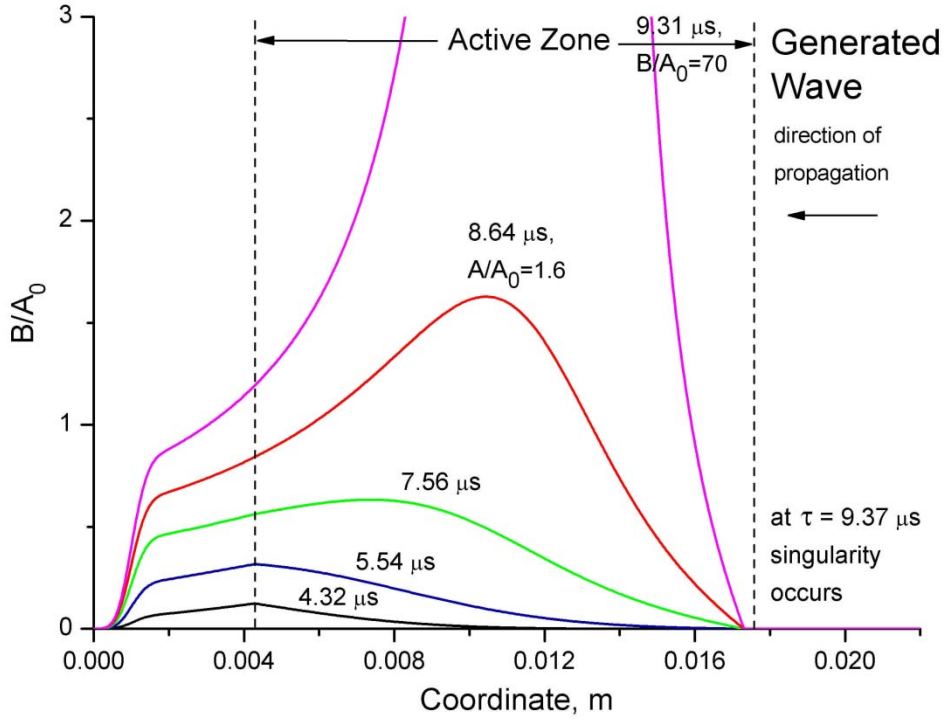

Figure 5.16. Supercritical time evolution of spatial distribution of normalized generated wave amplitude B/A_0 during three waves coupling process under parallel pumping without nonlinear phase shift. Distributions are shown for time moments: 4.32 μs (black), 5.54 μs (blue), 7.56 μs (green), 8.64 μs (red) and 9.31 μs (purple). At τ = 9.37 μs singularity occurs. $A_0 = 10^{-10}$, h_0 = 50 Oe, Γ = 1.04.

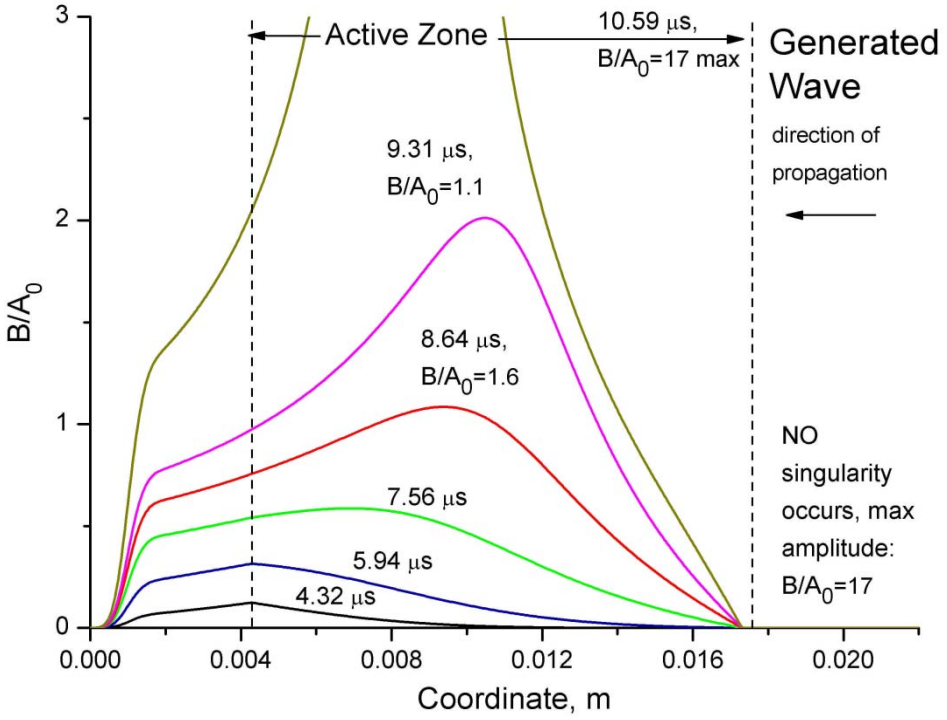

Figure 5.17. Supercritical time evolution of spatial distribution of generated wave amplitude B/A_0 during three waves coupling process under parallel pumping with nonlinear phase shift. Distributions are shown for time moments: 4.32 μs (black), 5.54 μs (blue), 7.56 μs (green), 8.64 μs (red), 9.31 μs (purple) and 10.59 μs (khaki). No singularity is observed. $A_0 = 10^{-10}$, h_0 = 50 Oe, Γ = 1.04.

Distributions of the generated wave are presented at the same time moments as distributions of the incident waves and are marked with the same colors. Without nonlinear phase shift generated wave demonstrates maximum amplitude amplification at the time 9.37 μs of B/A_0 = 77 that tends to infinity and reaches singularity at the time $\tau = 9.39\,\mu s$. The amplitude amplification of generated wave in the case when nonlinear phase shift is taken into account reaches its maximum value of B/A_0 = 17 at the time t = 10.59 μs and then starts oscillating. Explosive dynamics is not observed.

Obtained results demonstrate that perpendicular pumping geometry creates more favorable conditions for supercritical three waves coupling with considerably lower threshold in comparison with parallel pumping. The influence of nonlinear phase shift on the generated ultrasonic triads is also much lower in the perpendicular pumping model. Analysis of supercritical dynamics of a magnetoelastic resonator, presented in the Second Chapter of this work suggested, that nonlinear frequency shift can be compensated with the help of a proper phase modulation law. Similar technique can be developed for the coupling with travelling waves.

5.8.3 Nonlinear phase shift compensation

The resonance phase synchronism condition (5.22) can be also defined as:

$$\varphi_p = 2\varphi_A + \varphi_B\,, \tag{5.74}$$

where φ_p is the phase of pumping, φ_A and φ_B are the phases of incident and generated waves respectively. When nonlinear phase shift is neglected the condition (5.74) is fulfilled and in supercritical mode explosive instability is observed. However when cubic nonlinearity is introduced it creates an uncompensated phase shift that is proportional to the amplitudes of incident and conjugated waves and is given by:

$$\Phi = \varphi_p - 2\varphi_A - \varphi_B, \tag{5.75}$$

In contrast with magnetoelastic resonator model, in travelling waves model the value of nonlinear phase shift is different at every point of the medium. Supercritical time evolution

of the spatial distributions of nonlinear phase shift of three waves coupling under perpendicular pumping is presented in the Figure 5.18.

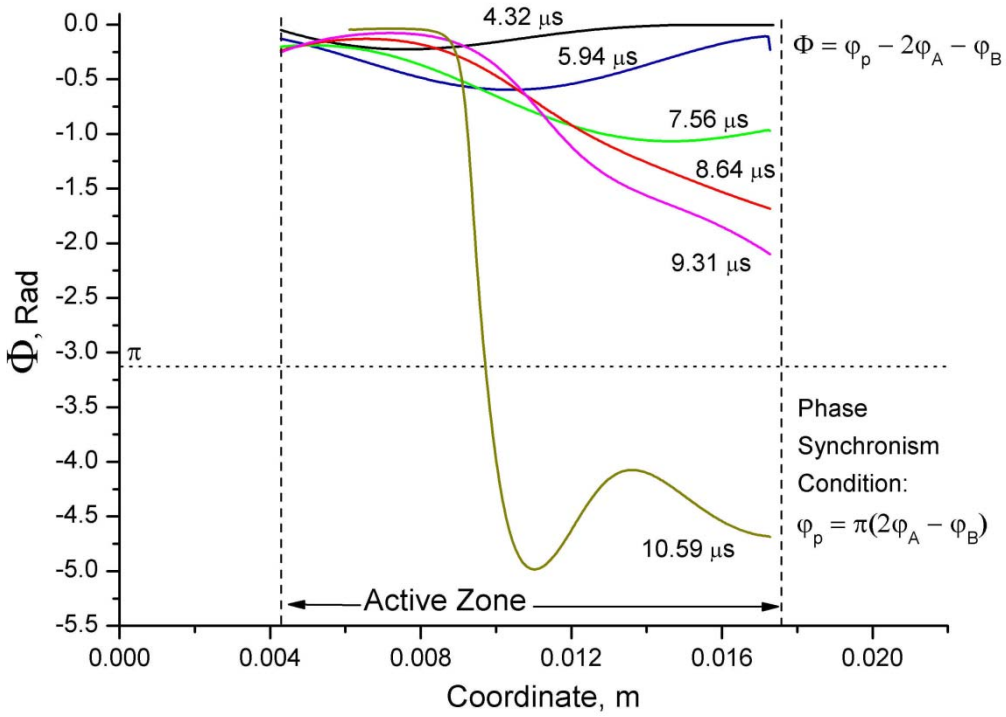

Figure 5.18. . Supercritical time evolution of the spatial distribution of nonlinear phase shift of three waves coupling under perpendicular pumping. Distributions are presented at the time moments: 4.32 μs (black), 5.54 μs (blue), 7.56 μs (green), 8.64 μs (red), 9.31 μs (purple) and 10.59 μs (khaki). $A_0 = 10^{-10}$, $h_0 = 50$ *Oe,* $\Gamma = 1.04$.

The Figure 5.18 corresponds to the supercritical time evolutions of spatial distributions of incident and generated waves, presented in the Figures 5.15 and 5.17 correspondingly. The phase shifts of incident and generated waves were calculated from imaginary and real parts of wave amplitudes as:

$$\varphi_A = \text{atan2}(A_i, A_r)\,, \varphi_B = \text{atan2}(B_i, B_r), \tag{5.76}$$

where atan2(*x,y*) is a variation of arctangent function that returns the angle of a complex point in radians with coordinates (*x,y*). The phase of pumping was considered to be constant. Figure 5.18 shows, that as the amplitude of oscillations grows, the phase is being shifted from the optimal value of $n\pi$ (where n = 0, |1|, |2|...) to the intermediary values. Phase shift distribution in the medium can be changed by introducing pumping field phase modulation. To introduce pumping phase modulation in the system of equations (5.73) the amplitude of three wave coupling can be presented as a complex number:

$$\Psi \to \Psi e^{-i\varphi} = \Psi\cos\varphi - i\Psi\sin\varphi\,, \tag{5.77}$$

where φ is the phase of pumping that can be modulated as $\varphi(t)$. Introducing (5.77) to (5.73) and applying new variables defined as:

$$D = (A_r B_r - A_i B_i), \qquad S = (A_i B_r + A_r B_i), \qquad D_A = (A_r^2 - A_i^2) \tag{5.78}$$

The final system of equations with pumping phase modulation becomes:

$$\begin{cases} \dfrac{\partial A_r}{\partial t} = -v_\perp(H)\dfrac{\partial A_r}{\partial z} - \dfrac{2\Psi\cos\varphi}{\omega_1}D + \dfrac{2\Psi\sin\varphi}{\omega_1}S - \dfrac{A_i}{\omega_1}(\alpha_{11}|A|^2 + \alpha_{12}|B|^2) \\ \dfrac{\partial A_i}{\partial t} = -v_\perp(H)\dfrac{\partial A_i}{\partial z} + \dfrac{2\Psi\cos\varphi}{\omega_1}S + \dfrac{2\Psi\sin\varphi}{\omega_1}D + \dfrac{A_r}{\omega_1}(\alpha_{11}|A|^2 + \alpha_{12}|B|^2) \\ \dfrac{\partial B_r}{\partial t} = v_\perp(H)\dfrac{\partial B_r}{\partial z} - \dfrac{2\Psi\cos\varphi}{\omega_2}D_A + \dfrac{2\Psi\sin\varphi}{\omega_2}2A_rA_i - \dfrac{B_i}{\omega_2}(\alpha_{22}|B|^2 + \alpha_{12}|A|^2) \\ \dfrac{\partial B_i}{\partial t} = v_\perp(H)\dfrac{\partial B_i}{\partial z} + \dfrac{2\Psi\cos\varphi}{\omega_2}2A_rA_i + \dfrac{2\Psi\sin\varphi}{\omega_2}D_A + \dfrac{B_r}{\omega_2}(\alpha_{11}|B|^2 + \alpha_{12}|A|^2) \end{cases} \tag{5.79}$$

The system of equations (5.79) describes three travelling waves coupling process in AFEP crystal under phase-modulated perpendicular pumping.

In the Second Chapter a law was derived for a magnetoelastic resonator that allowed complete nonlinear frequency shift compensation for a resonance mode via self-consistent pumping field modulation. In the case of travelling waves the value of nonlinear phase shift is different in every point, so full compensation is impossible. However for travelling waves in a system with high supercriticality parameter even partial compensation of the phase shift can help to manifest explosive dynamics.

In the present research the point with maximum oscillations amplitude in the medium was tracked and the phase of the pumping pulse was adjusted proportionally to the maximum amplitude to provide optimal conditions in that point. An optimal phase modulation law was empirically found to be proportional to the amplitude of incident wave as $\varphi_p(t) = -0.7\cdot 10^9\, A_{max}(t)$. Resulted singular phase modulation law was recorded and can be applied in experimental conditions. Numerical simulations of the system of equations (5.79) with the suggested phase modulation law are presented in the Figures 5.18 and 5.19 for incident and generated waves respectively.

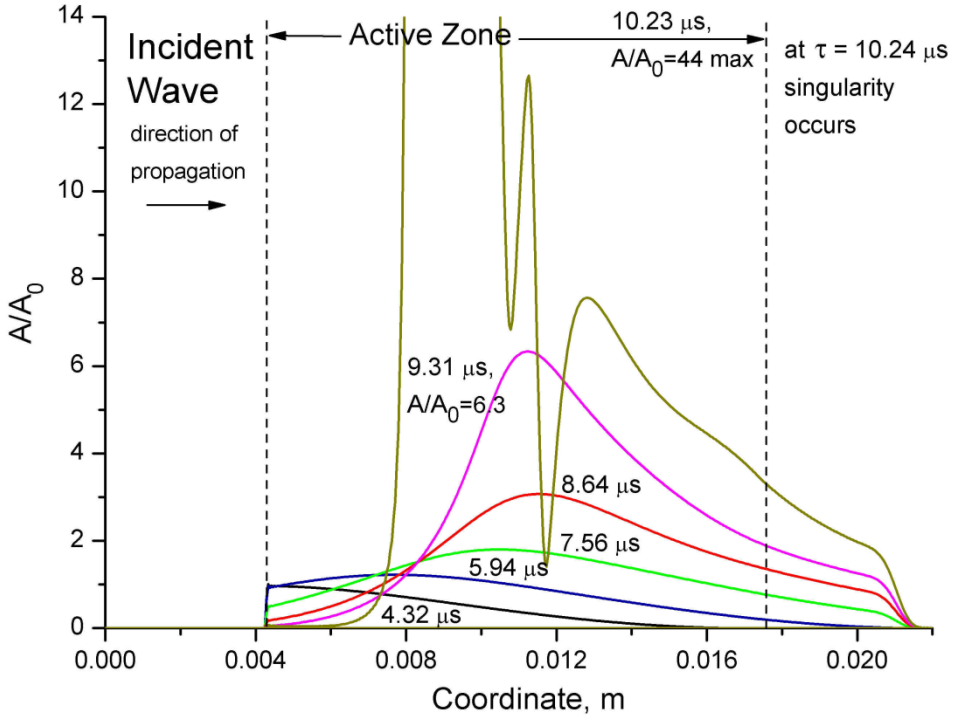

Figure 5.18. Supercritical time evolution of spatial distribution of normalized generated wave amplitude B/A_0 with nonlinear phase shift under perpendicualr modulated pumping. Distributions are presented at the time moments: 4.32 μs (black), 5.54 μs (blue), 7.56 μs (green), 8.64 μs (red), 9.31 μs (purple) and 10.23 μs (khaki). At τ = 10.24 μs singularity occurs. $A_0 = 10^{-10}$, h_0 = 50 Oe, Γ = 1.04.

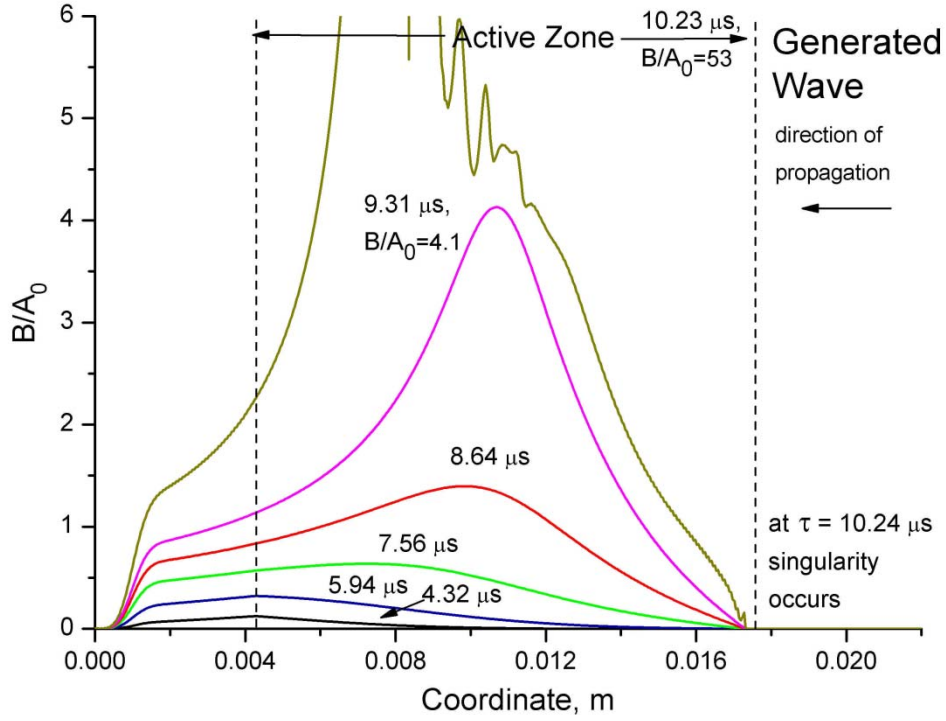

Figure 5.19. Supercritical time evolution of spatial distribution of normalized generated wave amplitude B/A_0 with nonlinear phase shift under perpendicualr modulated pumping. Distributions are presented at the time moments: 4.32 μs (black), 5.54 μs (blue), 7.56 μs (green), 8.64 μs (red), 9.31 μs (purple) and 10.23 μs (khaki). At τ = 10.24 μs singularity occurs. $A_0 = 10^{-10}$, h_0 = 50 Oe, Γ = 1.04.

The simulations with the suggested pumping field modulation law show clear explosive dynamics of the system; however the time evolution of the amplitudes distribution differs from the one observed for the system with neglected nonlinear phase shift. Explosion of the amplitudes occurred at the time $\tau_{s2} = 10.24$ μs which is more than the explosion time of $\tau_{s1} = 9.37$ μs for the system at the same threshold conditions and neglected contributions of nonlinearities. The shapes of incident and generated wave pulses were more distorted than in previously observed singularities. Spatial localization of the ultrasonic triads' generation also changed. For the singularity observed under modulated pumping it was first forming at the coordinate $z = 0.011$ *m* but then closer to the explosion it was moving backwards in the Active Zone with the singularity forming at the coordinate $z = 0.008$ *m*.

Supercritical dynamics of normalized maximum incident wave amplitude value during three-wave coupling process under modulated perpendicular pumping is presented in the Figure 5.20 with a red line. This curve tracks evolution of the highest amplitude point of the distributions presented in the Figure 5.18 and also describes linear law that was applied to modulate the phase of pumping field with corresponding proportionality constant $-0.7 \cdot 10^9$.

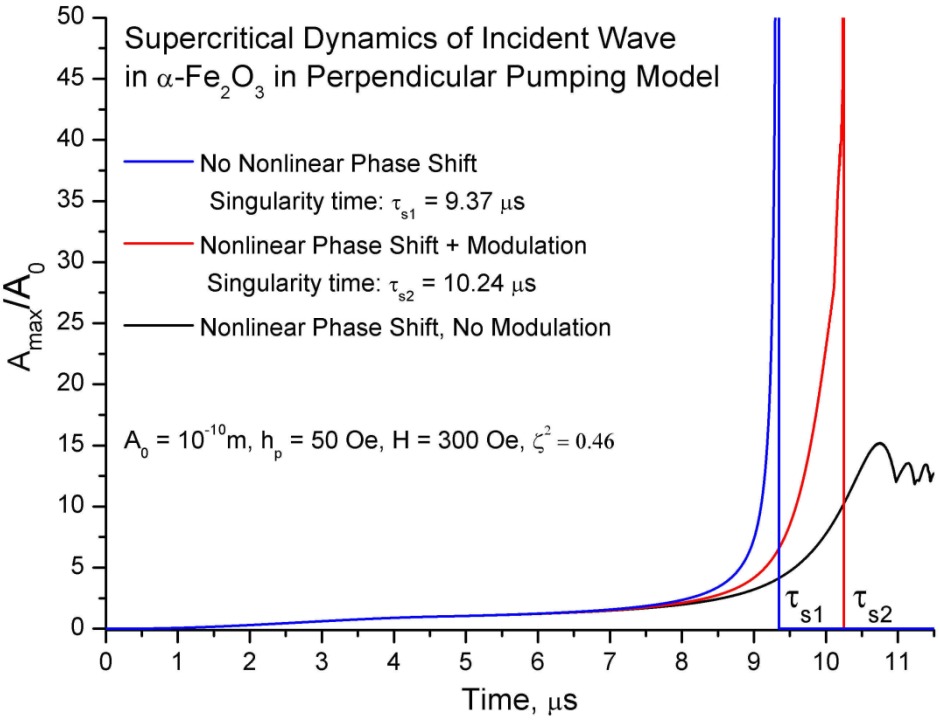

Figure 5.20. Supercritical dynamics of normalized maximum incident wave amplitude A_{max}/A_0 during three waves coupling process in perpendicular geometry: (blue) without nonlinear phase shift and non-modulated pumping, (red) with nonlinear phase shift and modulated pumping, (black) with nonlinear phase shift and non-modulated pumping. $A_0 = 10^{-10}$, $h_0 = 50$ Oe, $\Gamma = 1.04$.

The blue line in the Figure 5.20 shows supercritical dynamics of normalized maximum incident wave amplitude A_{max}/A_0 under perpendicular pumping for the case when nonlinear phase shift is neglected. This curve tracks evolution of the maximum amplitude point of the distributions presented in the Figure 5.14. Singularity times of both instabilities are shown in the figure as $\tau_{s2} = 10.24$ μs and $\tau_{s1} = 9.37$ μs in the same order.

The black line in the Figure 5.20 presents supercritical dynamics of normalized maximum incident wave amplitude value during three-wave coupling process under perpendicular pumping without modulation. This curve tracks evolution of the maximum amplitude point of the distributions presented in the Figure 5.15. Amplitude growth is limited and no singularity is observed. Maximum amplitude amplification is observed at the time moment 10.59 μs and then the amplitude starts oscillating.

5.9 Chapter V conclusion

Two anharmonic models of nonlinear three waves coupling in easy plane antiferromagnets for parallel and perpendicular electromagnetic pumping have been developed. The models take into account important contributions of square and cubic nonlinearities of a real AFEP crystal that were found to be the main causes of misphasing mechanism in ultrasound triads' generation.

A custom computer program has been created for numerical simulations of the models in time and space domains. The program was written in Fortran and uses advanced numerical methods for calculations. Numerical simulations of the developed models were conducted with the help of the program using the properties of magnetoelastic waves that have been studied experimentally on hematite crystal. Solutions showed that both models have instability thresholds. When the nonlinear phase shift was neglected in supercritical regime both models demonstrate explosive dynamics with spatial localization of ultrasound triads' generation. Thresholds of explosive instability for both models were found to depend on the amplitude of incident waves, their frequency, pumping field amplitude and magnetoelastic properties of the crystal. The value of instability threshold for perpendicular pumping geometry was found to be 2.58 times lower than for the parallel pumping geometry. This

considerable difference makes perpendicular pumping model more interesting for experimental studies of supercritical dynamics.

Introduction of square and cubic nonlinearity terms in the numerical simulations limited explosive dynamics of supercritical ultrasound triads' generation. These nonlinearities were causing nonlinear phase shift that affected the process. Misphasing was found to be lower in the model with perpendicular pumping geometry. Pumping field phase modulation was introduced in the perpendicular geometry model with a suggested empirical law of phase modulation. Supercritical dynamics of the model with suggested law demonstrated explosive behaviour as the modulation partially compensates the influence of nonlinear shift.

As a result the conducted studies of nonlinear three-waves coupling in anharmonic models have shown that explosive instability of magnetoelastic waves can be experimentally observed in strongly nonlinear easy plane antiferromagnets at feasible electromagnetic pumping fields of about 50 Oe applied perpendicularly to the bias magnetic field with proper modulation and incident wave amplitude values of 10^{-10} *m*.

Thesis Conclusion

Recently discovered nonlinear parametric instabilities manifest themselves in the form of multi-boson processes and possess some unique features. Three quasi-phonon excitations in easy plane antiferromagnet resonator have been analyzed on the basis of anharmonic approximation that takes into account energy terms up to the fourth order. Analysis showed that nonlinear parametric instability arises when threshold conditions of excitations are met. These conditions depend not only on the intensity of the pumping field, but also on the amplitude of initial oscillations. In supercritical mode three quasi-phonon excitations are expected to demonstrate explosive dynamics, which however is limited by other nonlinear effects. The main mechanism that limits supercritical explosive dynamics manifestation has been determined to be the nonlinear frequency shift that comes from strong cubic nonlinearity.

An advanced pumping field phase modulation technique has been proposed to compensate the nonlinear frequency shift. A proper consistent time-varying singular modulation law has been derived. Numerical solutions of the anharmonic equations of motion of magnetoelastic resonator with the parameters of a real easy plane antiferromagnetic crystal demonstrated explosive supercritical dynamics of three quasi-phonon excitations.

Suggested modulation law was used for experimental supercritical three quasi-phonon excitations. For the first time supercritical explosive dynamics of coupled triads of magneto-elastic waves in single mode regime was experimentally observed and studied in hematite single crystal resonator. New experimental method has been developed that allows arbitrary pumping pulse frequency modulation and continuous amplitude monitoring of magnetoelastic oscillations under electromagnetic pumping.

The studies were extended on another high temperature easy plane antiferromagnet – iron borate. Experimental studies of magnetoelastic parameters of iron borate were conducted in the temperature range 293 K – 77 K where crystal properties vary essentially. For the first time nonlinear frequency shift and quality factor of iron borate resonator were investigated at different temperatures. Supercritical explosive dynamics of three quasi-phonon excitations in

iron borate was studied at different operating points at 77 K and at 293 K. Low temperature conditions were found to be more favorable for three quasi-phonon excitations in the crystal.

In order to describe the behavior of magnetoelastic resonator at high oscillation amplitudes anharmonic approximation was found to be insufficient. Strongly nonlinear model of quasi-phonon triads' excitation has been developed that takes into account higher order nonlinearities. Numerical simulations of the strongly nonlinear model for supercritical excitations in hematite resonator and for iron borate resonator at 77 K and 293 K showed good agreement with experimentally obtained results, proving that the model can be used to describe resonator dynamics at high amplitudes.

Together with stationary waves researched in the resonators, travelling magnetoelastic waves present a great applied value. Nonlinear coupling of three travelling magnetoelastic waves under electromagnetic pumping has been considered in strongly nonlinear medium of easy plane antiferromagnetic crystal. Two models of ultrasound triads' interaction with different geometries of pumping have been developed. The first model considers pumping applied parallel to the bias magnetic field and the second model considers pumping applied perpendicular to the bias field. Both models are anharmonic and consider energy contributions up to the fourth order.

The models were numerically simulated with custom computer program that was written using Fortran language. Solutions showed that nonlinear coupling of the waves also has instability threshold that depends on the amplitude of the waves and on the amplitude of coupling pumping field. The value of instability threshold for perpendicular pumping geometry was found to be 2.58 times lower than for the parallel pumping geometry. This considerable difference makes perpendicular pumping model more interesting for experimental studies of supercritical dynamics.

In supercritical mode both models demonstrate explosive dynamics of the amplitudes of the waves with spatial localization of generated ultrasound triads. However, just like in magnetoelastic resonator, other nonlinear effects limit the amplification by nonlinear phase shift. Suggested pumping field phase modulation law helped to overcome this limitation and explosive supercritical dynamics of coupled waves was obtained in modeled magnetoelastic crystal with strong cubic nonlinearity of hematite.

Nonlinear parametric coupling of travelling waves has a great potential in real life applications, notably in wave phase conjugators and navigation. Initial amplitude threshold condition allows selective amplification of the signals. Explosive supercritical dynamics gives faster amplitude increase in comparison with linear parametric processes. Spatial localization of amplification permits spectra modulations and creation of short powerful wave pulses. Theoretical studies that used parameters of hematite have shown that supercritical nonlinear three travelling waves' coupling is experimentally feasible. Perpendicular geometry of applied pumping field is preferred for lower instability thresholds and proper phase modulation is required for nonlinear phase shift compensation.

Résumé étendu en Français

Les effets non linéaires représentent un problème très important pour la science moderne. En acoustique, les phénomènes non linéaires et paramétriques dans les solides sont très divers et sont un outil puissant pour la recherche scientifique sur les propriétés de la matière. Ces phénomènes présentent aussi un grand intérêt car ils peuvent être utilisés dans les applications ultrasonores diverses telles que la biomédecine et l'industrie pour le contrôle non-destructif, l'imagerie ultrasonore, le traitement des signaux, etc. Ces dernières années, les effets non linéaires dans les "solides mous" sont devenus des sujets d'actualités pour le diagnostic biomédical ultrasonore, par exemple. En particulier, la technique d'imagerie supersonique d'élasticité avec les ondes de cisaillement a été développée et utilisée dans l'élastographie. Les effets d'amplification du signal paramétrique et d'inversion du front d'onde ultrasonore sont bien connus et utilisés dans la conjugaison de phase. Ils sont basés soit sur des céramiques piézoélectriques PZT fortement non linéaires, soit sur des céramiques magnéto-acoustiques comme milieux actifs. La combinaison de cette technique avec l'imagerie d'harmoniques non linéaires permet la visualisation des fantômes isoéchogènes et augmente la résolution de l'imagerie.

Les effets paramétriques utilisés dans ces applications proviennent de la modulation des paramètres linéaires d'un système. Récemment, la recherche s'est étendue aussi aux effets paramétriques causés par la variation des paramètres non-linéaires dans les matières condensées et les systèmes micro-électromécaniques. Ce type de modulation a ouvert une nouvelle catégorie d'instabilités qui se manifestent comme des excitations couplées à multi-bosons. Ces effets ont été signalés auparavant uniquement en physique des plasmas. Les processus multi-bosons sont également intéressants en physique fondamentale, plus particulièrement dans le cas de la physique des particules élémentaires.

Dans les matériaux où les ondes acoustiques sont couplées avec des excitations d'autres natures, les non linéarités de couplage et du sous-système (piézo-électrique ou magnétique par exemple) introduisent une non linéarité effective aux excitations du sous-système élastique. Ceci se traduit alors par un changement des modules élastiques non linéaires pour les oscillations quasi-élastiques. Dans le cas des matériaux

antiferromagnétiques à haute température et à anisotropie "plan facile" (AFPF) comme α-Fe_2O_3 et $FeBO_3$, le changement des modules est exceptionnellement élevé en raison de la participation de l'interaction d'échange dans les oscillations des ondes de grande longueur. Cela introduit alors une anharmonicité effective géante dans les cristaux et font des AFPFs des milieux modèles, très pratiques pour les études des phénomènes de la dynamique non linéaire des milieux continus.

Les excitations acoustiques dans les milieux antiferromagnétiques se manifestent généralement comme des ondes hybrides magnéto-élastiques qui sont appelées quasi-phonons. Le couplage phonon-magnon exceptionnellement fort dans les AFPFs se manifeste en particulier pendant la génération paramétrique des paires de quasi-phonons. Ces paires peuvent être couplées avec l'aide de la modulation d'un champ électromagnétique. Le seuil de profondeur de modulation pour ces instabilités dépend des paramètres d'amortissement dans le milieu. On montre également, en régime supercritique, que la dynamique a une croissance exponentielle. Un certain nombre d'autres effets paramétriques et non linéaires ont aussi été prédits théoriquement et observés expérimentalement observé dans les AFPFs, y compris la génération paramétrique du son par le son, le doublement de la fréquence du son, la détection acoustique, etc.

La valeur de la non linéarité acoustique efficace dans les matériaux antiferromagnétiques à plan facile a une forte dépendance au champ magnétique externe. La modulation des paramètres non-linéaires élastiques favorise la génération des excitations multi-bosons. Les premières excitations stationnaires à trois quasi-phonons dans la matière condensée ont été théoriquement prédites et expérimentalement observées dans un cristal d'hématite sous pompage électromagnétique.

L'analyse théorique des triades de quasi-phonons paramétriquement excités a montré plusieurs particularités dynamiques qui diffèrent des nouvelles instabilités de paires de quasi-phonons. D'abord, les seuils d'instabilités non linéaires ne dépendent pas seulement de l'amplitude de pompage électromagnétique, mais aussi du nombre de quasi-phonons initiaux (c'est à dire de l'amplitude initiale des oscillations). De plus, ces instabilités montrent une dynamique supercritique explosive avec une augmentation rapide du nombre de triades de quasi-phonons générées jusqu'à une singularité des amplitudes des ondes couplées en un temps fini.

Les instabilités paramétriques résultant de la modulation des paramètres non linéaires d'un système ont également été détectées dans les structures MEMS. Le couplage non linéaire entre un réseau de micro-leviers a été modulé avec un champ électrique alternatif, conduisant à la formation des instabilités sous-harmoniques.

Les travaux théoriques suivants ont suggéré que pour l'interaction non linéaire des ondes propagatives magnéto-élastiques, la dynamique supercritique explosive est accompagnée d'une localisation spatiale des triades générées. En raison de la loi de conservation de l'énergie, la dynamique explosive d'un système est généralement causée par l'interaction entre les ondes à énergie positive (ondes normales) avec les ondes à énergie négative pour lesquelles l'augmentation d'amplitude correspond à la baisse d'énergie. Plusieurs travaux théoriques sur les interactions d'ondes positives et négatives ont été écrits avec très peu d'observations expérimentales, principalement en physique des plasmas.

Les instabilités paramétriques non linéares anticipées dans les matériaux antiferromagnétiques à plan facile montrent une dynamique supercritique explosive des trois ondes magnétoélastiques positives dans le cristal, sous pompage électromagnétique, avec des amplitudes tendant vers l'infini en un temps fini. Les excitations à trois-phonons couplées ont été observées expérimentalement dans le monocristal d'α-Fe_2O_3, mais la dynamique explosive des excitations supercritiques prédite théoriquement ne s'est pas manifestée en raison d'autres interactions dans le cristal, principalement le décalage de fréquence non linéaire (DFN) de modes magnéto-élastiques. L'observation expérimentale de la dynamique explosive des ondes magnéto-élastiques reste un but important à accomplir.

Ainsi le **but principal de ce travail** est la recherche théorique et expérimentale de la dynamique supercritique explosive des instabilités trois-phonons dans les matériaux antiferromagnétiques "plan facile" (AFPF): l'hématite α-Fe_2O_3 et le borate de fer $FeBO_3$.

Pour cela les **objectifs** suivants ont été fixés:

- Investigation des limitations de la dynamique explosive et développement de méthodes de compensation. Validation théorique des techniques développées.
- Recherche expérimentale de la dynamique supercritique explosive de l'excitation de trois quasi-phonons dans différents cristaux antiferromagnétiques à plan facile.

- Développement d'un modèle théorique fortement non linéaire de dynamique d'AFPF pour la description du couplage des trois quasi-phonons. Simulation numérique du modèle développé.
- Développement des modèles anharmoniques de couplage de trois ondes propageant en milieu fortement non linéaire.
- Simulations numériques d'interactions non linéaires supercritiques explosives de trois ondes magnétoélastiques dans les domaines temporels et spatiaux, sous pompage électromagnétique perpendiculaire et parallèle.

Ce travail a été soutenu par le Ministère français des affaires étrangères (Ambassade de France en Ukraine), la Fondation ukrainienne de la recherche fondamentale (subvention № F33.7/001), la Fondation russe de la recherche fondamentale (subvention № 09-02-00602-A) et le Programme de RAS "Acoustique des milieux naturels".

Le domaine des études présentées se situe dans la dynamique non linéaire des milieux continus, les effets multi-bosons et la dynamique des matériaux d'antiferromagnétiques de type plan facile.

Le sujet de la recherche concerne les propriétés magnéto-élastiques des cristaux d'AFPFs et le phénomène de couplage non linéaire des ondes magnéto-élastiques.

Les méthodes de la recherche utilisées dans ce travail comprennent des techniques impulsionnelles et continues d'excitation et d'enregistrement des oscillations basses fréquences de modes magnéto-élastiques. De nouvelles techniques ont été exclusivement développées : une pour la modulation singulière de phase de pompage ainsi qu'une pour l'enregistrement continu de l'amplitude sous pompage électromagnétique. Les simulations numériques effectuées dans les travaux utilisent des méthodes pseudo-spectrales, des couches parfaitement adaptées et la méthode d'Adams Bashforth pour les solutions des systèmes d'équations.

Nouveautés scientifiques de la recherche :

- Pour la première fois, les excitations de couplage des trois phonons ont été observées expérimentalement dans un monocristal de borate de fer.

- De même, la dynamique supercritique explosive des excitations de trois quasi-phonons dans les monocristaux d'hématite et de borate de fer a été observée et étudiée expérimentalement.
- La dynamique supercritique explosive des excitations de trois quasi-phonons dans les résonateurs magnétoélastiques
- Les propriétés magnétoélastiques de borate de fer ont été étudiées dans la plage de températures 77K - 293K. Pour la première fois, le décalage de fréquence non linéaire du mode magnétoélastique de borate de fer a été étudié expérimentalement.
- Le couplage non linéaire des trois ondes magnéto-élastiques en milieu anharmonique a été étudié. La dynamique supercritique explosive et la localisation spatiale de la génération des triades ultrasonores ont été signalées.

Portée pratique du travail :

- Une technique de compensation de décalage de fréquence non linéaire a été développée par modulation singulière précise de la phase de pompage.
- Une méthode expérimentale a été développée pour permettre la modulation arbitraire de la phase de pompage et l'enregistrement continu de l'amplitude des oscillations magnéto-élastiques sous pompage électromagnétique.
- Une nouvelle instabilité paramétrique qui découle de la modulation des paramètres non linéaires d'un système a été recherchée.
- Un modèle fortement non linéaire et une approximation anharmonique des excitations des trois quasi-phonons dans les résonateurs antiferromagnétiques de type plan facile ont été développés.
- Un programme pour simulations numériques de couplage non linéaire des ondes magnéto-élastiques a été créé. Ce programme simule le processus de couplage dans les domaines temporel et spatial.

Approbation des résultats de la thèse: les parties de ce travail ont été rapportées dans six conférences internationales. Les résultats principaux obtenus pendant les études ont été publiés dans quatre articles, dont trois dans les journaux scientifiques et un dans les actes de conférences.

Le manuscrit de thèse comporte 196 pages, réparties en cinq chapitres encadrés par une introduction et une conclusion générale**. Le premier chapitre** comporte une analyse très détaillé des phénomènes physiques magnéto-élastiques qui ont formé la base de la recherche présentée. Ce chapitre donne aussi une analyse de l'état de l'art dans les matériaux magnétoacoustiques et les processus multi-bosons. La dynamique des excitations couplées de sous-systèmes magnétiques et élastiques est considérée dans les matériaux magnétiquement ordonnés : ferromagnétiques, ferrites et antiferromagnétiques. Diverses instabilités paramétriques des ondes magnéto-élastiques qui découlent de la modulation des paramètres linéaires sont analysées. Les applications de ces instabilités paramétriques pour conjugaison de phase sont présentées. Il est démontré que les matériaux antiferromagnétiques à plan faciles possèdent un couplage magnétoélastique sans précédent et une anharmonicité effective géante qui peut être contrôlée et modulée par champ magnétique externe. Récemment découvertes, les instabilités paramétriques qui découlent de la modulation des paramètres non linéaires d'un système magnétoélastique sont analysées. Il est montré que les études théoriques ont prédit la dynamique explosive et la localisation spatiale de la dynamique supercritique de ces instabilités. Ces propriétés n'ont cependant pas encore été confirmées expérimentalement.

Le deuxieme chapitre est consacrée à l'analyse des mécanismes qui affectent la manifestation de la dynamique supercritique explosive des excitations à trois quasi-phonons dans les résonateurs magnéto-élastiques en régime monomode. Cette analyse est effectuée sur la base d'un modèle anharmonique developpé dans le chapitre pour les cristaux antiferromagnétiques à plan faciles. Le modèle est une approximation anharmonique limitée aux quatre premiers termes d'énergie. L'analyse montre que le décalage de fréquence non linéaire qui vient de la non-linéarité cubique est responsable de la limitation de la dynamique d'instabilité explosive. Afin de compenser le décalage de fréquence non linéaire une technique avancée a été proposée. Basé sur le fait que ce décalage a une dépendance en carré de l'amplitude des oscillations, une modulation singulière de phase de pompage a été suggérée. Les résultats de simulations numériques supercritiques de l'approximation anharmonique avec la loi de pompage proposée pour un résonateur en hématite sont présentés. Les résultats montrent la dynamique explosive quand l'amplitude des oscillations tend vers l'infini en un temps fini lorsque la modulation singulière est appliquée.

Le troisième chapitre est consacré aux études expérimentales de la dynamique explosive supercritique d'excitations à trois quasi-phonons en régime monomode. La recherche est effectuée sur deux résonateurs monocristallines magnéto-élastiques d'AFPF : l'hématite et le borate de fer. Les expériences sont effectuées à température ambiante pour α-Fe_2O_3 et pour $FeBO_3$. Elles sont effectuées à basses températures entre 77 K et 293 K lorsque les propriétés magnéto-élastiques diffèrent considérablement. Tout d'abord, les fréquences des modes de résonance magnéto-élastiques des échantillons sont déterminées et leurs propriétés sont étudiées, Sont également déterminé les dépendances des coefficients de couplage magnéto-élastiques dues au champ magnétique de polarisation, les décalages de fréquences non linéaires des modes magnéto-élastiques et les facteurs de qualité des modes. Pour la première fois la non-linéarité cubique du borate de fer est recherchée. Les résultats obtenus sont utilisés pour la détermination des points de fonctionnement et les lois de modulation de la phase pour la recherche de dynamique supercritique. Une nouvelle technique expérimentale qui a été développée pour la visualisation des oscillations des résonateurs sous pompage électromagnétique est montrée. Pour la première fois la dynamique explosive de l'instabilité paramétrique non linéaire est expérimentalement observée et étudiée dans les deux résonateurs quand les bonnes lois de modulation de phase sont appliquées au pompage. La corrélation entre expérience et modélisation du deuxième chapitre est réalisée aux basses amplitudes. La non corrélation aux amplitudes élevées est mise en évidence et expliquée.

Dans **le quatrième chapitre** un modèle fortement non linéaire d'excitations à trois quasi-phonons en régime monomode est développé pour décrire la dynamique des résonateurs aux amplitudes élevées. Le modèle considère les non-linéarités magnéto-élastiques en dehors de l'approximation anharmonique développée dans le deuxième chapitre. Le modèle développé est numériquement simulé avec les paramètres de l'hématite expérimentalement étudiés et les paramètres du borate de fer étudiés aussi à 293 K et à 77 K. Les résultats sont comparés avec les simulations numériques de l'approximation anharmonique et les données obtenues expérimentalement. Le modèle fortement non linéaire démontre une bonne corrélation avec les observations expérimentales de l'instabilité explosive et rend correctement compte des expériences.

Dans **le cinquième** et dernier **chapitre** le phénomène de couplage non linéaire de trois ondes magnéto-acoustiques dans un milieu magnéto-élastique à anisotropie magnétocristalline planaire est considéré. Deux modèles de couplage anharmonique des ondes sont développées

qui correspondent à pompage électromagnétique en géométrie parallèle ou perpendiculaire par rapport à champ magnétique de polarisation. Les modèles développés utilisent les valeurs réelles des non linéarités cristallines d'AFPFs jusqu'aux termes de quatrième ordre d'énergie inclus. Il est montré que ces termes introduisent un décalage de phase non-linéaire dans la génération de triades ultrasonores. Les seuils d'instabilités sont déterminés. Un programme exclusivement créé pour cette étude en utilisant le langage de programmation Fortran et simulant le processus de couplage dans les domaines temporel et spatial est également décrit. Les modèles développés sont simulés à l'aide de ce programme et les paramètres d'excitation et pompage nécessaires pour l'observation du couplage supercritique de trois ondes dans le cristal d'hématite sont déterminés. Les simulations numériques montrent que la configuration perpendiculaire est préférable pour les expériences. La dynamique explosive et la localisation spatiale des triades sont observées lorsque le déphasage non-linéaire est négligé. L'introduction des non-linéarités ajoute un déphasage qui limite la dynamique des instabilités. Une loi de modulation du pompage est suggérée pour aider à surmonter cette limitation et manifester la dynamique explosive et la localisation spatiale des ondes magnétoélastiques couplées même avec les non linéarités de cristaux hématites.

La **conclusion générale** de la thèse est présentée à la fin du manuscrit et elle résume les résultats obtenus dans les études menées sur les instabilités explosives des ondes magnéto-élastiques. Les perspectives d'utilisation du couplage paramétrique non linéaire des ondes magnétoélastiques dans les applications diverses sont aussi considérées, notamment en conjugaison de phase, amplification sélective des signaux acoustiques et génération des impulsions à haute puissance

References

[1] A. I. Akhiezer, "Magnetoelastic Interaction in Ferromagnetic Crystal" J. Phys. USSR **10** (2), 216 – 231 (1946).

[2] E. A. Turov, Y.P. Irhin "Spectrum of Oscillations of Elastic Ferromagnetic Medium" Fiz. Met. Metalov. **3** (1), 15 – 17 (1956).

[3] E. G. Spenser, R. C. LeCraw. "Magnetostatic Resonance in Yttrium Iron Garnet" Phys. Rev. Lett. **7** (1), 241 – 243 (1958).

[4] A. I. Akhiezer, V. G. Baryahtar, S. V. Peletminsky "Coupled Magnetoacoustic Waves and Ferroacoustic Resonance" Sov. Phys. JETP **35** (1), 15 – 17 (1958).

[5] C. Kittel "Interaction of Spin Waves and Ultrasonic Waves in Ferromagnetic Crystals" Phys. Rev. **110** (4), 836 – 841 (1958).

[6] R. C. LeCraw, E. G. Spencer, E. I. Gordon "Extremely Low Loss Acoustic Resonance in Single-Crystal Garnet Spheres" Phys. Rev. Lett. **6** (11), 620 – 622 (1961).

[7] O.Yu. Belyaeva, L.K. Zarembo, S.N. Karpachev "Magnetoacoustics of ferrites and magnetoacoustic resonance" Sov. Phys. Usp. **35** (2), 106 – 122 (1992).

[8] V.V. Lemanov, G.A. Smolensky "Hypersonic Waves in Crystals", Sov. Phys. Usp. **15,** 708 – 727 (1973).

[9] J. R. Eshbach "Spin-Wave Propagation and the Magnetoelastic Interaction in Yttrium Iron Garnet", J. Appl. Phys. **34** (4), 1298 – 1304 (1963).

[10] R. W. Bierig, R. I. Joseph, E. Schlomann "Magnetoelastic Propagation in YIG Rods Surrounded by Magnetic Sleeves" IEEE Trans. Sonics Ultrason. **SU-13** (3), 82 – 84 (1966).

[11] H. Matthews "Elastic-Wave Amplification in Yttrium Iron Garnet at Microwave Frequencies" Phys. Rev. Lett. **12** (12), 325 – 327 (1964).

[12] Z. F. Donaghey, F. A. Olson "Parametric Amplification of Magnetostatic, Magnetoelastic and Acoustic Waves for Microwave Delay at Room Temperature" Electron. Lett. **1** (6), 158 – 160 (1965).

[13] D. R. Jackson "Magnetoelastic Bandwidth Compression" Proceedings IEEE **59** (1), 20 – 25 (1971).

[14] R. W. Damon "Relaxation Effects in the Ferromagnetic Resonance" Rev. Mod. Phys. **25**, 239 – 245 (1953).

[15] N. Bloembergen, S. Wang "Relaxation Effects in Para- and Ferromagnetic Resonance" Phys. Rev. **93**, 72 – 83 (1954).

[16] H. Suhl "The Theory of Ferromagnetic Resonance at high Signal Powers" Phys. Chem. Sol. **1** (4), 209 – 227 (1957).

[17] F. R. Morgenthaler "Microwave Phonon Instabilities Associated with Ferromagnetic resonance" Proc. IRE **50**, 2139 – 2140 (1962).

[18] B. A. Auld, R. E. Tokheim, D. K. Winslow "Pumping Effects Contributing to the Excitation of Phonon Instabilities in Ferromagnetic Insulators" J. Appl. Phys. 34 (8), 2281 – 2286 (1963).

[19] B. A. Auld "Transversely Pumped Magnetoelastic Instabilities" J. Appl. Phys. **36** (3), 689 – 698 (1965).

[20] R. L. Comstock "Parametric Coupling of the Magnetization and Strain in a Ferromagnet. II. Parametric Excitation of magnetic and Elastic Plane Waves" J. Appl. Phys. **34** (5), 1465 – 1468 (1963).

[21] R. W. Damon, H. van de Vaart "Dispersion of Spin Waves and Magnetoelastic Waves in YIG", Proc. IEEE **53**, 348 – 354 (1965).

[22] R. W. Damon, H. van de Vaart "Microwave Pulse Echoes with Variable Time Delay by Parametric Pumping of Travelling Spin Waves" Appl. Phys. Lett. **6** (10), 194 – 196 (1965).

[23] R. W. Damon, H. van de Vaart "Parametric Amplification of Magnetoelastic Waves YIG at 8.7 Gc/sec" Appl. Phys. Lett. **6** (8), 152 – 154 (1965).

[24] H. Van de Vaart, M. I. Grace, R. W. Damon "Parametric Amplification of Microwave Magnetoelastic Waves in YIG at Room Temperature" Electr. Lett. **1** (5), 122 (1965).

[25] H. Van de Vaart, H. D. Lyons, R.W. Damon "Parametric Excitation and Amplification of Magnetoelastic Waves" J. Appl. Phys. **38** (1), 360 – 374 (1967).

[26] F. R. Morgenthaler "Harmonic Resonance in Small Ferromagnetic Ellipsoids" J. Appl. Phys. **30** (4), S157 – S159 (1959).

[27] E. Schlomann, J. Green, V. Milano "Recent Developments in Ferromagnetic Resonance at High Power Levels" J. Appl. Phys. **31** (5), S386 – S385 (1960).

[28] E. H. Turner "Interaction of Phonons and Spin Waves in Yttrium Iron Garnet" Phys. Rev. Lett. **5** (3), 357 – 358 (1960).

[29] R. L. Comstock, R. C. LeCraw "Instability of Elastic Waves by Time-Varying Elastic Modulus in Ferromagnets" Phys. Rev. Lett. **10** (6), 219 – 220 (1963).

[30] E. Schlomann "Longitudinal Susceptibility of Ferromagnets in Strong RF Fields" J. Appl. Phys. **33** (2), 527 – 534 (1962).

[31] F. A. Olsen "Study of Magnetoelastic Interactions by Parallel Pumping" J. Appl. Phys. **34** (4), 1281 – 1283 (1963).

[32] J. P. Sage "Parallel Pumping of Phonons in Yttrium Iron Garnet at 114 MHz" J. Appl. Phys. **42** (1), 343 – 351 (1971).

[33] J. P. Sage "Physical Theory of the Phonon Parallel Pump Instability" J. Appl. Phys. **41** (6), 2502 – 2504 (1971).

[34] P. Gottlieb, H. Suhl "Saturation of Ferrimagnetic resonance with Parallel Pumping" J. Appl. Phys. **33** (4), 1508 – 1514 (1962).

[35] J. D. Bierlein, P. M. Richards "Harmonic Generation and Parametrically Coupled Spin Waves in Yttrium Iron Garnet" Phys. Rev. B **1** (11), 4342 – 4357 (1970).

[36] V. E. Zakharov, V. S. L'vov, S. S. Starobinets "A New Mechanism of Limitation of the Amplitude of Spin Waves in Parallel Pumping" Phys. Sol. State **11**, 2047 – 2055 (1969).

[37] V. E. Zautkin, V. E. Zakharov, V. S. L'vov, S. L. Musher, S. S. Starobinets "Parallel Pumping of Spn Waves in YIG Mono-Crystals" Sov. Phys. JETP **35** (5), 926 – 933 (1973).

[38] V. E. Zakharov, V. S. L'vov, S. S. Starobinets "Spin-Wave Turbulence Beyond the Parametric Excitation Threshold" Sov. Phys. Usp. **17** (6), 896 – 919 (1975).

[39] V. Preobrazhensky "Overthreshold Nonlinearity of Parametric Sound Wave Phase Conjugation in Solids" Jpn. J. Appl. Phys. **32** (5B), 2247 – 2251 (1993).

[40] B. Ya. Zel'dovich, N. F. Pilipetsky, V. V. Shkunov "Principles of Phase Conjugation" (Springer Verlag, Berlin, 1985).

[41] M. Fink, D. Cassereau, A. Derode, C. Prada, Ph. Roux, M. Tanter, J.-L. Thomas, Wu F. "Time-reversed acoustics", Rep. Prog. Phys. **63** (12), P. 1933 – 1995 (2000).

[42] V. Preobrazhensky "Parametrically Phase Conjugate Waves: Applications in Nonlinear Acoustic Imaging and Diagnostics", Phys. Usp. 49 (1), 98 – 102 (2006).

[43] R. B. Thomson, C. F. Quate "Nonlinear interaction of microwave electric fields and sound in $LiNbO_3$", J. Appl. Phys. **42** (3), 907 – 919 (1971).

[44] A. P. Brysev, F. V. Bunkin, D. V. Vlasov, L. M. Krutianskii, V. L. Preobrazhenskii, A. D. Stakhovskii, "Parametric phase conjugation of an ultrasonic wave in a ferrite" Sov. Phys. Acoust. **34**, 642–643 (1989).

[45] A. Brysev, P. Pernod, V. Preobrazhensky "Magneto-Acoustic Ceramics for Parametric Sound Wave Phase Conjugators" Ultrasonics **38**, 834 – 837 (2000).

[46] L. O. Svaasand, "Interaction between elastic surface waves in piezoelectric materials" Appl. Phys. Lett. **15**, 300 – 302 (1969).

[47] K. Yamamoto, P. Pernod, V. Preobrazhensky, "Visualization of Phase Conjugate Ultrasound Waves Passed Through Inhomogeneous Layer" Ultrasonics **42**, 1049 – 1052 (2004).

[48] M. Ohno "Generation of Acoustic Phase Conjugate Waves Using Nonlinear Electroacoustic Interaction in $LiNbO_3$" Appl. Phys. Lett. **54**, 1979 – 1980 (1989).

[49] N. S. Shiren, R. L. Melcher, T. G. Kazyaka "Multiple-Quantum Phase Conjugation in Microwave Acoustics" IEEE J. Quantum Electronics **22** (8), 1457 – 1460 (1986).

[50] M. Ohno, K. Takagi, "Acoustic Phase Conjugation in Highly Nonlinear PZT Piezoelectric Ceramics" Appl. Phys. Lett. **64**, 1620 – 1622 (1993).

[51] M. Ohno, K. Takagi "Enhancement of the acoustic phase conjugate reflectivity in nonlinear piezoelectric ceramics by applying static electric or static stress fields" Appl. Phys. Lett. **69**, 3483 – 3485 (1996).

[52] A. P. Brysev, F. V. Bunkin, D. V. Vlasov, and Yu. E. Kazarov "Experimental Realization of POFUZ on Lithium Niobate" Sov. Phys. Tech. Lett. **8**, 237 (1982).

[53] V. I. Reshetzky "Phase Conjugate Reflection and Amplification of a Bulk Acoustic Wave in Piezoelectric Crystals" J. Phys. C: Solid State Phys. **17** (33), 5887 – 5891 (1984).

[54] P. Pernod, V. Preobrazhensky "Parametric Phase Conjugation of a Wide-Band Acoustic Pulse in Supercritical Mode" Appl. Phys. Lett. **76** (3), 387 – 389 (2000).

[55] Yu. Pyl'nov, P. Pernod, V. Preobrazhensy "Low Frequency Emission by Nonlinear Interaction of Phase Conjugate Ultrasound Waves" Acta Acoustica **89** (6), 942 – 947 (2003).

[56] A. Merlen, V. Preobrazhensky, P. Pernod "Supercritical Parametric Phase Conjugation of Ultrasound. Numerical Simulation of Nonlinear and Nonstationary Mode" J. Acoust. Soc. Am. **112** (6), 2656 – 2665 (2002).

[57] O. Bou Matar, V. Preobrazhensky, P. Pernod "Two-Dimensional Axisymmetric Numerical Simulation of Supercritical Phase Conjugation of Ultrasound in Active Solid Media" J. Acoust. Soc. Am. **118** (5), 2880 – 2890 (2005).

[58] A. Brysev, L. Krutyansky, P. Pernod, V. Preobrazhensky "Acoustic Microscope Based on Magneto-Elastic Wave Phase Conjugator" Appl. Phys. Lett. **76**, 3133 – 3135 (2000).

[59] Yu.V. Pyl'nov, P. Pernod, V. Preobrazhensky "Acoustic Imaging by Second Harmonic of Phase-Conjugate Wave in Inhomogeneous Medium" Appl. Phys. Letts. **78** (4), 553 – 555 (2001).

[60] L.Krutyansky, P. Pernod, A. Brysev, F.Bunkin, V.Preobrazhensky "Supercritical Parametric Wave Phase Conjugation as an Instrument for Narrowband Analysis in Ultrasonic harmonic imaging" IEEE Trans. UFFC **49** (4), 409 – 414 (2002).

[61] A. P. Brysev, F. V. Bunkin, D. V. Vlasov, L. M. Krutyansky, V. L. Preobrazhensky, A. D. Stakhovsky. "Regenerative Amplification Mode of Acoustic Waves and Phase Conjugation in Ferrite" Acoust. Phys. **34** (6), 986 – 990 (1988).

[62] A. Brysev, L. Krutyansky, P. Pernod, V. Preobrazhensky "Nonlinear Ultrasonic Phase Conjugate Beams and Their Application in Ultrasonic Imaging" Acoust. Phys. **50** (6), 623 – 640 (2004).

[63] S.V. Preobrazhensky, V.L. Preobrazhensky, P. Pernod, "Second Harmonic Generation by Phase Conjugate Ultrasonic Wave in Medium with Nonlinear Inclusion", Phys. Wave Phenom. **13** (1), 24 – 29 (2005).

[64] S. Preobrazhensky, V. Preobrazhensky, O. Bou Matar, P. Pernod, Proc. of the 8th French Acoustic Conf (on CD), France, Tours, p.67 (2006).

[65] L. Krutyanskiy, V. Preobrazhensky, P. Pernod, O. Bou Matar "Nonlinear Imaging of Isoechogenic Phantoms Using Phase Conjugation of The Second Acoustic Harmonic" Phys. Wave Phenom. **15** (3), 186 – 190 (2007).

[66] Yu. Pyl'nov, V. Preobrazhensky "Principles of Ultrasonic Velocimerty by Means of Nonlinear Interaction of Phase Conjugate Waves" Proc. IEEE Ultrasonics Symp., Montreal, vol. **3**, p. 1612 (2004).

[67] Preobrazhensky V.L., Pernod Ph., Pyl'nov Yu.V., Krutyansky L.M., Smagin N.V., Preobrazhensky S.V. "Nonlinear Acoustic Imaging of Isoechogenic Objects and Flows Using Ultrasound Wave Phase Conjugation", Acta Acoustica **95** (1), 36 (2009).

[68] M. Tanter "Application du Retournement Temporel à l'Hyperthermie Ultrasonore de Cerveau" Thèse de doctorat de l'université Paris 7 (1999).

[69] A. Brysev, L. Krutyansky, P. Pernod et al. "Ultrasonic testing of steel tubes by supercritical parametric wave phase conjugation" IEEE Ultrasonics Symposium, vol. **3**, 2295 – 2297 (2004).

[70] B. Kevin, A. Antonio, L. Andres "Examination Of Time Reversal Acoustics in Shallow Water and Applications to Noncoherent Underwater Communications" J. Acoust. Soc. Am. **113** (6), 3095 – 3110 (2003).

[71] A. P. Brysev, F.V. Bunkin, L. M. Krutyansky, N.V. Smagin "Phase Conjugation for measuring Ultrasound Absorption in Inhomogeneous Media" Phys. Wave Phenom. **18** (2), 143 (2010).

[72] E. A. Turov, V. G. Shavrov "Broken Symmetry and Magnetoacoustic Effects in Ferro- and Antiferromagnets" Sov. Phys. Usp. **26** (7), 429 – 462 (1983).

[73] S. V. Peletminsky "Coupled Magnetoelastic oscillations in Antiferromagnets" JETP 1959 **37** (2), 452 – 457 (1959).

[74] M. A. Savchenko "Coupled Magnetoelastic Waves in Antiferromagnets" Fiz. Tverd. Tela **6** (3), 864 – 872 (1964).

[75] V. I. Ozhogin "Exchange Enhancement in Antiferromagnets" IEEE Trans. Magn. **12** (1) p. 19 (1976).

[76] V. I. Ozhogin, V. L. Preobrazhensky "Nonlinear dynamics of coupled systems near magnetic phase transitions of the order-order type". Journ. of Magn. and Magn. Materials **100** (1), "Magnetism of Nineties" 544 – 571 (1991).

[77] E. G. Rudashevsky, T. A. Shalnikova "Antiferromagnetic Resonance in Hematite" Proc. of 3rd Reg. Conf. "Physics and Techniques of Low Temperatures" in Prague, p. 84 – 86 (1963).

[78] A. Tasaki, S. Lida "Magnetic Properties of synthetic single crystal of α-Fe_2O_3" J. Phys. Soc. Jap. **17** (8), 1148 – 1154 (1963).

[79] A. S. Borovik-Romanov, E. G. Rudashevsky "Influence of Spontaneous Striction on Antiferromagnetic Resonance in Hematite" Sov. Phys. JETP **47** (6), 2095 – 2101 (1964).

[80] E. A. Turov, V. G. Shavrov "Energy Gap in Ferro- and Antiferromagnets due to Magnetoelastic Energy" Fiz. Tverd. Tela **7** (1), 217 – 226 (1965).

[81] M. Nielsen, H. B. Moller, P. A. Lindgard, A. R. Mackintosh "Magnetic Anisotropy in Rare-Earth Metals" Phys. Rev. Lett. **25** (20), 1451 – 1454 (1970).

[82] W. Jantz, W. Wetting "Spin Wave Dispersion of Iron Borate at Small Wavectors" Appl.Phys. **15** (4), 399 – 407 (1978).

[83] L. V. Velikov, A. S. Prokhorov, E. G. Rudashevsky, V. N. Seleznev "Antiferromagnetic Resonance in $FeBO_3$" Sov. Phys. JETP **39** (5), 909 – 915 (1974).

[84] Petrakovsky G.A., Pankrats A.I. "The Magnetoelastic Coupling in $FeBO_3$" Proc. ICM'76, Amsterdam, North-Holland **3**, 447 – 1448 (1977).

[85] A. G. Berezin, V. G. Shavrov "Antiferromagnetic Resonance in Cubic Crystals" Sov. Phys. JETP **72** (6), 2362 – 2366 (1977).

[86] V. I. Sokolov, O. I. Shevalyavsky "Antiferromagnetic Resonance in Cubic Crystals" Sov. Phys. JEPT **72** (6), 2367 – 2374 (1977).

[87] V. G. Bar'yakhtar, I. M. Vitebskii, Yu. G. Pashkevich, V. L. Sobolev, V. V. Tarasenko "Striction Effects and Dynamics of the Magnetic Subsystem in Spin-Reorientation Phase Transitions: Symmetry Aproach" Sov. Phys. JETP **87** (9), 1028 – 1037 (1984).

[88] I. E. Dikhshtein, E. G. Tarasenko, V. G. Shavrov "Effect of Pressure of Magnetoacoustic Resonance in Uniaxial Antiferromagnets" Sov. Phys. JETP **40** (2), 404 – 407 (1975).

[89] A. M. Kadomtseva, R. Z. Levitin, Yu. F. Popov, V. N. Seleznev, V. V. Usov "Magnetic and Magnetoelastic Properties of Single Crystals" Fiz. Tverd. Tela **14** (1), 214 – 217 (1972).

[90] I. E. Dikhshtein, V. V. Tarasenko, V. G. Shavrov "Magnetoelastic Waves in Orthoferrites" Fiz. Tverd. Tela **25** (4), 1107 – 1113 (1977).

[91] V. D. Buchelnikov, V. V. Tarasenko, V. G. Shavrov "Relaxation Processes in Magnets near Orientation Phase Transitions" Fiz. Tverd. Tela **25** (10), 3019 – 3024 (1983).

[92] M. H. Seavey "Acoustic Resonance in the Easy-Plane Weak Ferromagnets α-Fe_2O_3 and $FeBO_3$" Sol. State Comm. **10** (2), 219 – 225 (1972).

[93] N. N. Evtiheev, S. A. Pogozhev, V. P. Preobrazhensky, N. A. Ekonomov "Dependences of Acoustic Parameters of Hematite on Temperature and Bias Field" Sov. Phys. Acoust. **30** (M), 544 – 546 (1984).

[94] J. Iensen, S. B. Palmer "Field Dependence of the Elastic Constant C_{66} in the Basal-Plane Ferromagnet Terbium" J. Phys. C: Solid State Phys. **12**, 4573 – 4583 (1979).

[95] A. M. Balboshov, N. K. Denshin, A. I. Izotov, M. A. Sdvizhkov, L. T. Tsimbal "Anomality of Acoustic Properties of $ErFeO_3$" Fiz. Tverd. Tela **31** (7), 279 – 280 (1989).

[96] R. C. LeCraw, T. Kasuya "Long-Wavelength Collective Excitations in Ferromagnetic Insulators. I. Strong Coupling of Acoustic Modes to Spin Wave Modes" Phys. Rev. **130** (1), 50 – 57 (1963).

[97] R. L. Comstock, B. A. Auld "Parametric Coupling of the Magnetization and Strain in a Ferrimagnet. I. Parametric Excitation of Magnetostatic and Elastic Modes" J. Appl. Phys. **34** (5), 1461 – 1464 (1963).

[98] V. I. Ozhogin, P. P. Maksimenkov "Antiferromagnetic Resonance Investigation of the Magnetoelastic Interaction in Hematite" Sov. Phys JETP **38** (2), 324 – 328 (1974).

[99] E. A. Andrushak, N.N. Evtihiev, S. A. Pogozhev, V.L. Preobrazhensky, N.A. Ekonomov, Sov. Phys. Acoust. **27**, 179 (1981)

[100] M. H. Seavey "Magnon - Phonon Interaction and Determination of Exchange Constants in $CsMnF_3$" Phys. Rev. Letts. **23** (3), 132 – 135 (1969).

[101] V.I. Ozhogin, A. Yu. Yakubovskii "Parametric Pairs in Antiferromagnet with Easy Plane Anisotropy" Sov. Phys. JETP **40** (1) 144 – 153 (1975).

[102] B. Ya. Kotyuzhanskii, L.A. Prozorova "Parametric Excitation of Spin Waves in Antiferromagnetic $MnCO_3$" Sov. Phys. JETP **36** (6), 1165 - (1973).

[103] B. Ya. Kotyuzhanskii, L.A. Prozorova "Parametric Excitation of Magnons in Antiferromagnetic $CoCO_3$" Sov. Phys. JETP **61** (1), 128 – 132 (1985).

[104] N. N. Evtikheev, V. L. Preobrazhensky, M. A. Savchenko, N. A. Ekonomov "Nonlinear Electroacoustic Transformation of Information in High Temperature Antiferromagnet" Vopr. Radioelektron. Ser. Obshchetekhn. **5**, 124 – 136 (1978).

[105] I. B. Pleshakov "Parametric Excitations of Magnetoelastic Oscillations in Hematite in Weak Fields" Fiz. Tverd. Tela **74** (9), 1629 – 1633 (2005).

[106] W. Wettling, W. Jantz, "High-Intensity Brillouin Scattering from Parametrically Excited Phonons in $FeBO_3$" Appl. Phys. **19** (2), 175 – 179 (1979).

[107] V. S. Lutovinov, M. A. Savchenko. In abstracts of papers presented at the All-Union Conf. on Physics of Magnetic Phenomena, Kharkov, p.85 (1979).

[108] A. V. Andrienko, L. V. Podd'akov "Parallel Pumping of Phonons in Antiferromagnetic $FeBO_3$ by a Microwave Magnetic Field" Sov. Phys. JETP **68** (6), 1224 – 1228 (1989).

[109] A. V. Andrienko, L. V. Podd'akov, V. L. Safonov "Parametric Excitation of Magneoelastic Waves in Single Crystals of $CoCO_3$ and $FeBO_3$" Sov. Phys. JETP **74** (3), 579 – 587 (1992).

[110] V. A. Krasilnikov, T. A. Mamatova, V. G. Prokoshev "Parametrical Amplification while Wave Phase Conjugation of Magnetoelastic Wave in Hematite", Sol. State Phys. **28**, 615 – 617 (1986).

[111] L. K. Zarembo, V. A. Krasil'nikov "Nonlinear Phenomena in the Propagation of Elastic Waves in Solids" Sov. Phys. Usp. **13** (6), 778 – 797 (1971).

[112] V.I. Ozhogin and V.P. Maksimenkov "Easy Plane Antiferromagnet for Applications: Hematite" IEEE Trans. Magn. **Mag-8** (3), 645 (1972).

[113] V. I. Ozhogin and V. L. Preobrazhenskii "Effective Anharmonicity of the Elastic Subsystem of Antiferromagnets" Sov. Phys. JETP **46** (3), 523 – 529 (1977).

[114] V.L. Preobrazhensky, M.A. Savchenko, N.A. Ekonomov "Nonlinear Self-Action of Elastic Waves in Easy Plane Antiferromagnet" JETP Lett. **28** (2), 93 – 97 (1978).

[115] V.I. Ozhogin, A.Yu. Lebedev, A.Yu.Yakubovsky "Frequency Doubling and Acoustic Doubling in Hematite" JETP Lett. **27** (6), 333 – 336 (1978).

[116] V.A. Krasil'nikov, T.A. Mamatova, V.G. Prokoshev, Sov. Tech. Phys. Lett. **10**, p. 506 (1984).

[117] A. Yu. Lebedev, V. I. Ozhogin, A. Yu. Yakubovskiy "Stimulated Acoustic Raman Scattering in an Antiferromagnet" JETP Lett. **34** (1), 22 – 24 (1981).

[118] P. Pernod, V. Preobrazhensky "Dynamic Control of Elasticity by Means of Ultrasound Excitation in Antiferromagnet" Journ. of Magn. and Magn. Mater. **184**, 173 – 178 (1998).

[119] A. O. Kiselev, V. I. Ozhogin, V. L. Perobrazhensky "Bistability of Above-Threshold Oscillations of Parametric Magnetoelastic Waves in Hematite" JETP Lett. **52** (2), P. 83 – 86 (1990).

[120] V. L. Preobrazhenskiĭ, V. V. Rudenko, P. Pernod, V. I. Ozhogin "Three-Phonon Coupled Excitations in an Antiferromagnet" JETP Lett. **86** (5), 348 – 351 (2007).

[121] V. Preobrazhensky, O. Bou Matar, P. Pernod. "Explosive Dynamics and Localization of Wave Triads in a Coupled Magnetoelastic System" Phys. Rev. E **78**, 046603 (2008).

[122] R. Diehl, W. Jantz, B. I. Nolang, W. Wetlling "Growth and Properties of Iron Borate $FeBO_3$" Current Topics in Materials Science, Uppsala **11** (3), 241 – 387 (1984).

[123] M. Jona-Lasinio, L. Pricoupenco "Three Resonant Ultra-Cold Bosons: Off-Resonance Effects" Phys. Rev. Lett. **104**, 023201 (2010).

[124] T. Kraemer, M. Mark, P. Waldburger, J. G. Danzl, C.Chin, B. Engeser, A. D. Lange, K. Pilch, A. Jaakkola, H.-C. N¨agerl and R. Grimm , "Evidence for Efimov Quantum States in an Ultracold Gas of Caesium Atoms" Nature 440, 315 – 316 (2006).

[125] D. J. Kaup, A. Reiman, A. Bers "Space-Time Evolution of Nonlinear Three-Wave Interactions. I. Interaction in a Homogeneous Medium" Rev. Mod. Phys. **51** (2), 275 – 309 (1979).

[126] L. A. Ostrovski, S. A. Rybak, L. Sh. Tsimring "Negative Energy Waves in Hydrodynamics" Sov. Phys. Usp. **29** (11), 1040 – 1052 (1986).

[127] B. R. Safdi, H. Segur "Explosive Instability due to Four Wave Mixing" Phys. Rev. Lett. **99** (24), 245004 (2007).

[128] R. Sugaya, M. Sugawa, H. Nomoto "Experimental Observation of Explosive Instability Due to a Helical Electron Beam" Phys. Rev. Lett. **39** (1), 27 – 31 (1977).

[129] T. Honzawa, T. Hoshina, K. Takahashi "Observation of Instabilities due to Three-Wave Interaction during Nonlinear Pump Wave Modulation" Phys. Plasmas **8** (3), 734 – 743 (2001).

[130] Yu. Fetisov, V. Preobrazjensky, P. Pernod, "Bistability in a Nonlinear Magnetoacoustic Resonator" J. Commun. Tech. Electon. **51** (2), 218 – 230 (2006).

[131] V.P. Sobolev, M.A. Savchenko, V.L. Preobrazhensy "Phonon Relaxation in Antiferromagnets with Dislacations" Sov. Phys. Solid State **20** (8), (1978).

[132] A. Chiaramonti et al. "Optical Growth of Single Crystal α-Fe_2O_3 from a $CaFe_4O_7$-Based Solvent" Crystal Growth & Design **4** (4), 749 – 753 (2004).

[133] V. V. Rudenko, V. N. Berzhansky, S. N. Polulyakh, P. Pernod, V.L. Preobrazhensky "Magnetoelastic Waves in Parametrically Active Nickel Ferrite Spinels", Phys. Wave Phenom. **16** (1), 24 (2008).

[134] O. Bou Matar, V. Preobrazhensky, P. Pernod "2D Numerical Simulation of Supercritical Phase Conjugation of Ultrasound in Active Solid Media" IEEE – UFFC, pp. 227 – 228 (2004).

[135] O. Bou Matar, V. Preobrazhensky, P. Pernod "Two-Dimensional Axisymmetric Numerical Simulation of Supercritical Phase Conjugation of Ultrasound in Active Solid Media" J. Acoust. Soc. Am. **118** (5), 2880 – 2890 (2005).

[136] J. P. Berenger "A Perfectly Matched Layer for the Absorption of Electromagnetic Waves" J. Comput. Phys. **114**, 185 – 200 (1994).

[137] J. P. Roden, S. D. Gedney "Convolutional PML (CPML): An Efficient FDTD Implementation of the CFS-PML for Arbitrary Media" Microwave Opt. Technol. Lett. **27**, 334 – 339 (2000).

[138] J. Zhu, C. Q. Ru, A. Mioduchowski "High-Order Subharmonic Parametric Resonance of Nonlinearly Coupled Micromechanical Oscillators" Eur. Phys. J. B **58**, 411 – 421 (2007).

[139] J. Zhu, C. Q. Ru, A. Mioduchowski "High-order Subharmonic Parametric Resonance of Multiple Nonlinearly Coupled Micromechanical Oscillators" Acta Mech. **212**, 69 – 81 (2010).

[140] M. B. Strugatsky, K. M. Skibinsky "Acoustic Resonances in Antiferromagnet $FeBO_3$" J. Magn. Magn. Mater. **309** (1), 64 – 70 (2007).

Instabilité Explosive des Ondes Magneto-Élastiques

Récemment découvri instabilités paramétriques non linéaire se produirent lorsque le paramètre non linéaire d'un système est modulé. Ces instabilités ont été signalées sur les ondes magnétoelastique comme couplage de trois quasi-phonons sur pompage électromagnétique. Les études théoriques prédisent dynamique supercritique explosive de ces instabilités limitée par la décalage de fréquence.

Dans cette recherche la dynamique supercritique des instabilités paramétriques non linéaires est étudiée dans deux antiferromagnétiques "plan facile" (AFEP): hématite α-Fe2O3 et fer borate FeBO3. Ces matériaux possèdent non-linéarité acoustique efficace immense. Mécanismes de limitation de la dynamique explosive ont été analysés à l'aide de l'approximation anharmonique. Compensation par modulation singulier de phase de pompage a été suggéré et théoriquement vérifiée.

Cette compensation a été utilisée pour la recherche expérimentale de la dynamique supercritique explosive des excitations trois quasi-phonon aux résonateurs magnétoelastiques. Les études sur borate de fer ont été réalisées dans la gamme de température 77 K - 293 K où les paramètres magnétoélastique du cristal varie essentiellement. Modèle fortement non linéaire des excitations trois quasi-phonon dans AFEPs a été développé. Des simulations numériques du modèle sont en accord avec les résultats expérimentaux.

Les études théoriques de couplage de trois ondes magnétoelastique progressives sont effectuées sur la base de modèles théoriques qui a suggéré de prendre en compte la non-linéarité cubes. Des simulations numériques des modèles suggèrent un comportement explosif et la localisation spatiale des triades généré.

Mots – clés :

- Ondes non linéares
- Hématite
- Borate de fer
- Ondes élastiques
- Ondes acoustiques
- Instabilité explosive
- Couplage trois-phonons
- Dynamique supercritique

Explosive Instability of Magneto-Elastic Waves

Recently discovered nonlinear parametric instabilities occur when nonlinear parameter of a system is modulated. These instabilities were reported on magnetoelastic waves as three quasi-phonon coupling under electromagnetic pumping. Theoretical studies suggested supercritical explosive dynamics of these instabilities. Experimentally such singular behavior is limited by strong nonlinear frequency shift.

Presented work studies supercritical dynamics of nonlinear parametric instabilities in two easy plane antiferromagnets (AFEP): hematite α-Fe_2O_3 and iron borate $FeBO_3$. These materials possess unprecedented effective acoustic nonlinearity due to high magneto-elastic coupling. Limiting mechanisms of explosive dynamics were analyzed with the help of anharmonic approximation. Nonlinear frequency shift compensation via singular pumping field phase modulation was suggested and theoretically approbated. This technique was successfully used for experimental observation and investigation ofx supercritical explosive dynamics of three quasi-phonon excitations in magnetoelastic resonators. Iron borate studies were performed in the temperature range 77 K – 293 K where magnetoelastic parameters of the crystal vary essentially. Strongly nonlinear model of three quasi-phonon excitations in AFEPs was developed. Numerical simulations of the model showed good agreement with experimental results.

Theoretical studies of three travelling magnetoelastic waves coupling are performed on the basis of suggested theoretical models that take into account cubic nonlinearity of real AFEP crystals. Numerical simulations of the models suggest explosive behavior and spatial localization of generated triads.

Keywords :

- Nonlinear waves
- Hematite
- Iron borate
- Elastic waves
- Acoustic waves
- Explosice instability
- Three phonons coupling
- Supercritical dynamics